INSTITUTE OF PARTICLE SCIENCE & ENGINEERING

UNIVERSITY OF LEEDS

Single Droplet Drying at High Temperatures

Andrew Bayly

PhD students: Wael Ebrahim, Tien Nguyen

School of Chemical and Process Engineering

University of Leeds

UK

IFPRI Annual Meeting, 2018, Edinburgh, UK

What is different about high temperatures?

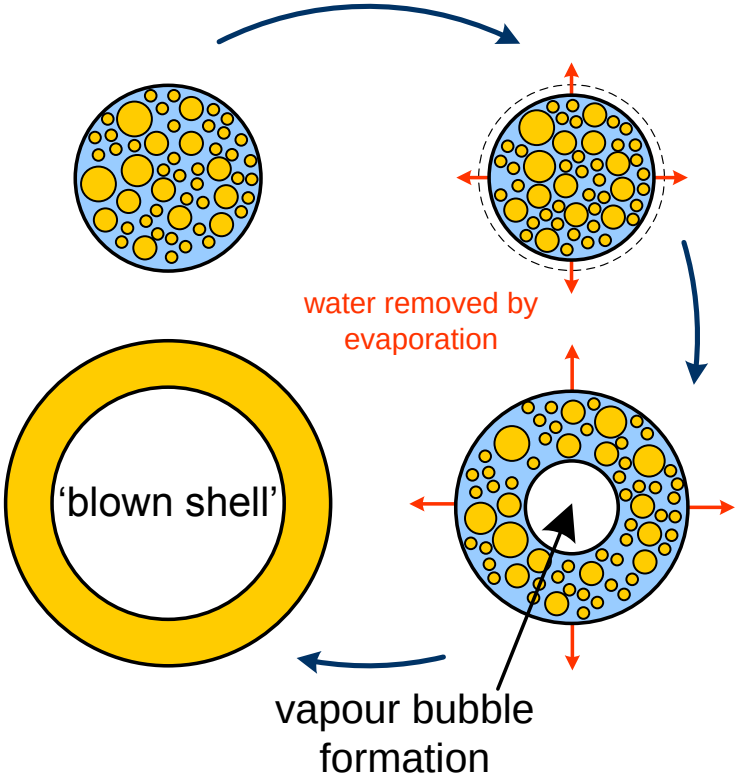

Bubble nucleation leads to mechanical deformation, puffing, and very significant changes in physical and functional properties

Droplet Drying History

UNIVERSITY OF LEEDS

Drying kinetics ⇄ Structural evolution

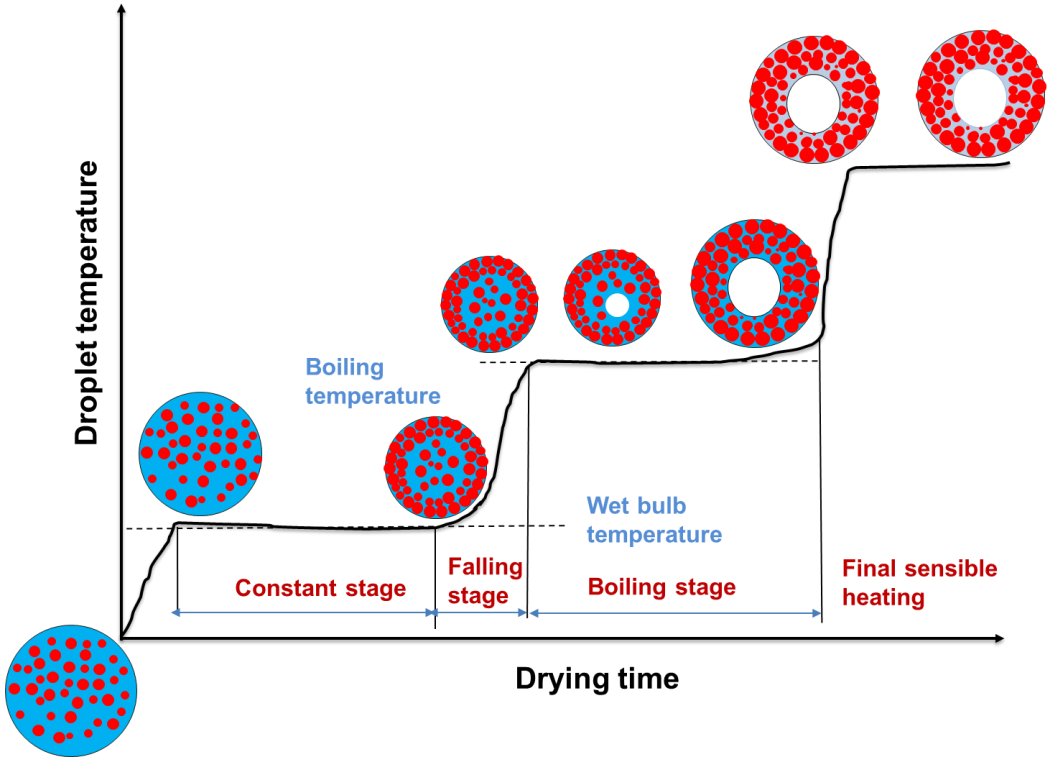

The temperature history and morphological changes of a droplet in a spray dryer

High Temperature Drying

UNIVERSITY OF LEEDS

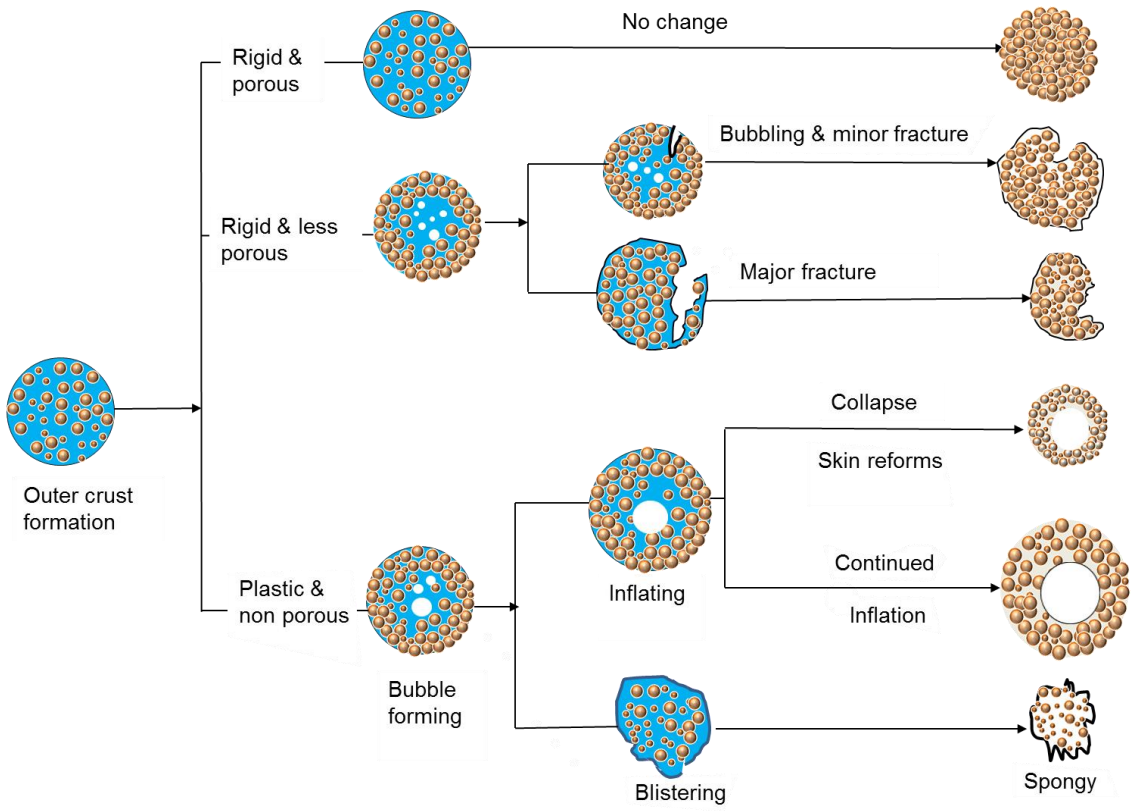

Bubble formation and nucleation leads to mechanical deformation, puffing and changes to the morphological development

(adapted from Charlesworth, D. and Marshall, W. 1960. *AIChE Journal*. 6. pp 9-23.)

Work Programme

UNIVERSITY OF LEEDS

Goal: regime map based on material properties

- Drying rig development for experimental mapping
- Material property method development
- Modelling – incorporation of structural development

Material Categories

- Amorphous, glassy - *e.g.* polymers, many foods
  - skin forming, plastic, polymeric, ~ gels
- Suspensions and colloids *e.g.* TiO_2, silica
  - diffusivity a function of packing, primary particle size
- Crystallizing – *e.g.* inorganic salts
  - nucleation and growth

Phase transition → micro-structure → material property evolution during drying drives macro-structure *i.e.* morphology

Material Categories

UNIVERSITY OF LEEDS

- Amophous/glassy – **HPMC, Sucrose, Silicate**
- Suspensions and colloids - Ti02, silica
- Crystallizing – Na2SO4, Ascorbic Acid

Mapping behaviours

UNIVERSITY OF LEEDS

Even on a relatively uniform spray dryer. The morphologies are different, significant distribution of properties.

Why:
- drop size
- distributed drying histories
- stochastic nature of structure development

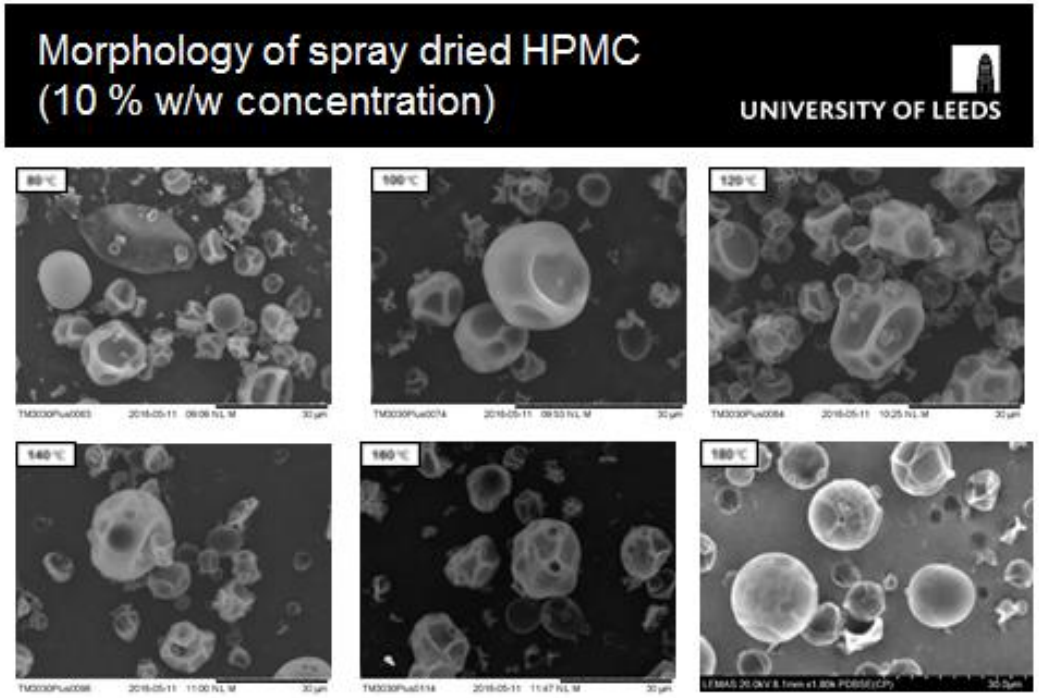

Establish method with controlled drying single or mono-dispersed droplets

Drying Methods

UNIVERSITY OF LEEDS

- Suspended droplet/filament
- Drop tube/chain
- Levitator
  - Acoustic
  - Electrodynamic balance (EDB)

Experimental – recent focus

UNIVERSITY OF LEEDS

Filament rig

- rig and technique development
- quantitative analysis
- expanding material space
    - viscosity range
    - silicate

Drop tube – in place

Filament Drying Rig

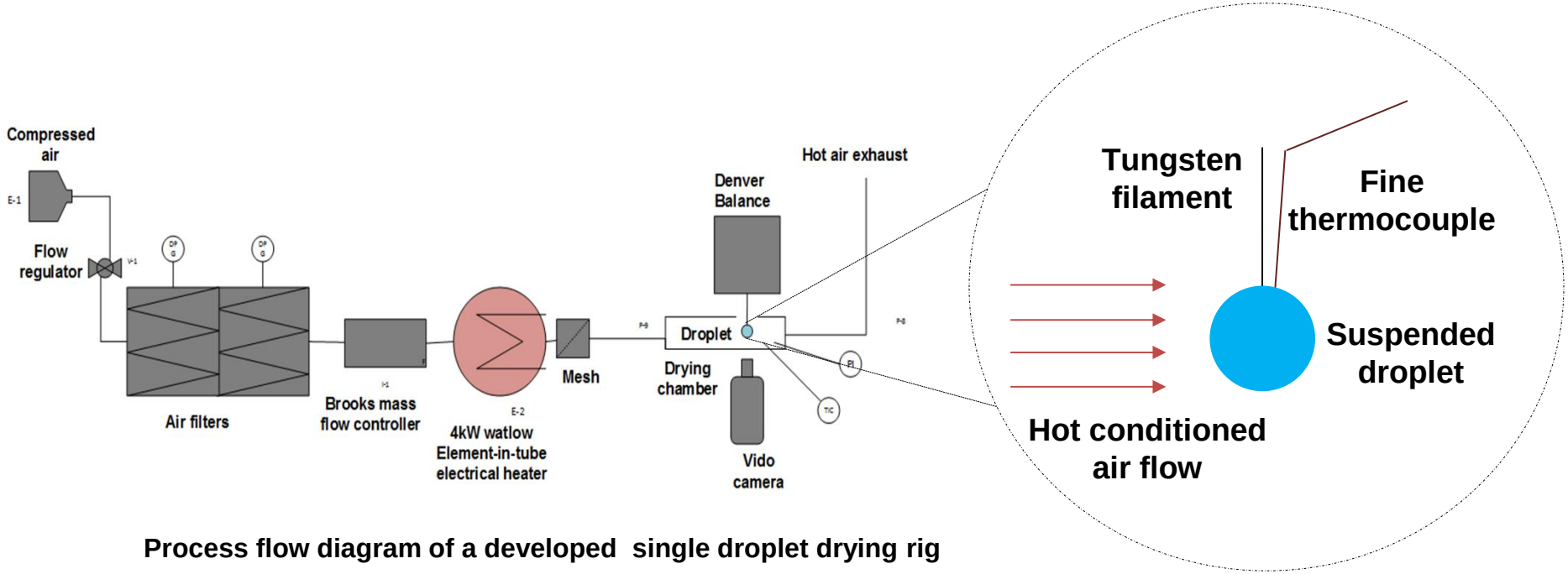

Process flow diagram of a developed single droplet drying rig

Filament Drying Rig

UNIVERSITY OF LEEDS

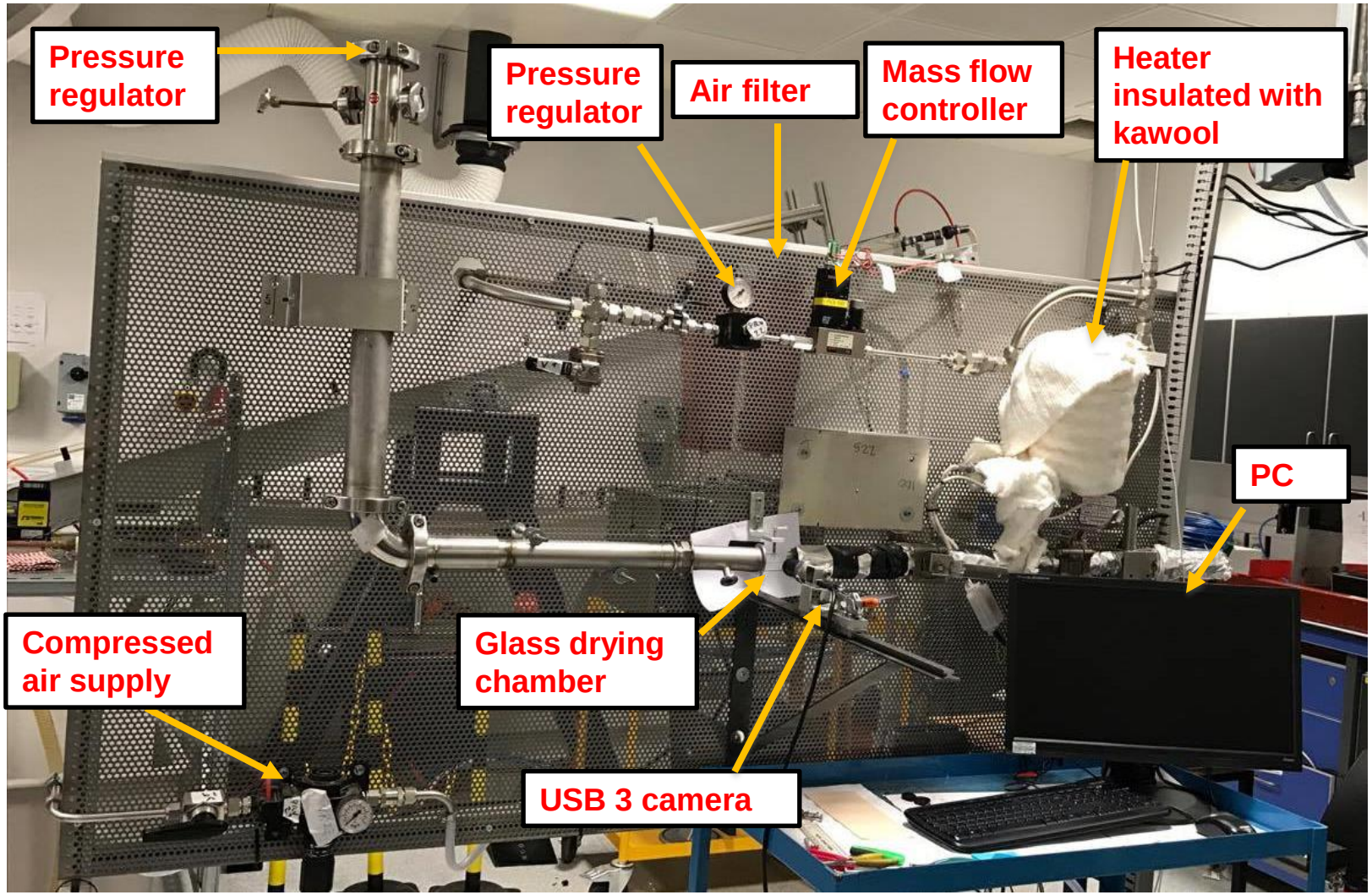

Mark 2 - Version

Single Droplet Drying Rig

UNIVERSITY OF LEEDS

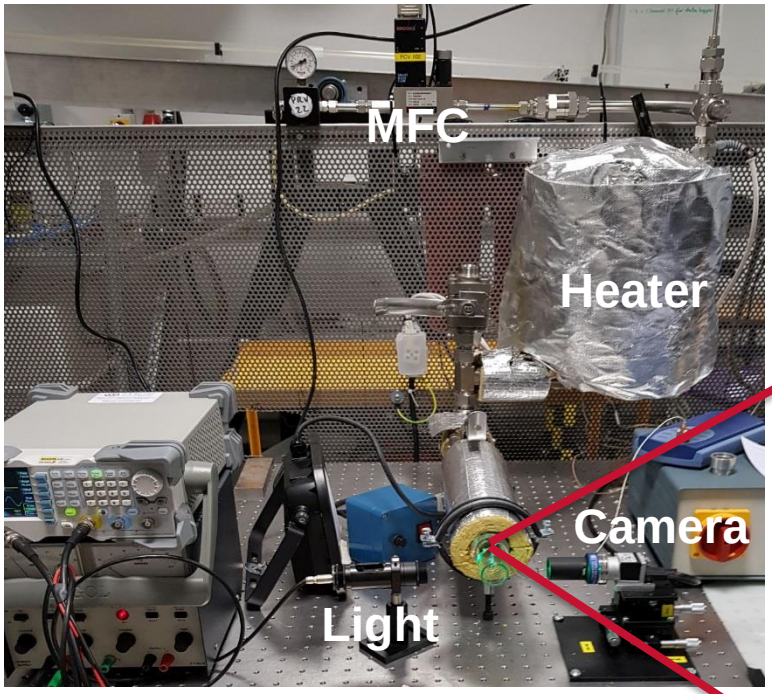

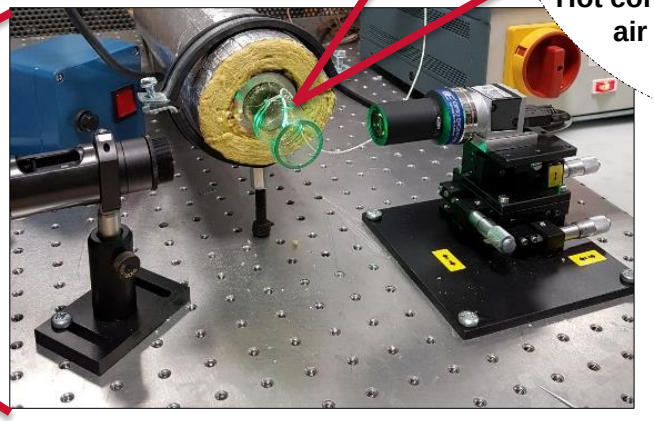

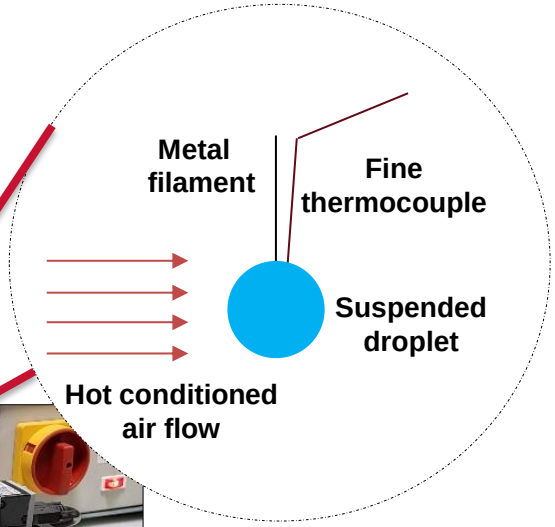

Sucrose - T_{air} = 190˚ C , 45 %, d_{init} = 1.5 mm inflation/defalation cycles

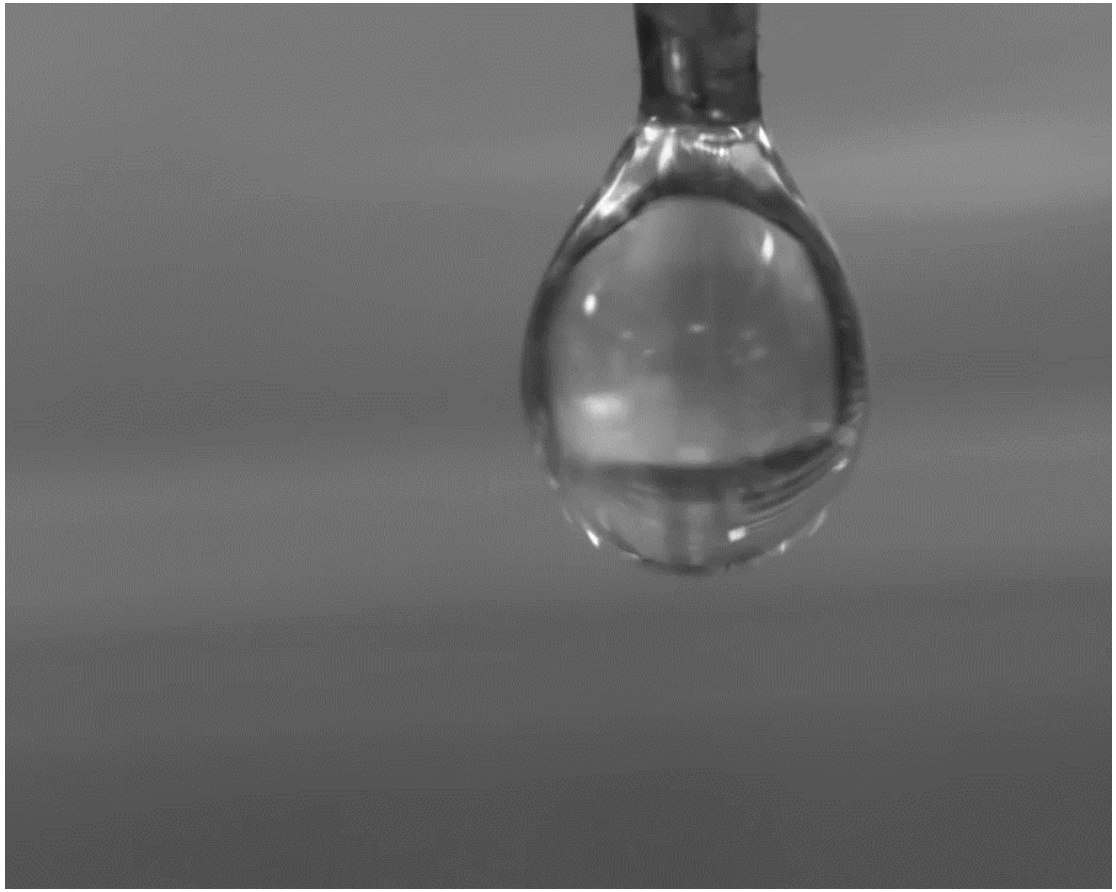

Sucrose - T_{air} = 190° C , 45 %, d_{init} = 1.5 mm inflation/defalation cycles

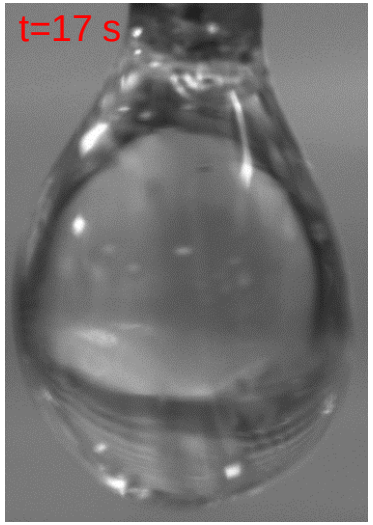

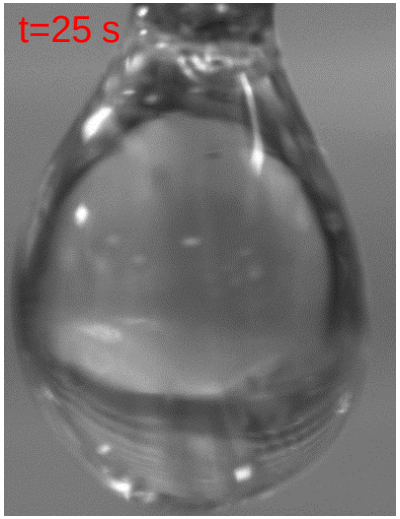

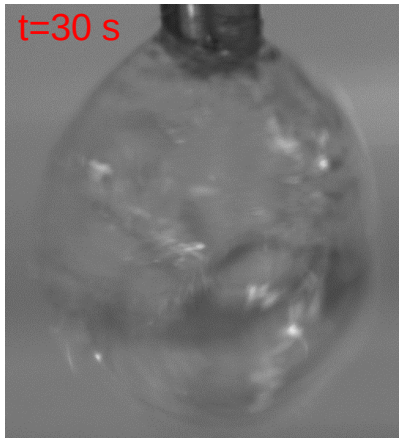

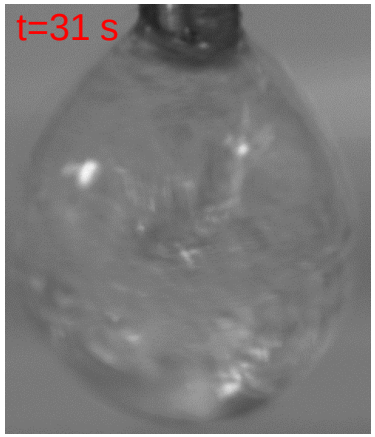

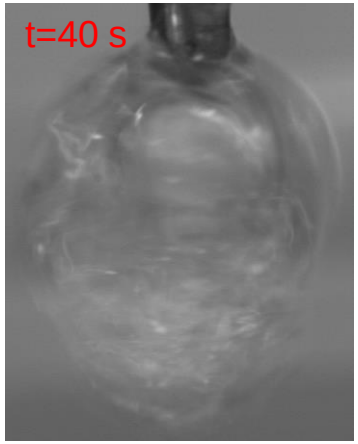

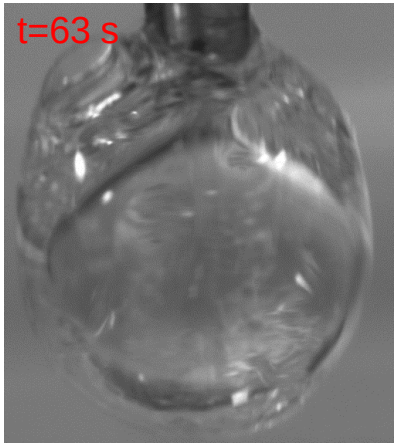

Sucrose - T_{air} = 180° C , 15 %, d_{init} = 1.7 mm
inflation/defalation cycles

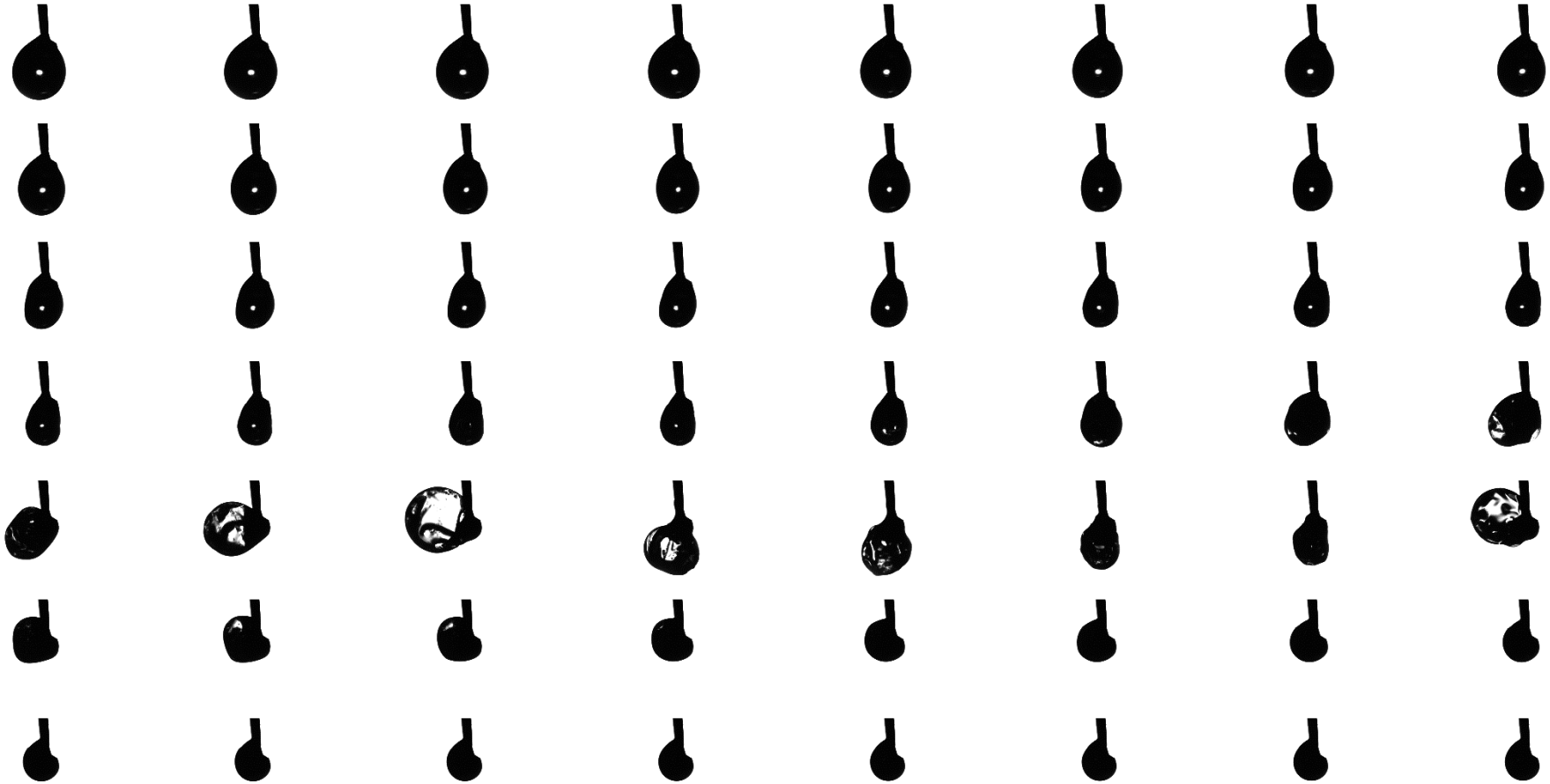

Sucrose - T_{air} = 180°C , 15 %, d_{init} = 1.7 mm
inflation/defalation cycles

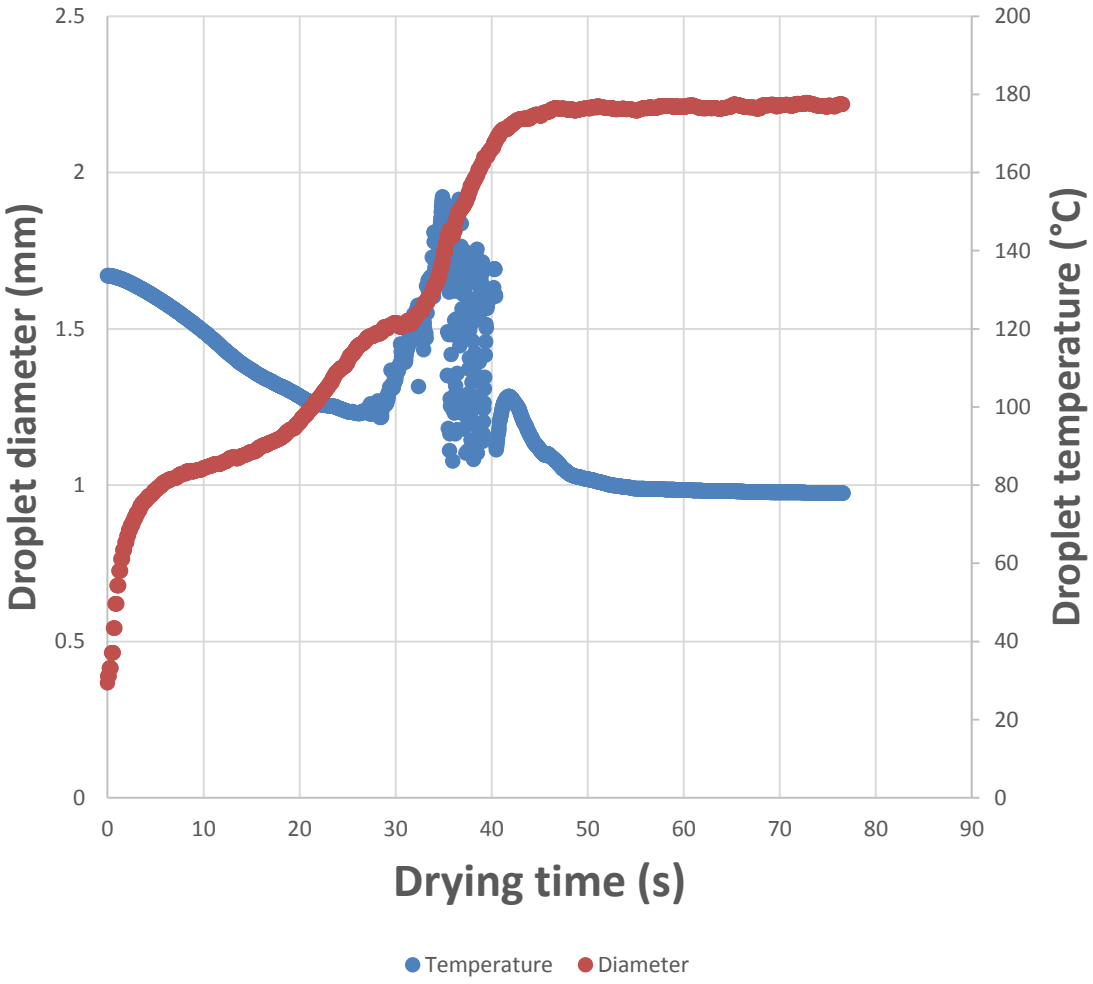

Morphology Evolution of HPMC in water

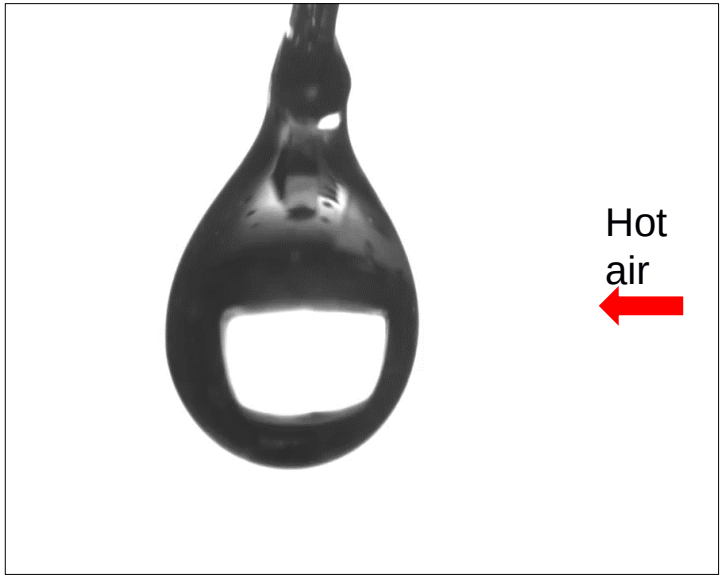

HPMC 15% w/w, T_{air} = 72°C

HPMC: 15% w/w, T_{air} = 180°C

HPMC in water - T_{air} = 72°C , 15 %, d_{init} = 2.5 mm
shrinkage and buckling

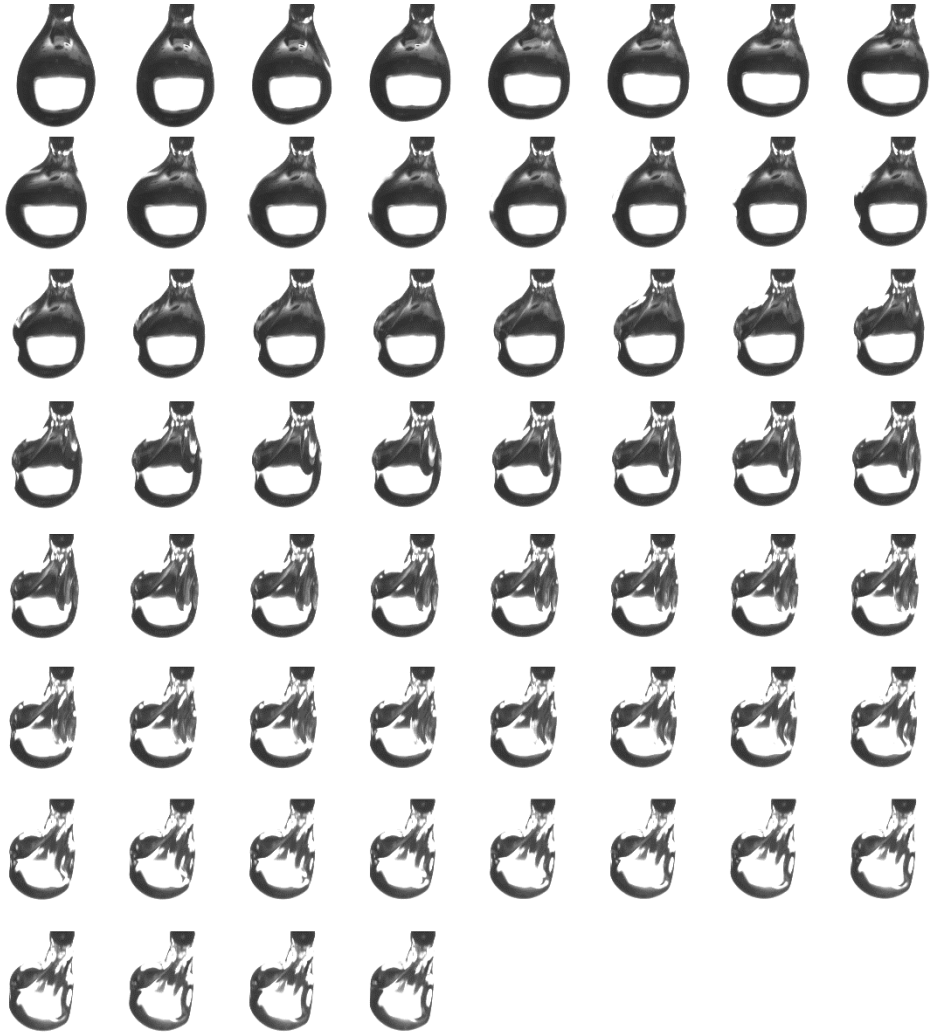

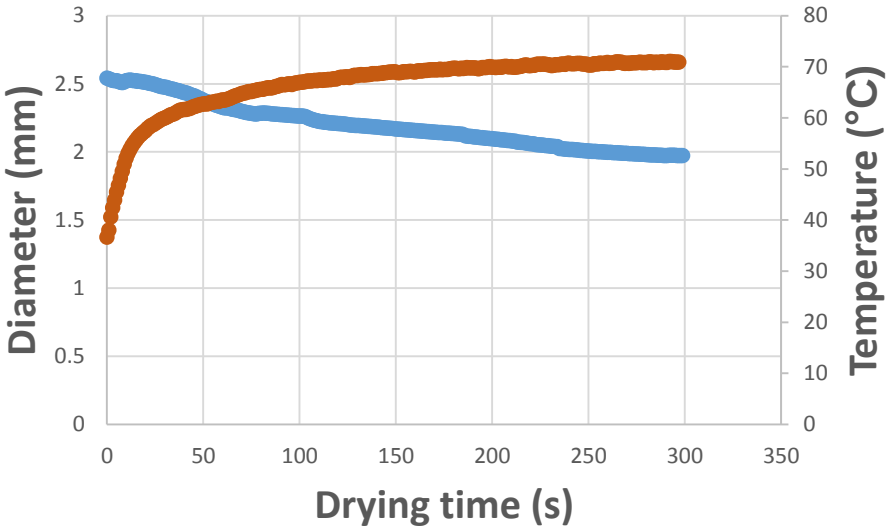

HPMC in water - T_{air} = 180°C , 5 %, d_{init} = 2.2 mm
shrinkage and buckling

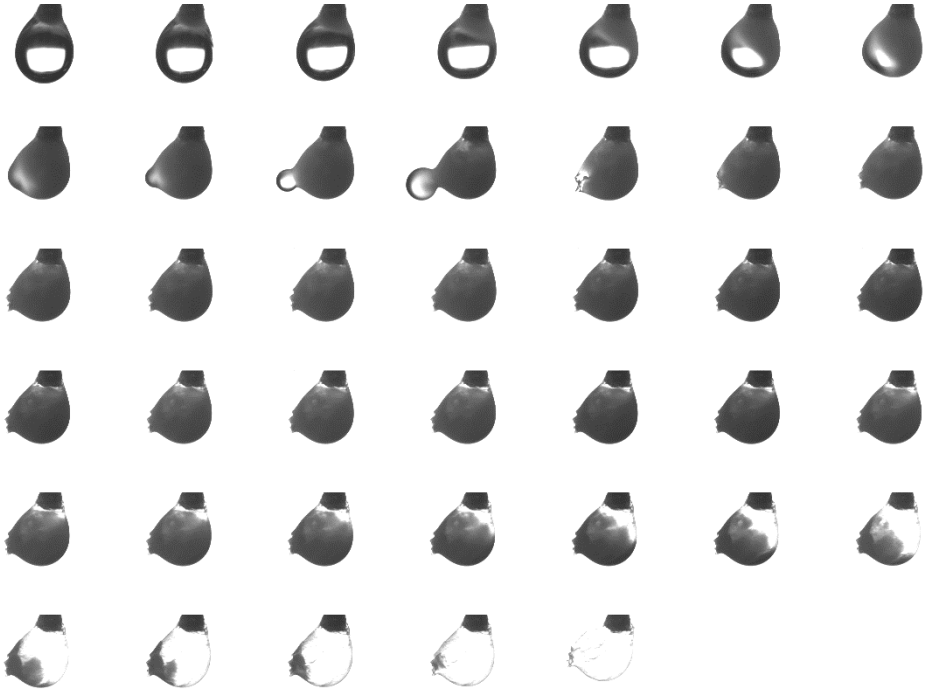

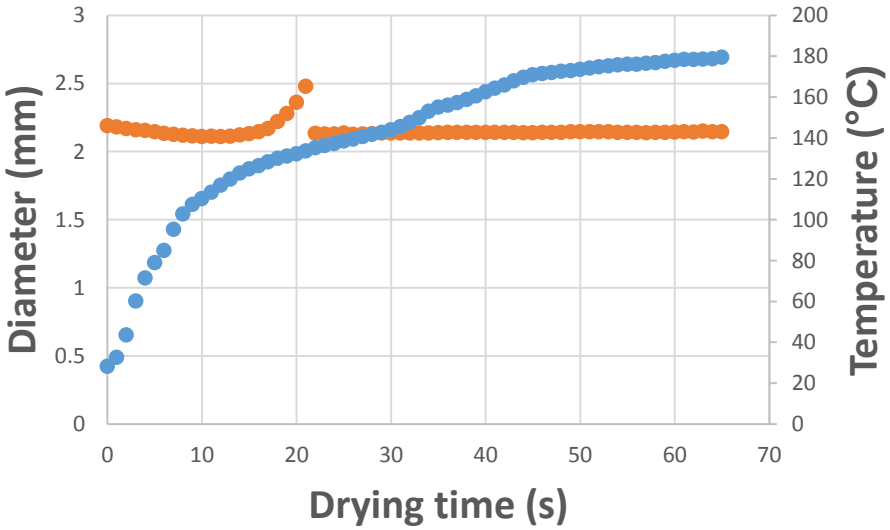

Structure of final dried HPMC particles

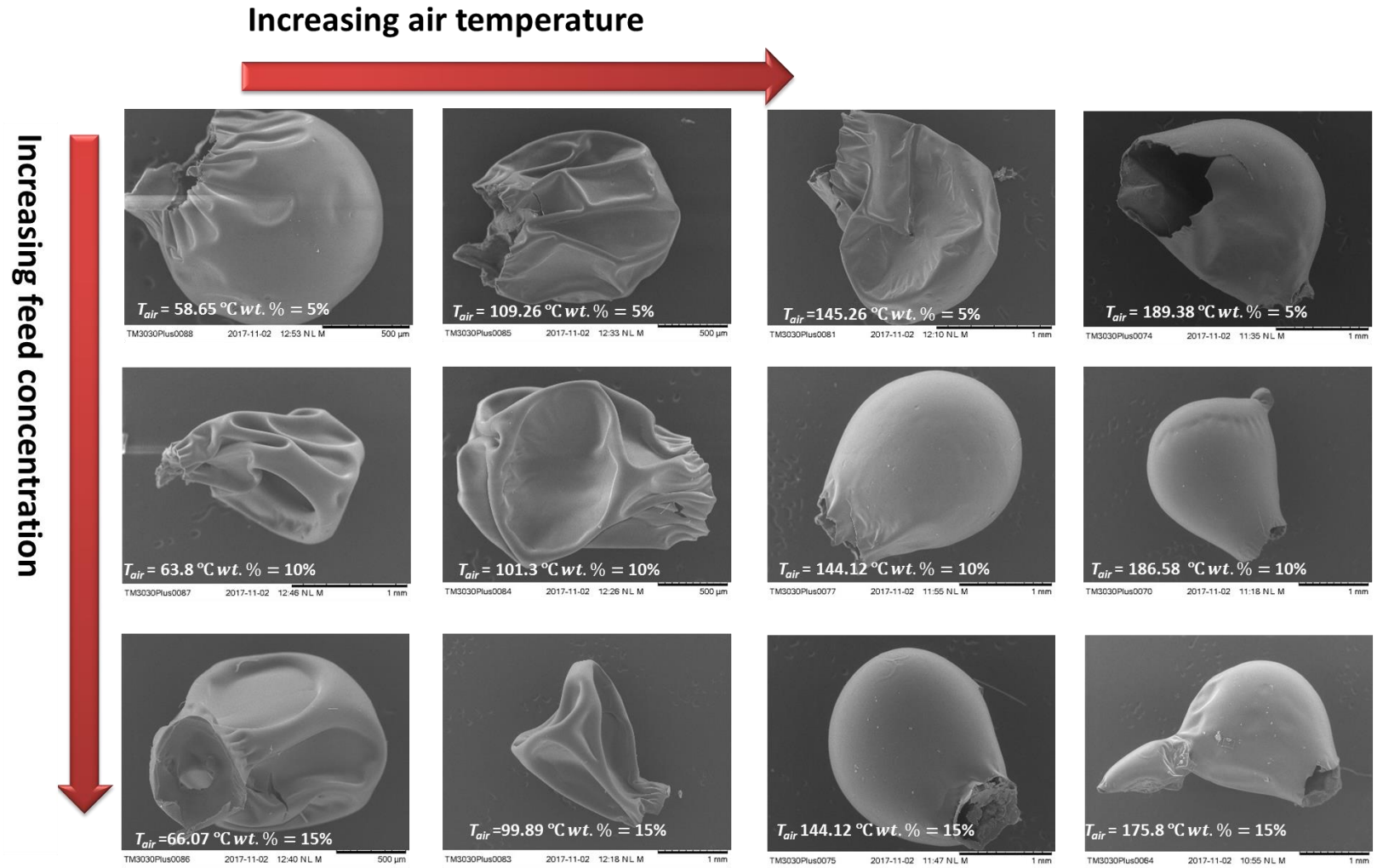

Spray dried HPMC (15%w/w)

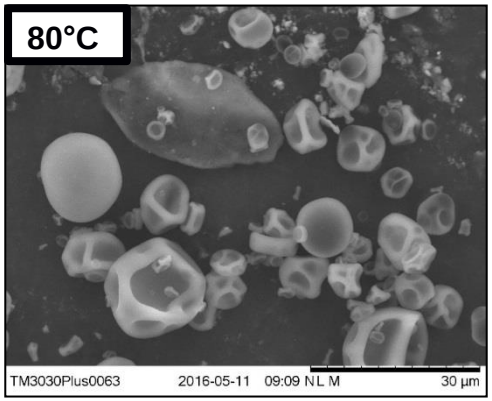

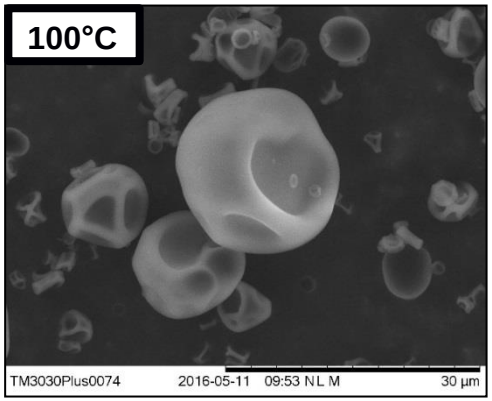

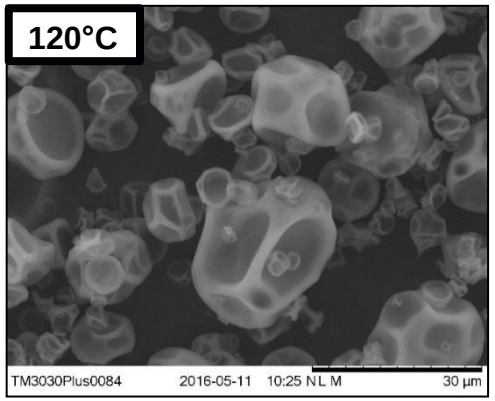

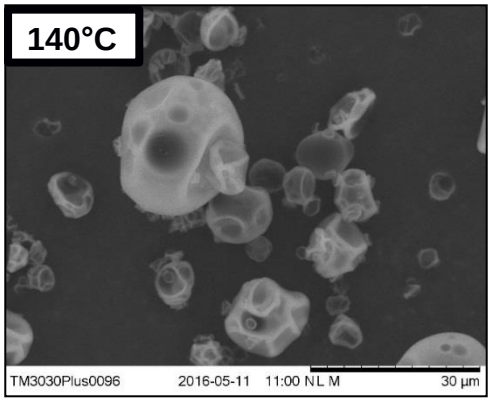

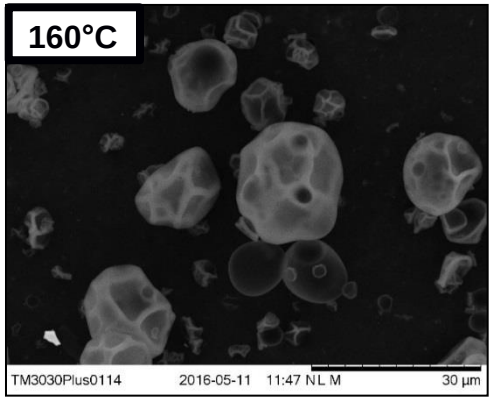

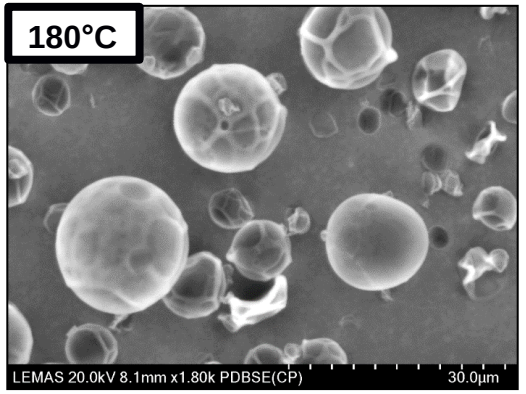

Buckled morphologies at low temperature, smoother morphologies at high temperature

HPMC in acetone–water - T_{air} = 180°C , 15 %, d_{init} = 2.8 mm — partial inflation

HPMC droplet: 15% w/w HPMC in 70:30 w/w acetone: water, T_{air}=180°C

HPMC in acetone–water - T_{air} = 180°C , 5 %,

d_{init} = 1.8 mm — partial inflation

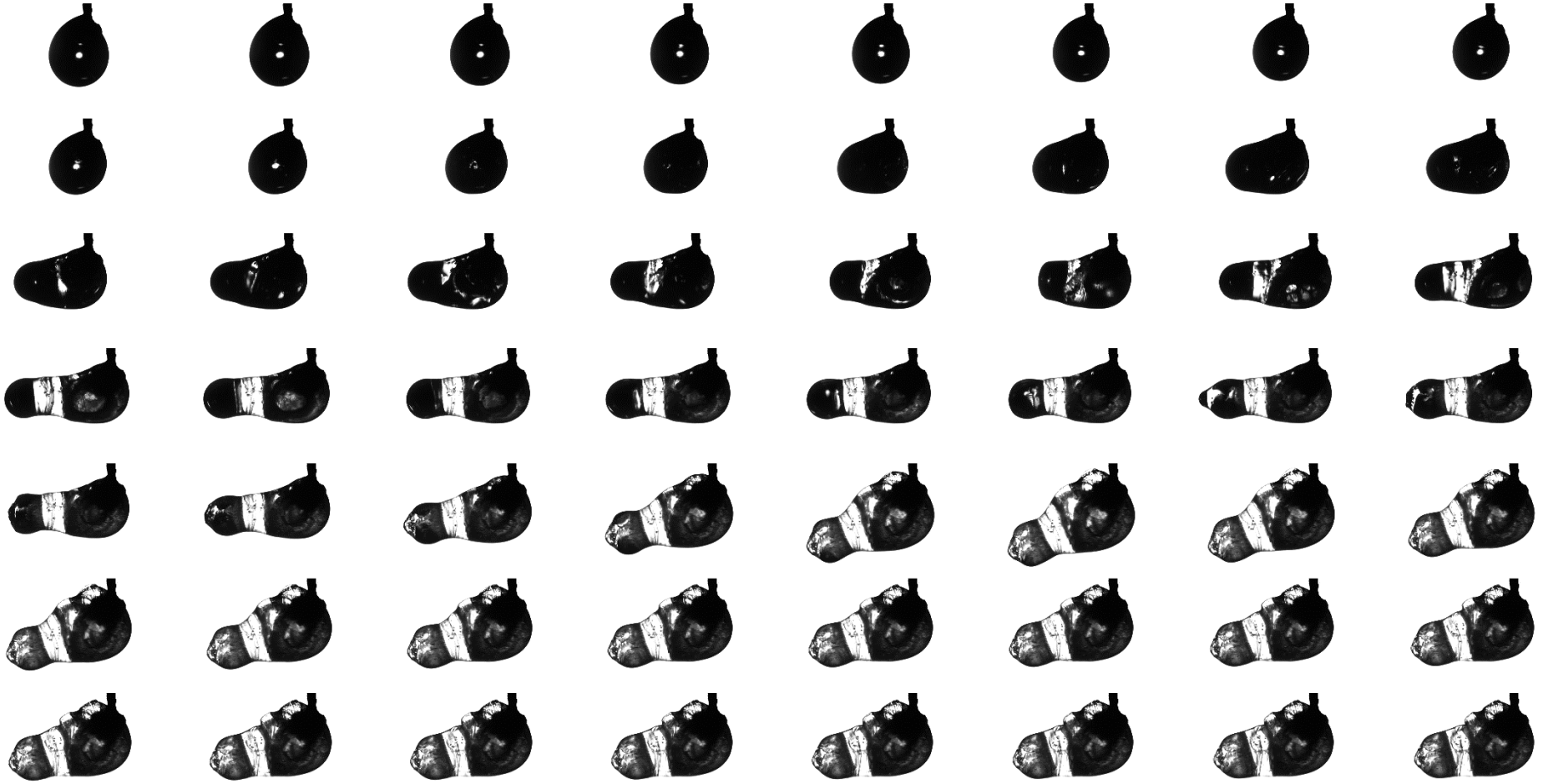

HPMC in acetone–water - T_{air} = 180°C , 5 %, d_{init} = 1.8 mm — partial inflation

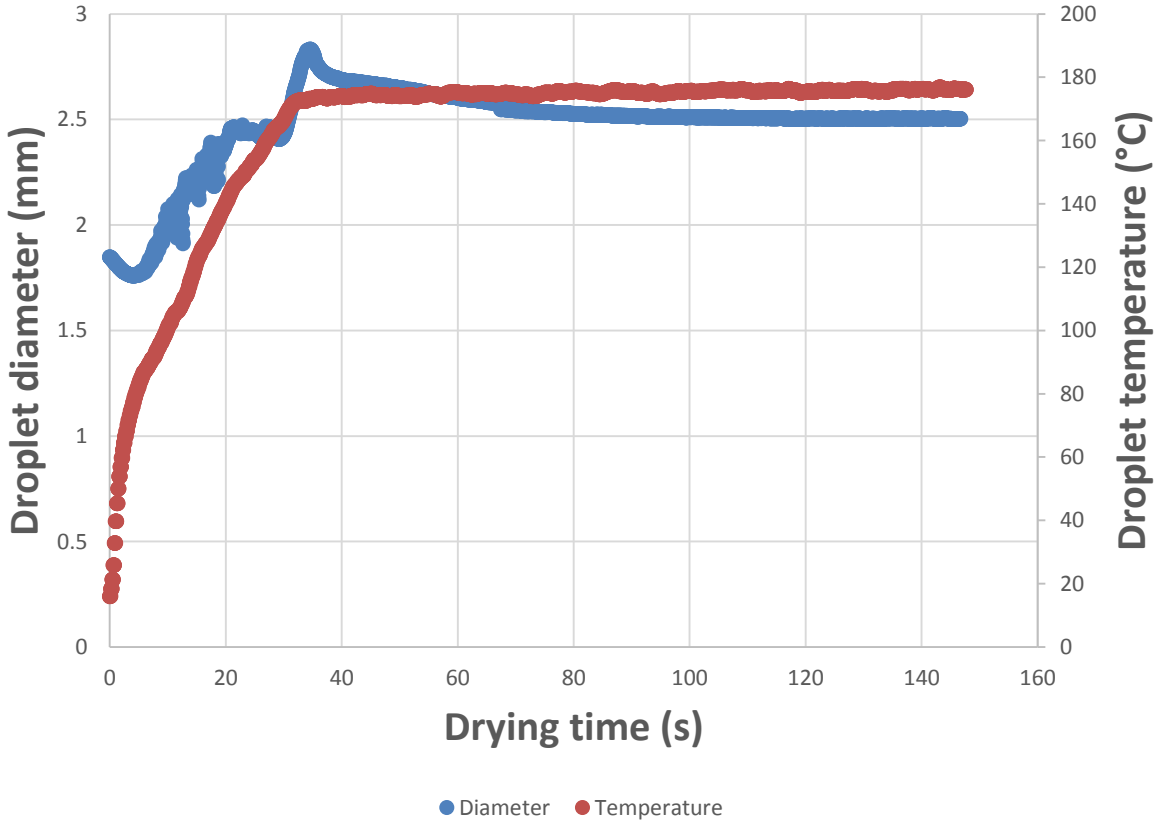

Sodium silicate - T_{air} = 180°C , 40 %, d_{init} = 1.6 mm
puffing behaviour

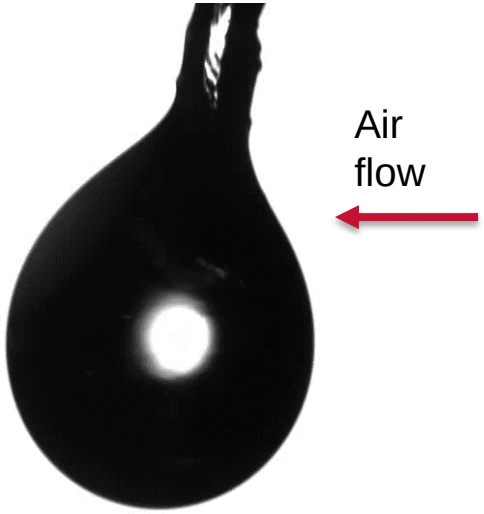

Sodium silicate: 40% w/w, T_{air}=180°C

Sodium silicate - T_{air} = 180°C , 40 %, d_{init} = 1.6 mm
puffing behaviour

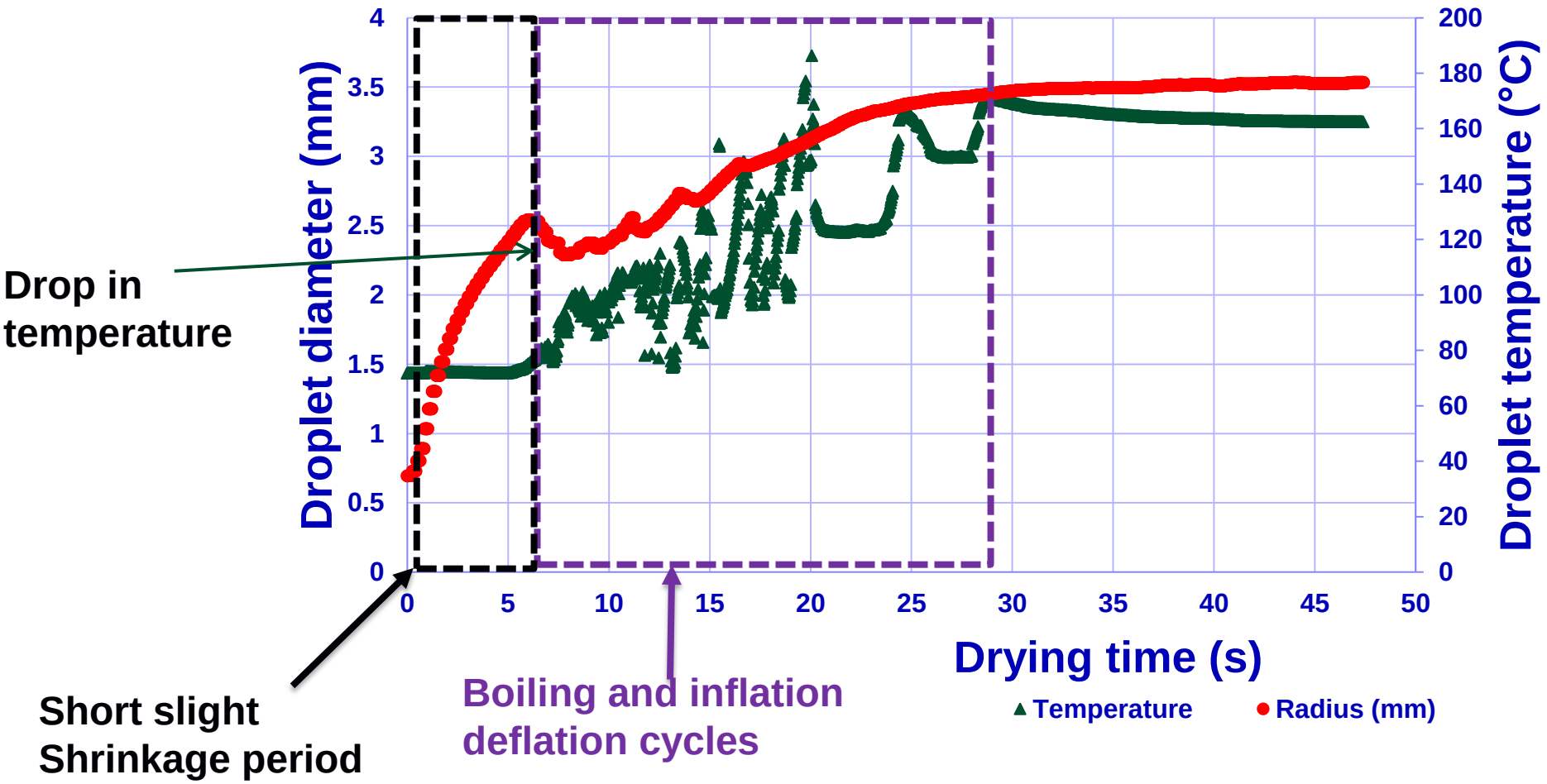

Spray dried Sodium Silicate

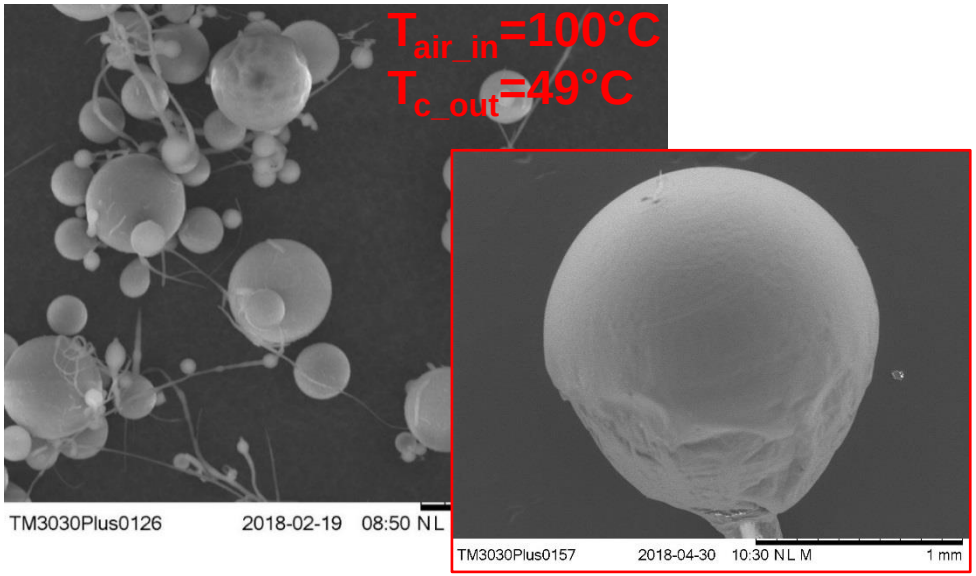

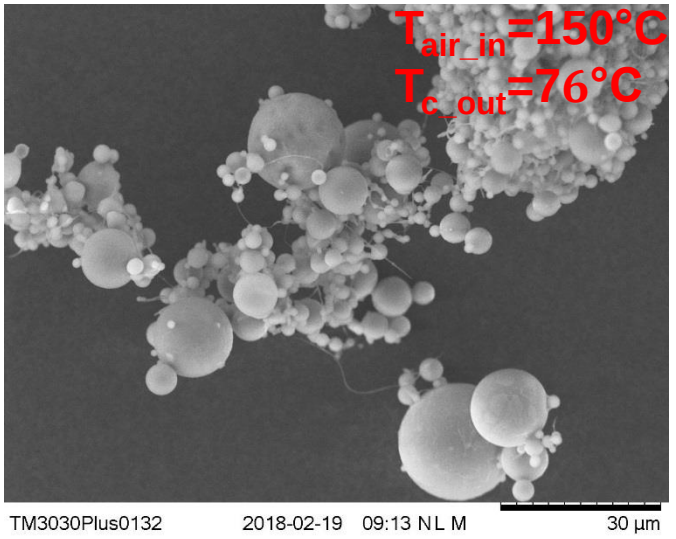

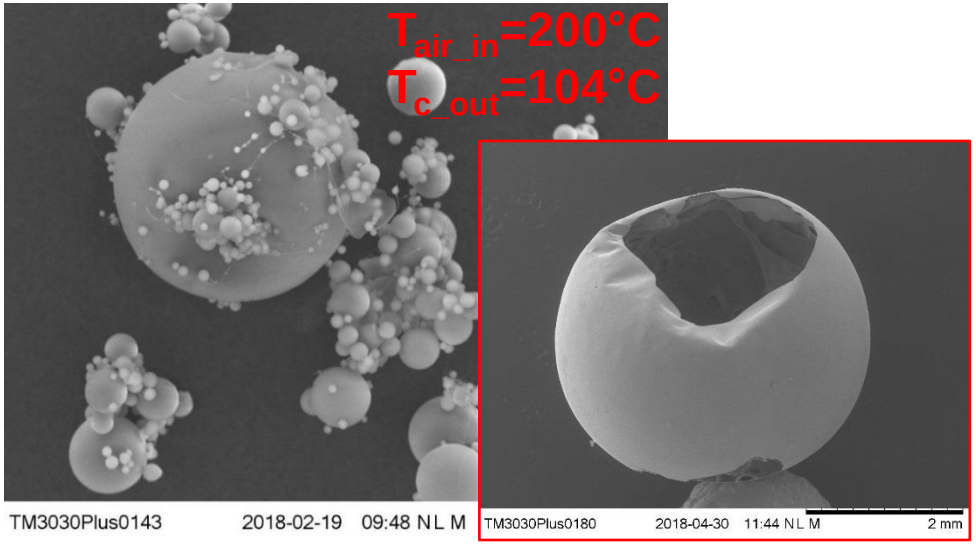

- Spray dried sodium silicate show puffed particles
- Spray drying results in agreement with single droplet drying experiments

***T_{c_out} represents the chamber outlet temperature**

Sucrose — D^2/D_0^2 and T_{drop} vs $t/\tau d$

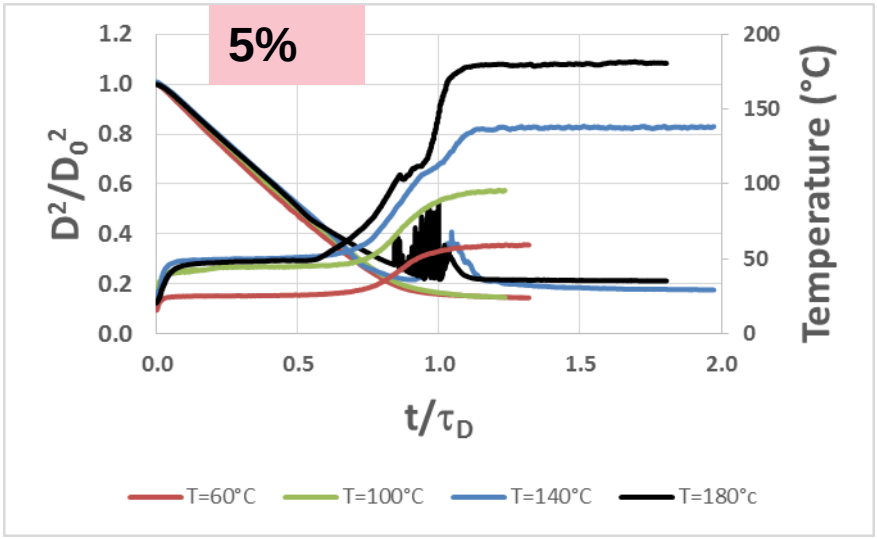

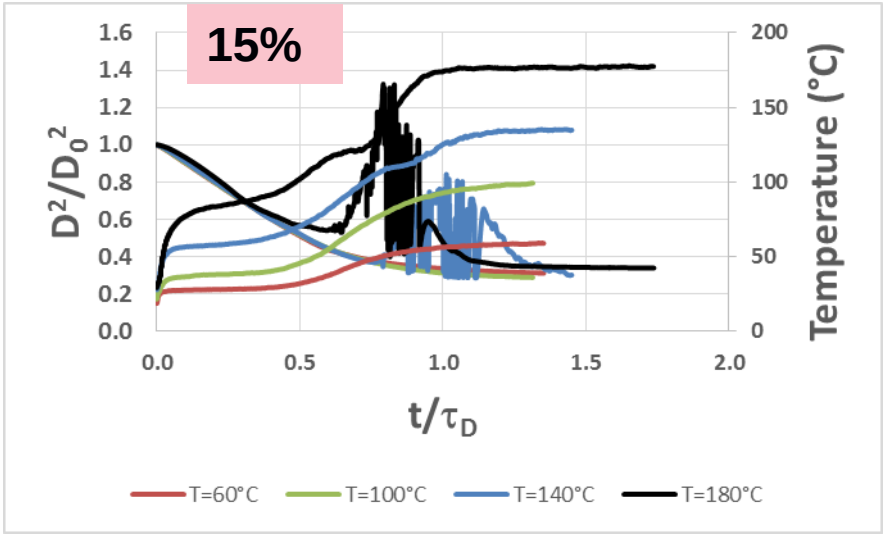

HPMC — D^2/D_0^2 and T_{drop} vs $t/\tau d$

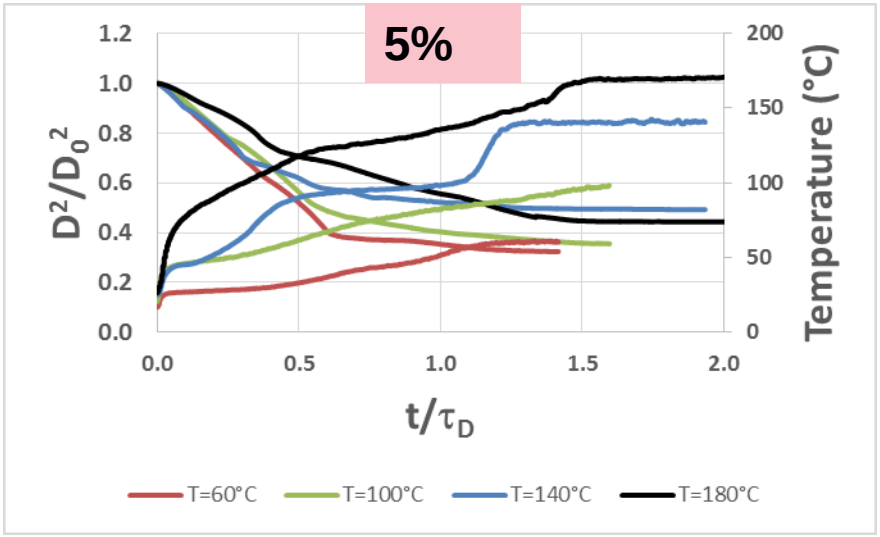

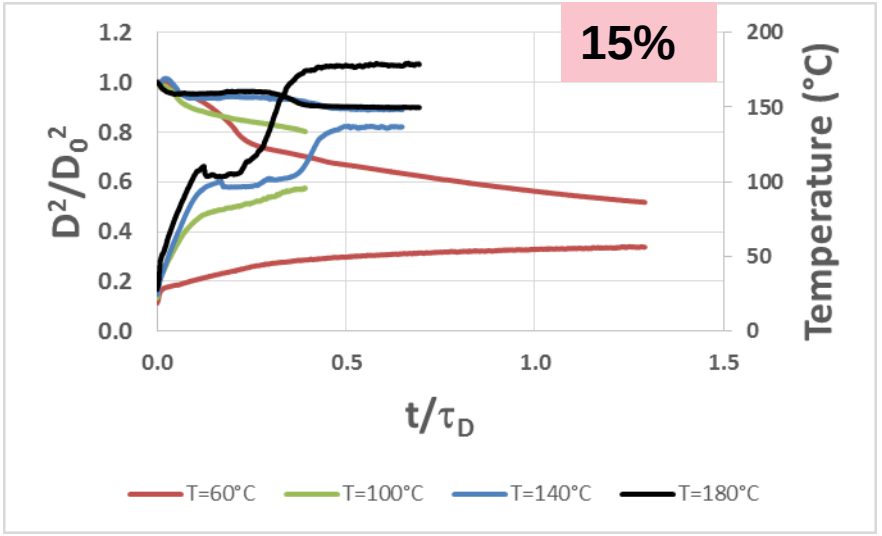

Silicate — D^2/D_0^2 and T_{drop} vs $t/\tau d$

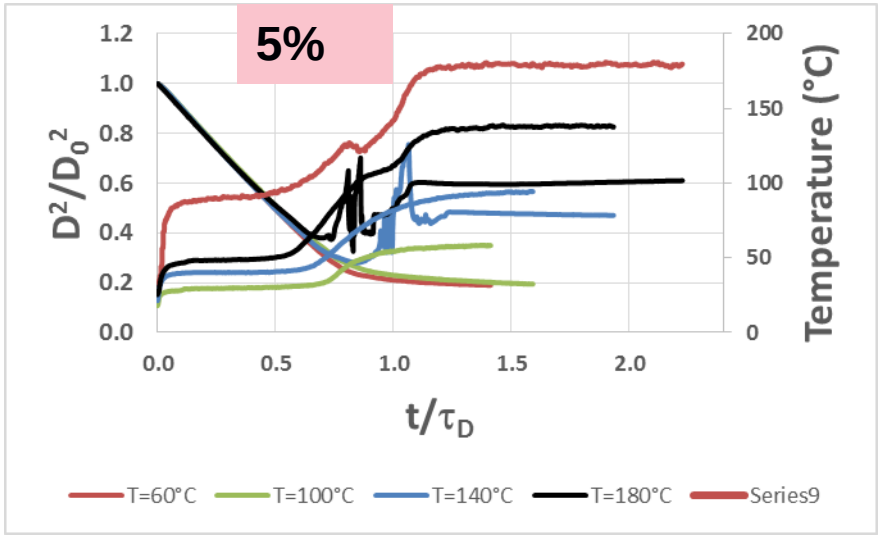

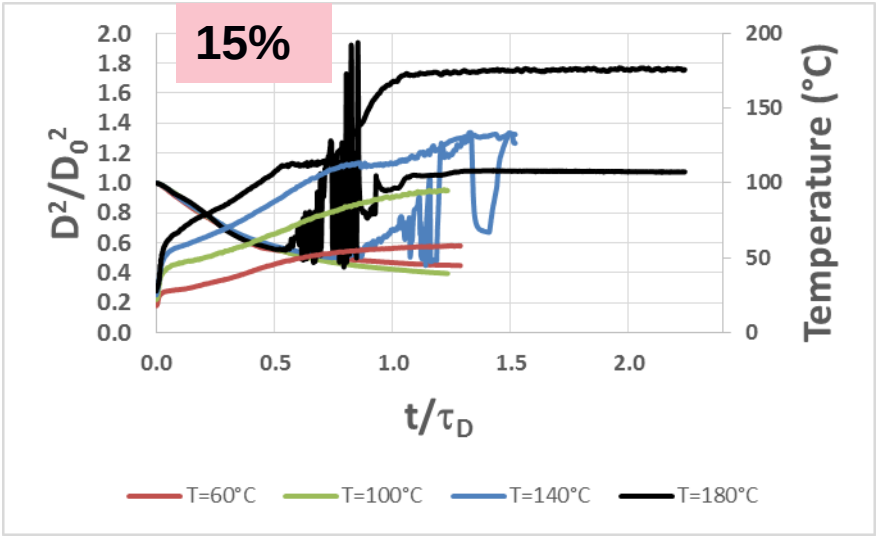

Peclet number and D/D_0 at key stages

5% Sucrose

T (°C)	D_0 (mm)	Solid diffusivity (mm^2/s)	Evaporation rate (k) (mm^2/s)	Pe_0	D/D_0 @ Boiling	D/D_0 Max	D_f/D_0
60	1.64	3.32E-03	1.20E-02	**0000.5**	-	-	0.38
100	1.75	3.32E-03	2.16E-02	**0000.8**	-	-	0.38
140	1.57	3.32E-03	3.36E-02	**0001.3**	0.46	1.000	0.42
180	1.63	3.32E-03	5.58E-02	**0002.1**	0.53	1.000	0.46

5% HPMC

T (°C)	D_0 (mm)	Solid diffusivity (mm^2/s)	Evaporation rate (k) (mm^2/s)	Pe_0	D/D_0 @ Boiling	D/D_0 Max	D_f/D_0
60	1.64	2.93E-06	1.10E-03	**0046.9**	-	-	0.57
100	1.75	2.93E-06	1.90E-02	**0809.7**	-	-	0.60
140	1.57	2.93E-06	3.01E-02	**1282.7**	0.72	1.000	0.70
180	1.63	2.93E-06	3.51E-02	**1495.8**	0.91	1.000	0.67

5% Silicate

T (°C)	D_0 (mm)	Solid diffusivity (mm^2/s)	Evaporation rate (k) (mm^2/s)	Pe_0	D/D_0 @ Boiling	D/D_0 Max	D_f/D_0
60	1.64	1.96E-04	1.11E-02	**0007.1**	-	-	0.44
100	1.75	1.96E-04	2.22E-02	**0014.2**	-	-	0.69
140	1.57	1.96E-04	3.38E-02	**0021.5**	0.53	1.000	0.44
180	1.63	1.96E-04	4.71E-02	**0030.0**	0.62	1.000	0.78

Peclet number and D/D_0 at key stages

15% Sucrose

T (°C)	D_0 (mm)	Solid diffusivity (mm^2/s)	Evaporation rate (k) (mm^2/s)	Pe_0	D/D_0 @ Boiling	D/D_0 Max	D_f/D_0
60	1.62	3.32E-03	1.20E-02	**0000.5**	-	-	0.56
100	1.59	3.32E-03	2.26E-02	**0000.9**	-	-	0.54
140	1.60	3.32E-03	3.12E-02	**0001.2**	0.65	1.00	0.55
180	1.67	3.32E-03	6.33E-02	**0002.4**	0.74	1.15	0.58

15% HPMC

T (°C)	D_0 (mm)	Solid diffusivity (mm^2/s)	Evaporation rate (k) (mm^2/s)	Pe_0	D/D_0 @ Boiling	D/D_0 Max	D_f/D_0
60	1.57	2.69E-07	7.70E-03	**3579.8**	-	-	0.72
100	1.45	2.69E-07	4.70E-03	**2185.0**	-	-	0.90
140	1.57	2.69E-07	1.09E-02	**5067.4**	0.97	1.00	0.94
180	1.50	2.69E-07	1.73E-02	**8042.8**	0.98	1.00	0.95

15% Silicate

T (°C)	D_0 (mm)	Solid diffusivity (mm^2/s)	Evaporation rate (k) (mm^2/s)	Pe_0	D/D_0 @ Boiling	D/D_0 Max	D_f/D_0
60	1.49	1.96E-04	9.70E-03	**0006.2**	-	-	0.67
100	1.55	1.96E-04	2.04E-02	**0013.0**	-	-	0.63
140	1.72	1.96E-04	3.06E-02	**0019.5**	0.75	1.16	1.23
180	1.63	1.96E-04	4.07E-02	**0025.9**	0.71	1.50	1.40

Summary of Morphology Evolutions

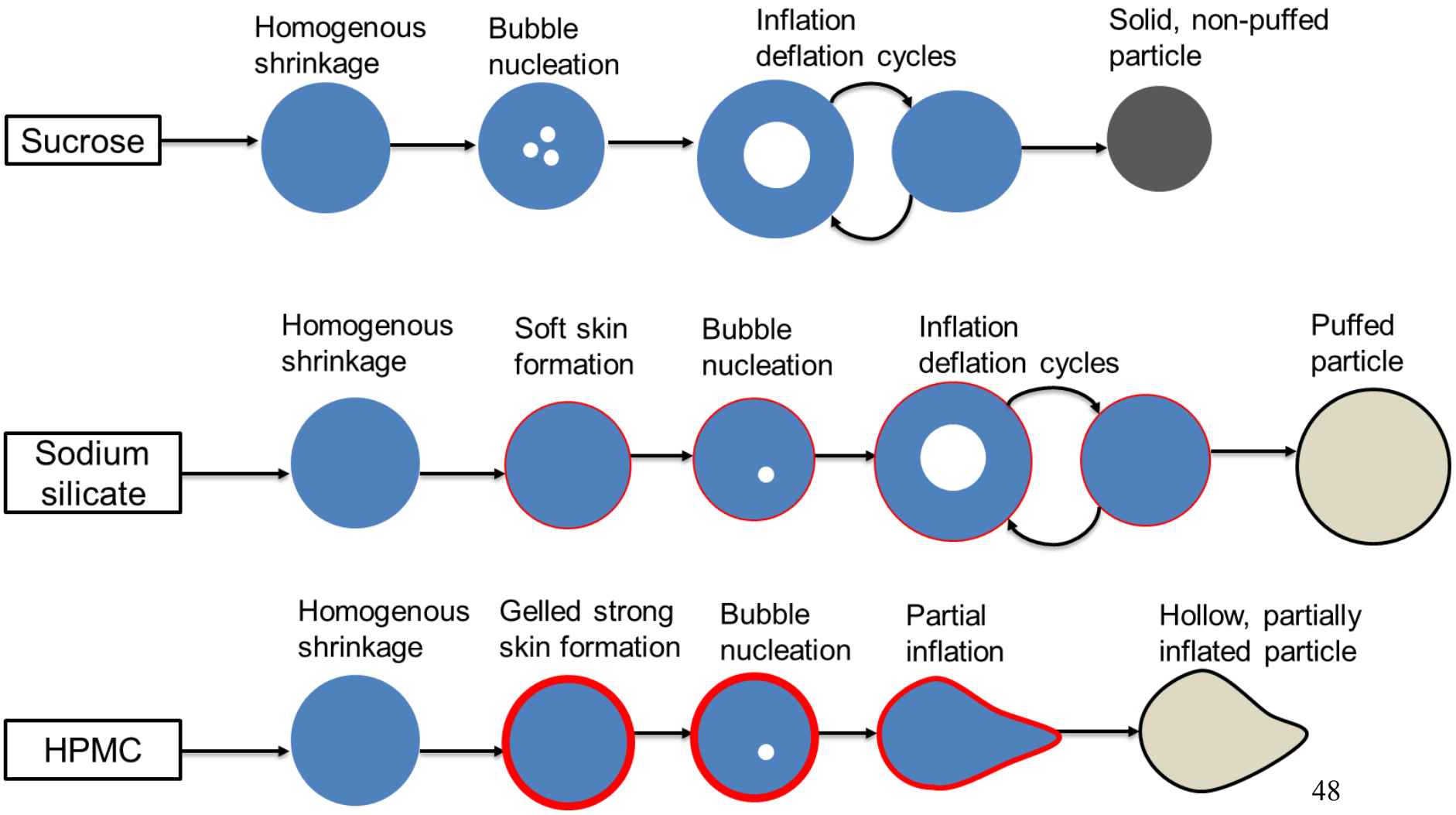

Importance of material properties

UNIVERSITY OF LEEDS

Material properties of the system as it dries determine behaviour:

Transport – diffusivity, porosity

Thermodynamics - water activity

Structure - Rheo-mechanical properties

Phase changes clearly important to all these properties.

Sucrose morphology

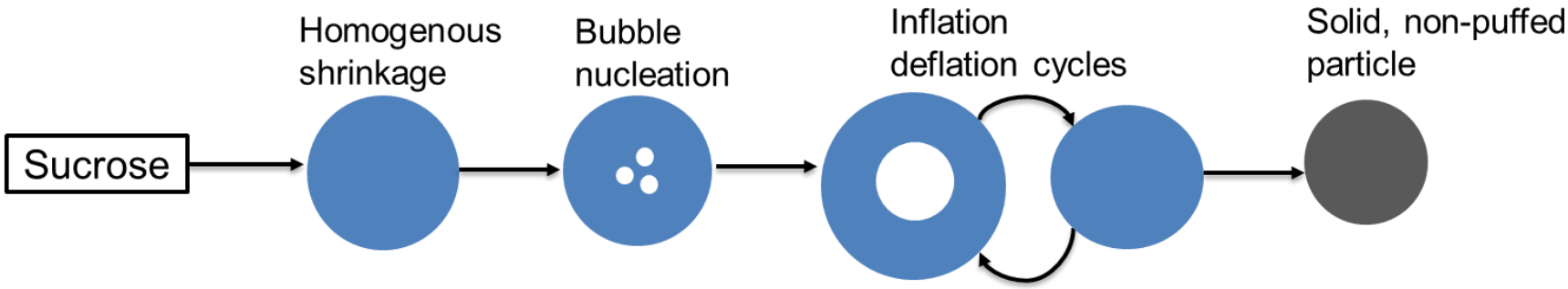

Low viscosity at high temp. and low water % – bubble's burst, surface tension draws liquid back

http://notsohumblepie.blogspot.com/2010/05/lollipops-sugar-science-ramblings.html

HPMC morphology

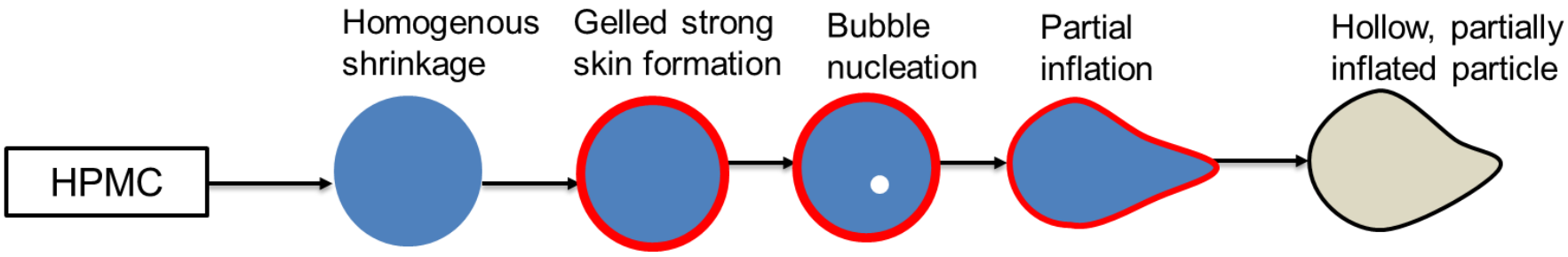

Sol-gel transition critical to material properties

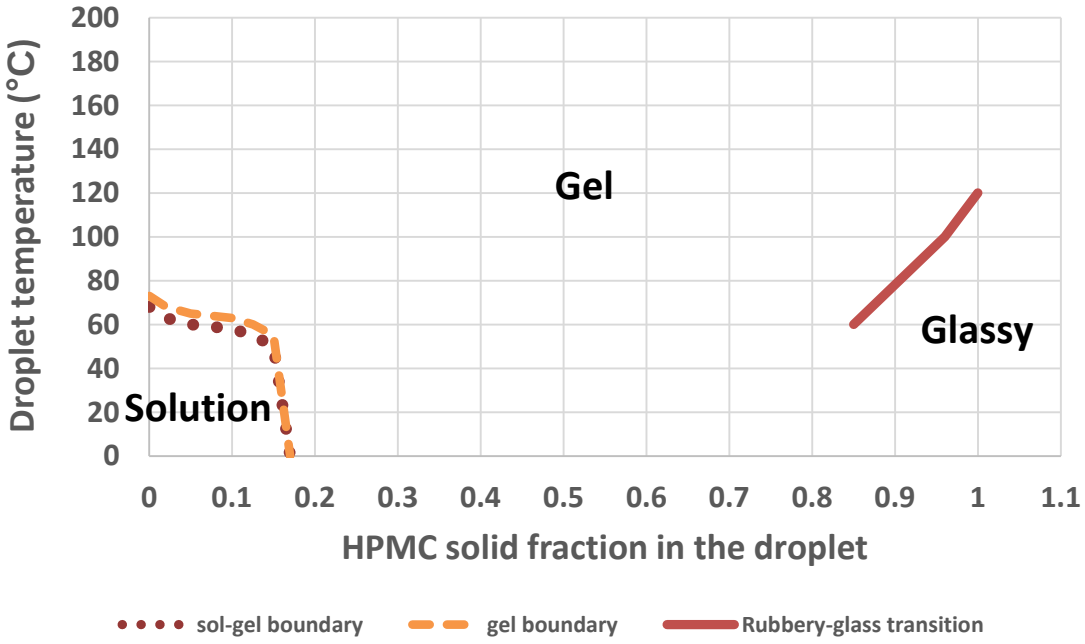

HPMC morphology

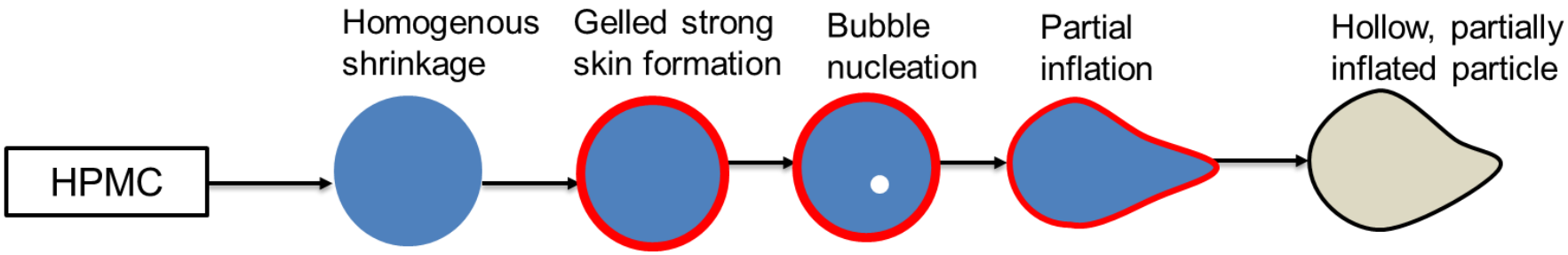

Drying trajectory super imposed on phase diagram

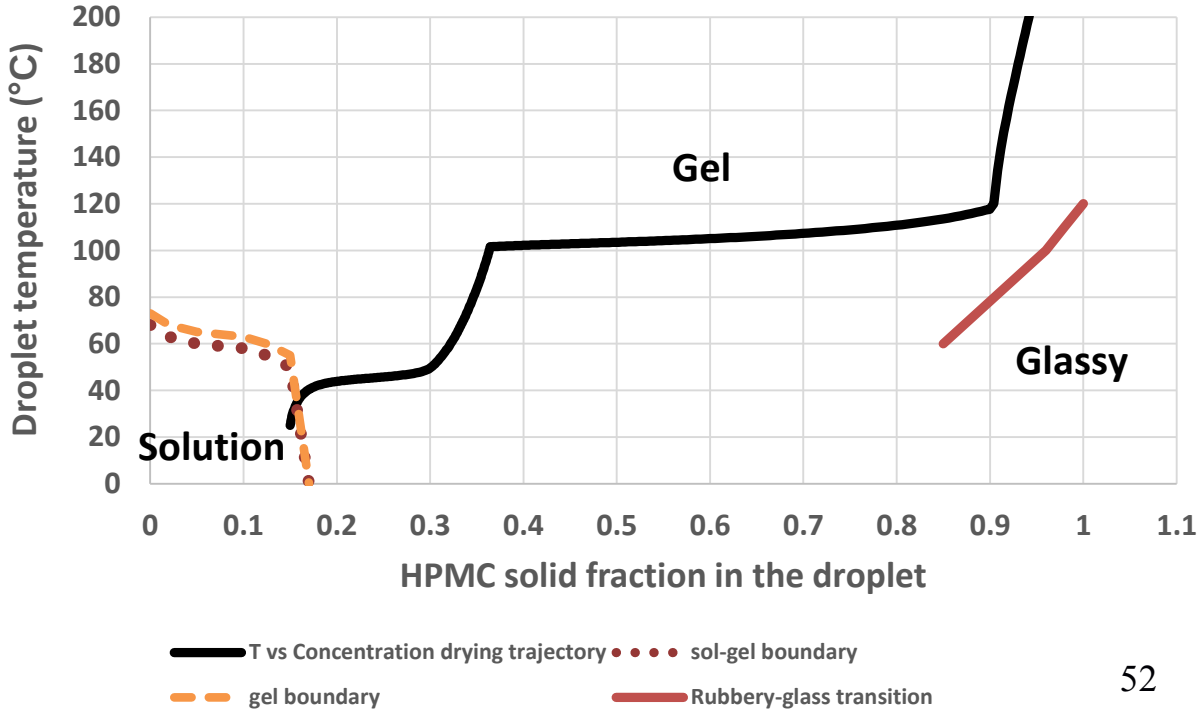

HPMC morphology

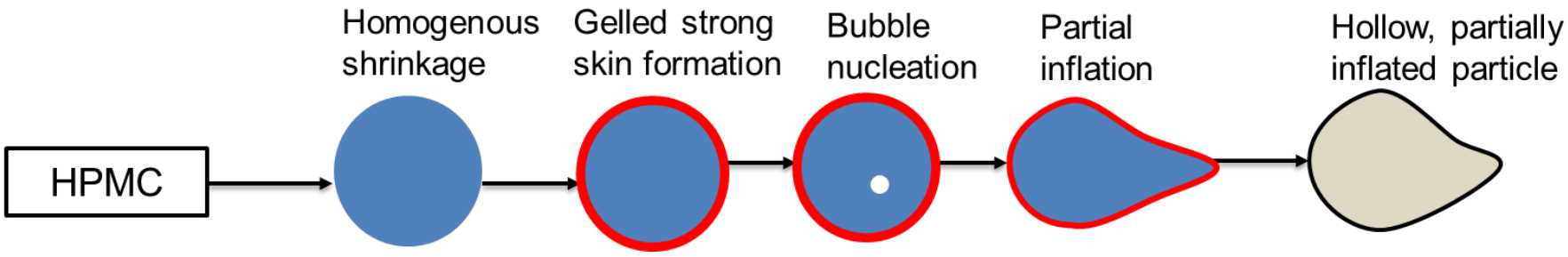

- Surface rapidly goes through gel boundary forms elastic solid
- Boiling occurs inside gel shell, stretches a little and occasionally ruptures
- Strong enough to resist buckling

  - does pressure helps resist bucking?

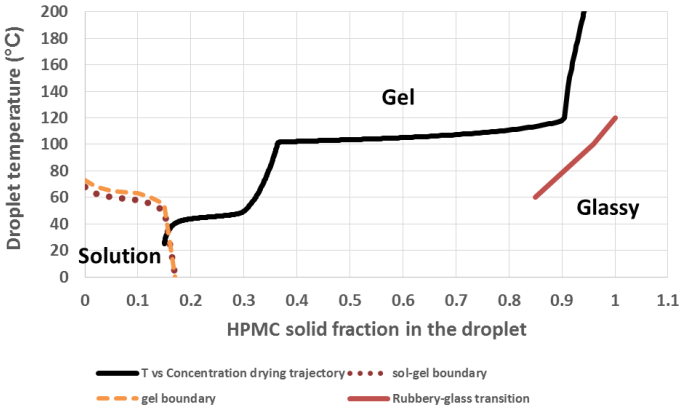

Sodium Silicate

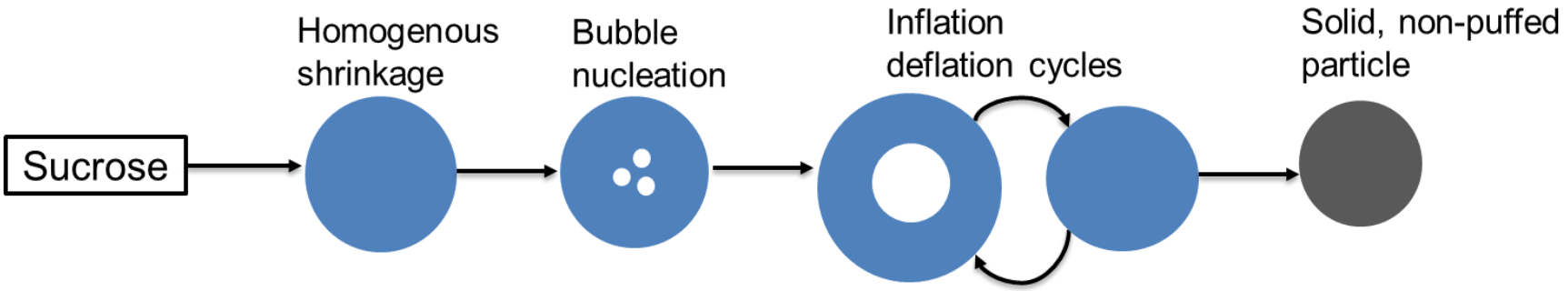

- Higher viscosity than sucrose, more stable bubbles
- Transition to elastic solid whilst inflated
- Shell strong enough to maintain shape and not buckle
- Pressure helps resist buckling

Rheology/ mechanical properties evolution during drying

- HPMC - phase change -> surface gels -> elastic solid occasionally ruptures, strong enough to resist buckling pressure helps resist bucking.

- Sucrose – lower viscosity, still low enough to shrink when low water content reduced and vapour pressure reduced

- Silicate – higher viscosity, balance between pressure becomes elastic solid strong enough to resist buckling

Questions: balance between pressure, role of porosity in these systems

Rig development – droplet mass loss

- 6 decimal place balance evaluated and order placed

Comparison of mass loss balance vs image analysis

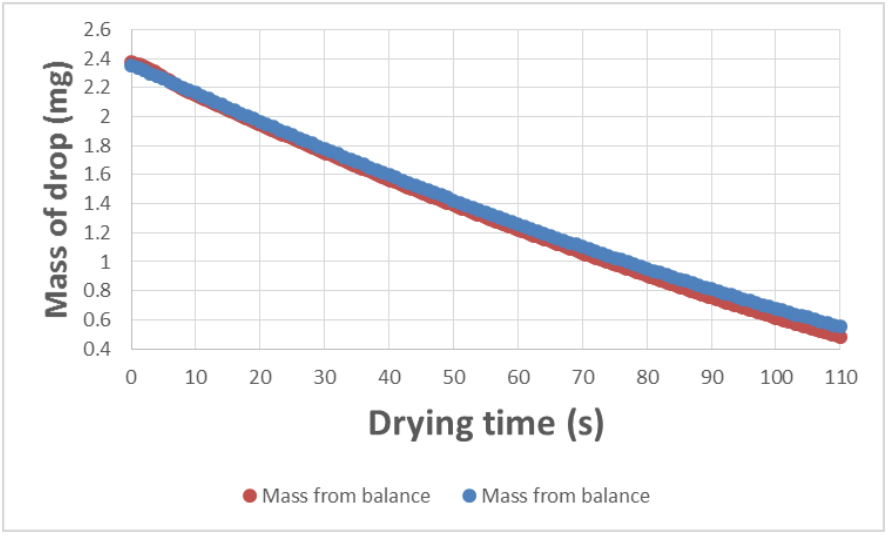

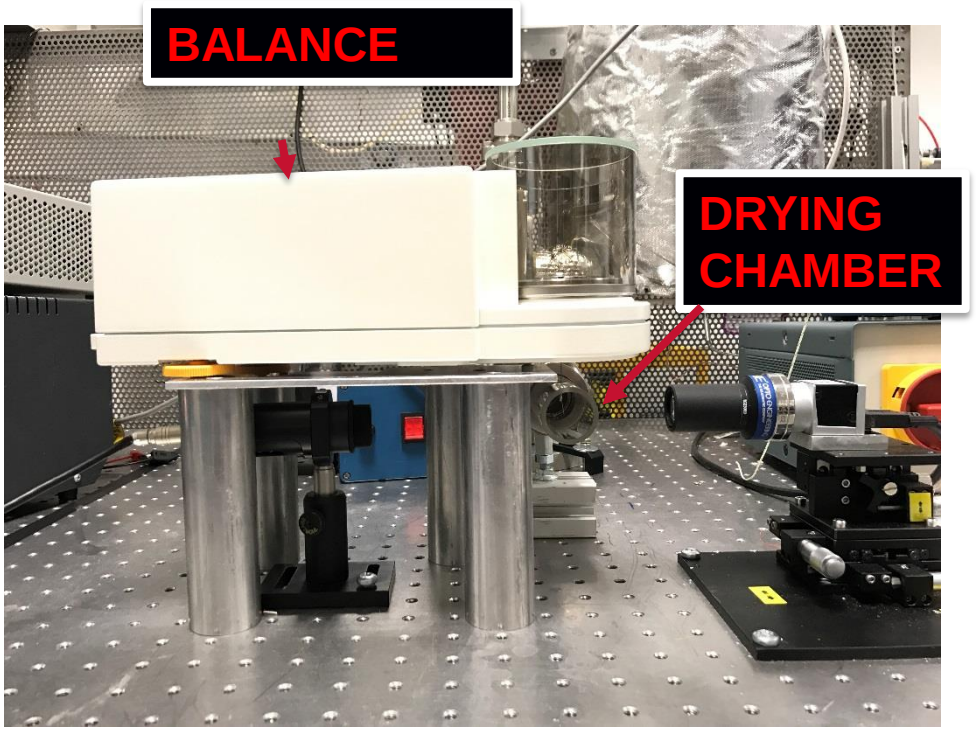

Drop Tube

Droplet generator rig schematic

UNIVERSITY OF LEEDS

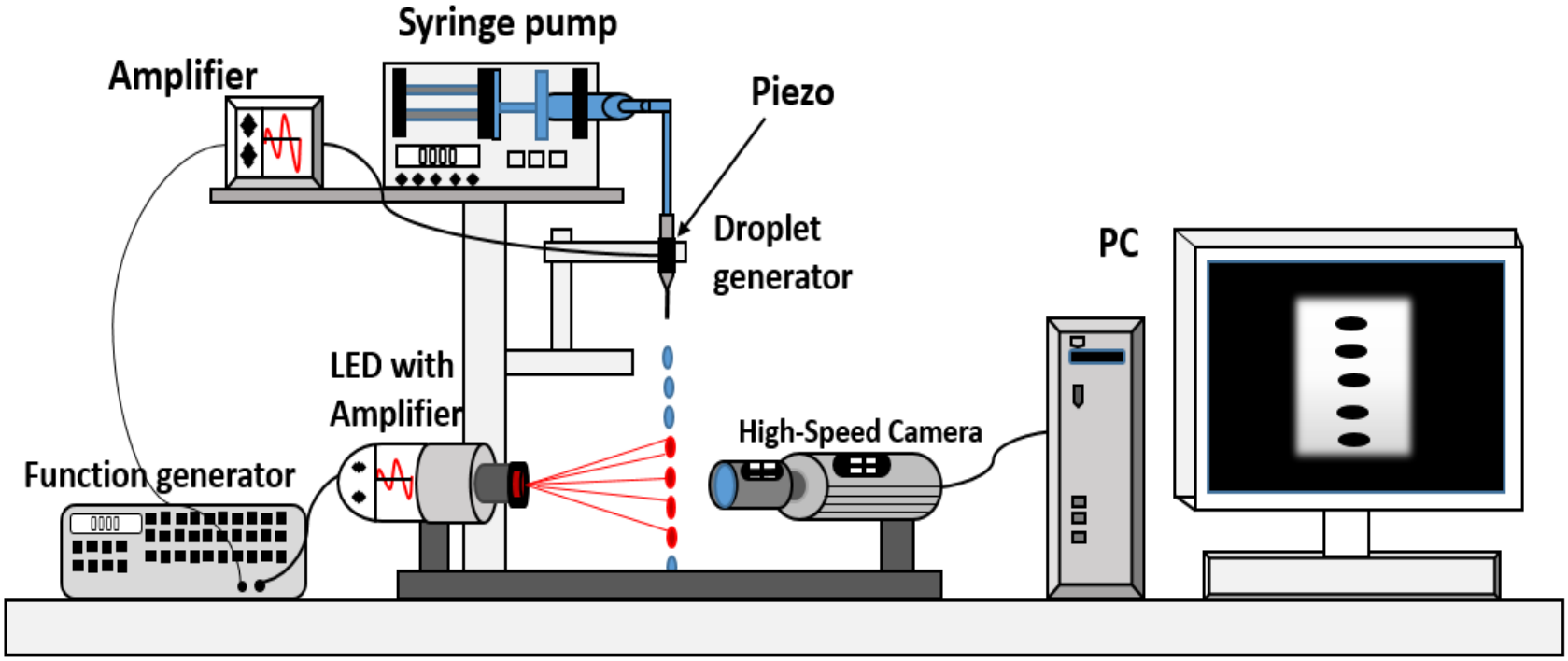

Drop Tube – mondispersed atomiser

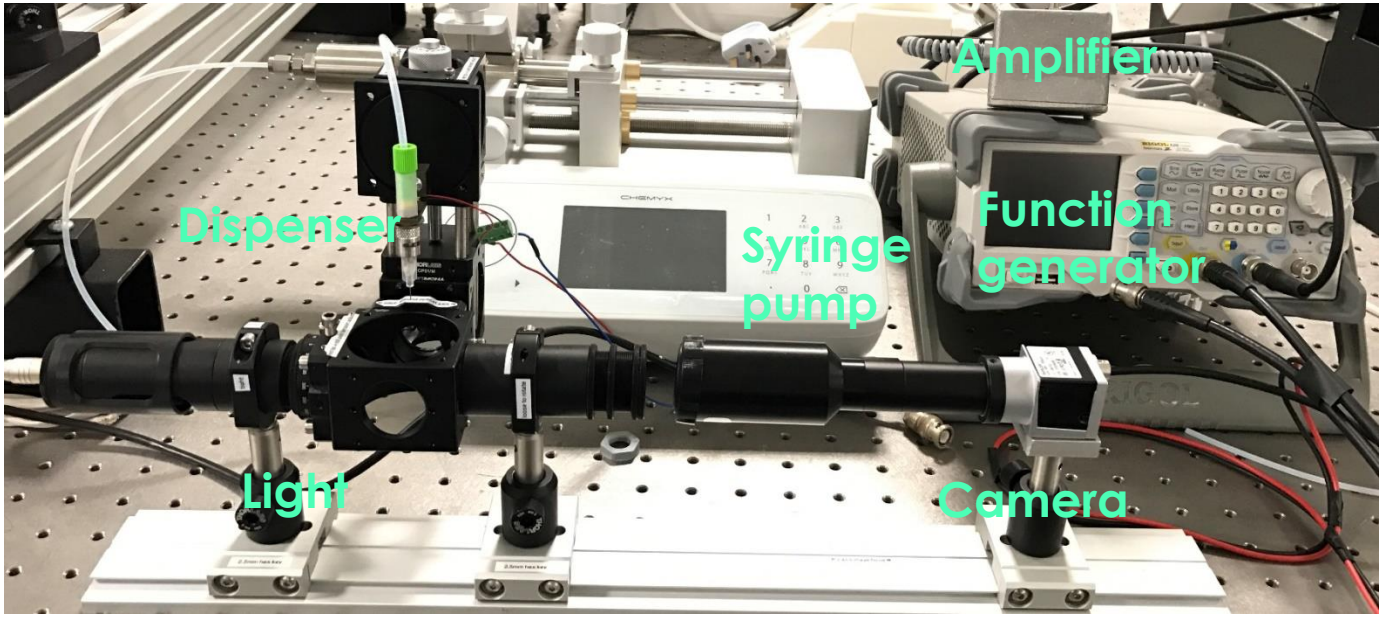

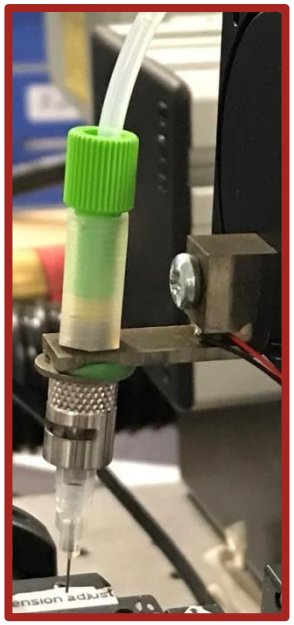

Experimental Summary

Experimental development for regime mapping: Single droplet filament rig developed, upgrades to imaging, geometry, control, droplet handling and analysis. Drop tube now in place. Mass measurement technique successfully evaluated.

Mapping: Detailed investigation of sucrose, HPMC, sodium silicate. HPMCs with different viscosity and different solvent investigated. Behaviours linked to phase change and material properties

Material properties: Evaluation of rheologies, diffusivities. Atomic Force Microscope investigated for solid material measurement.

Modelling Approach

UNIVERSITY OF LEEDS

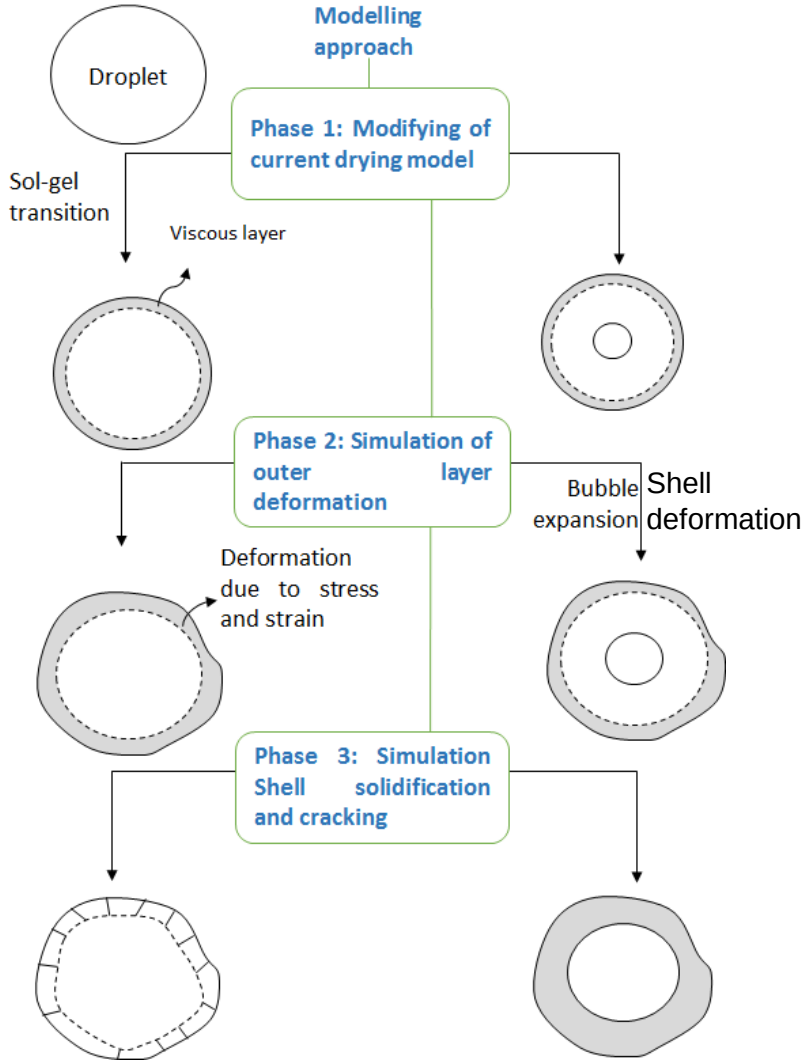

Predict droplet morphology development – couple mass transfer, fluid and mechanical models

Challenges:

- Material property definition
- Numerical methods

Bubble expansion (no drying)

UNIVERSITY OF LEEDS

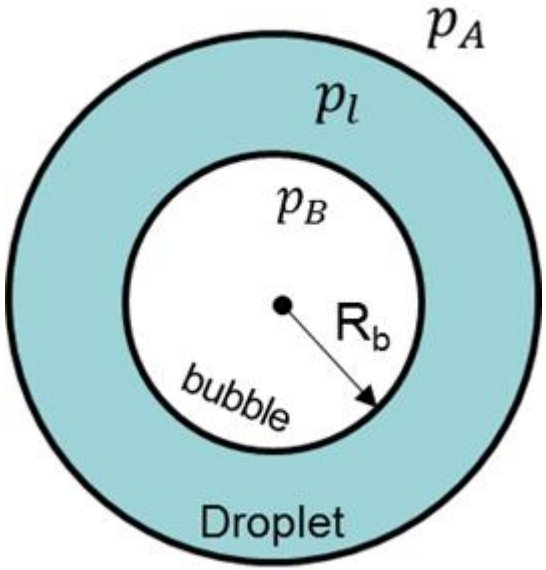

- Matlab
  - 1-D spherically symmetric
  - Modified Rayleigh-Plesset eqn
- Finite Volume (Fluent)
  - 2/3D with VOF
- Finite Element (Comsol)
  - 2/3D

Model system

UNIVERSITY OF LEEDS

- Apply Rayleigh-Plesset approach to bubble in drop

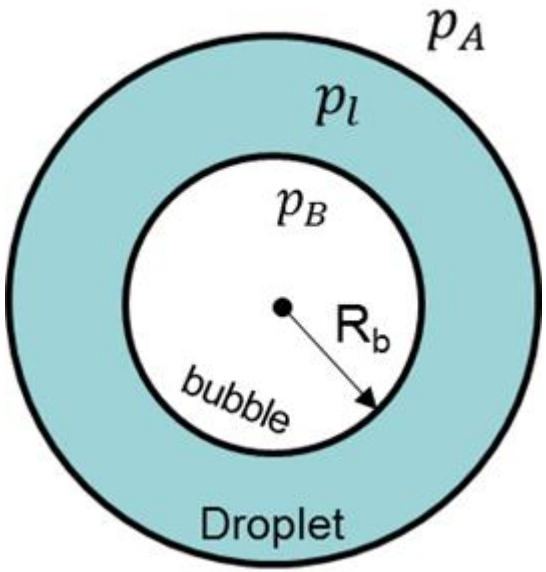

$$p_B - p_A = \left[R_D\rho_A + \rho_L\left(1 - \frac{R_D}{R_B}\right)\right]\frac{d^2R}{dt^2} + \left[\frac{3}{2}(\rho_A + \rho_L) \pm 2\rho_L\frac{R_B}{R_D} + \frac{\rho_L}{2}\left(\frac{R_B}{R_D}\right)^4\right]\left(\frac{dR}{dt}\right)^2 + 2S\left(\frac{1}{R_B} + \frac{1}{R_D}\right) + 4\left(\frac{\mu_A}{R_D} + \frac{\mu_L}{R_B}\right)\frac{dR}{dt}$$

Assumption:

- Perfectly spherical bubble and droplet
- Isothermal
- Incompressible liquid droplet
- Ideal gas behaviour in the bubble and air domain.

Initial Conditions

UNIVERSITY OF LEEDS

- A system of a 200 microns bubble in 1mm liquid water droplet in an air domain
- Boundaries condition: outlet boundaries at atmospheric pressure.
- Initial bubble relative pressure: 5k Pa
- Initial water relative pressure: 0 Pa
- Simulation method: Two-phase laminar flow with moving mesh.
- Solver: Backward differentiation formula (BDF).

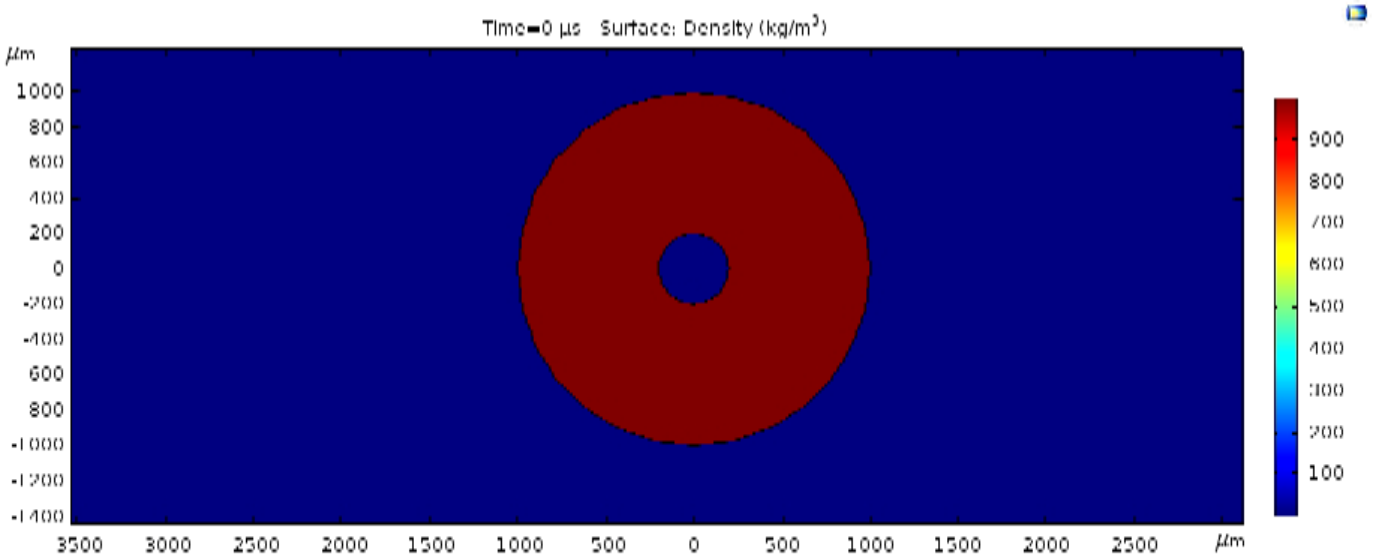

Pressure/Size Oscillations

UNIVERSITY OF LEEDS

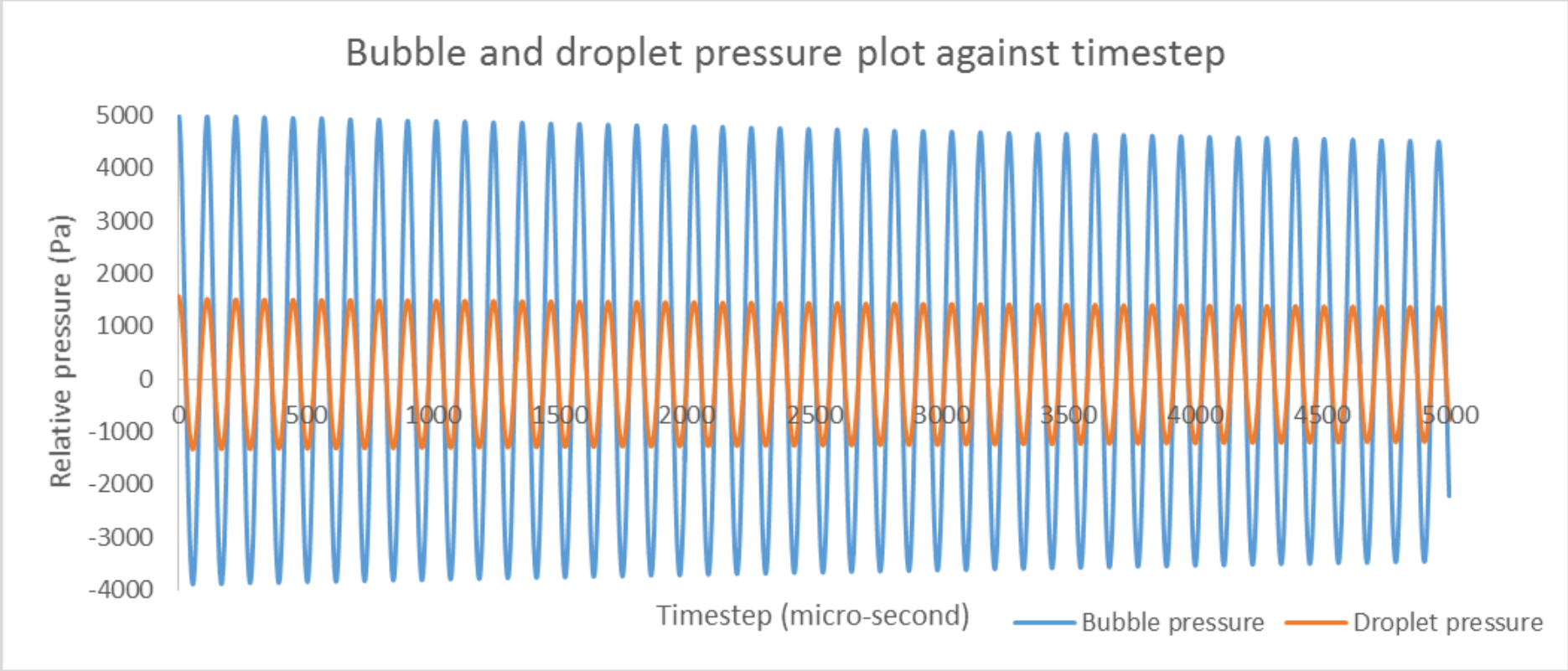

Effect of liquid viscosity on the bubble oscillation

UNIVERSITY OF LEEDS

- Liquid viscosity : 0.001009 , 0.01009 and 0.1009 Pa.s

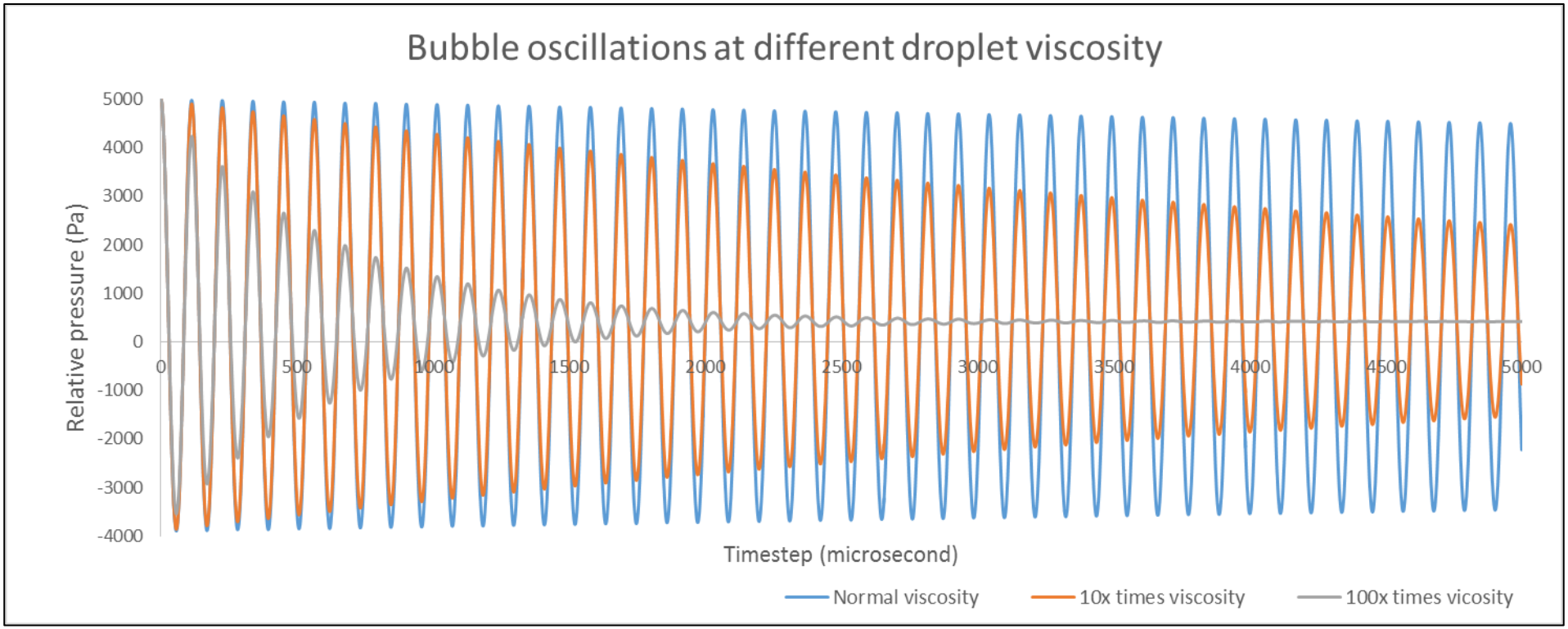

Effect of initial bubble and droplet size on the bubble oscillation

UNIVERSITY OF LEEDS

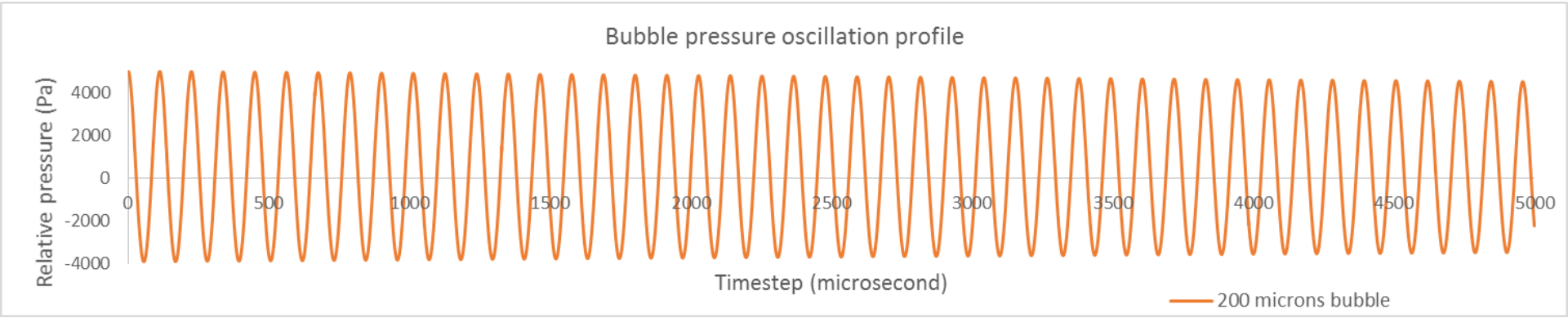

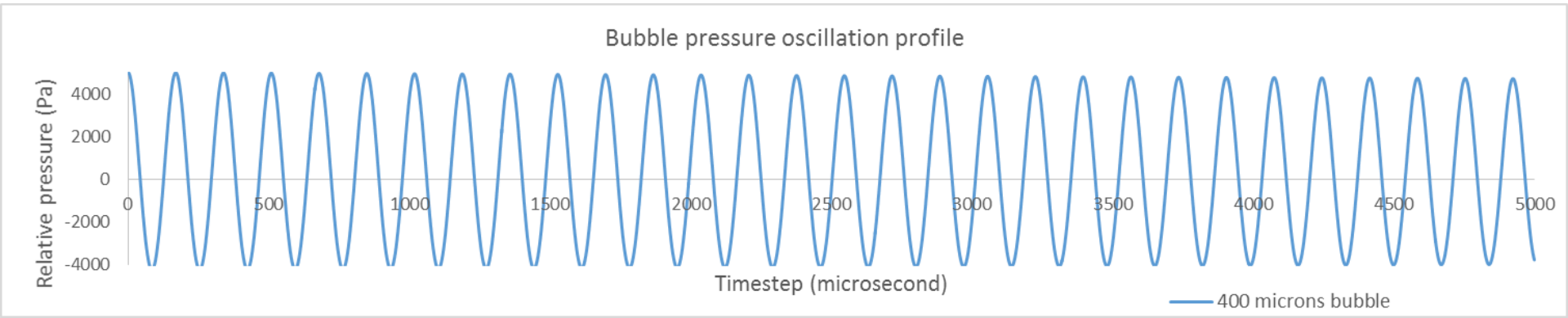

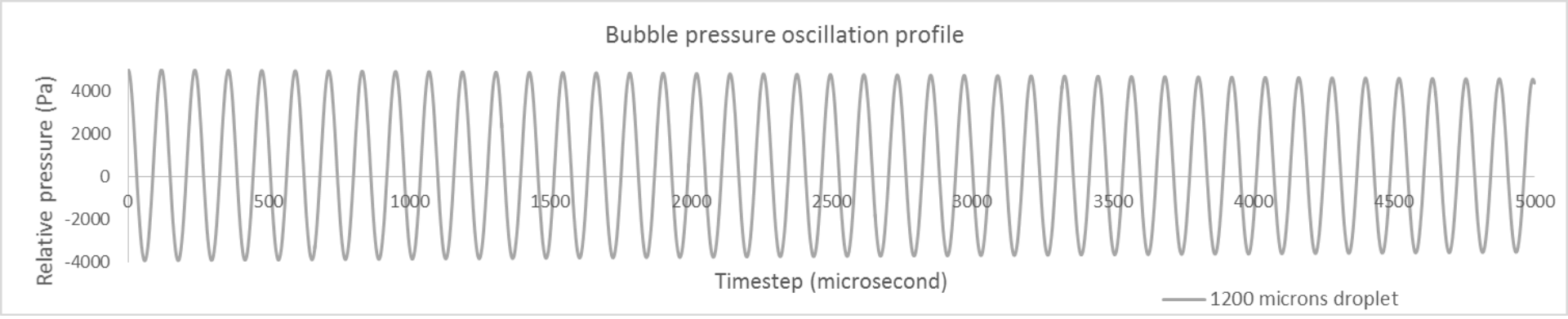

Offset Bubble

UNIVERSITY OF LEEDS

Velocity field

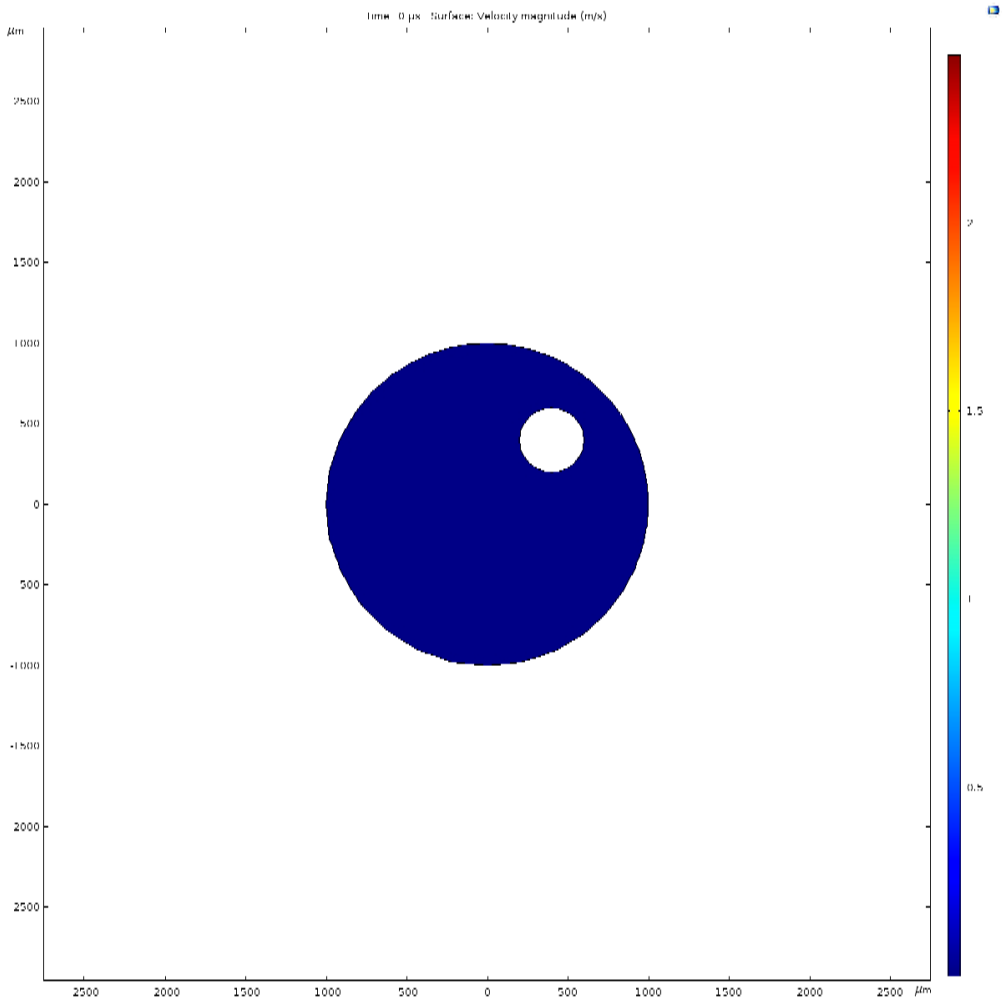

External pressure lowered

UNIVERSITY OF LEEDS

- A system of a 200 microns bubble in 1mm liquid water droplet in an air domain.
- Boundaries condition: boundary pressure lowered.
- Initial bubble relative pressure: 0 Pa
- Initial water relative pressure: 0 Pa
- Simulation method: Two-phase laminar flow with moving mesh.
- Solver: Backward differentiation formula (BDF).

Bubble Velocity Field

UNIVERSITY OF LEEDS

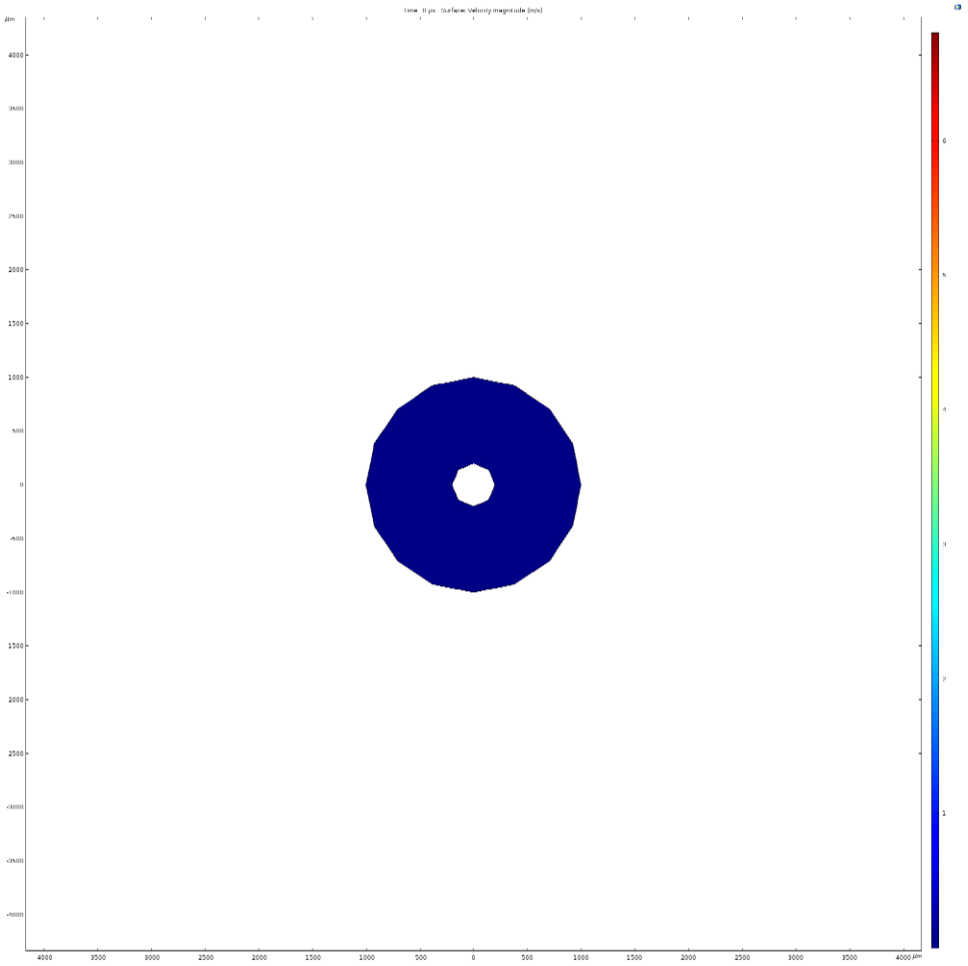

Off-set bubble – velocity field

UNIVERSITY OF LEEDS

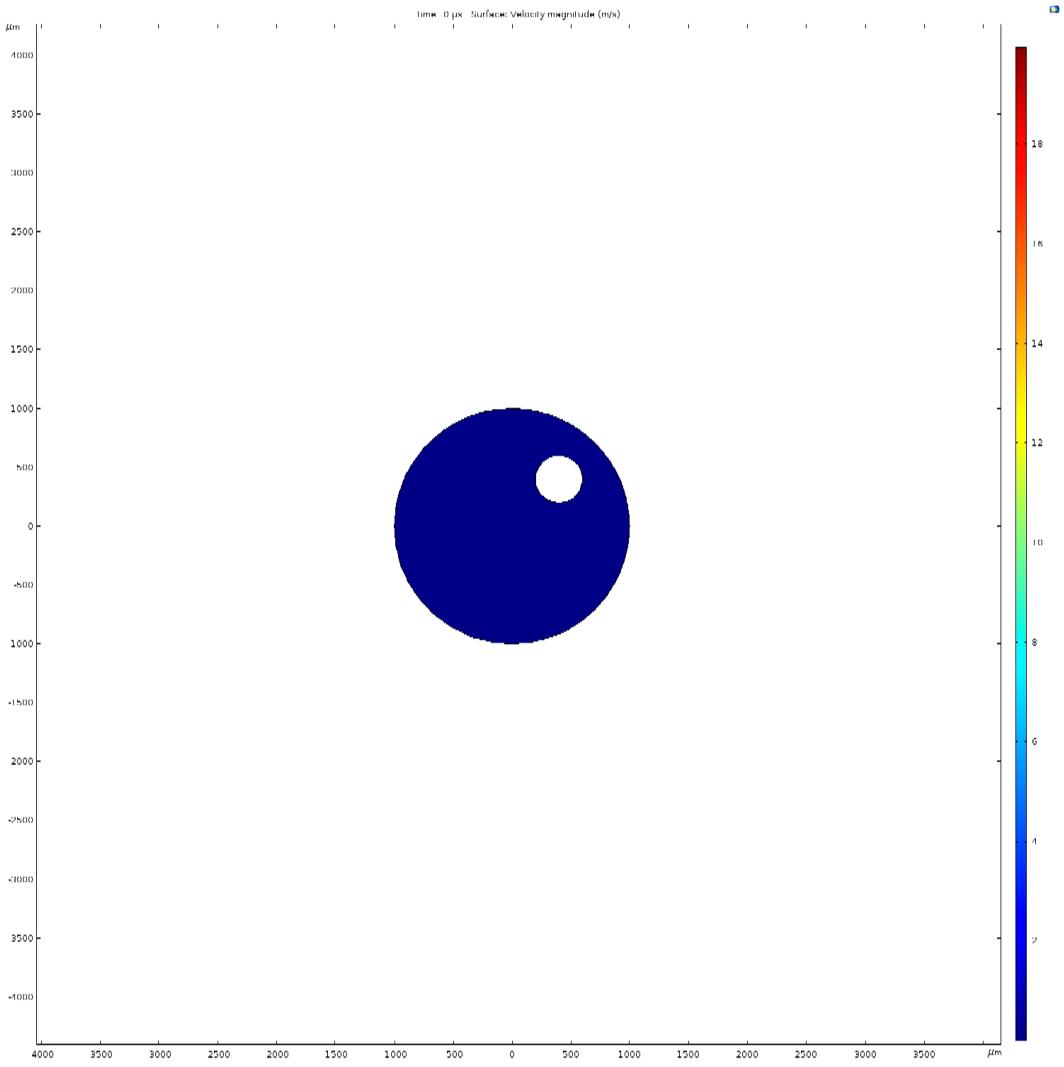

Summary

UNIVERSITY OF LEEDS

- Robust method for quantitatively assessing drying kinetics and morphology development
- Morphology driven by material property differences at low % H20 and high T and phase change
- Modelling – bubble expansion models allows exploration of system variables

Future Focus

UNIVERSITY OF LEEDS

Goal: regime map based on material properties

- Filament rig – weight with time
- Drop tube – size and comparison
- Regime Map – combine kinetics and diffusivity models
- Modelling – coupling a drying model with bubble growth model
- Material properties – from filament rig? Collaboration.

Acknowledgements

Group:
Dr. Muzammil Ali – CFD modelling supervision
Karrar Al-Dirawi – atomization rig development

Leeds technicians – rig builds

Leeds academics:
Prof. Phil Threfall Holmes – atomiser, drying rig expertise
Prof. Nik Kapur – atomiser expertise

Funding: IFPRI, EPSRC, University of Leeds,

See you at the poster

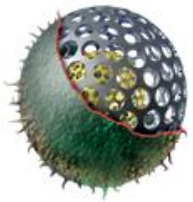

INSTITUTE OF
PARTICLE SCIENCE
& ENGINEERING

UNIVERSITY OF LEEDS

Material properties

- Rheology and solute diffusivity as function of moisture content and temperature

$$D = \frac{kT}{6\pi\eta R_h}$$

K is the Boltzmann's constant
T is the absolute temperature
η is the dynamic viscosity at the absolute temperature
r is the hydrodynamic radius
$[\![\eta]\!]$is the intrinsic viscosity
M is the molecular weight
N is Avogadro number

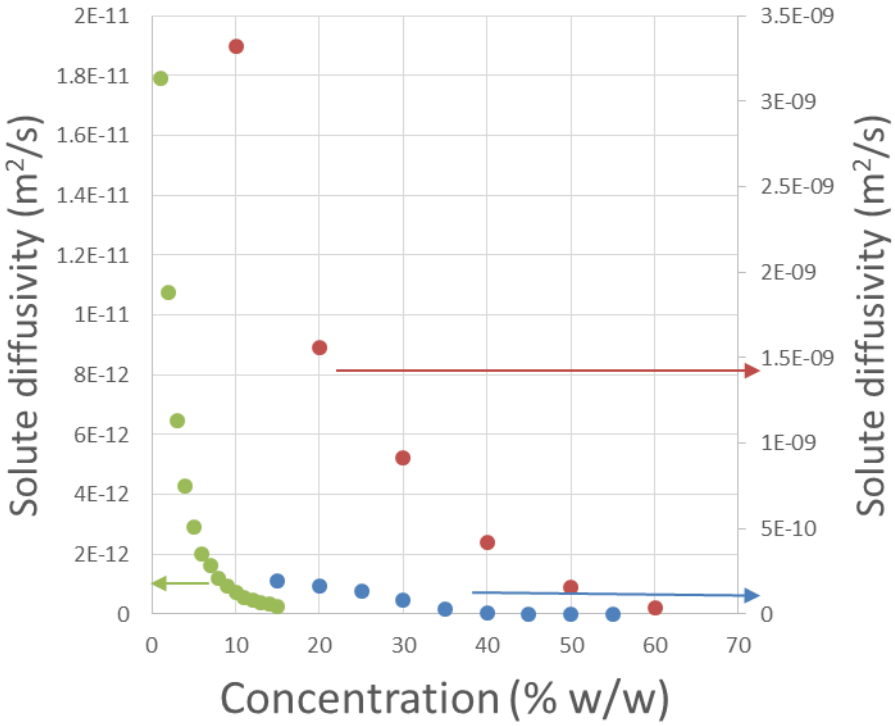

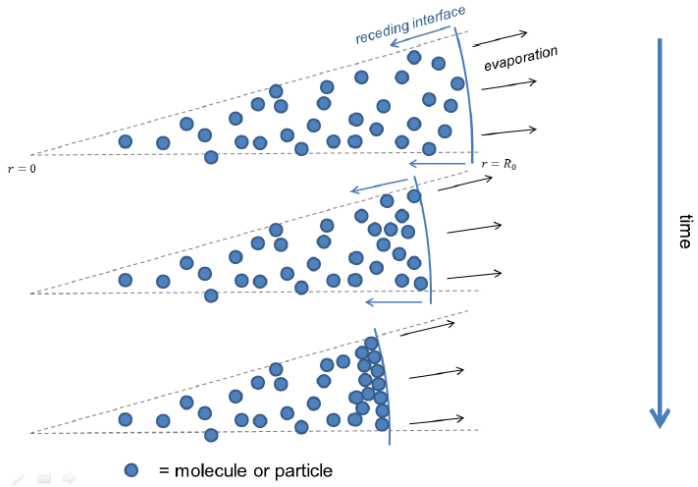

Figure 10 Schematic demonstrating shell formation at the surface of a drying droplet

Bayly, 2015. Structure development during drying- a review of the state of the art

NC STATE UNIVERSITY
http://danielslab.physics.ncsu.edu

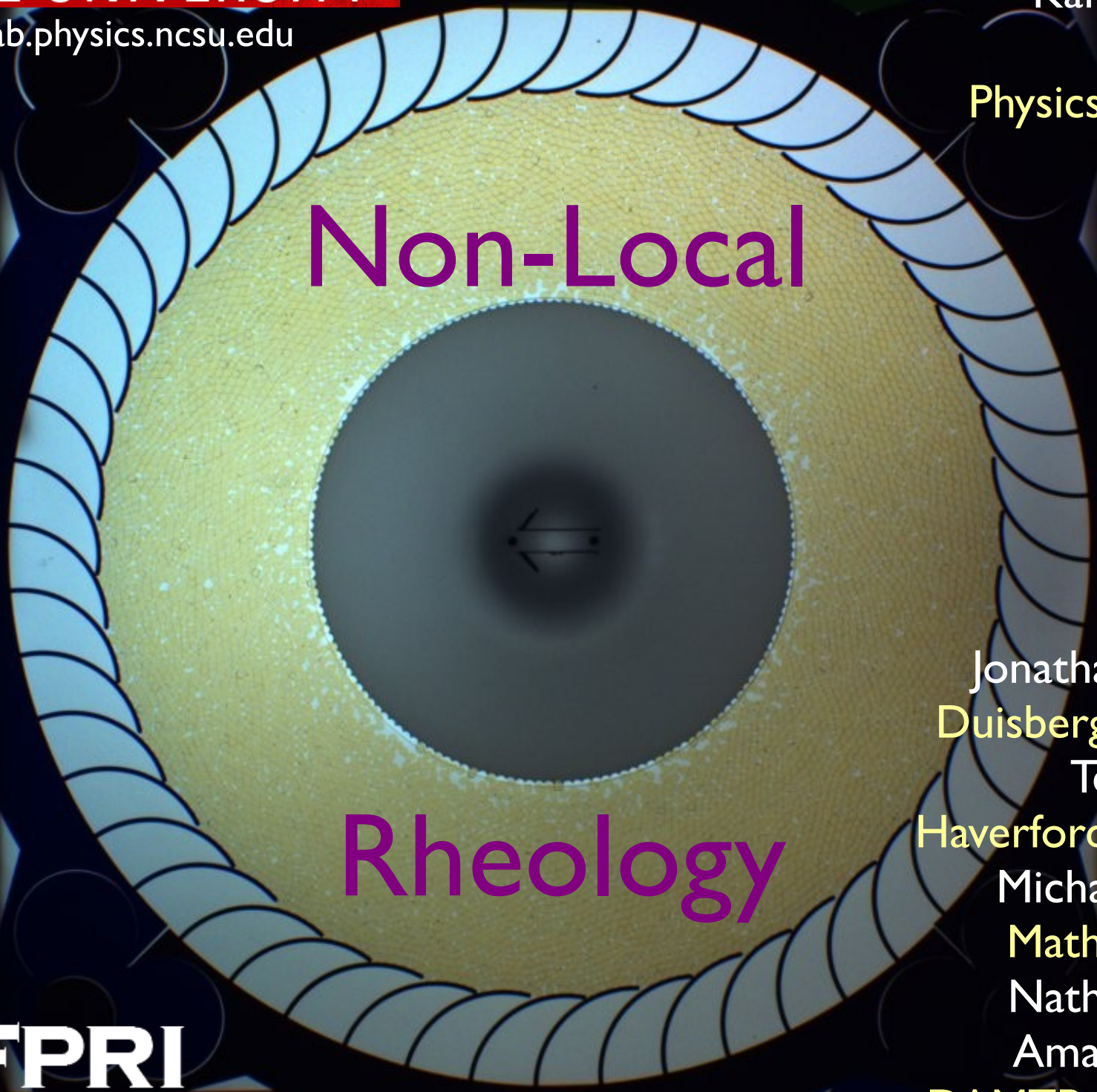

Non-Local Rheology

Karen Daniels
Zhu Tang
Physics, NC State

Jonathan Kollmer
Duisberg/NC State
Ted Brzinski
Haverford/NC State
Michael Shearer
Math, NC State
Nathalie Vriend
Amalia Thomas
DAMTP, Cambridge

NSF
IFPRI
International Fine Particle Research Institute

Problem Statement

- There is no first-principles, general theory of intermediate granular flow that predicts the rheological response as a function of particle size/shape/friction
- Currently: use empirical relations fit to bulk data for that particular flow geometry and particles
- Needed: An improved understanding of how **particle properties** control the rheology of granular materials, independent of geometry

Kamrin & Koval. PRL (2012)

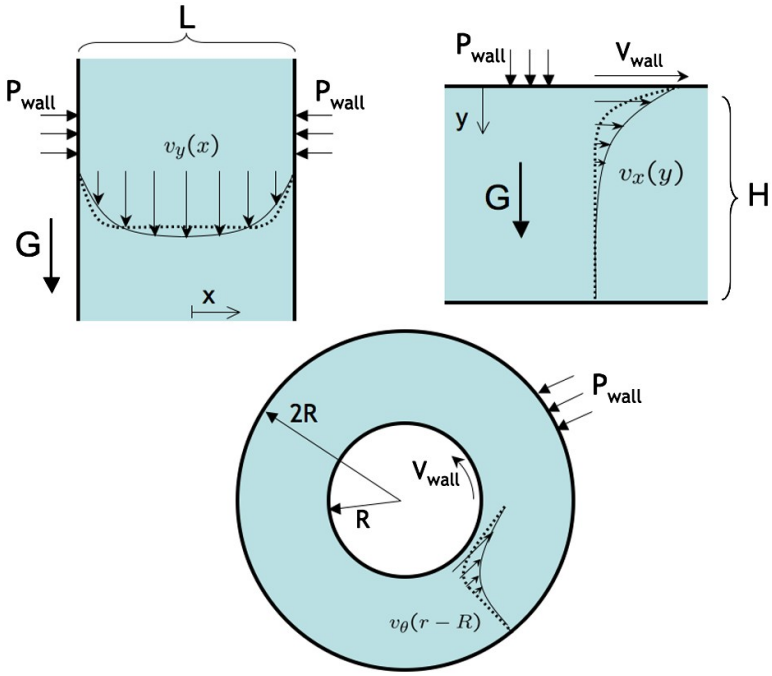

Local Granular Rheology

- inertial number: ratio $I = \frac{\dot{\gamma}\, d}{\sqrt{P/\rho}}$ between
  - micro timescale T to squeeze a particle into a hole
  - macro timescale $(1/\dot{\gamma})$ of deformation
  - large I corresponds to rapid flow

- stress ratio: ratio $\mu = \frac{\tau}{P}$ between
  - shear stress
  - normal pressure

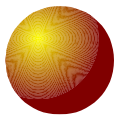

density ρ
diameter d

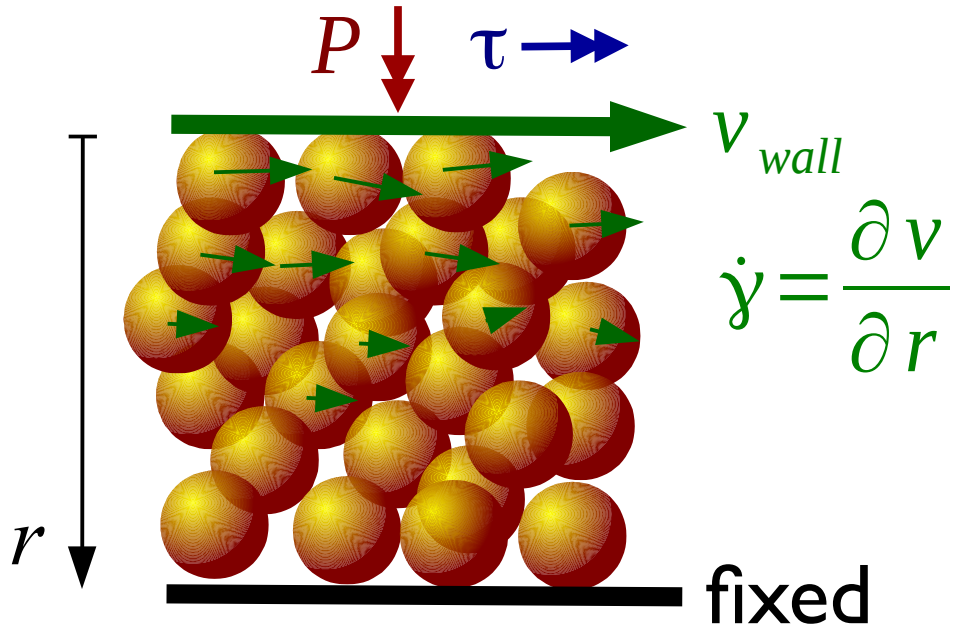

Kamrin Nonlocal Rheology I

- define granular fluidity: $g \equiv \dot{\gamma}/\mu$
  - macroscopic susceptibility of a granular region to flow
- locally, model the granular material as a Bingham fluid:

$$g_{loc} = \frac{\dot{\gamma}_{loc}}{\mu} \approx \sqrt{\frac{P}{\rho d^2}} \frac{\mu - \mu_s}{b\,\mu} \; for \; \mu > \mu_s \qquad (0 \; for \; \mu \le \mu_s)$$

- μ_s: incipient yield stress ratio (Coulomb failure)
- b: sets magnitude of local fluidity

[measured values]

[model parameters]

Kamrin & Koval. PRL (2012); Henann & Kamrin. PNAS (2013), PRL (2014), Soft Matter (2014); Zhang & Kamrin (2017)

Kamrin Nonlocal Rheology II

- granular fluidity: $g \equiv \dot{\gamma}/\mu$
- fluidity is determined by both local fluidity and a non-local, cooperative effect (beyond Bagnold scaling):

$$g = g_{loc} + \xi^2 \nabla^2 g$$

- the cooperative length scale ξ is set by

$$\frac{\xi}{d} = A\sqrt{\frac{1}{|\mu - \mu_s|}}$$

[measured values]

[model parameters]

How do μ_s, A, b depend on particle properties?

Kamrin & Koval. PRL (2012); Henann & Kamrin. PNAS (2013), PRL (2014), Soft Matter (2014); Zhang & Kamrin (2017)

$$\mu(r) = \frac{\tau(r)}{P}$$

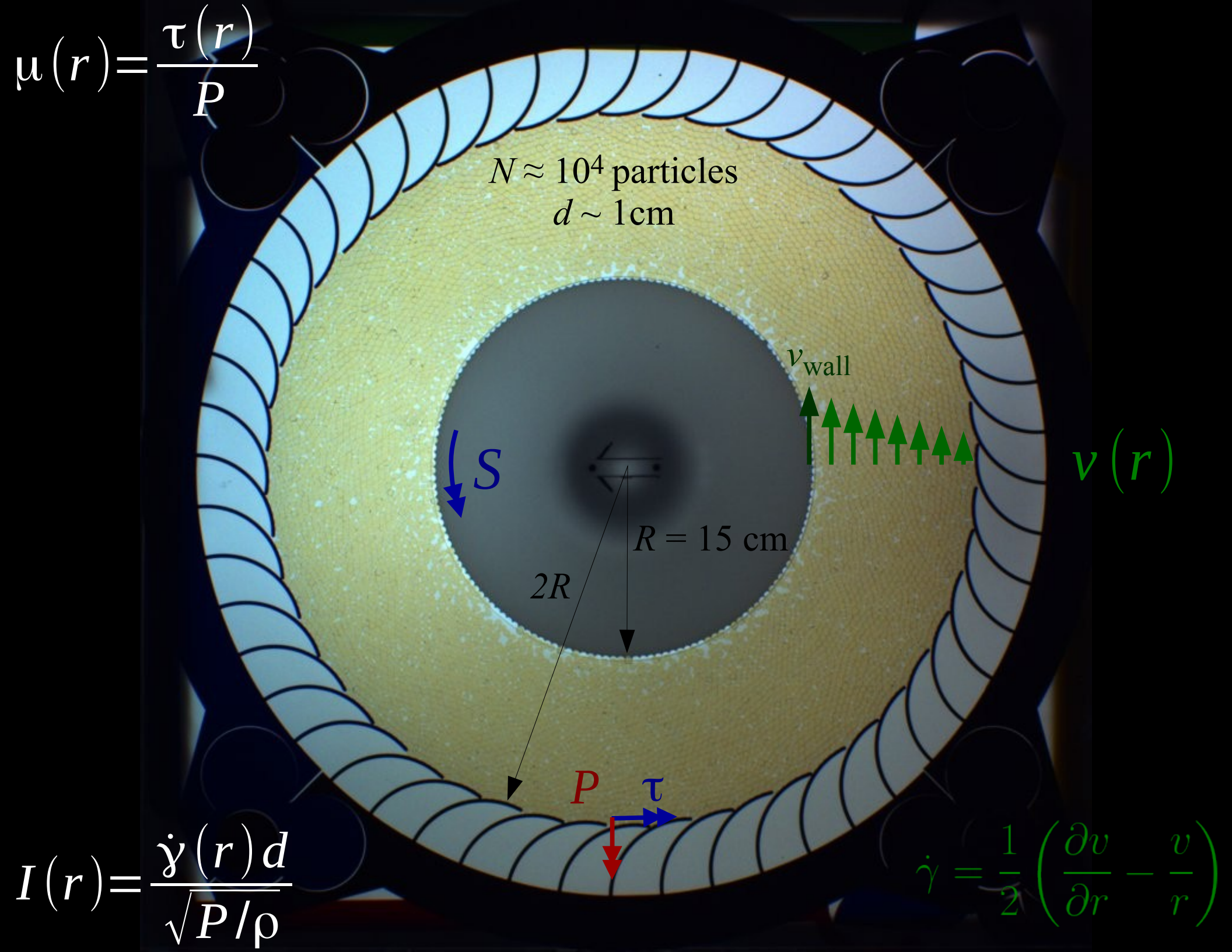

$$I(r) = \frac{\dot{\gamma}(r)\, d}{\sqrt{P/\rho}}$$

$$\dot{\gamma} = \frac{1}{2}\left(\frac{\partial v}{\partial r} - \frac{v}{r}\right)$$

Success of Nonlocal Rheology (Year 2)

- Experiments on the same particles in 6 different flows (2 packing fractions, 4 speeds)
- For two different nonlocal models (cooperative, gradient)
  - Capture the shape of $\mu(I), \nu(r)$
  - Lengthscale diverges at μ_s
  - One set of fit parameters captures all 6 datasets
- New interpretation of μ_s

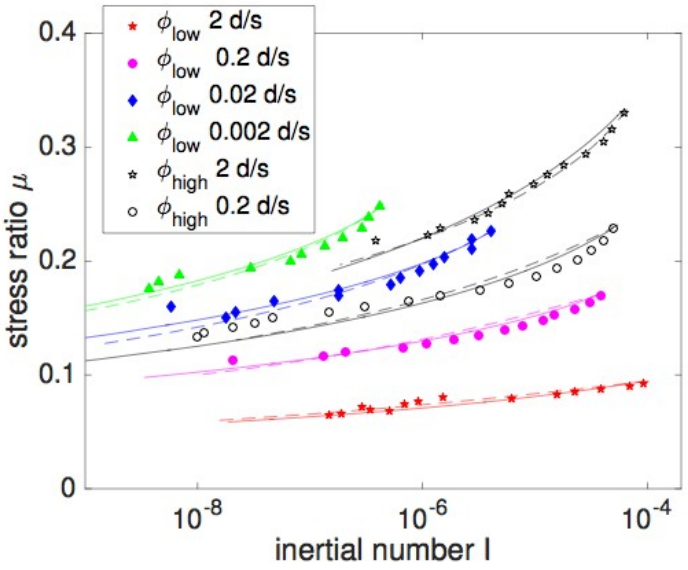

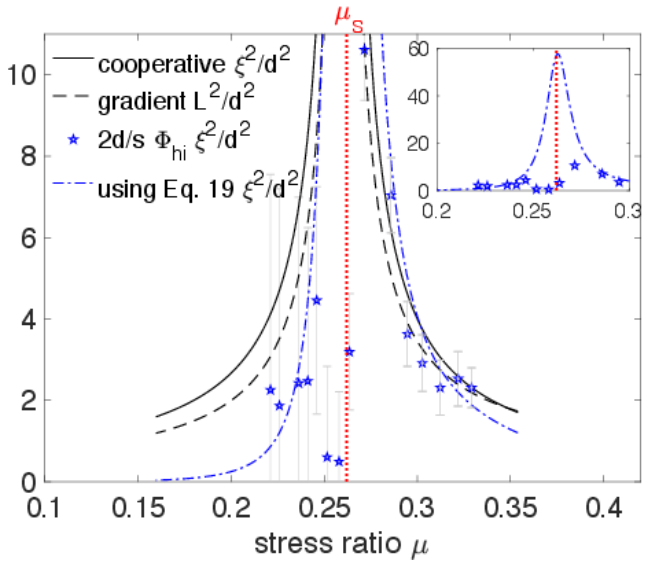

Experiments on particle shape at 2 fixed values of P

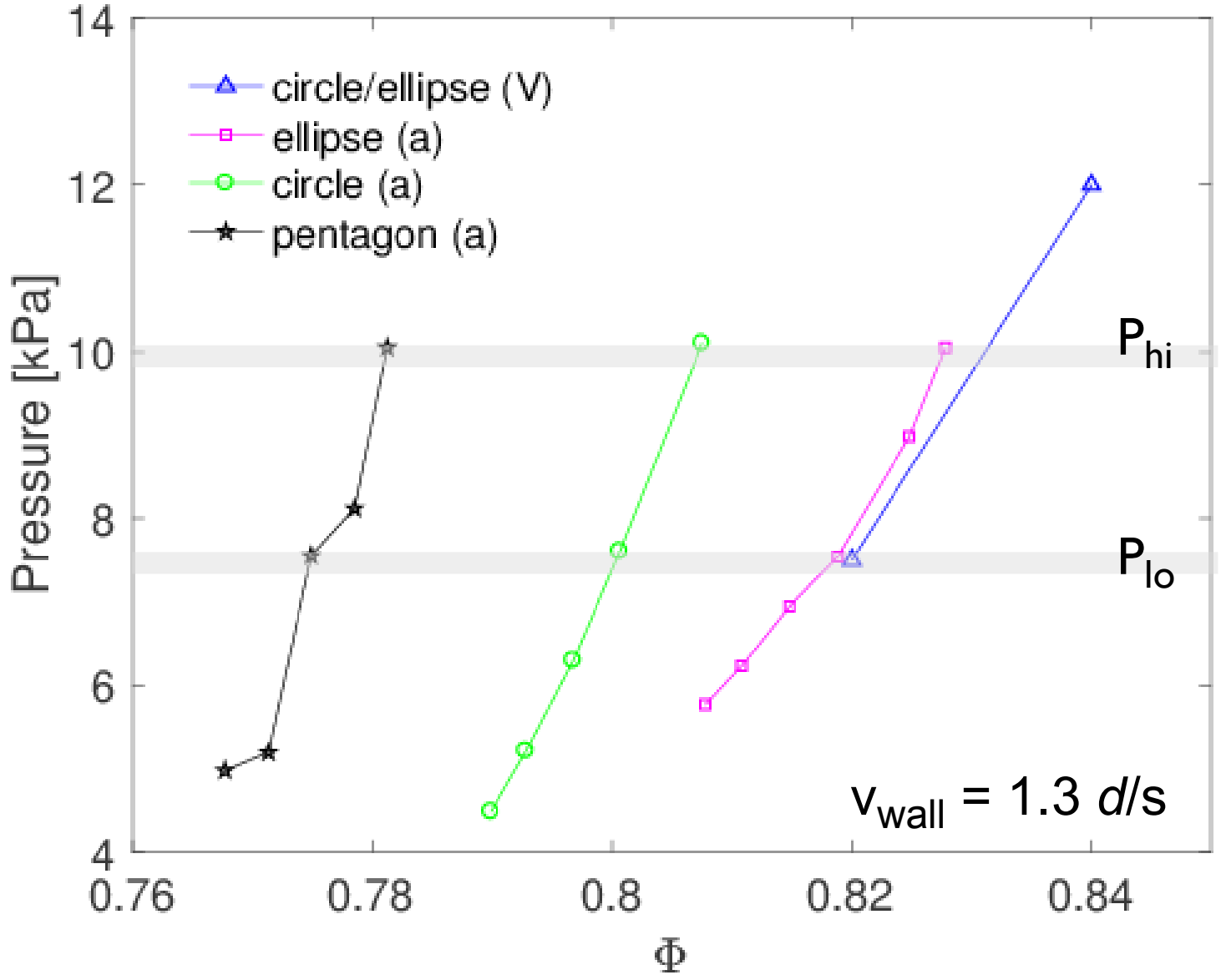

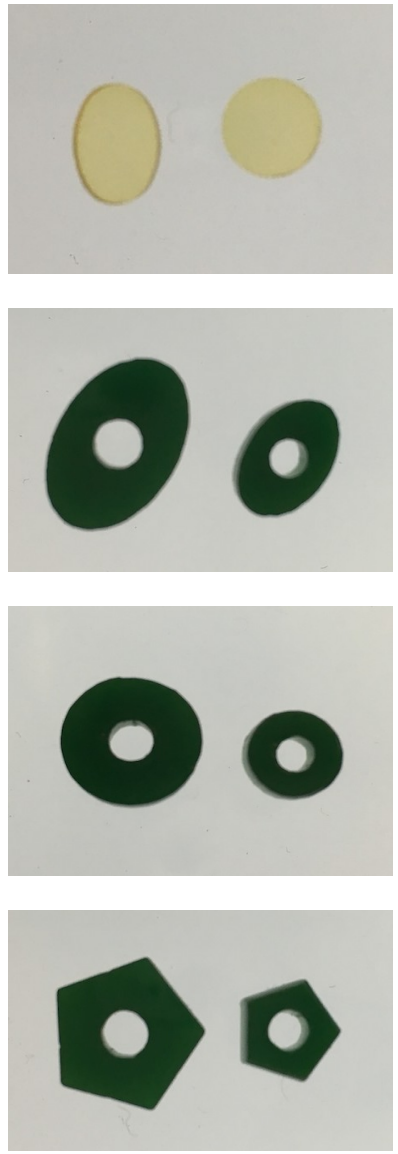

Success of Nonlocal Rheology (I)

$$\mu(r) = \frac{\tau(r)}{P}$$

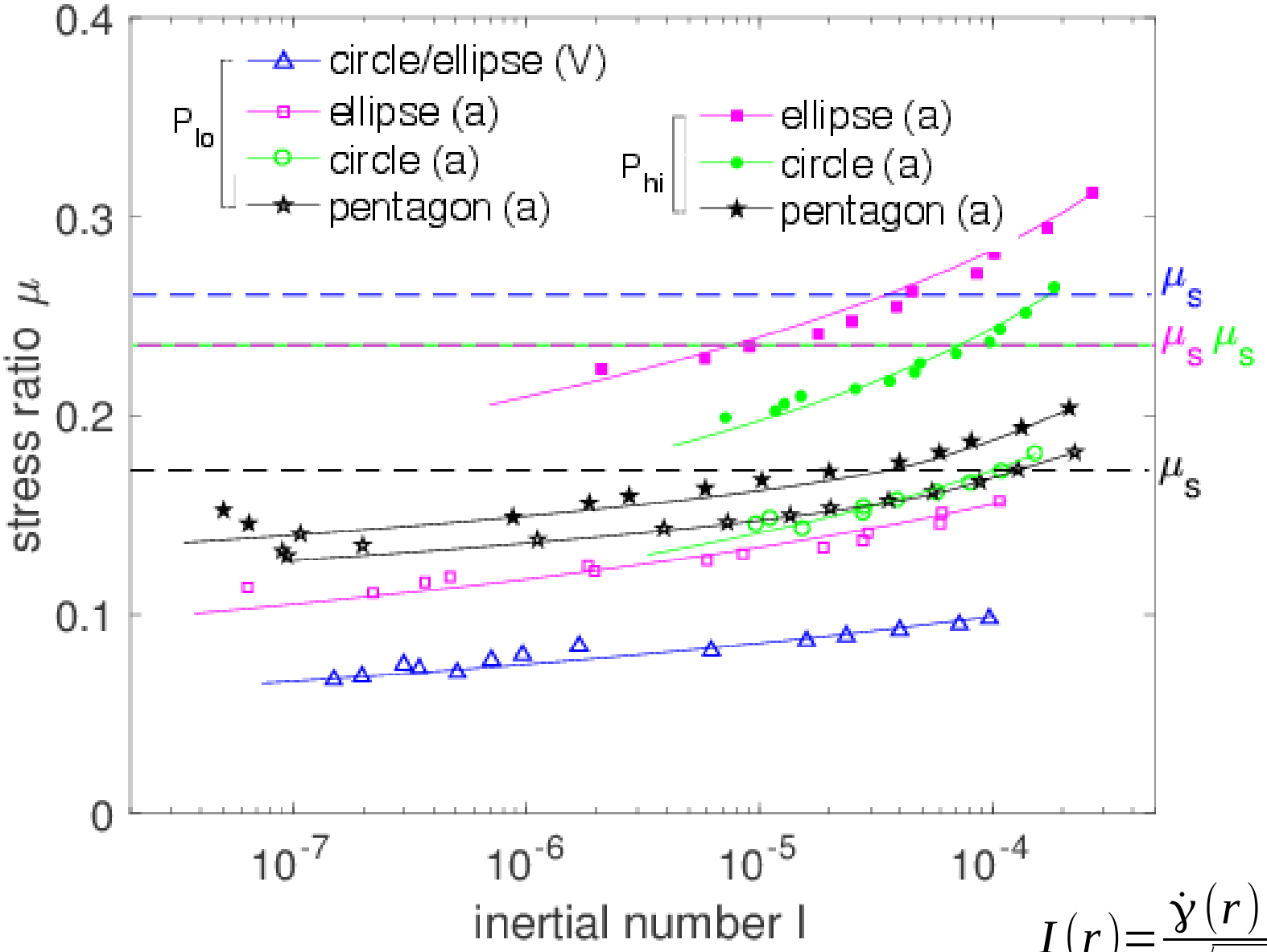

$$I(r) = \frac{\dot{\gamma}(r)\ d}{\sqrt{P/\rho}}$$

Success of Nonlocal Rheology (II)

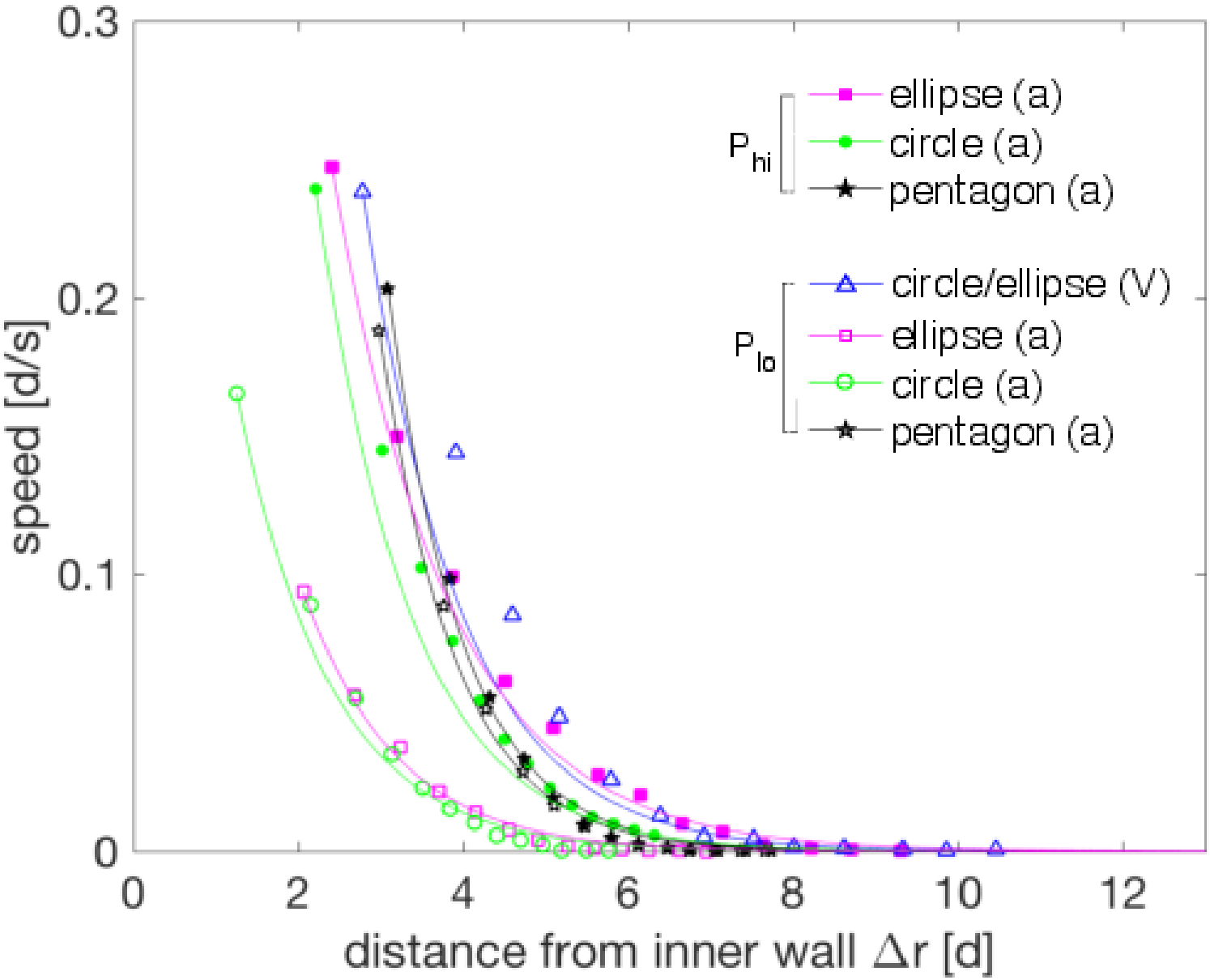

Success of Nonlocal Rheology (III)

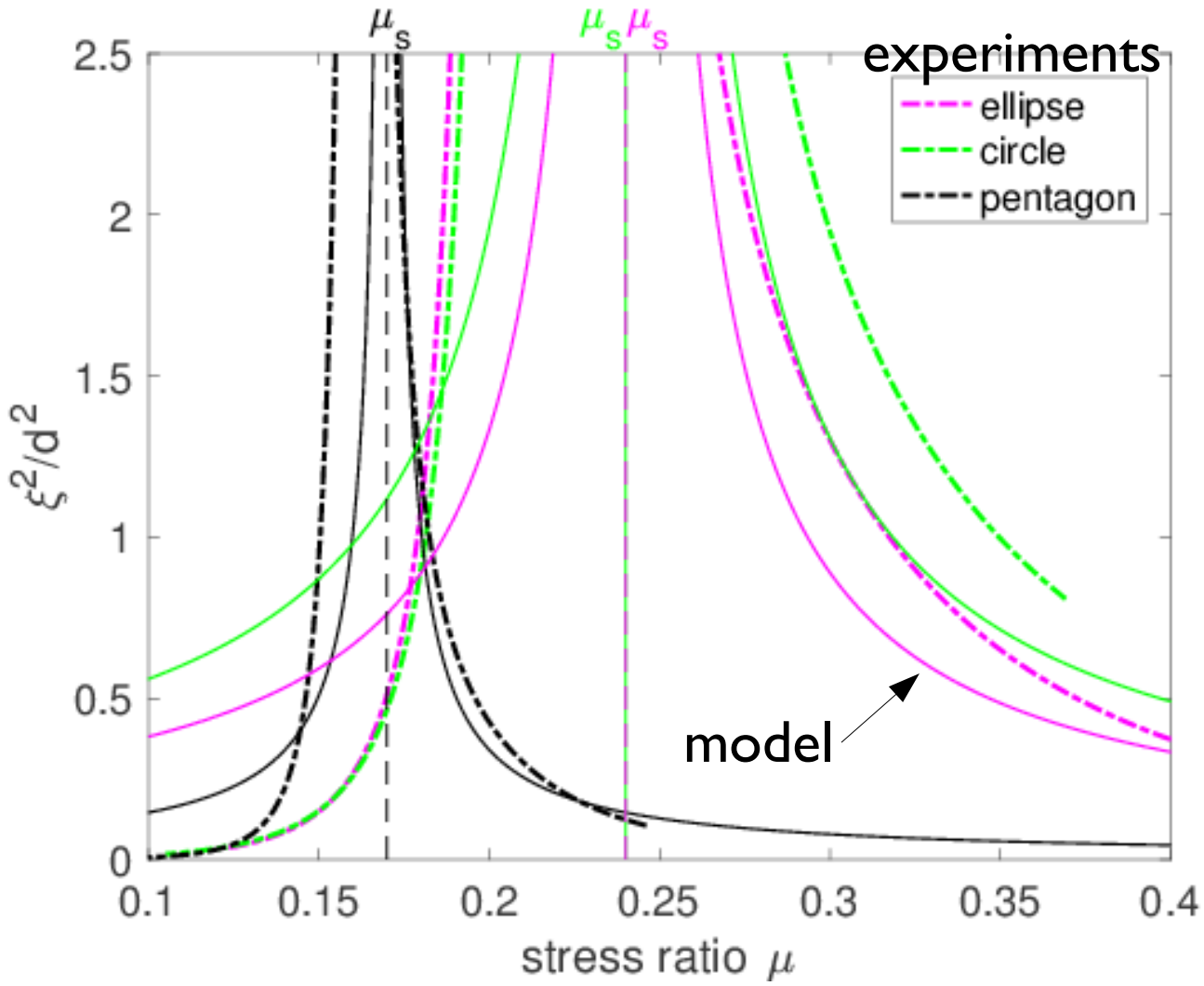

What sets the parameters?

	Vishay circles/ellipses	acrylic ellipses	acrylic circles	acrylic pentagons
μ_s	0.26 ± 0.02	0.24 ± 0.02	0.24 ± 0.02	0.17 ± 0.01
b	1.1 ± 0.3	1.1 ± 0.5	1.1 ± 0.6	1.1 ± 0.6
A	0.402 ± 0.003	0.231 ± 0.003	0.280 ± 0.003	0.101 ± 0.001

- μ_s (yield stress ratio)
  - determined by slow-shear experiments, consistent with calculated $\xi(\mu)$ curves
  - shape-dependent for same material
- b: local parameter
  - insensitive to material, shape
- A: nonlocal parameter
  - sensitive to both shape and material

Particle-scale interpretation of fluidity?

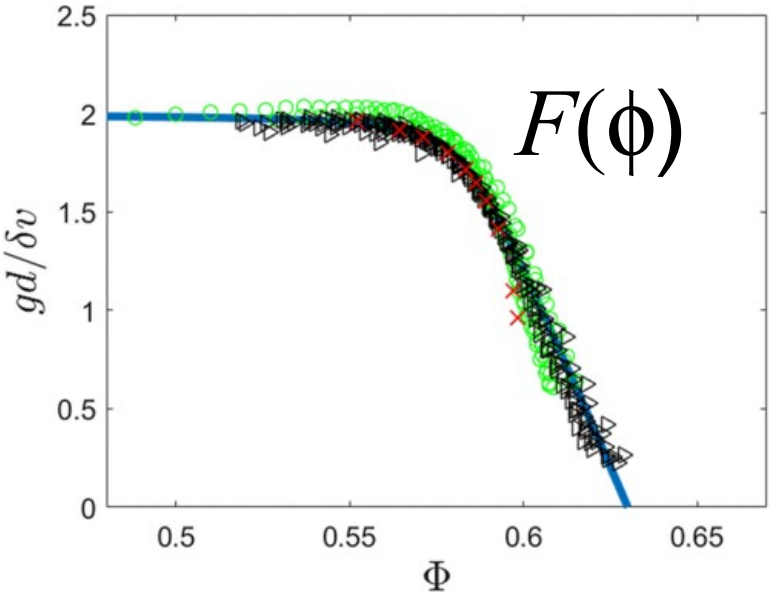

Zhang & Kamrin. *PRL* (2017)

$$g = \frac{\delta v}{d} F(\phi)$$

Prediction: g determined by universal function $F(\phi)$

Observation: $F(\phi)$ is shape-dependendent & may be affected by crystallization at higher pressures

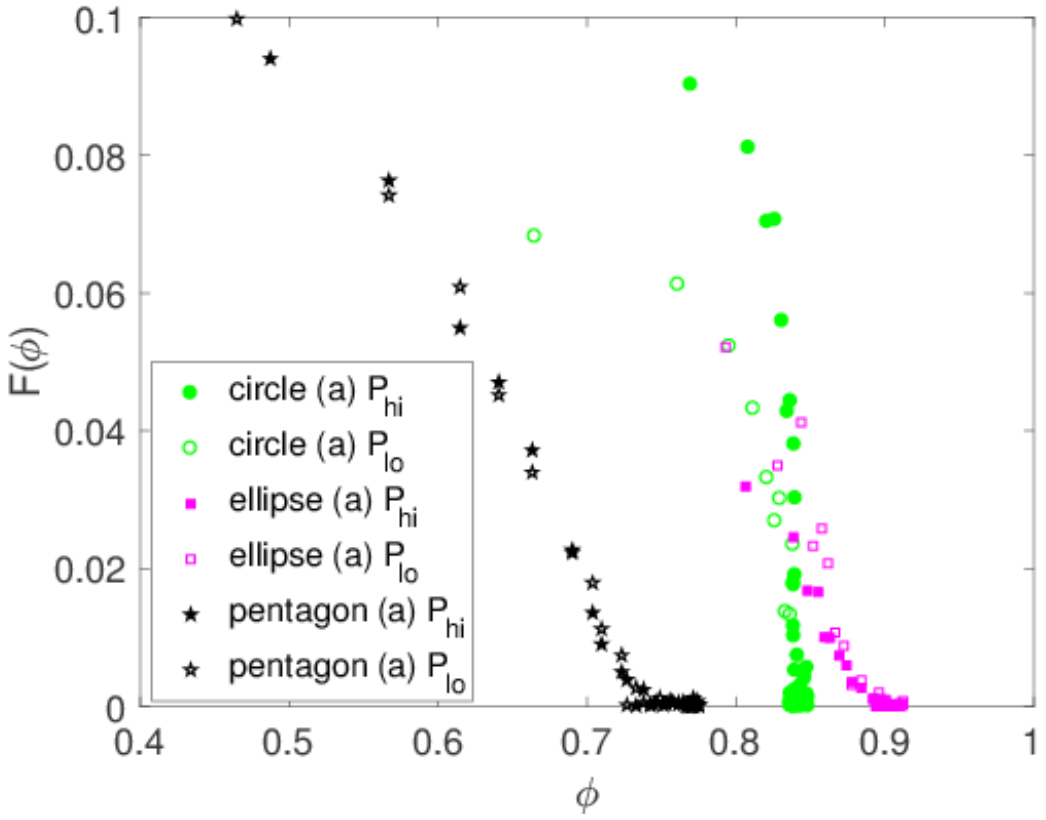

Conclusions

- can determine a set of nonlocal model parameters for each set of particles → reuse at different flow speeds, pressures
  - each set of parameters successfully fits $\mu(I)$, $v(r)$, $\xi(\mu)$
- first nonlocal rheology experiments as a function of particle properties
  - begin to identify which model parameters are associated with which particle properties
  - particle-scale fluidity is no longer a universal function

Renewal: experiments to determine generalizations for predetermining boundary conditions

Next talk: collaboration to test nonlocal rheology in intermediate chute flows

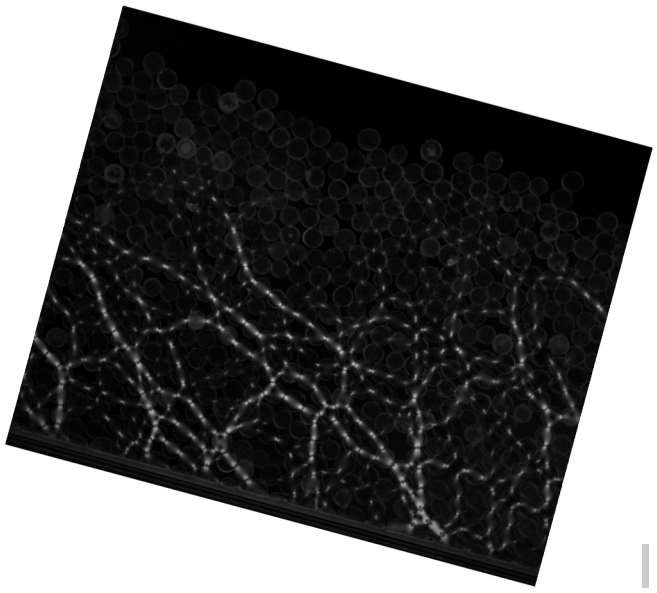

Photoelasticity displays forces

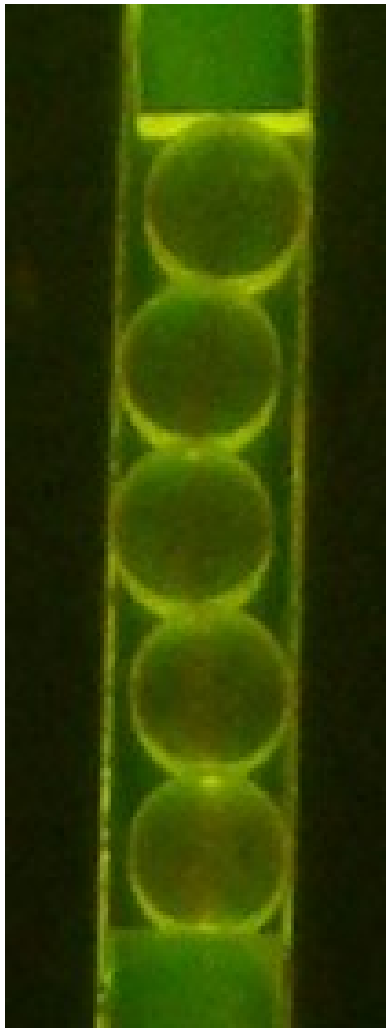

low
force

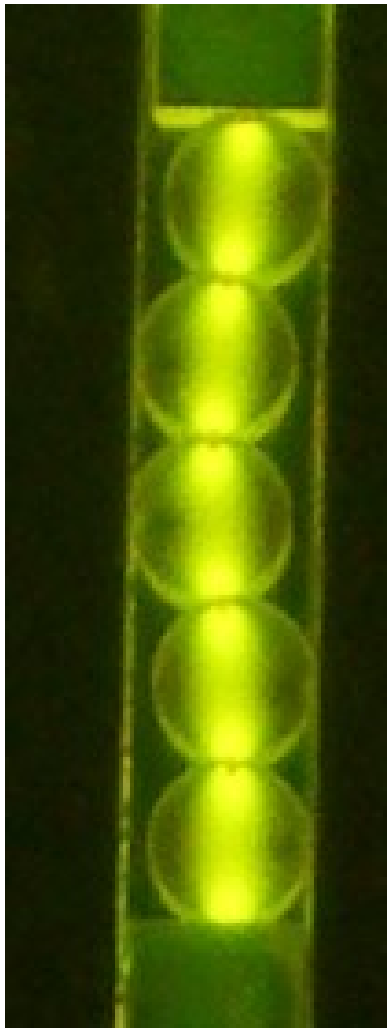

medium
force

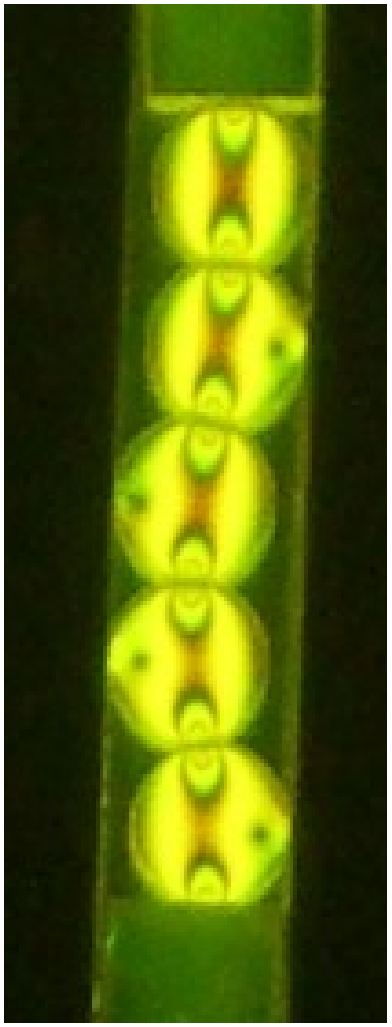

high
force

Classic technique: e.g. Frocht 1941

Measuring Interparticle Contact Forces

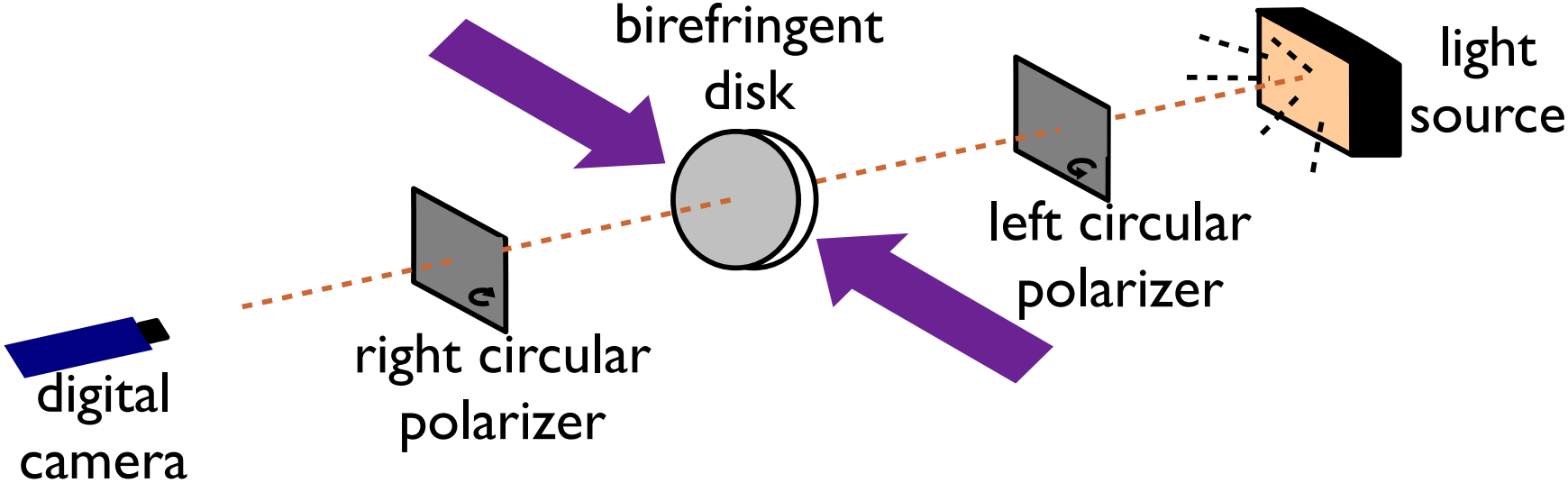

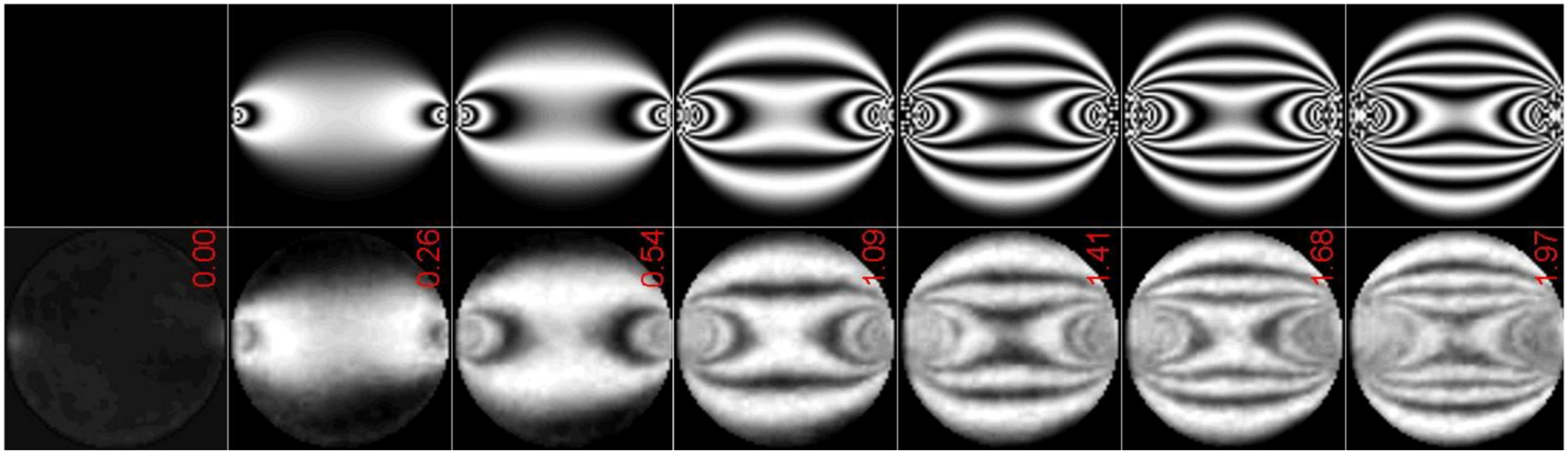

Daniels, Kollmer, Puckett. *Rev. Sci. Inst.* (2017) https://github.com/jekollmer/PEGS

Calculating Fringes

- The intensity of the fringe pattern is given by

$$I = I_0 \sin^2 \frac{\pi(\sigma_1 - \sigma_2) h C}{\lambda}$$

- $(\sigma_1 - \sigma_2)$ is the *principal stress difference* at that point
- h is the material thickness
- λ is the wavelength of light
- C is the *stress-optic coefficient* (a material property, also λ-dependent)

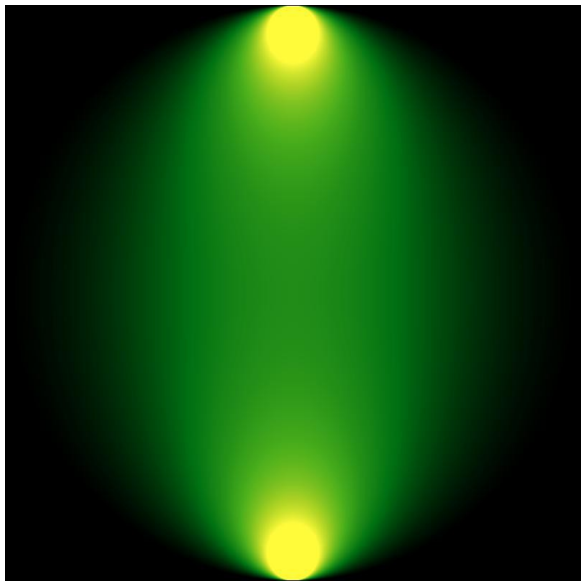

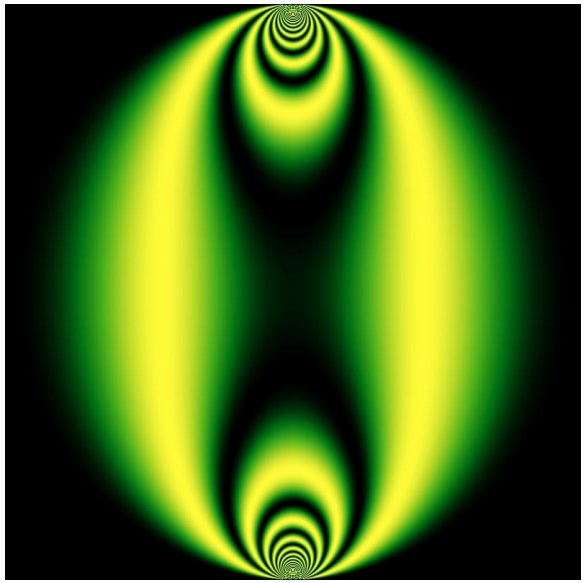

Step 1: Locate all Contacts

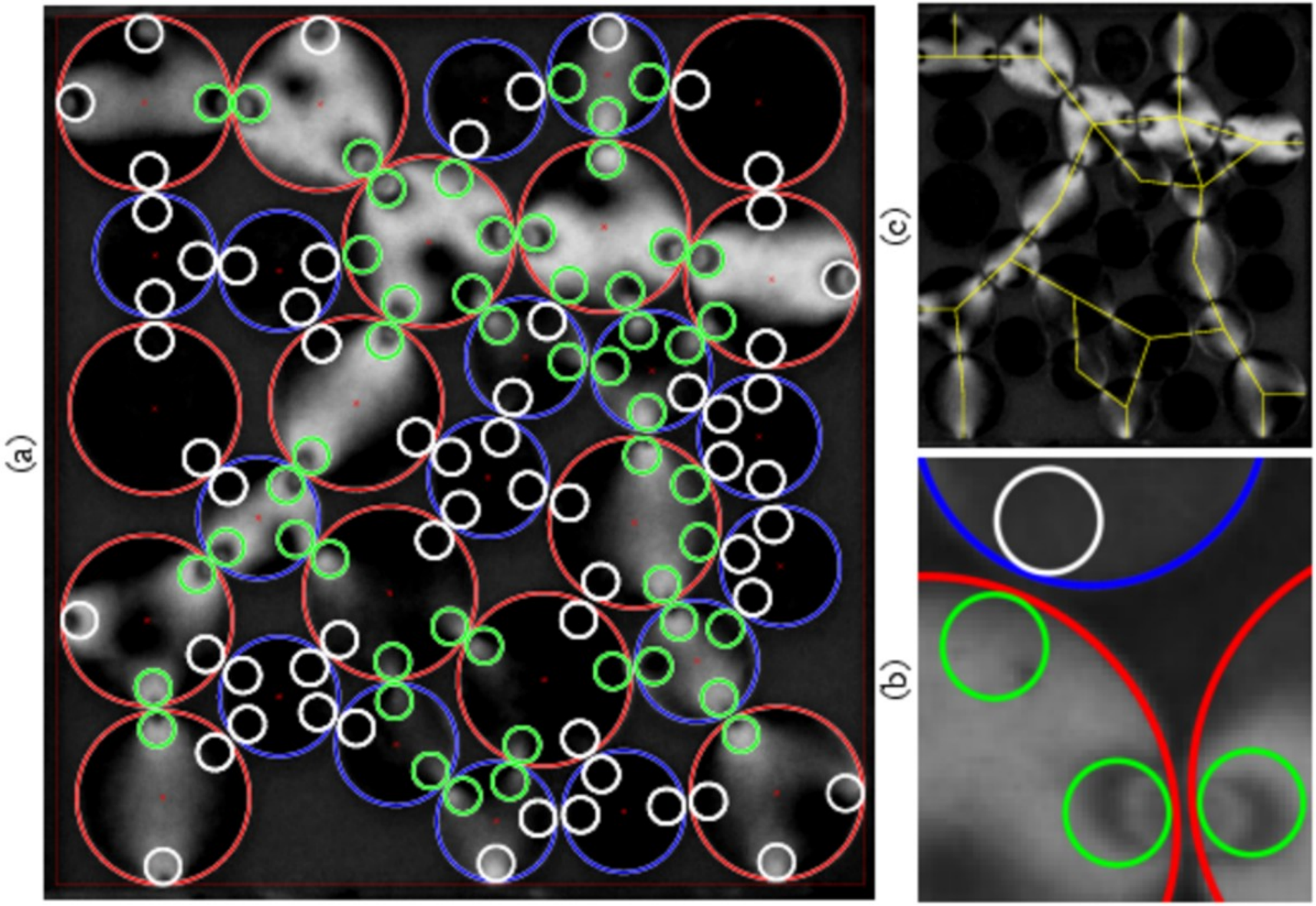

Daniels, Kollmer, Puckett. *Rev. Sci. Inst.* (2017) https://github.com/jekollmer/PEGS

Step 2: Photoelastic Inversion

pseudo-image

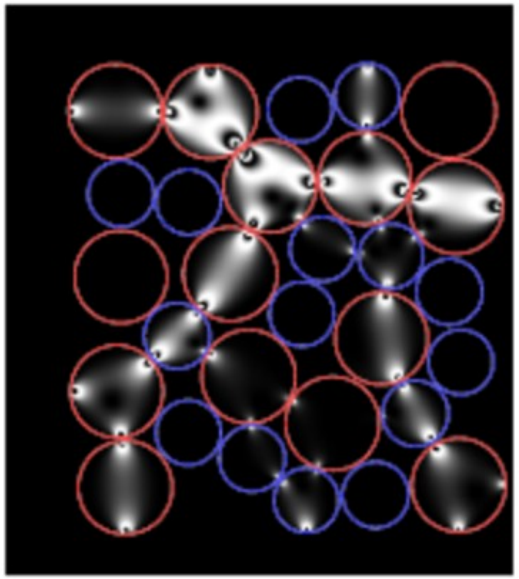

Result: vector force at each contact

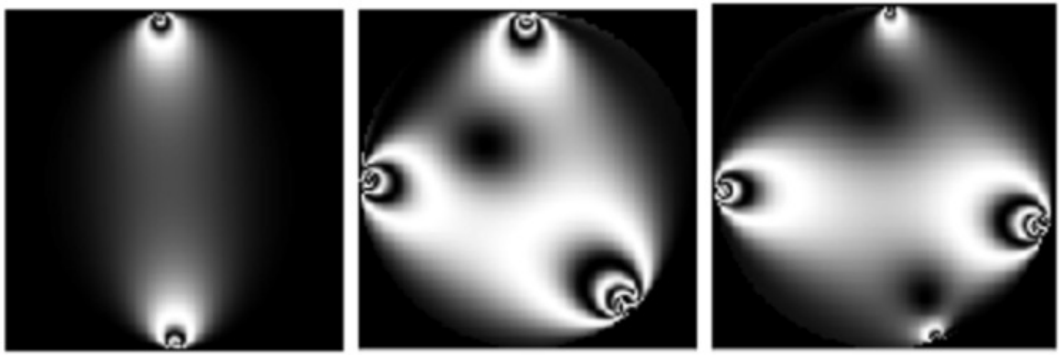

optimize fringe pattern (can't use force/torque balance each disk!)

image

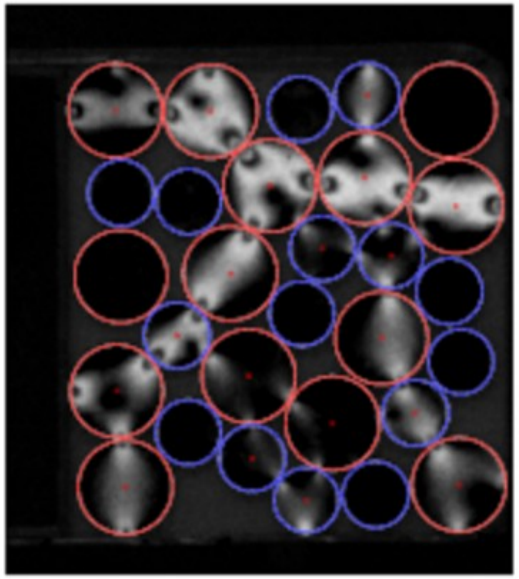

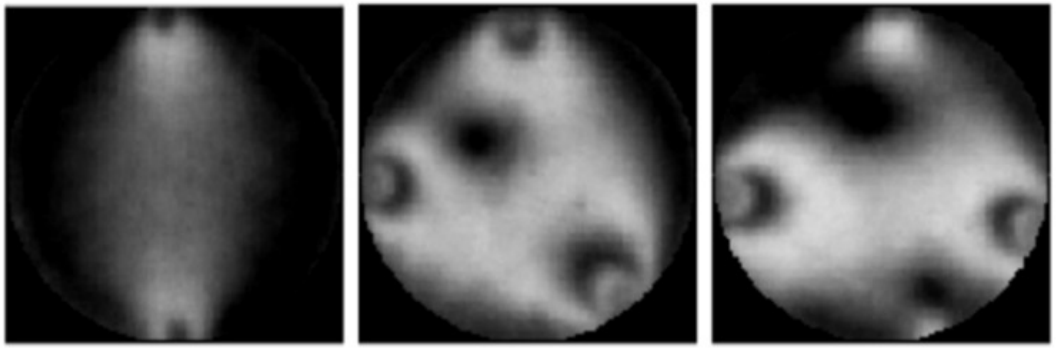

Daniels, Kollmer, Puckett. *Rev. Sci. Inst.* (2017) https://github.com/jekollmer/PEGS

Non-local effects in intermediate flows

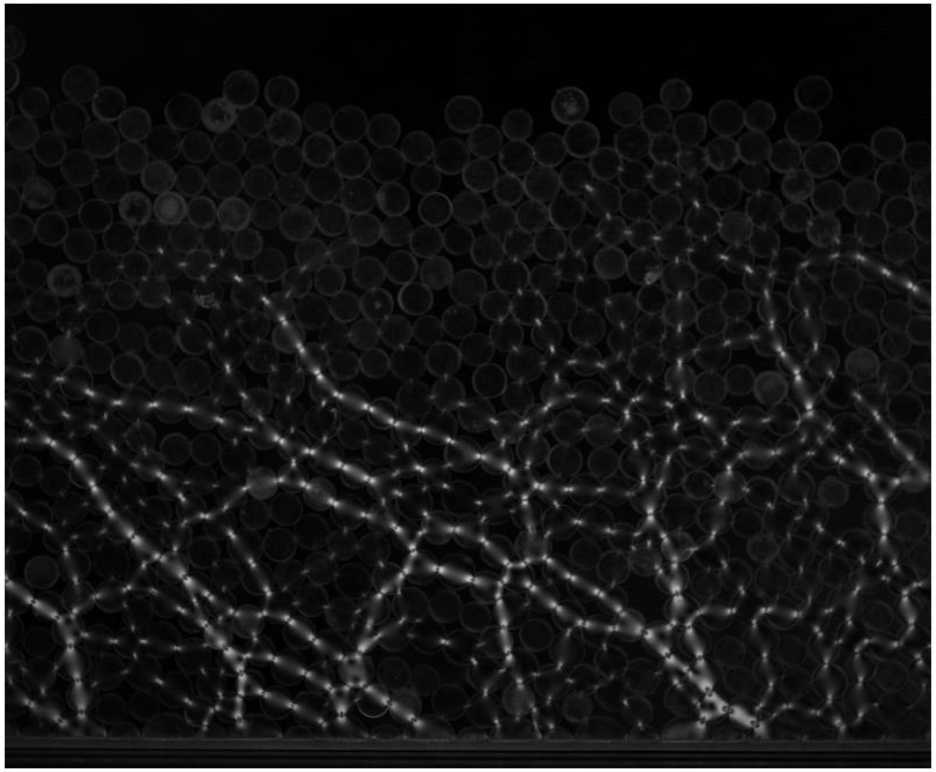

Nathalie M. Vriend[1] and Karen Daniels[2]

with Amalia Thomas[1] and Zhu Tang[2]

[1] DAMTP, University of Cambridge, UK

[2] Department of Physics, North Carolina State University, USA

June 25th, 2018

Photoelasticity in avalanches

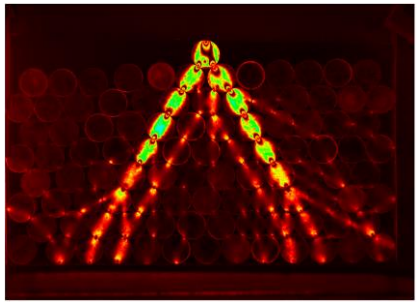

"Force chains"

- Principles:
  - Shows change of refractive index when stressed
  - Calibration between pattern and stress

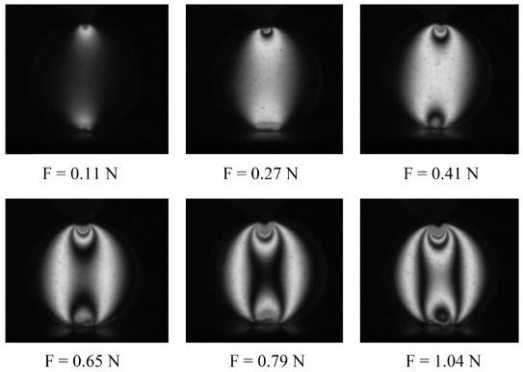

"Calibration"

- Novelty:
  - Custom-made, stress-free particles*
  - Dynamic interactions across milliseconds
    → No force equilibrium

- Potential:
  - Measuring non-local effects and rheology in intermediate flows!

* Procedure perfected by Amalia Thomas (PhD-student in DAMTP)

New “optical” segregation chute

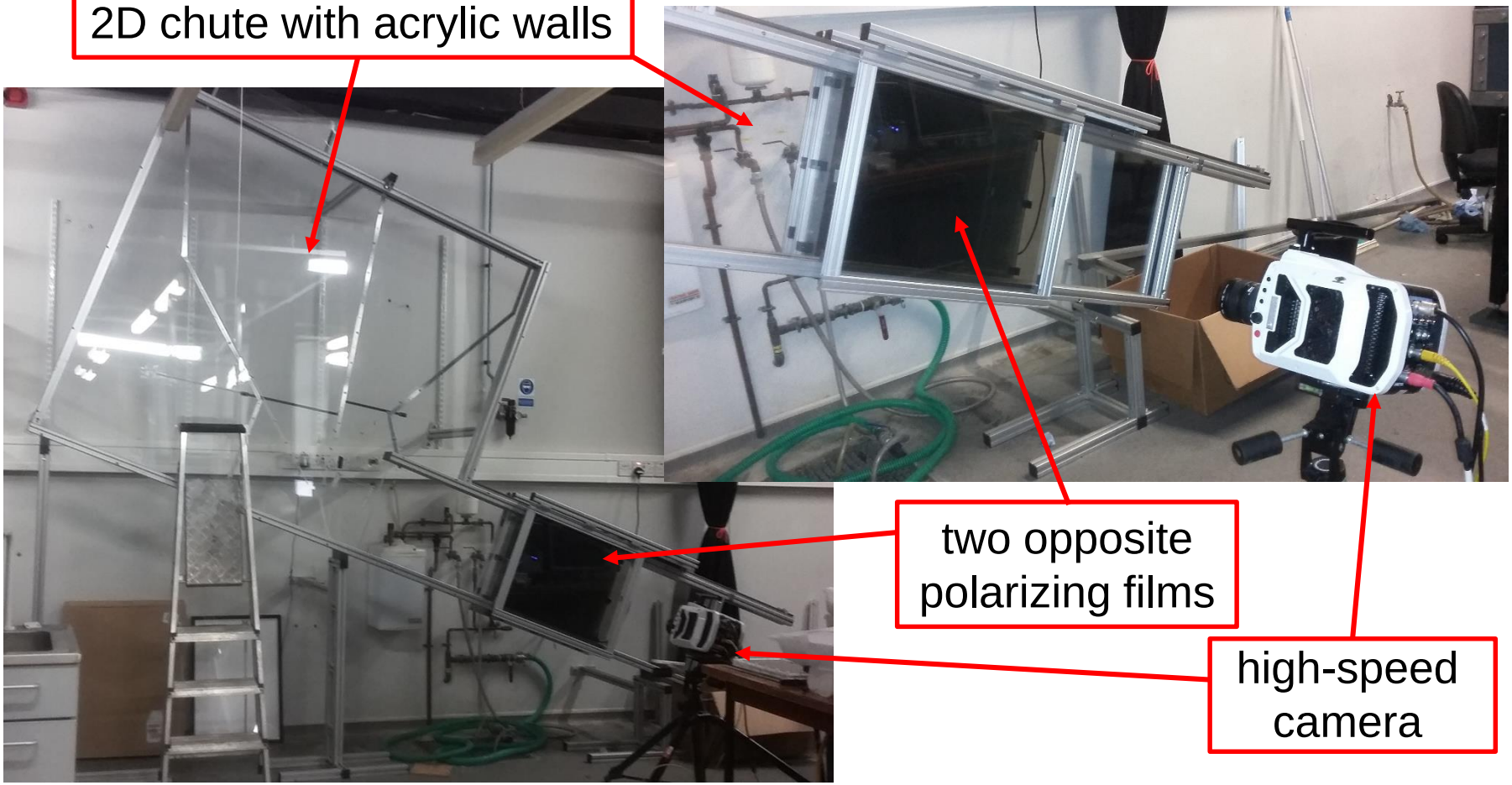

20 - 30s continuous 2D avalanches with constant height & flux!

Inclined at $\theta = 20°$, flux at $Q \approx 0.0564$ m^2/s, measurements at 0.25 cm from inlet

Continuous avalanche down a 2D chute

- Dynamical measurements of granular rheology:
  - Technique sensitive to F > 0.01 N
  - Force equilibrium does not hold!

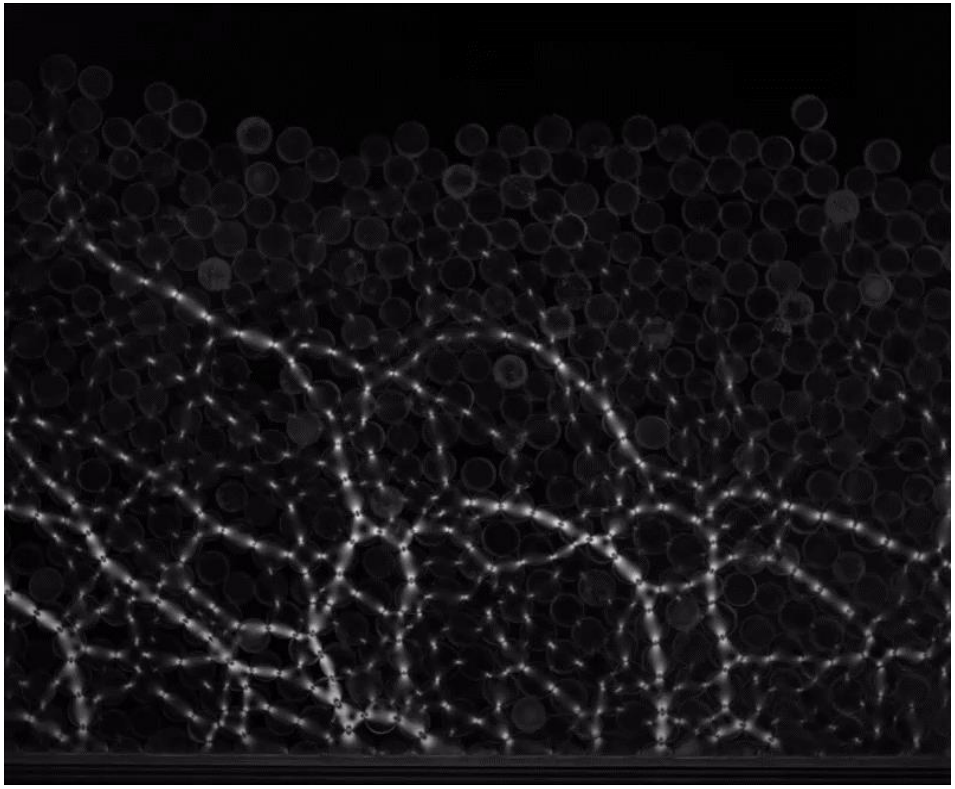

Collected at 1000fps,
Slowed down x66.66

Frictional base: alternating 1.2 & 2.1 cm particles

Extracting quantitative data

- Using coarse-graining for downstream velocity U:
  - Static & moving regions: linear at top, frozen at bottom
- Shear rate $\dot{\gamma}$:
  - Near surface: $\dot{\gamma}$ = 7 s^{-1}
  - Decreasing downwards

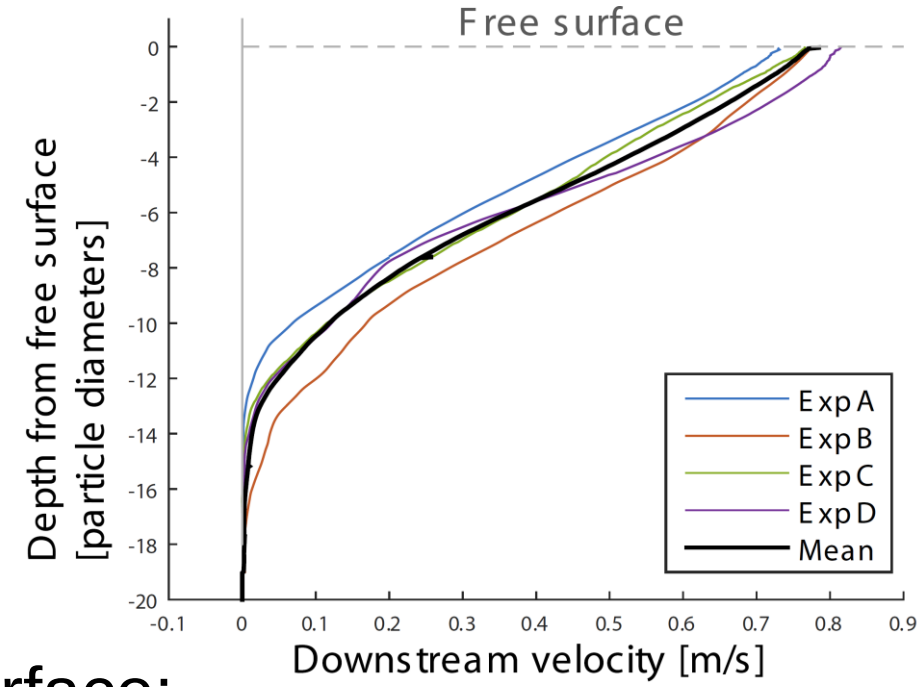

- Intermediate flow near surface:
  - Inertial number: $I = \frac{\dot{\gamma} d}{\sqrt{P/\rho}} \approx 0.25$

Frictional base, flowing material: D = 1.1 – 1.3 cm particles, 4 identical repeats

Extracting quantitative data (2)

- Using coarse-graining for stress components $\vec{\sigma}$:

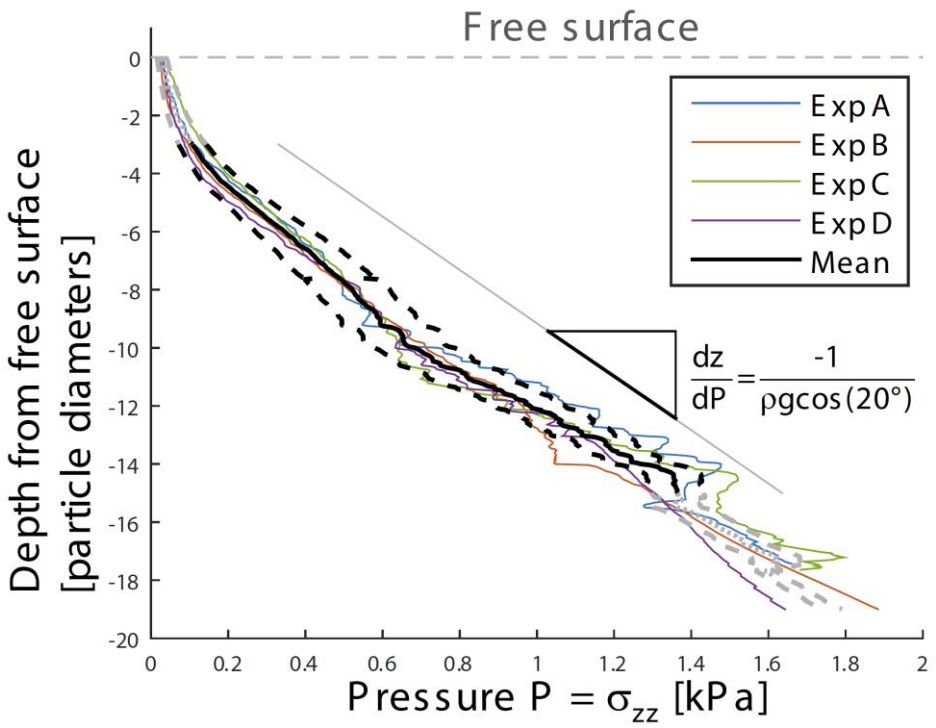

- Hydrostatic force balance:
  - $\sigma_{zz} = (h - z)\rho g cos(\theta)$
  - $\sigma_{zx} = (h - z)\rho g sin(\theta)$
- Systematic error at surface
  - for F < 0.01 N
- Symmetry in stresses?
  - $\sigma_{xz} \neq \sigma_{zx}$ (some rotation)
  - $\sigma_{xx} = \sigma_{zz}$ (no lateral stresses)
- Calculate friction coefficient μ:
  - $\mu = \sigma_{xz}/\sigma_{zz}$

Frictional base, flowing material: D = 1.1 – 1.3 cm particles, 4 identical repeats

Interpretation of quantitative data (1)

- Calculating friction coefficient & fluctuations:

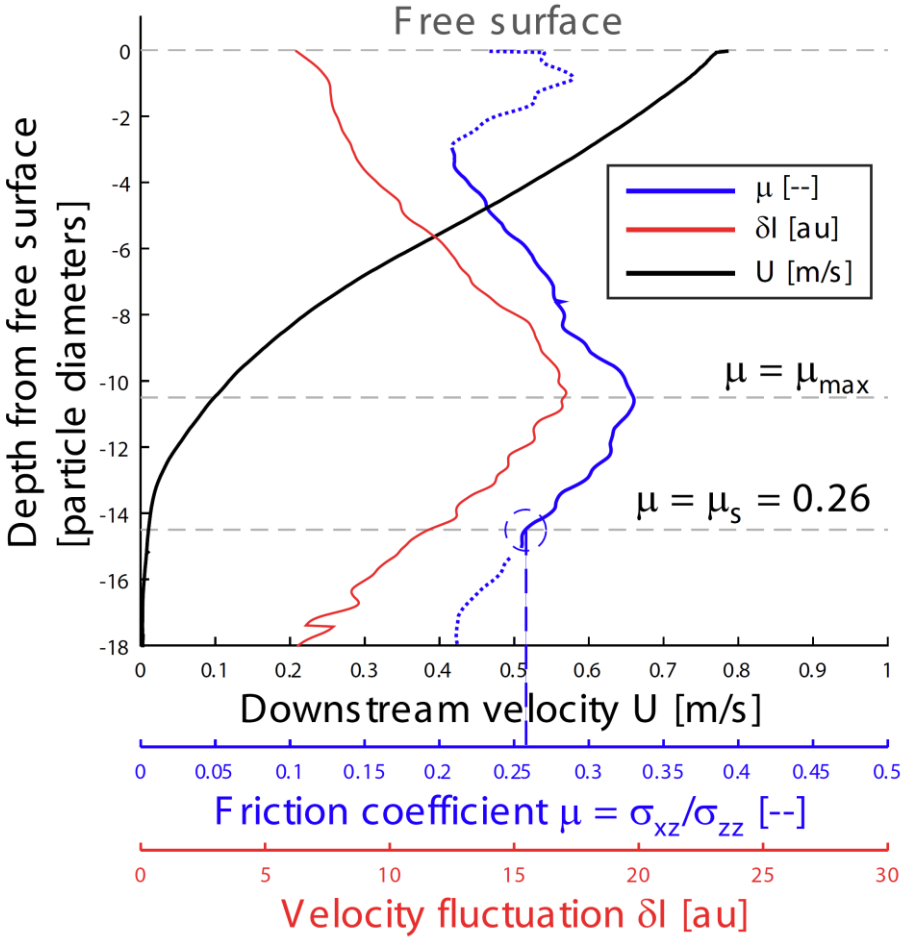

- Calculate friction coefficient μ:
  - Stress ratio: $\mu = \frac{\sigma_{xz}}{\sigma_{zz}}$
  - Location: $\mu > \mu_s$ and maximum μ
- Velocity fluctuations $\delta I(z)$ from pixel intensity I(x,z,t):

$$I'(x,z,t) = I(x,z,t) - \langle I(x,z,t)\rangle_t$$

$$\delta I(x,z) = \sqrt{\langle I'^2(x,z,t)\rangle_t}$$

$$\delta I(z) = \langle \delta I(x,z)\rangle_x$$

- Downstream velocity profile U
  - Transition static – dynamic

Frictional base, flowing material: D = 1.1 – 1.3 cm particles, 4 identical repeats

Interpretation of quantitative data (2)

- Compare fluctuations $\delta I(z)$ and friction coefficient μ:

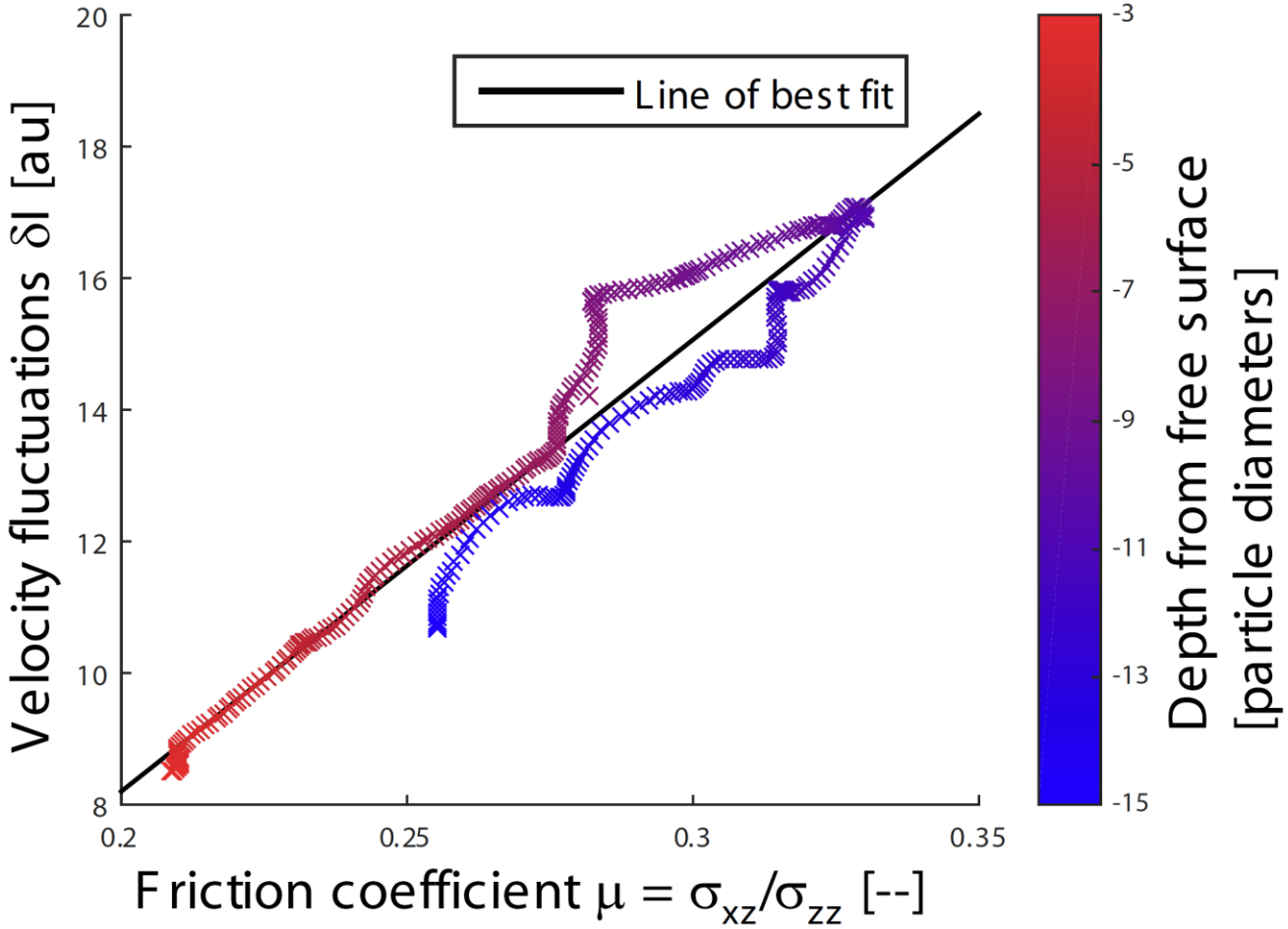

Highly correlated with correlation coefficient 0.967

Interpretation of quantitative data (3)

- Calculation of non-local parameters:

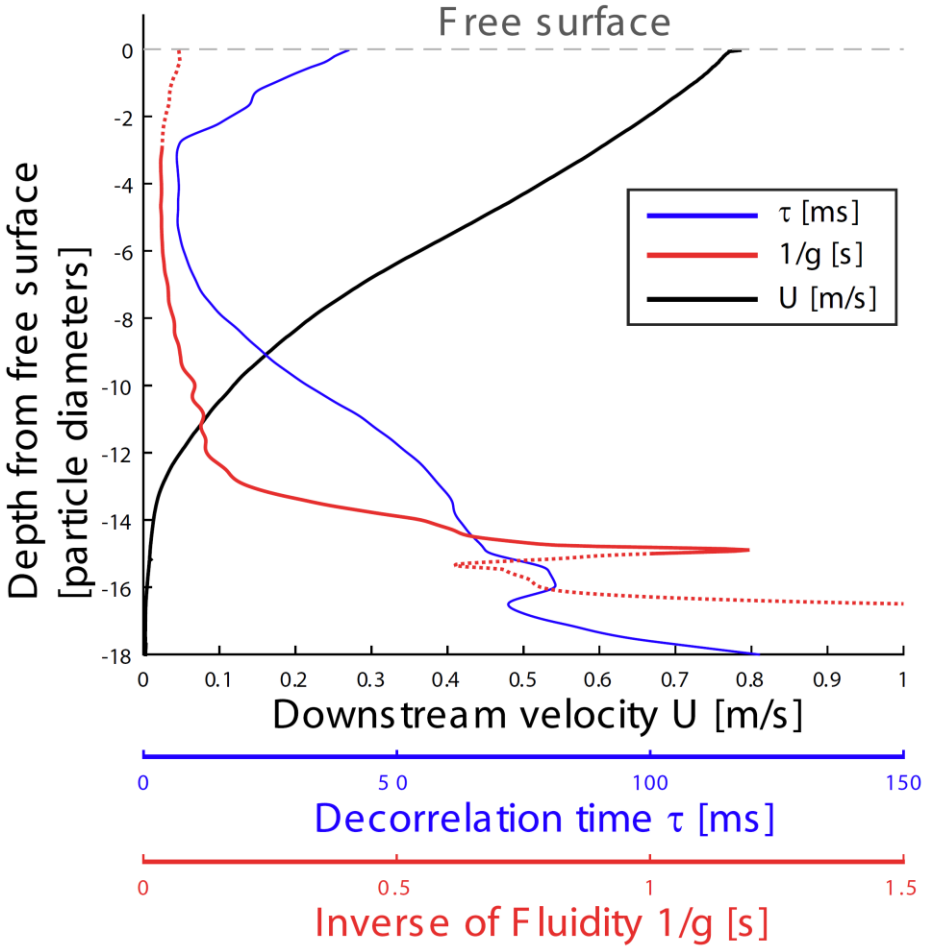

- Calculate granular fluidity g:
  - $g = \frac{\dot{\gamma}}{\mu}$
  - Steadily decreasing with depth
- Temporal decorrelation τ(z) from decaying autocorrelation

$$I'(x,z,t) = I(x,z,t) - \langle I(x,z,t)\rangle_t$$

$$r(x,z,k) = \frac{\sum_{t=1}^{N_t-k} I'(x,z,t)I'(x,z,t+k)}{\sum_{t=1}^{N_t} I'(x,z,t)^2}$$

$r_k = Ce^{-k\tau}$, with lag k

$$\tau(z) = \langle \tau(x,z)\rangle_x$$

- Downstream velocity profile U
  - Transition static – dynamic

Interpretation of quantitative data (4)

- Compare temporal decorrelation τ with fluidity g:

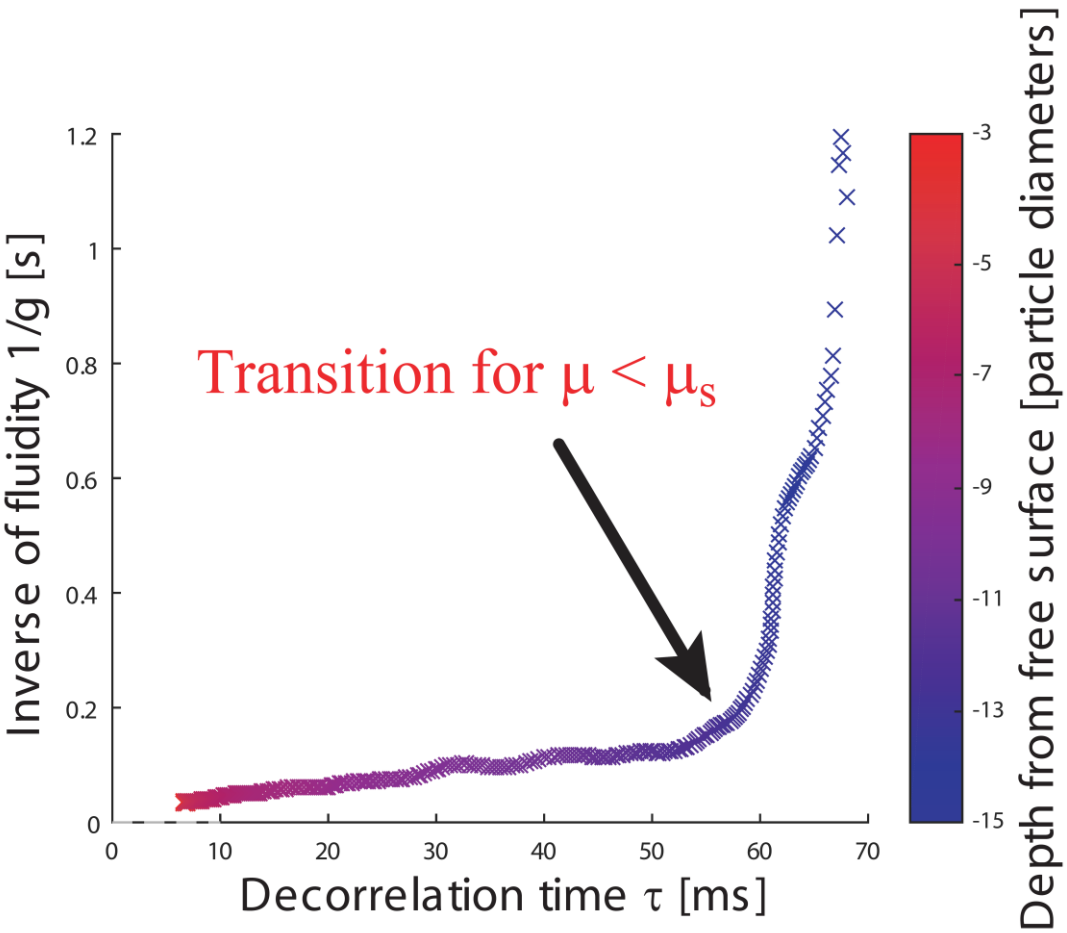

Highly correlated, for z = 3 – 12 D, with correlation coefficient 0.994

Conclusion

- Experimental apparatus to explore intermediate flows
  - Intermediate inertial numbers, probing non-local effects
- Non-local region between static and flowing layer:
  - Increasing hydrostatic pressure, decreasing velocity and shear
  - Maximum friction coefficient in non-local regime
- Correlation:
  - High between velocity fluctuations and friction coefficient
  - High between inverse of fluidity and decorrelation time for flowing part of the flow
  - Transition in correlation between flowing and quasi-static region

Extra

- Back-up slides

Extra: Extracting data (1)

- Normal and shear stresses as a function of depth:

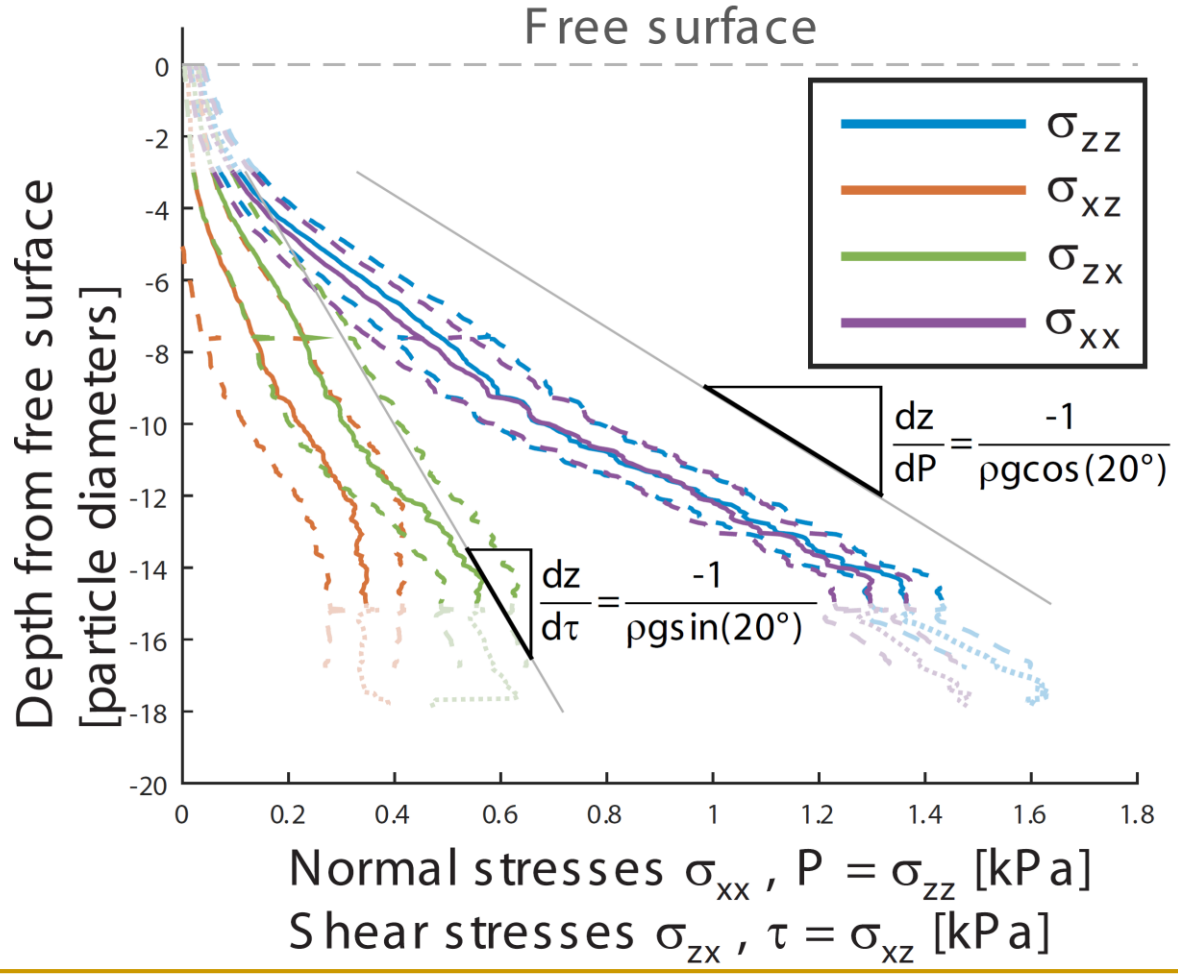

Extra: Extracting data (2)

- Friction coefficient as a function of depth: $\mu = \frac{\sigma_{xz}}{\sigma_{zz}}$

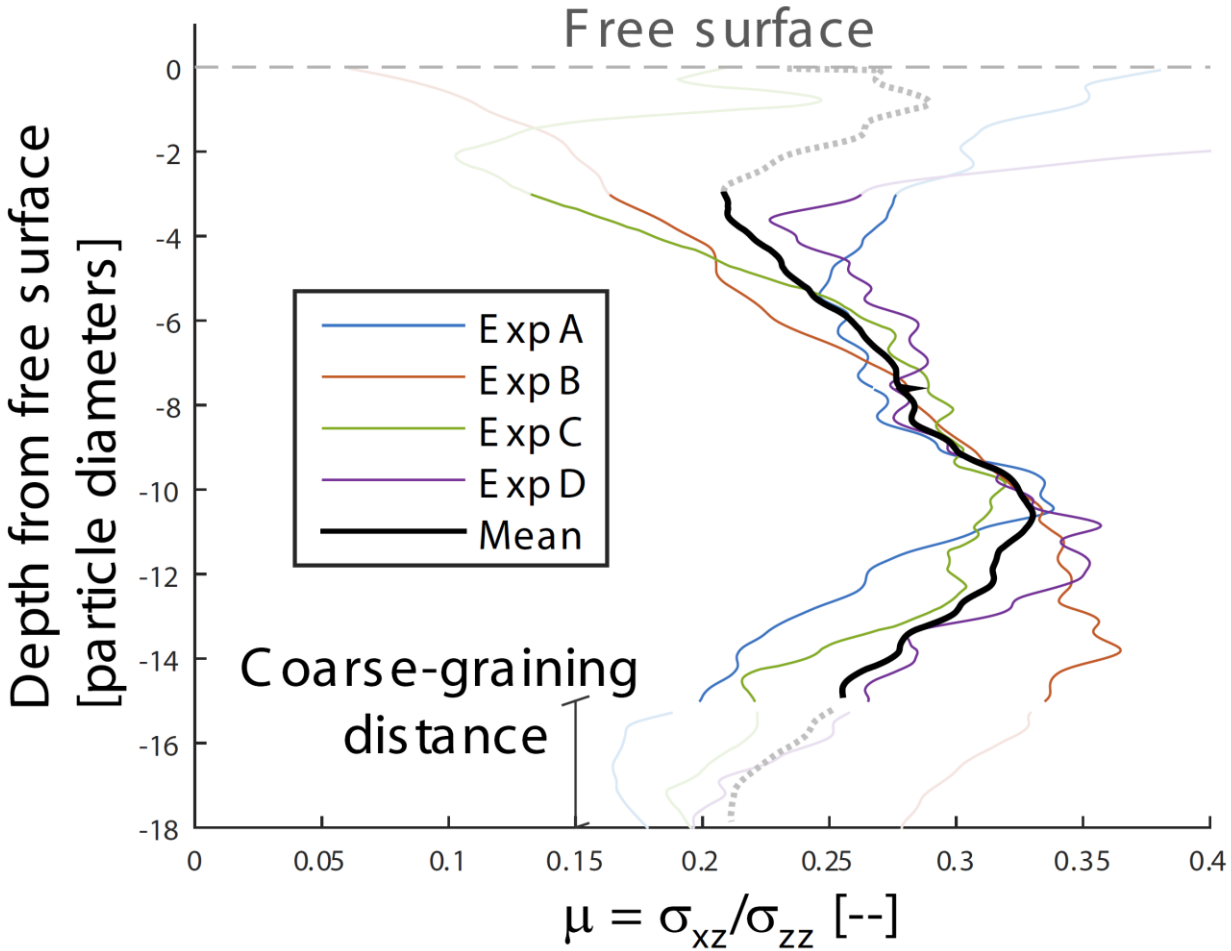

Extra: Extracting data (3)

- Velocity fluctuation as a function of depth:

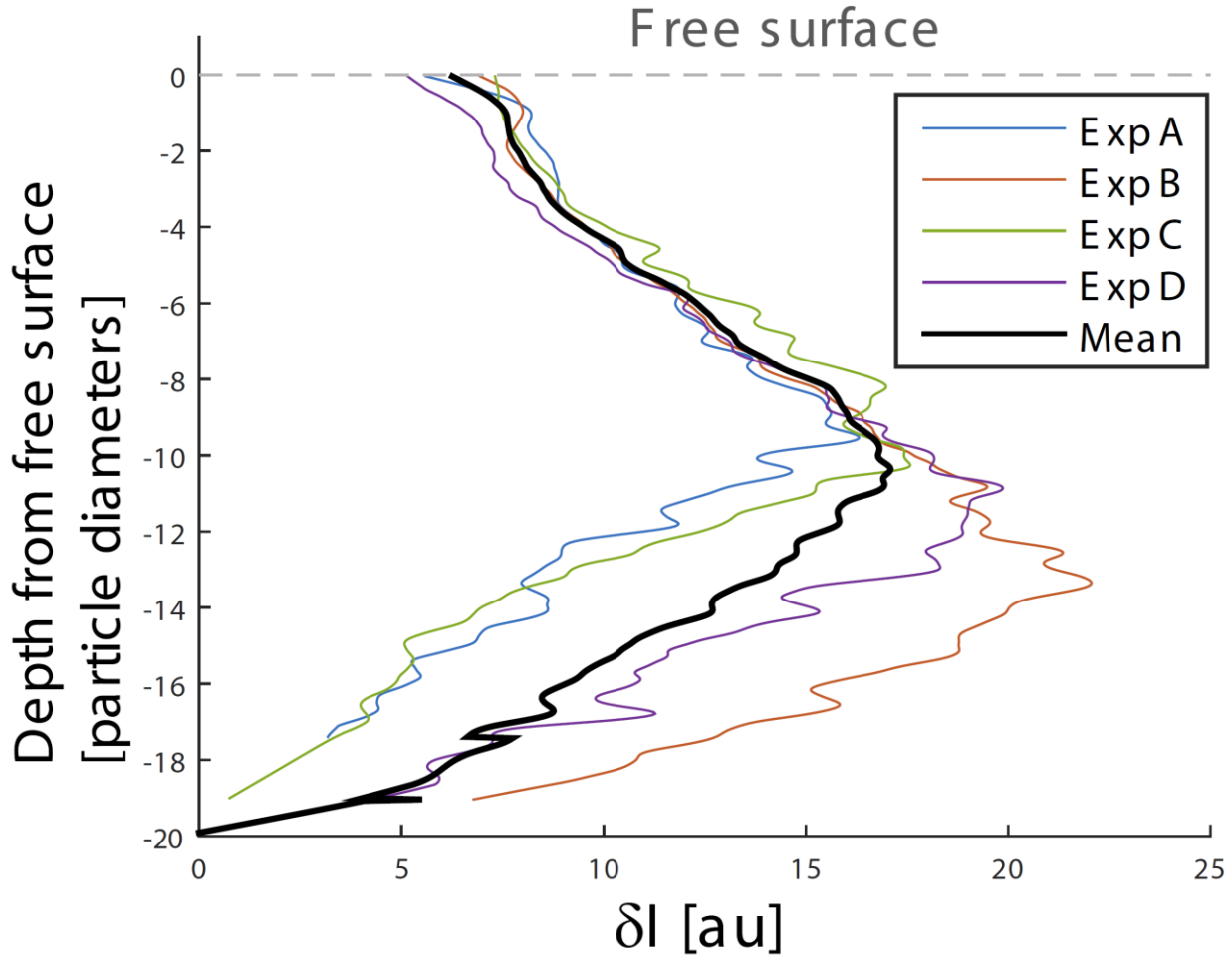

Extra: Extracting data (4)

- Temporal fluctuation as a function of depth:

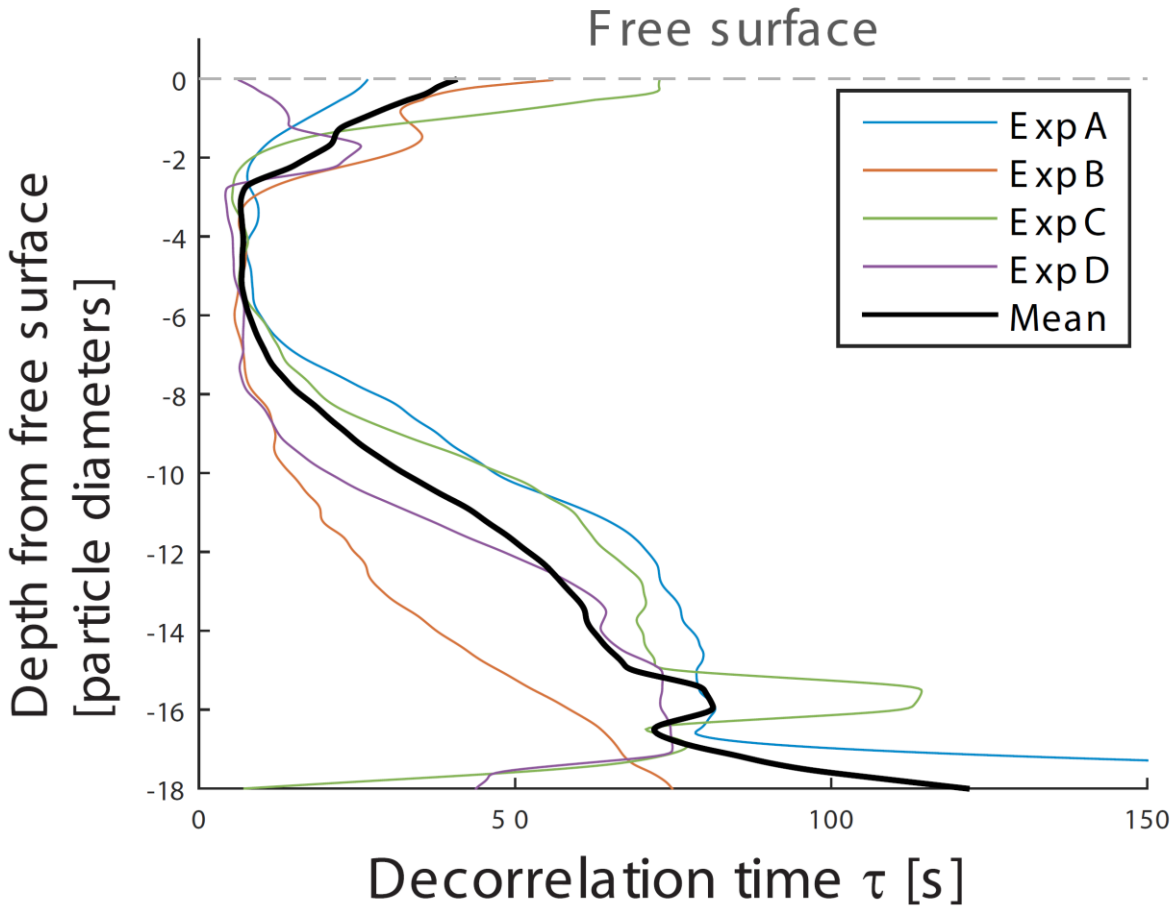

Extra: Extracting data (5)

- Shear rate as a function of depth:

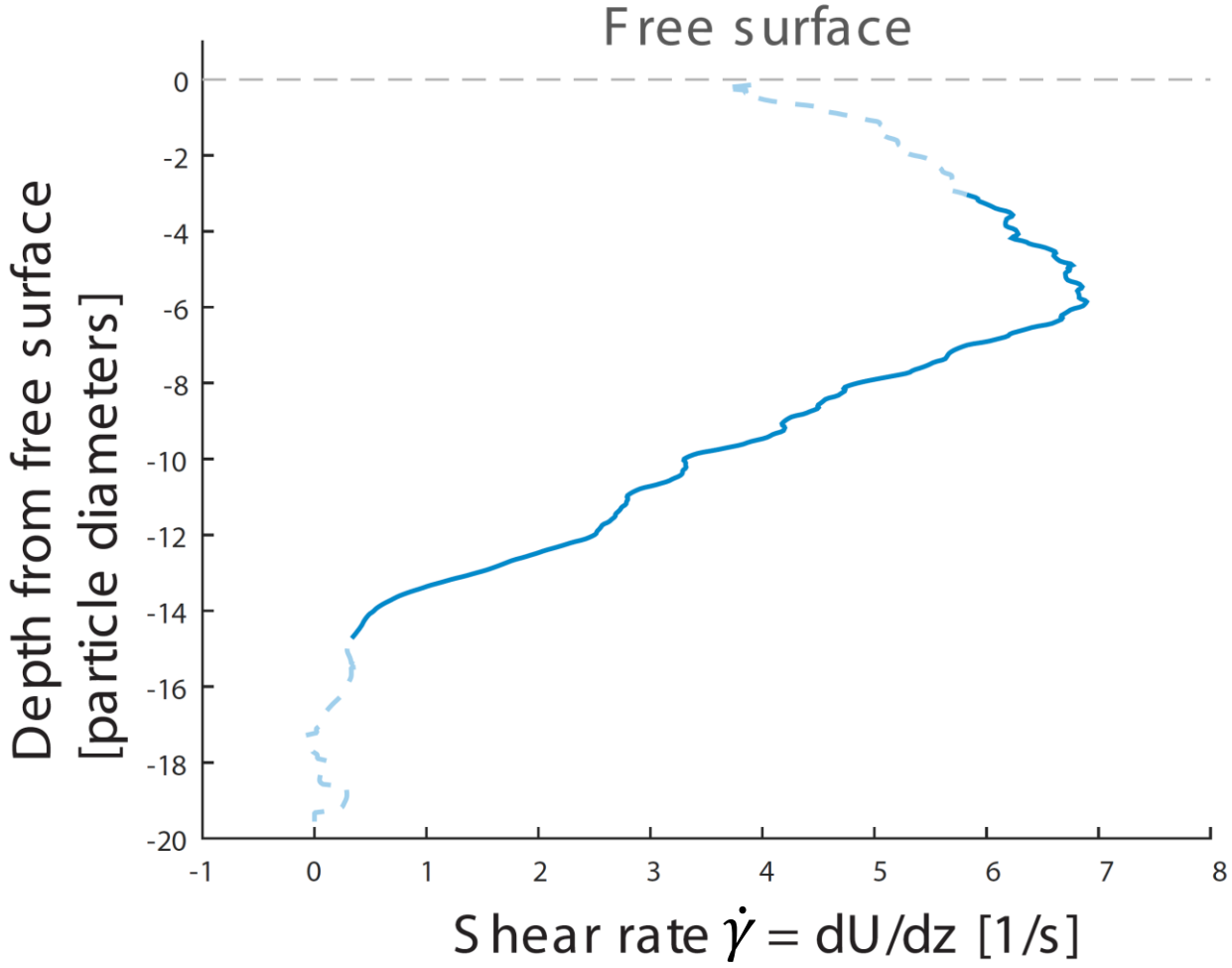

Extra: Extracting data (7)

- Inertial number as a function of depth:

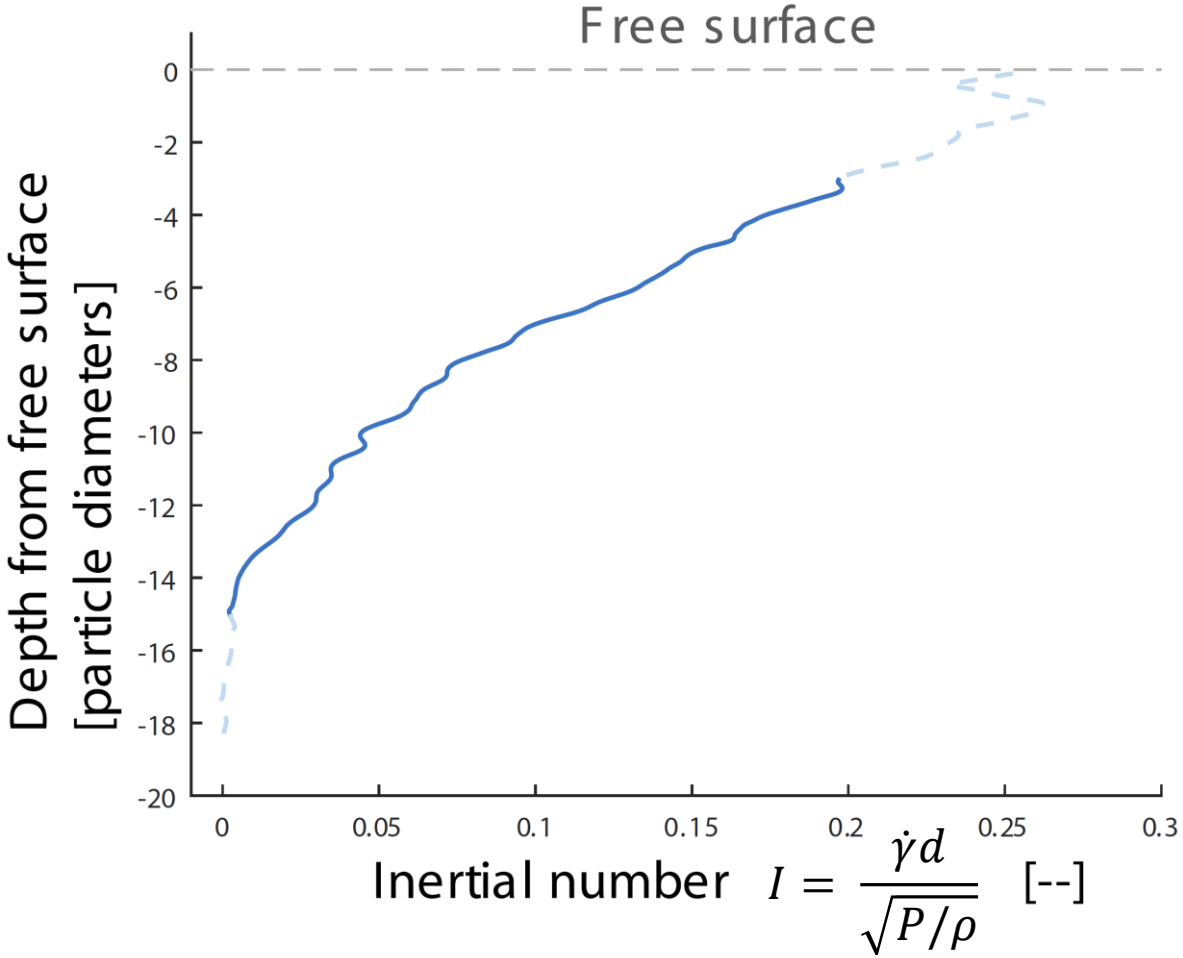

Extra: Extracting data (6)

- Fluidity as a function of depth:

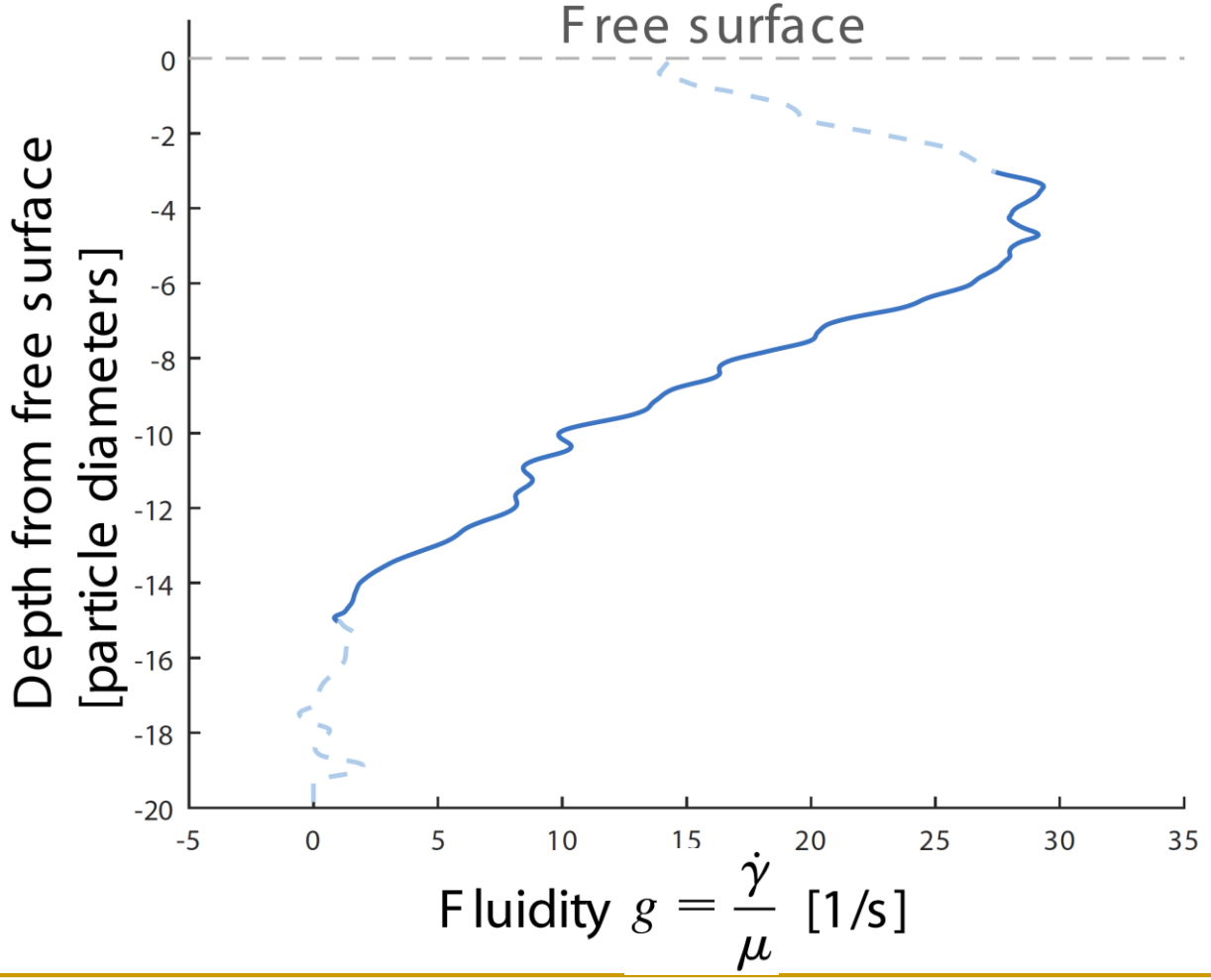

“Prediction of the Effect of Solvents and Impurities/Additives on Crystal Shape and Growth Kinetics”

ADDICT
Advanced Design and Development of Industrial Crystallization Technology

Michael Doherty

UCSB Chemical Engineering

Abstract

“The goal of this research is to develop a practical engineering tool for predicting the relative growth rates (growth kinetics) and morphology of solution-grown faceted crystals, including the effects of solvent (Phase 1 of the research), and impurities/ additives (Phase 2).”

Context: Equilibrium shape
(easy to predict but often inaccurate)

EQ shape: face growth rate proportional to face surface energy

$$R_{hkl} \propto \gamma_{hkl}$$

EQ shape prediction for urea

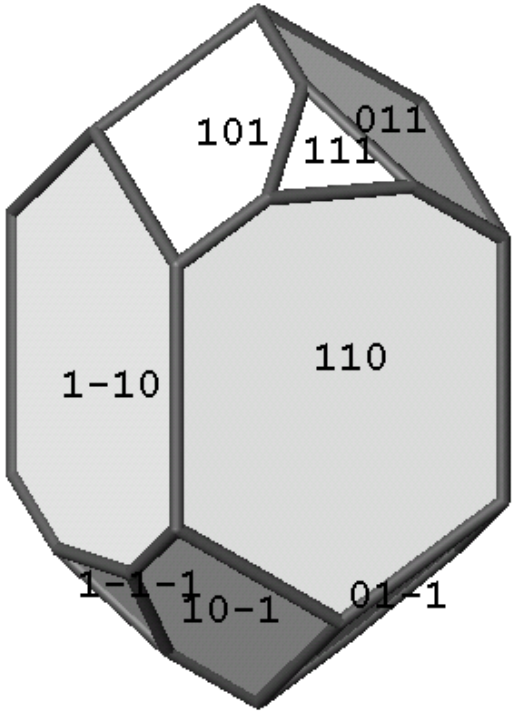

Actual urea vapor growth shape

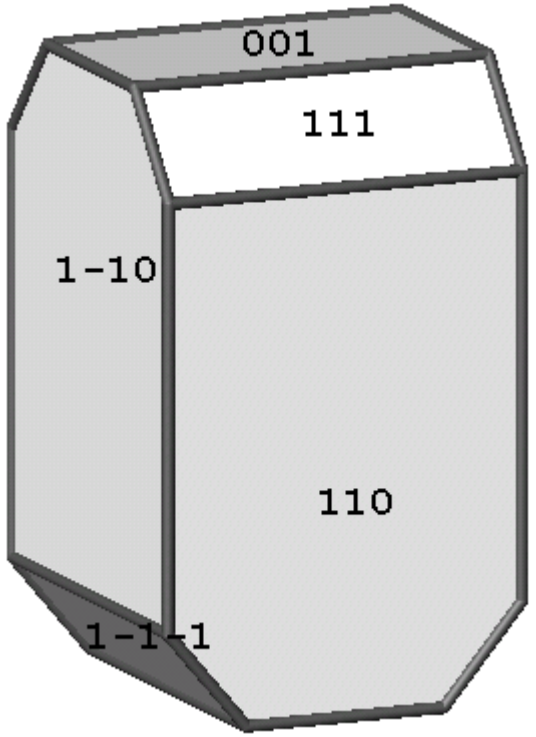

3

Context: Non-mechanistic growth models
(easy to predict but often inaccurate)

BFDH model

$$R_{hkl} = \frac{1}{d_{hkl}}$$

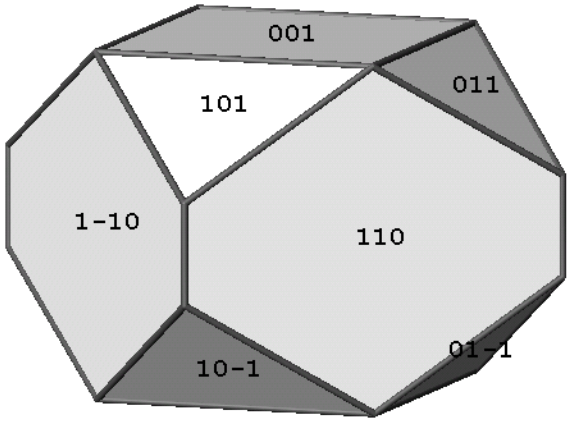

BFDH prediction for urea

Attachment energy (AE) model

$$R_{hkl} \propto E_{hkl}^{att}$$

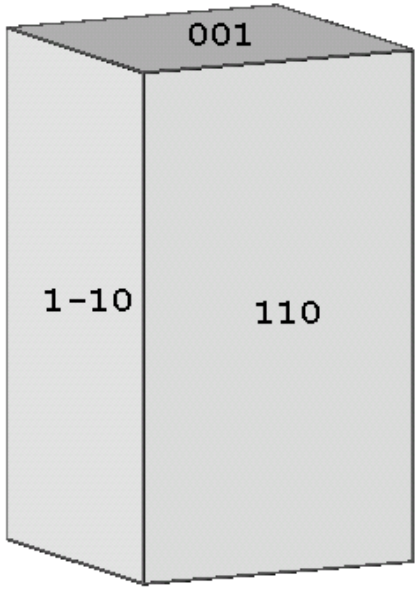

AE prediction for urea

Actual urea vapor growth shape

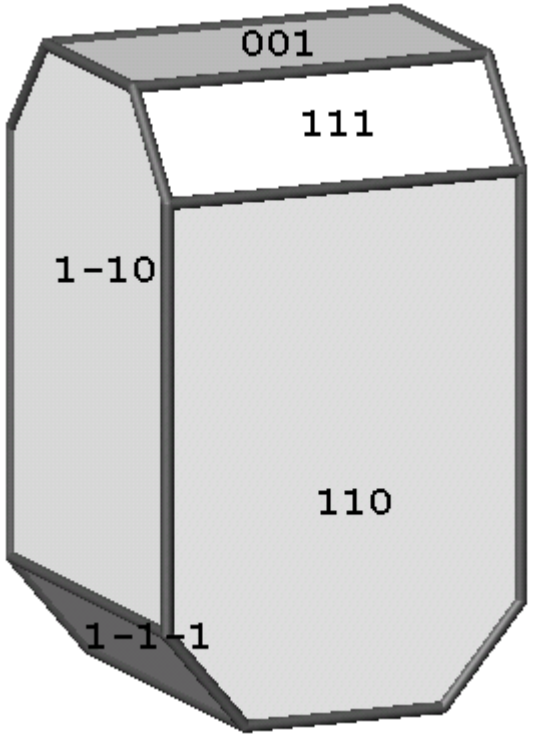

4

Lovastatin

AE shape

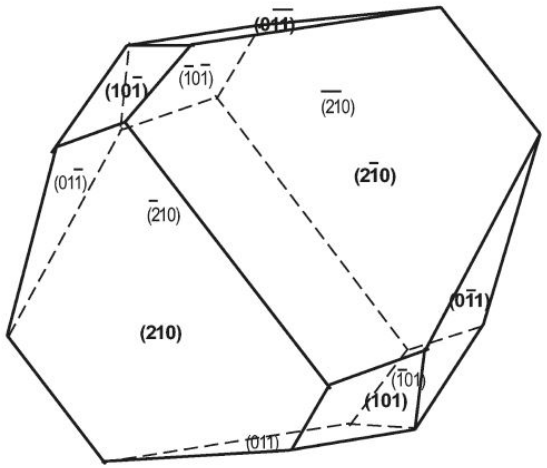

Figure 28. The attachment energy morphology of lovastatin.

Experimental growth shape

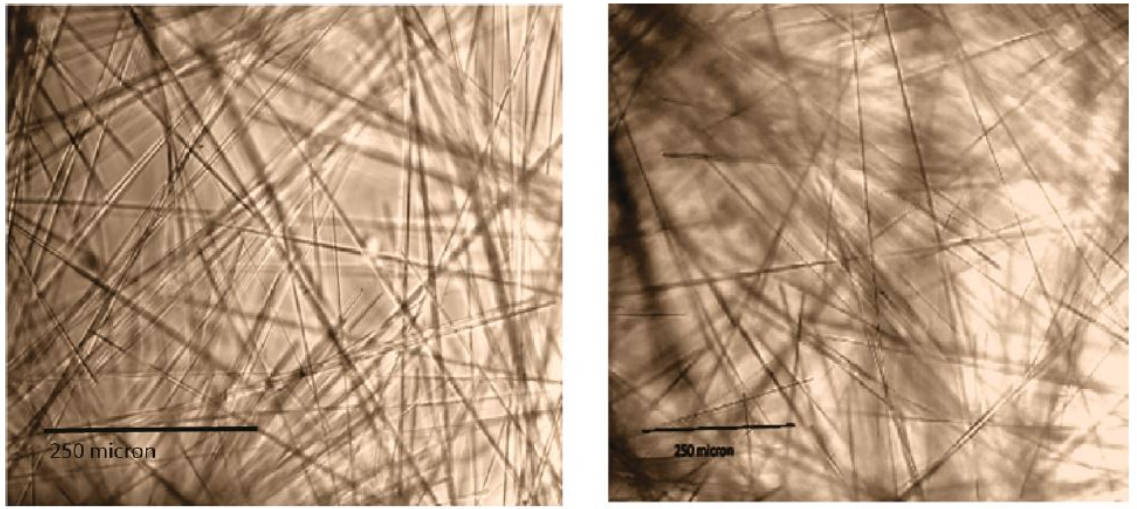

a) b)

Figure 27. The experimental steady-state morphology of lovastatin grown from (a) isopropanol, (b) methanol.

5

Context: Mechanistic vs. non-mechanistic

	Equilibrium	BFDH	Attachment energy	Mechanistic
Solvent	X		X	X
Supersaturation				X
Temperature				X
Speed / ease	X	X	X	
Future upgrades				X

Equilibrium
Not accurate
(growth governed by kinetics)

BFDH
Can't account for growth conditions at all – **not useful for engineering**

Attachment energy
Can't account for supersaturation, **can't be developed** further

Mechanistic
Much more **complicated**, but can account for **all growth conditions** and **can be improved**

6

ADDICT executes a multiscale mechanistic framework

Models at each scale feed info back and forth

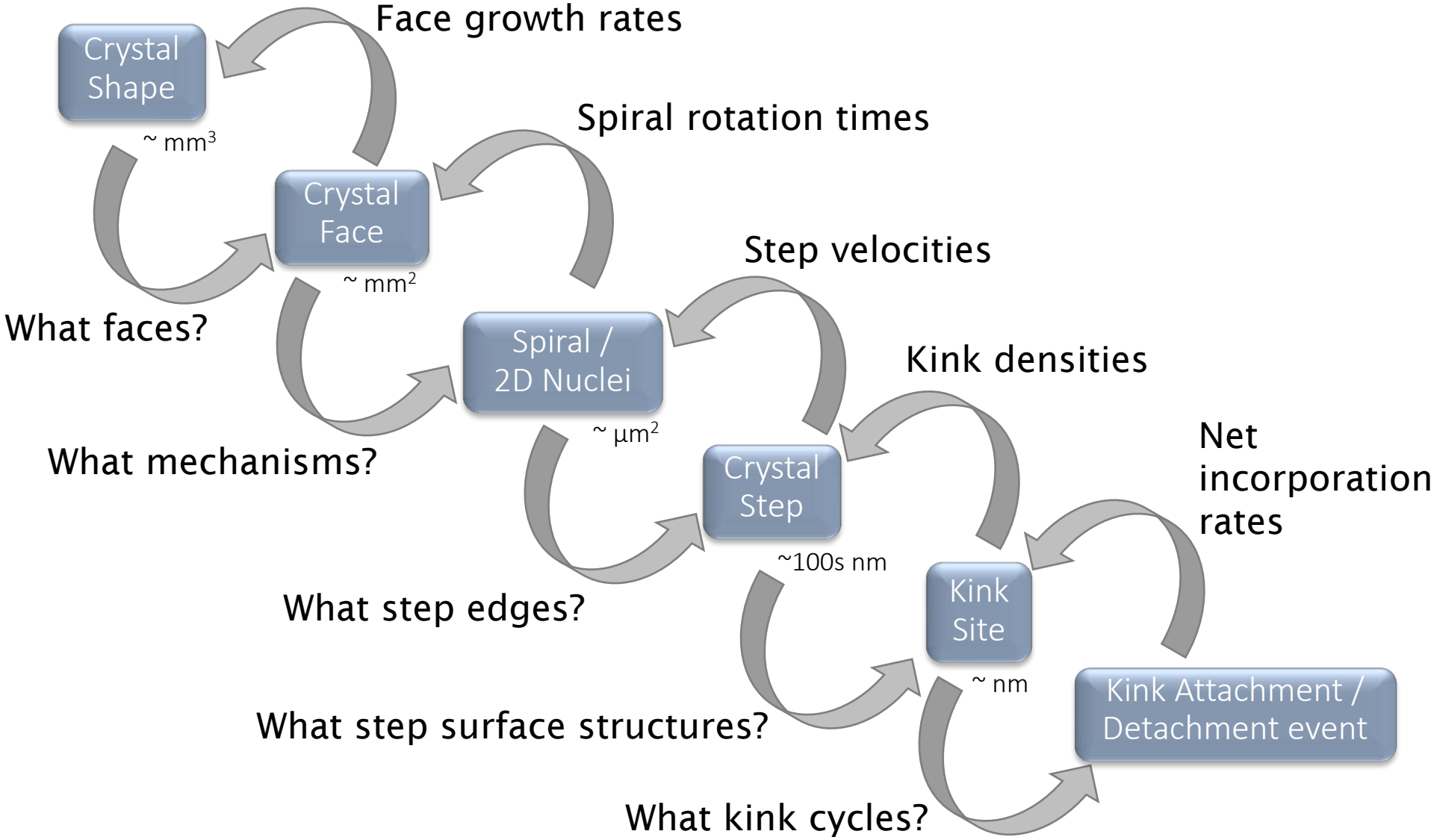

7

Solvent Effects

All crystal surface energies are modified to account for the solvent

$$\gamma_{XS} = \gamma_X + \gamma_S - W_{ad,XS}$$

Crystal
Solid-state
GAFF force field

Solvent
Solubility parameters
Beerbower correlations

Interfacial model
Van Oss, Chaudhury & Good
(match interactions by adhesion: dispersive, electron-accepting, electron-donating)

$$W_{ad} = 2\sqrt{\gamma_1^d \gamma_2^d} + W_{ad}^{AB}$$

$$W_{ad}^{AB} = 2\sqrt{\gamma_1^+ \gamma_2^-} + 2\sqrt{\gamma_1^- \gamma_2^+}$$

8

Lovastatin

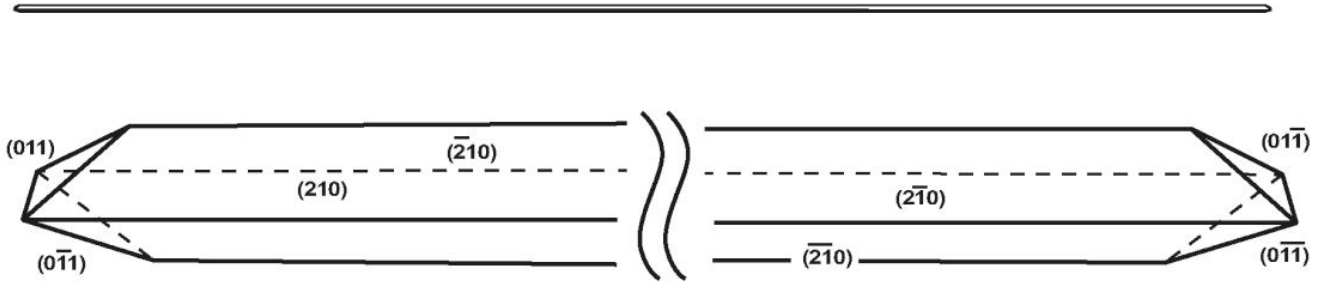

Figure 26. Predicted steady-state morphology of lovastatin.

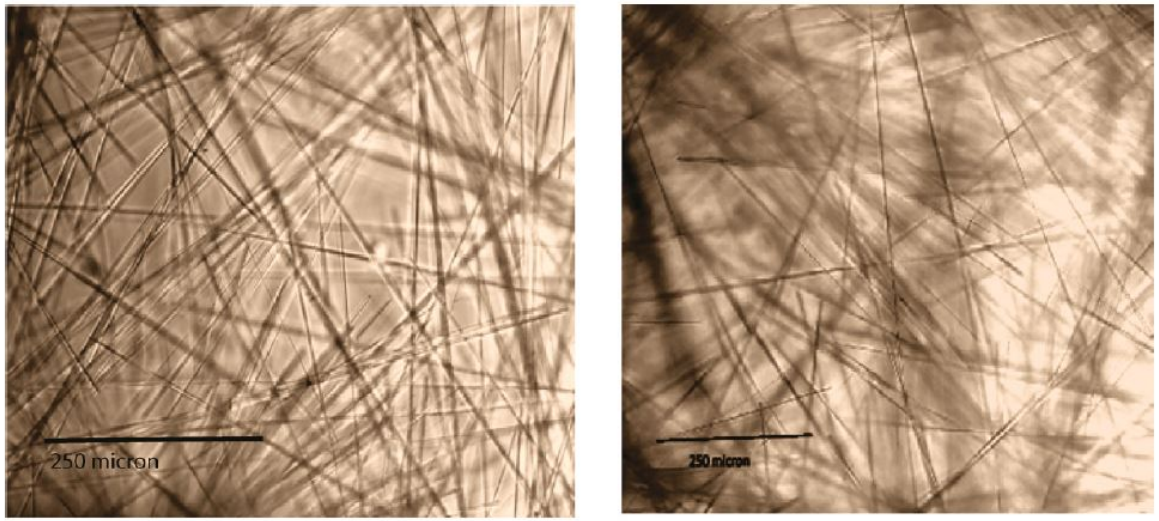

Figure 27. The experimental steady-state morphology of lovastatin grown from (a) isopropanol, (b) methanol.

9

Example – Olanzapine

Sun et al, Cryst. Growth Des., 2018 DOI: 10.1021/acs.cgd.7b01389

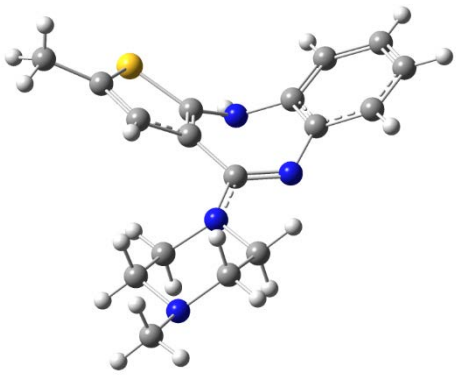

Olanzapine molecule

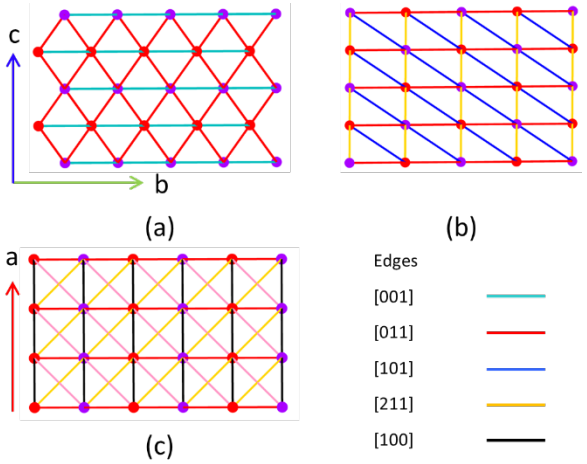

Olanzapine bond chains by face

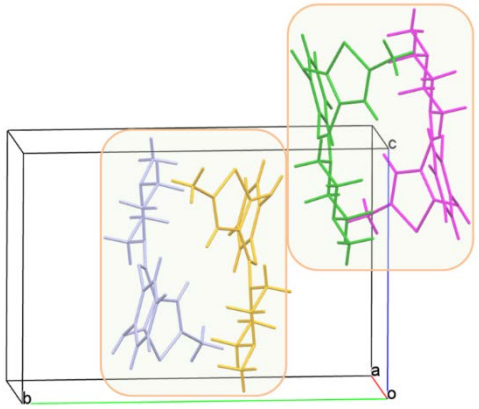

Olanzapine unit cell

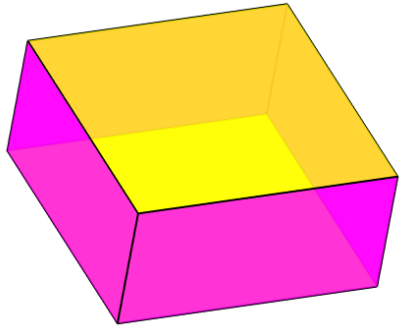

Calculated olanzapine vapor shape

Olanzapine solution shapes (calculated + experimental)

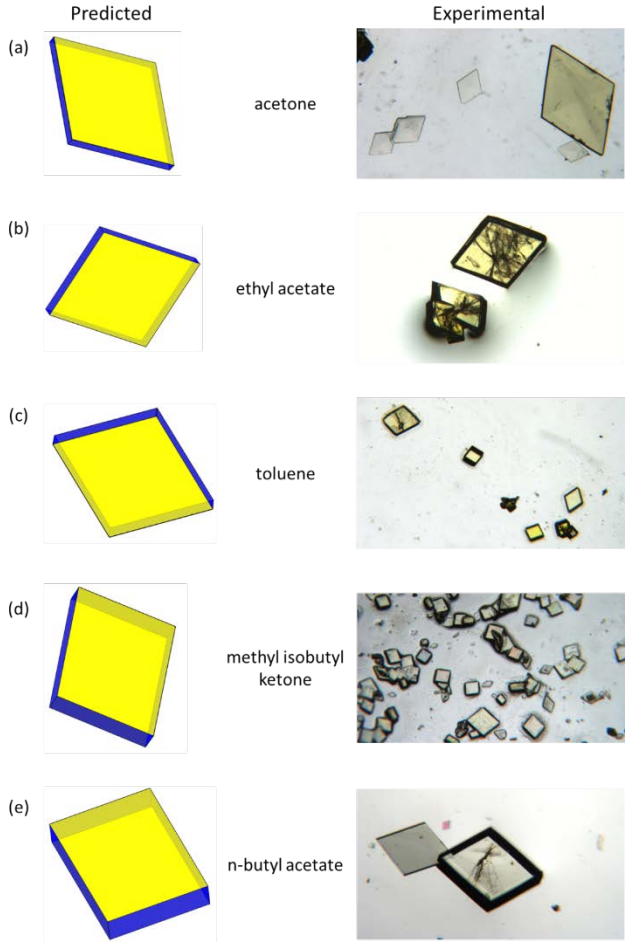

10

Results for NaCl agree with experimental growth rates

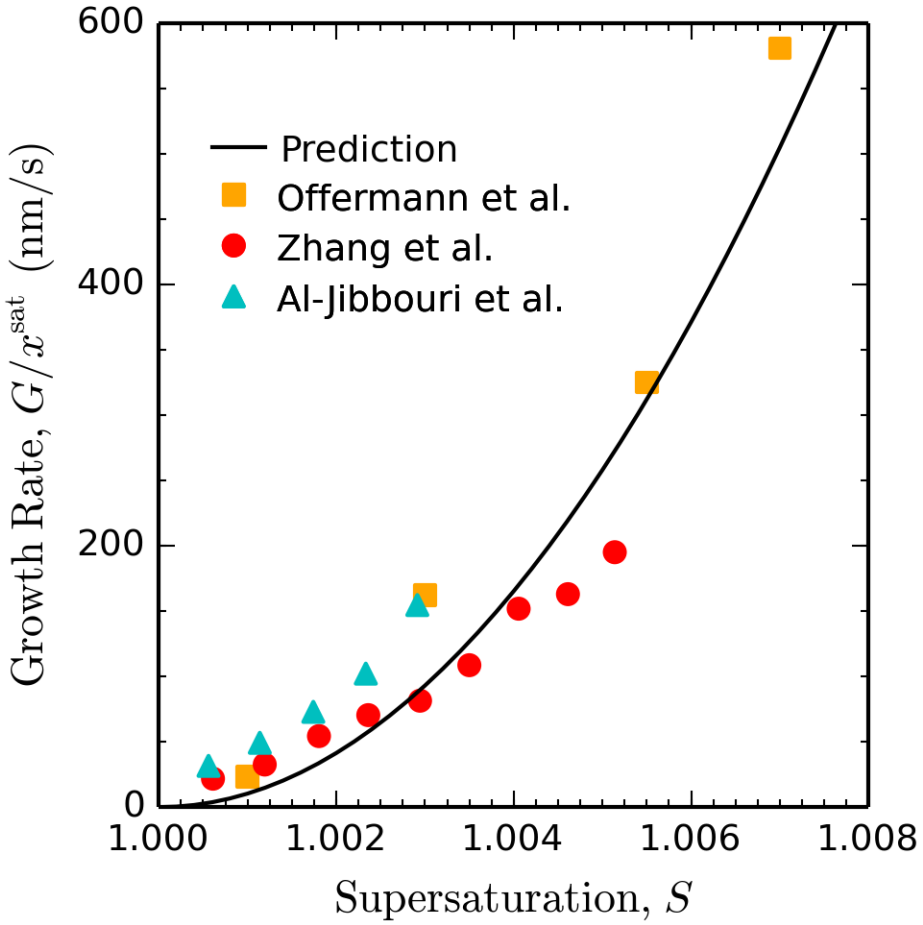

ADDICT could incorporate attachment & detachment model in the future (area of current research)

Absolute growth rate predictions will ONLY be possible using a mechanistic model

Offermann et al. *Cryst. Res. Technol.* 1995, *30*, 651-8
Zhang et al. *Cryst. Res. Technol.* 1996, *31*, 19-25
Al-Jibbouri et al. *J. Cryst. Growth* 2002, *234*, 237-46

Next Steps For 2019

- Test ADDICT for complex crystalline solutes (Z’ = 2 or greater)
- Test for supersaturation-dependent shapes
- Create detailed output and log files (shapes of spirals & 2D nuclei, …)

End

Scale: Crystal

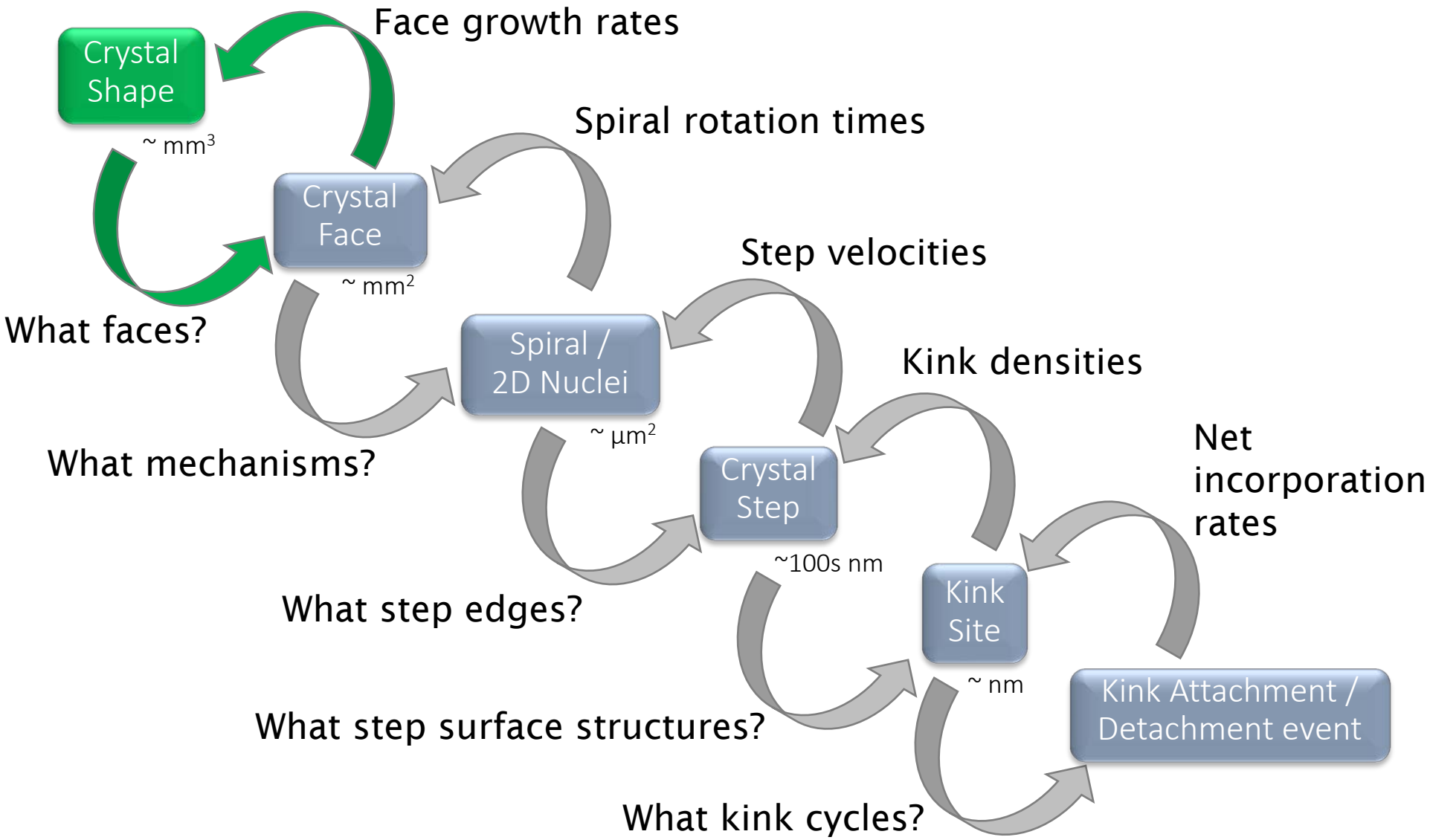

14

Scale: Crystal

The crystal shape depends on relative growth rates

Goal: predict crystal shape
Scale: entire crystal

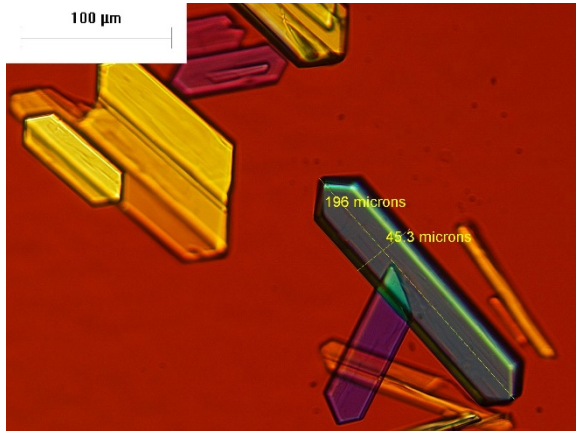

ADDICT

- Predicts faces (space group, energetics)
- Finds edges (energetics, surface physics)
- Calculates growth rates
- Renders morphology

Frank-Chernov condition calculates steady-state growth shape

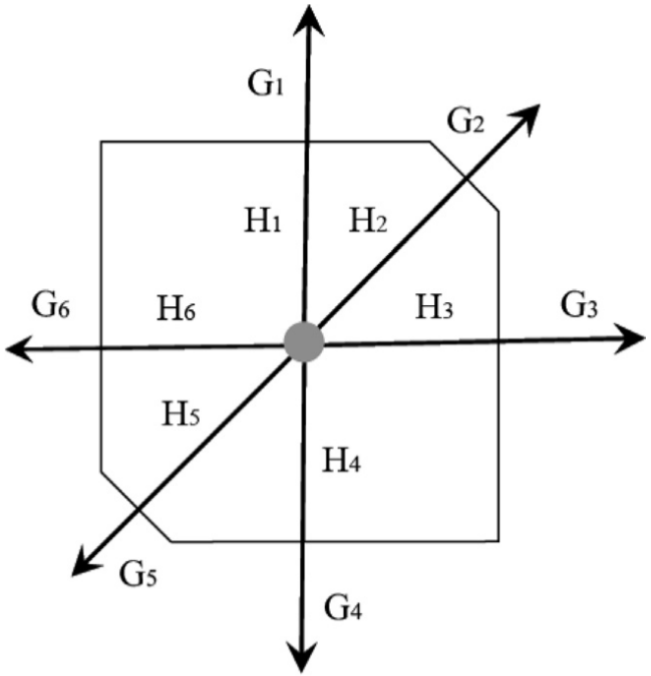

$$\frac{G_1}{H_1} = \frac{G_2}{H_2} = \cdots = \frac{G_5}{H_5} = \frac{G_6}{H_6}$$

Next - reduce modeling scale to a single face

15

Scale: Face

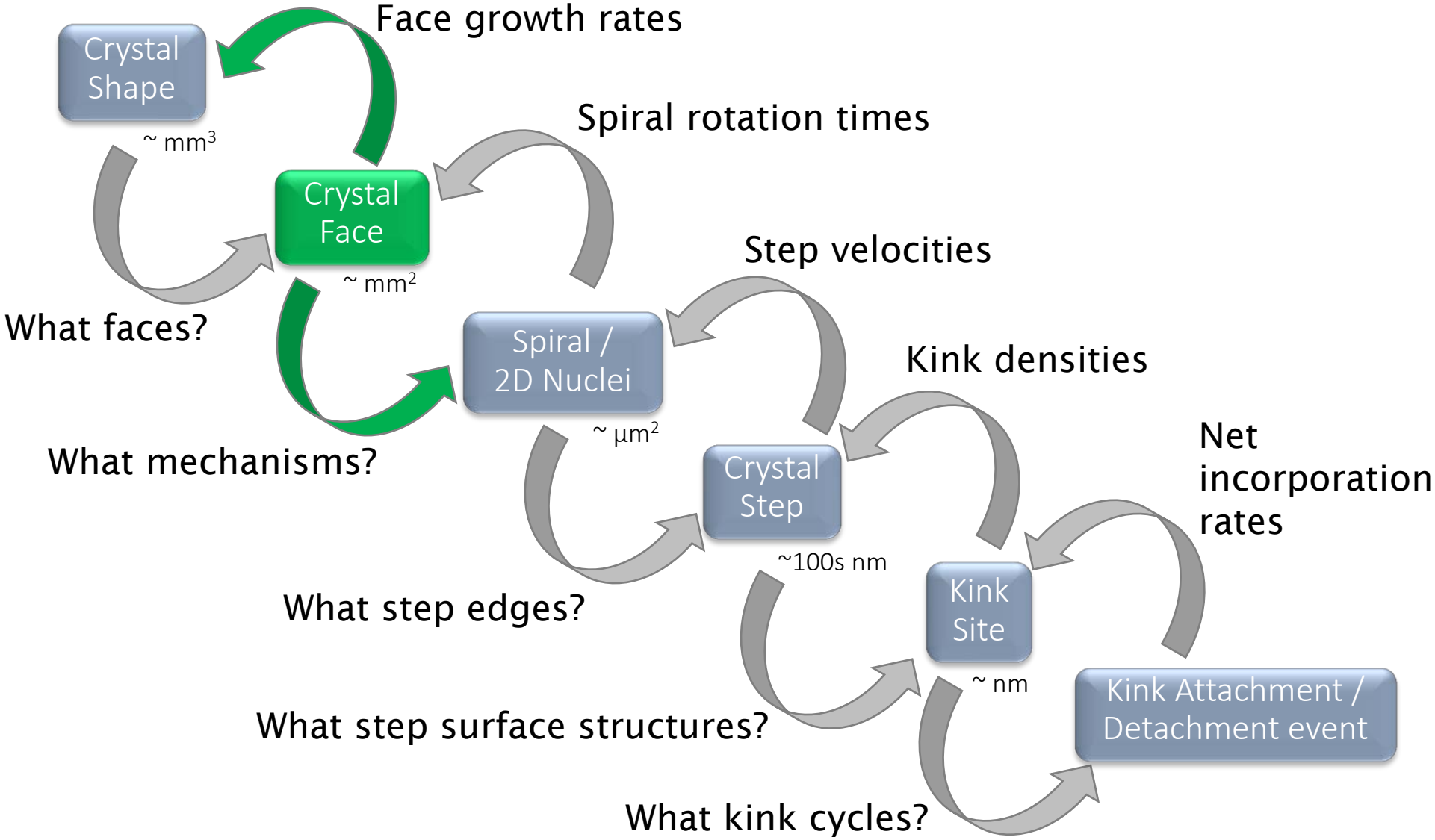

16

Scale: Face

The growth rate of a crystal face depends on which mechanisms are operating

Goal: predict face growth rate
Scale: single crystal face

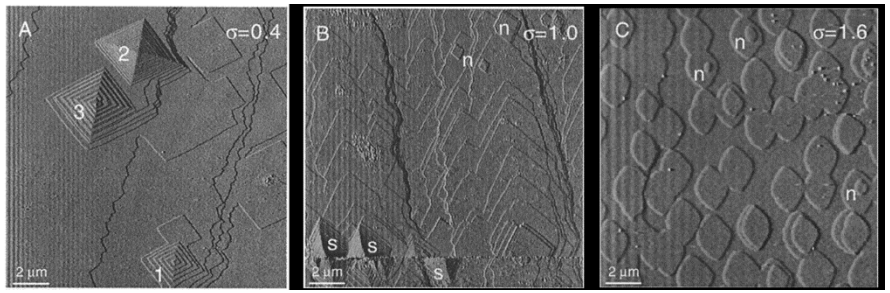

ADDICT

- Finds slice
- Finds step edges
- Calculates growth via multiple mechanisms (spirals, 2D nucleation)
- Predicts fastest (dominant) mechanism

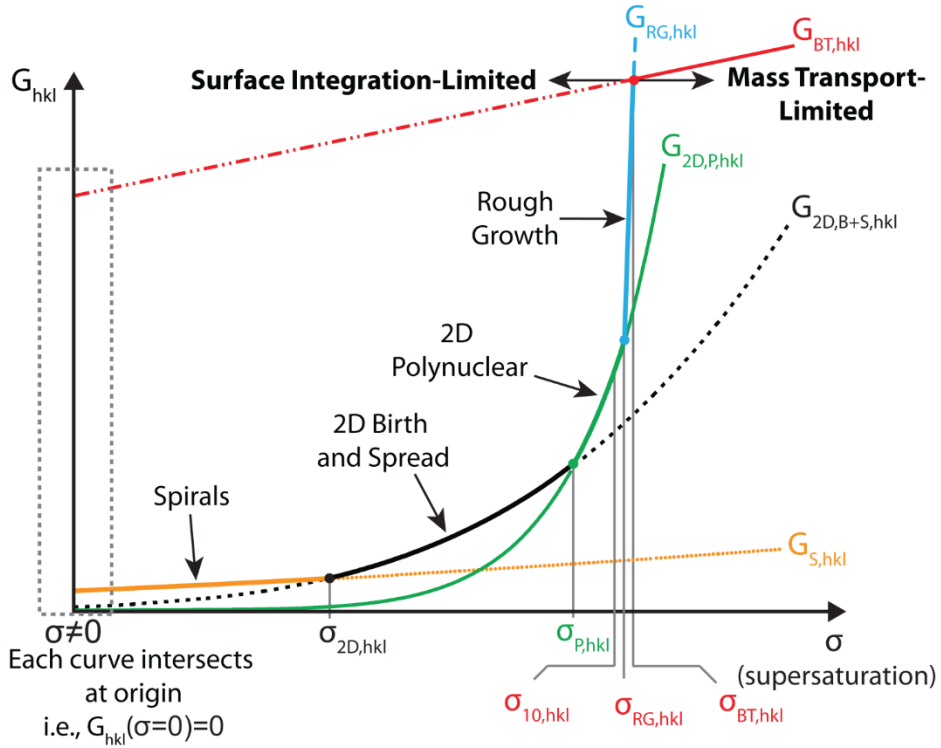

17

Scale: Face

ADDICT contains models for both spiral and 2D nucleation

$$G_{hkl} = \left(\frac{h}{\tau}\right)_{hkl}$$

Interplanar spacing

Time to complete layer (mechanism-dependent)

Spirals

$$\tau_S = \sum_{i=1}^{N} \frac{l_{C,i+1}\ \sin(\alpha_{i,i+1})}{v_i}$$

Time for each side to reach critical length (spiral rotation time)

2D Birth & Spread
(Initial nuclei areas negligible)

$$\theta_{2D,B+S} = \int_0^t JA(t-\tau)\mathrm{d}\tau$$

$$\tau_{2D,B+S} = (Jf)^{-1/3}$$

$$f \equiv \frac{1}{6}\sum_{i=1}^{N} v_i v_i^t$$

Time to cover face with growth of nuclei which form at constant rate J

2D Polynuclear
(Growth areas negligible)

$$\theta_{2D,P} = JA_C\ t$$

$$\tau_{2D,P} = (JA_c)^{-1}$$

Time to cover face with patchwork of critically-sized nuclei

Next – reduce modeling scale to single growth spiral / 2D nucleus

18

Scale: Spiral, 2D Nucleus

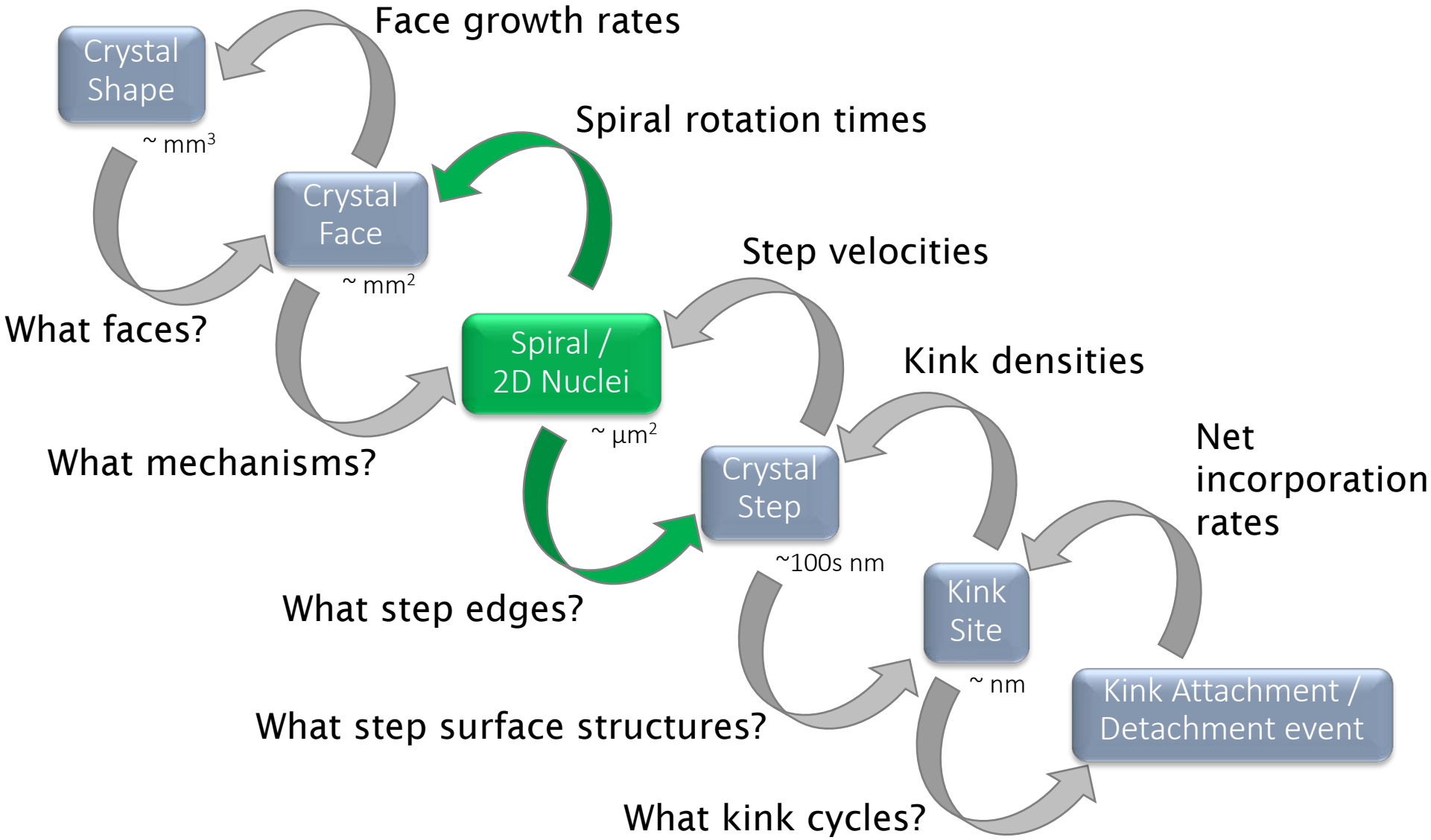

19

Scale: Spiral

Spiral growth depends on step motion around a dislocation

Goal: describe spiral growth
Scale: single growth spiral on surface

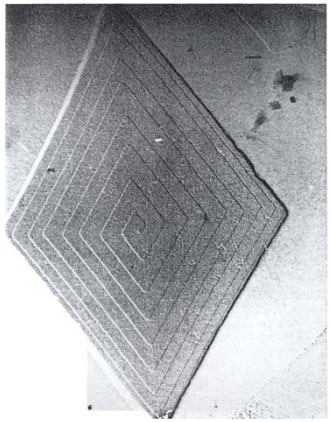

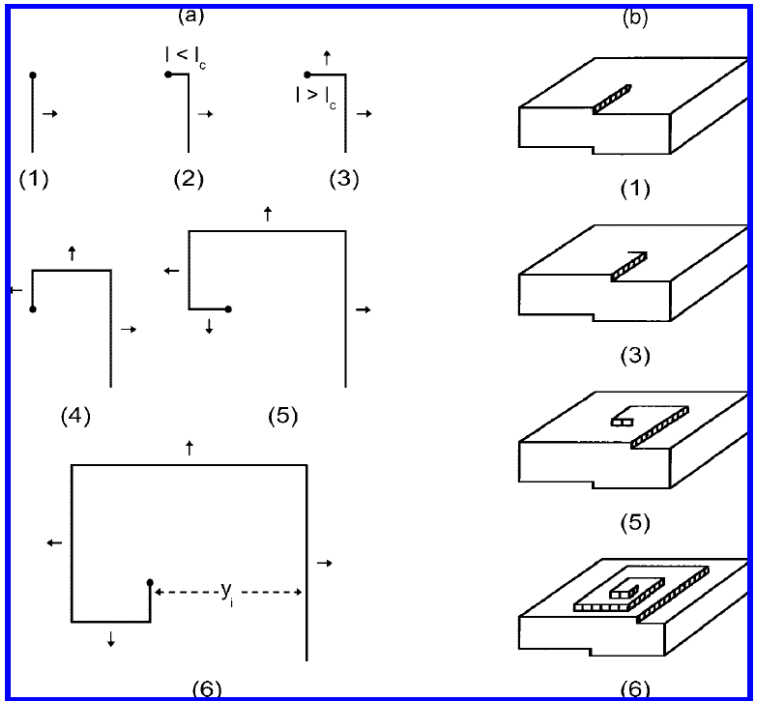

Determine rotation time resulting from successive step emergence

ADDICT

- Calculates angles
- Calculates critical lengths
- Calculates step velocities

Next - reduce modeling scale to a single step

20

Scale: Crystal Step

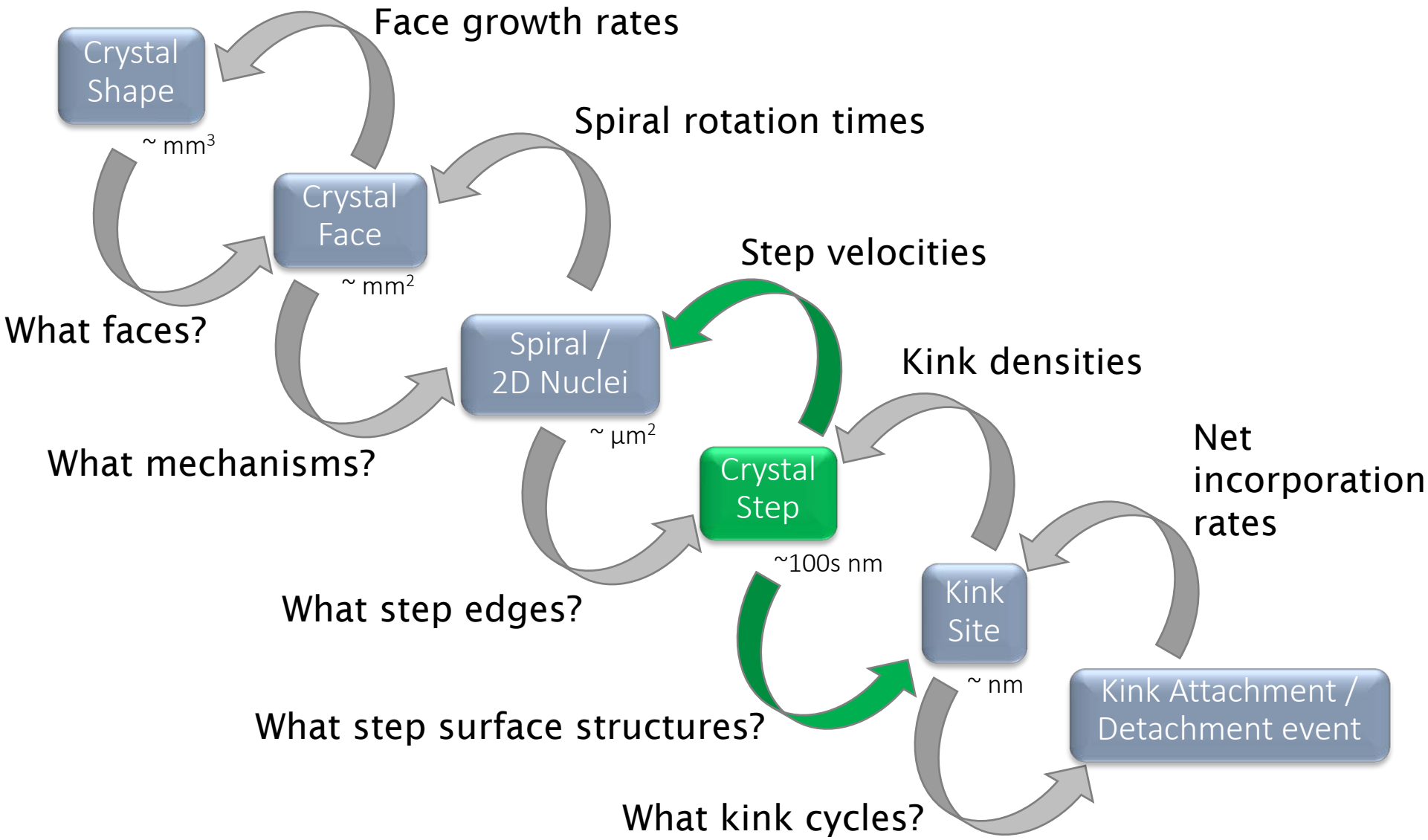

21

Scale: Crystal Step

Steps move due to growth unit incorporation at kink sites

Goal: predict step motion
Scale: single crystal step

Consider number of kinks on step and net speed of each

ADDICT

- Find rows
- Find growth units
- Organize bonds
- Find kinks
- Aggregate effects from all kinks on each step

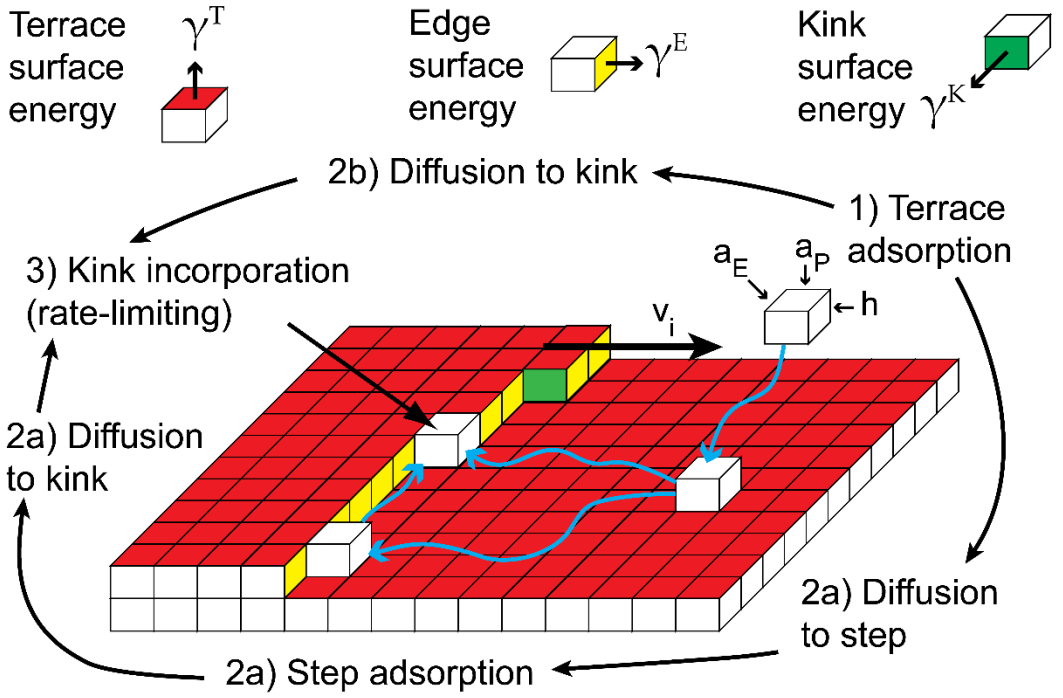

Centrosymmetric step: single kink site
Non-centrosymmetric step: many kink sites!

Next - reduce modeling scale to a single kink

22

Scale: Kink Site

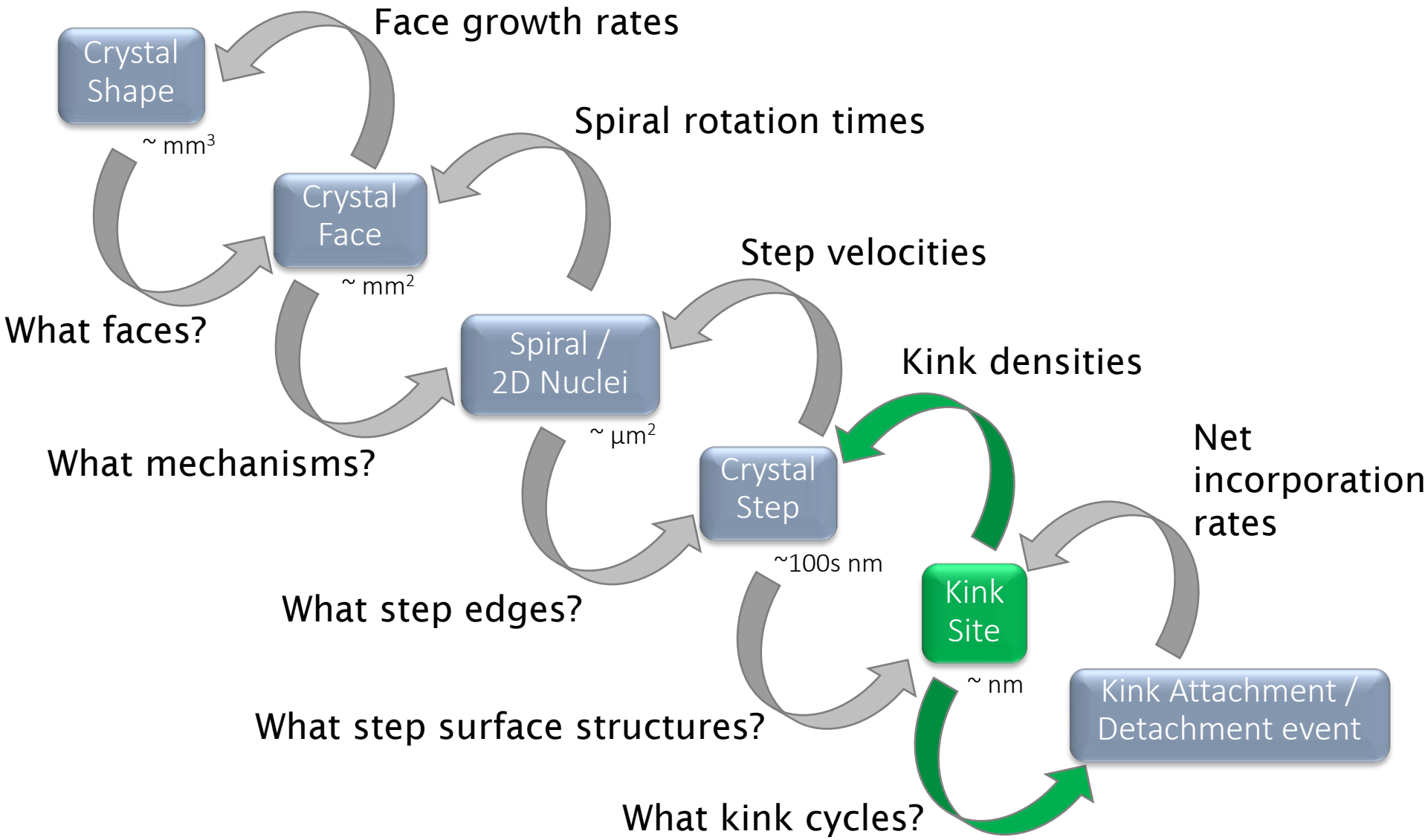

23

Scale: Kink Site

The net incorporation rate at kink site results from cycles of attachment

Goal: predict kink motion
Scale: kink site

$$u_i = n \frac{(j^+)^n - \prod_{k=1}^{n} j_{k,i}^-}{\sum_{r=1}^{n} (j^+)^{n-r} (j_i^-)^{r-1}}$$

ADDICT

- Calculate surface energies
- Calculate kink density
- Calculate net incorporation rates
- Calculate transformations / annihilations

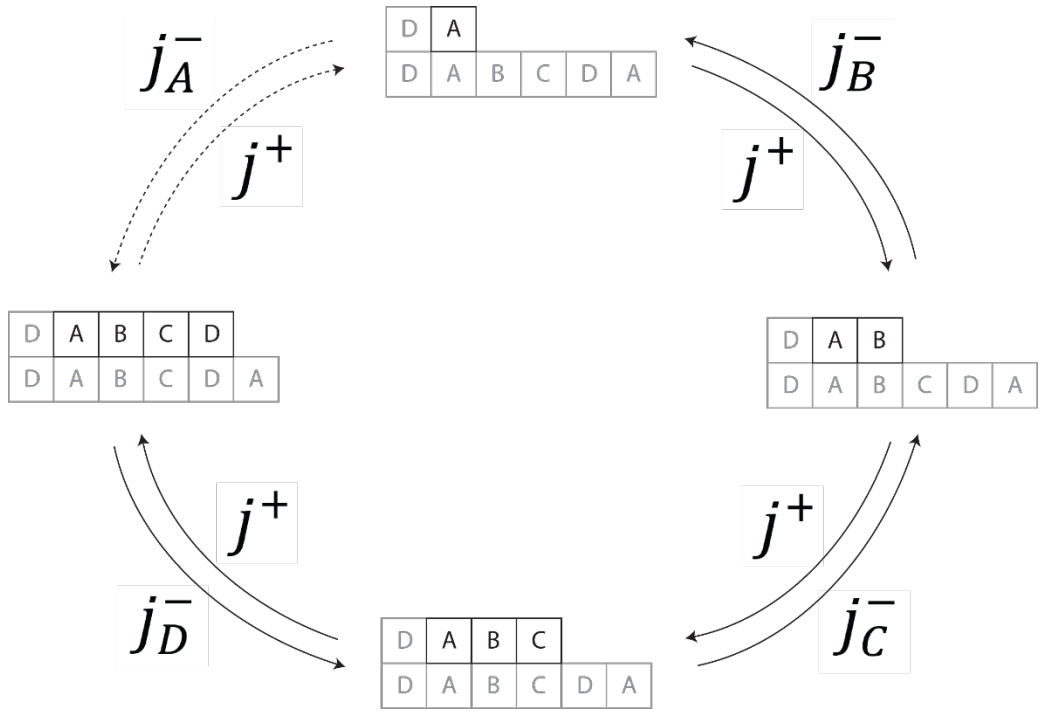

Next - reduce modeling time scale to single attachment/detachment event

24

(Time)Scale: Kink Attachment/Detachment Event

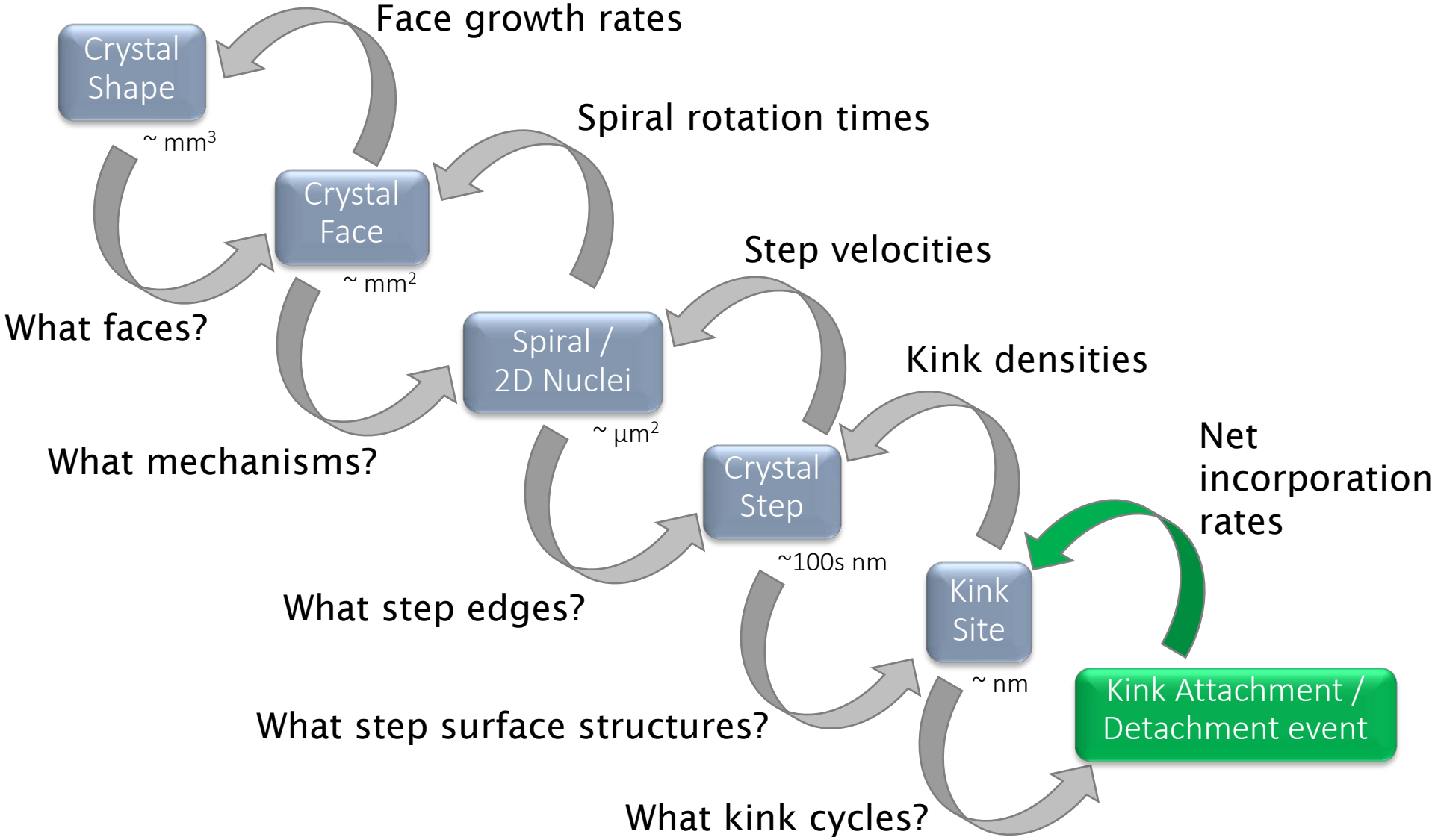

25

(Time)Scale: Kink Attachment/Detachment Event

Kink attachment is limited by desolvation kinetics

Goal: predict rate of event
Scale: single molecular event

ADDICT

- Estimates detachment work

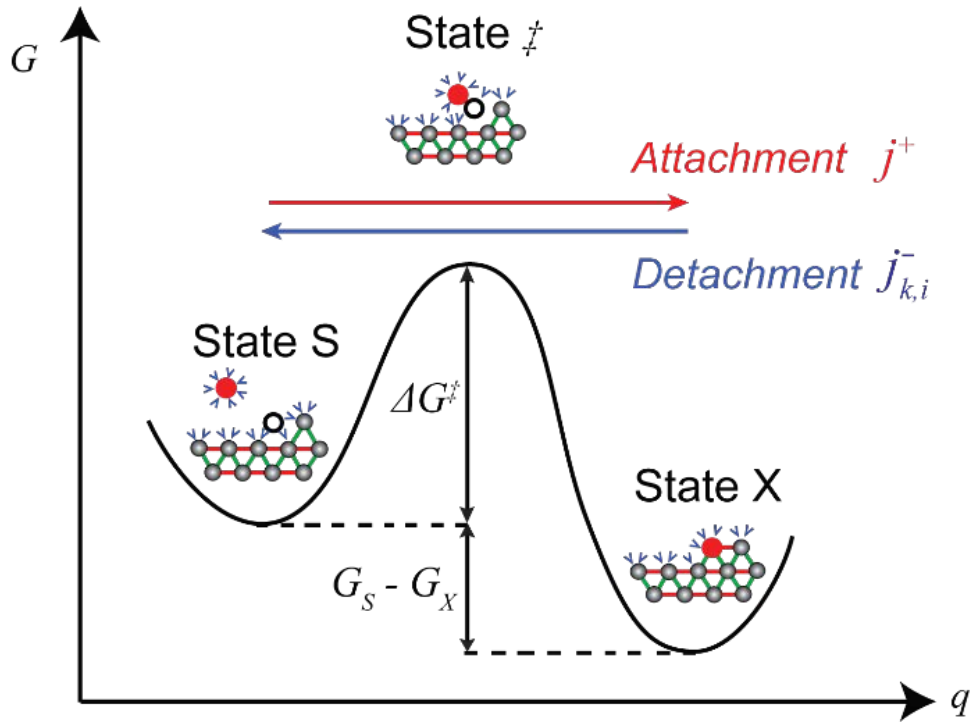

Current assumption: isotropic desolvation barrier (enables relative growth rates, not absolute)

26

ADDICT is a shape prediction tool

Computational screening can **target** experiments

Inputs

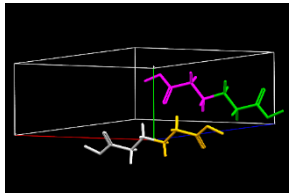

Crystallography + Growth conditions
- Solvent
- Supersaturation
- Temperature

ADDICT

Interpret crystal	Energetic calculations	Mechanistic models
• Describe growth units	• Organize interactions	• Spiral growth

Outputs

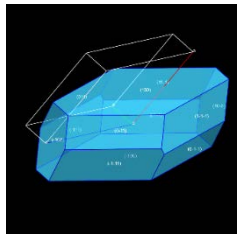

Crystal shape
Lattice energy
Spiral & 2D nucleation and growth shapes
Mechanistic info (faces, steps, kinks etc.)
Morphology map

Question:
How can we engineer the morphology by changing growth conditions?

ADDICT:
Fast computational screening + mechanistic insight into modifications can aid selection of growth conditions

27

Then use solvent sweep to shortlist solvents

Investigate shortlisted solvents experimentally

Crystallography

- Specific polymorph
- Pure organic molecule
- Future: cocrystals/ solvates, organic salts

Growth conditions

- 47 solvents
- Supersaturation
- Temperature

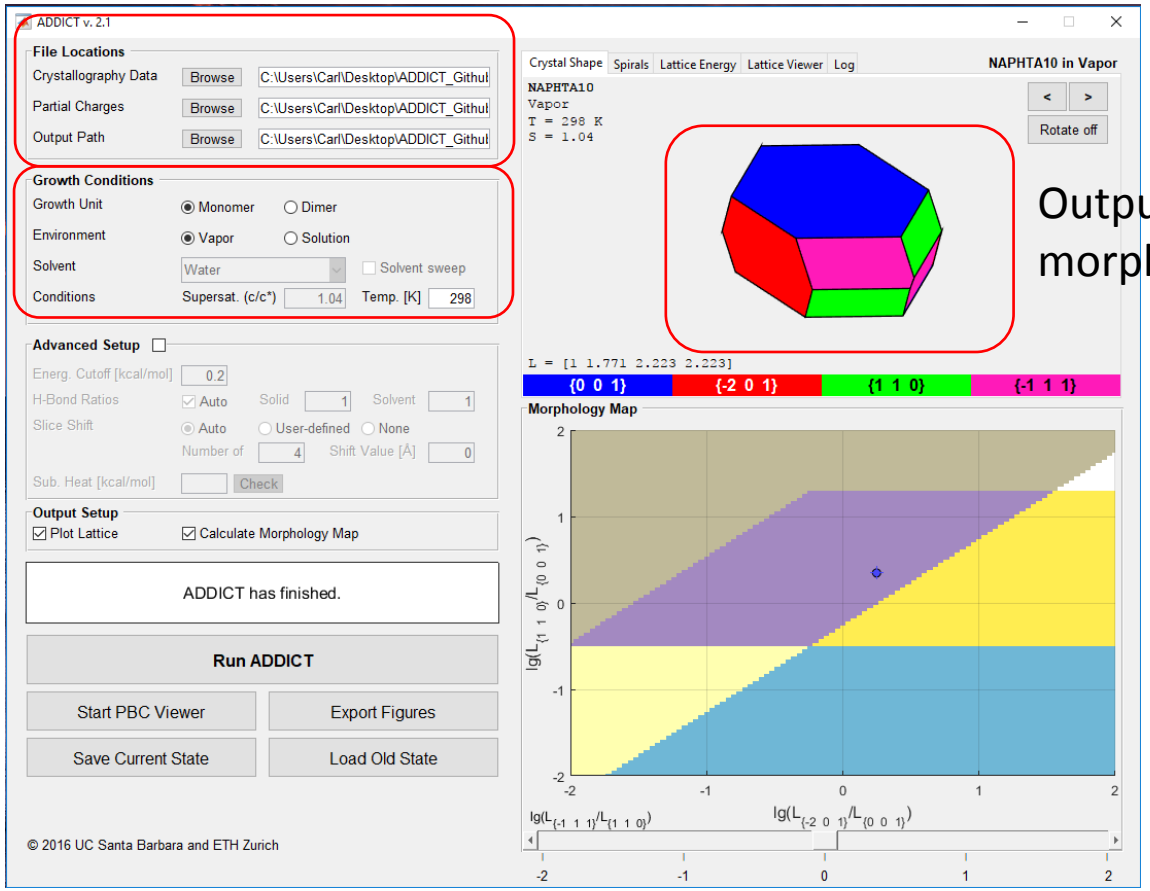

Output = predicted morphology

Morphology map plots results of solvent sweep

28

Morphology map can display hypothetical morphologies

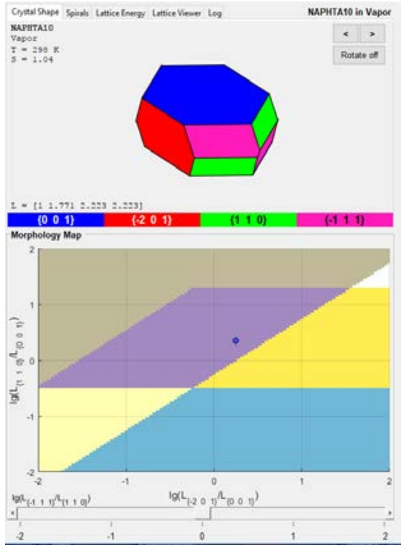

Predicted

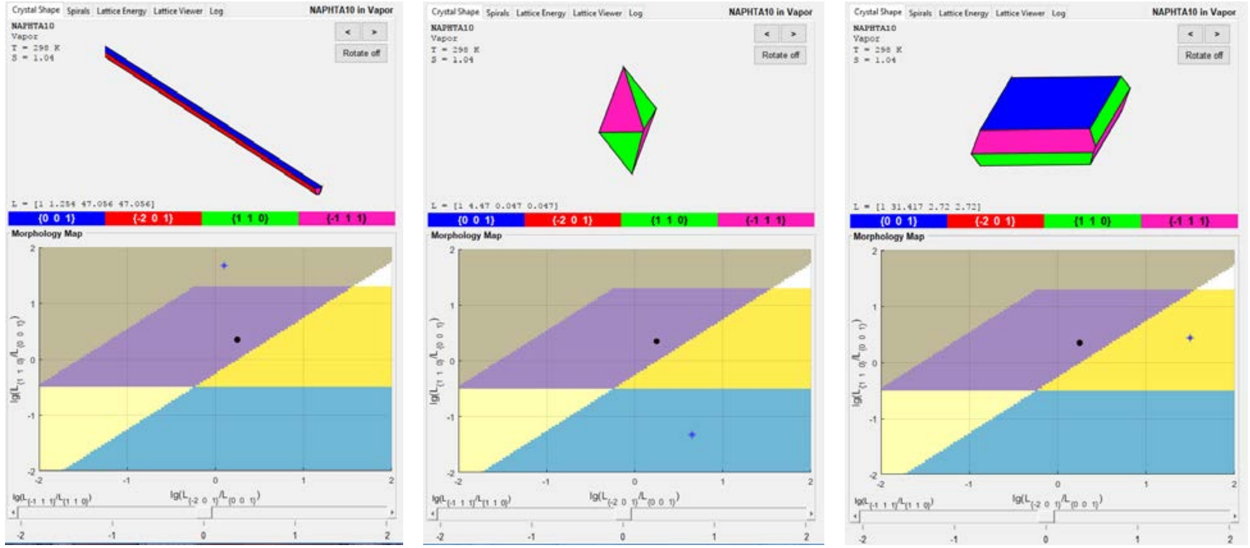

Hypothetical

Predicted morphologies plotted on map, but can explore map to find improved shapes

Map may provide insight about how to modify growth conditions
(what relative face growth rates are needed?)

29

ADDICT crystallography input = mol2 file of unit cell

Obtained using Mercury

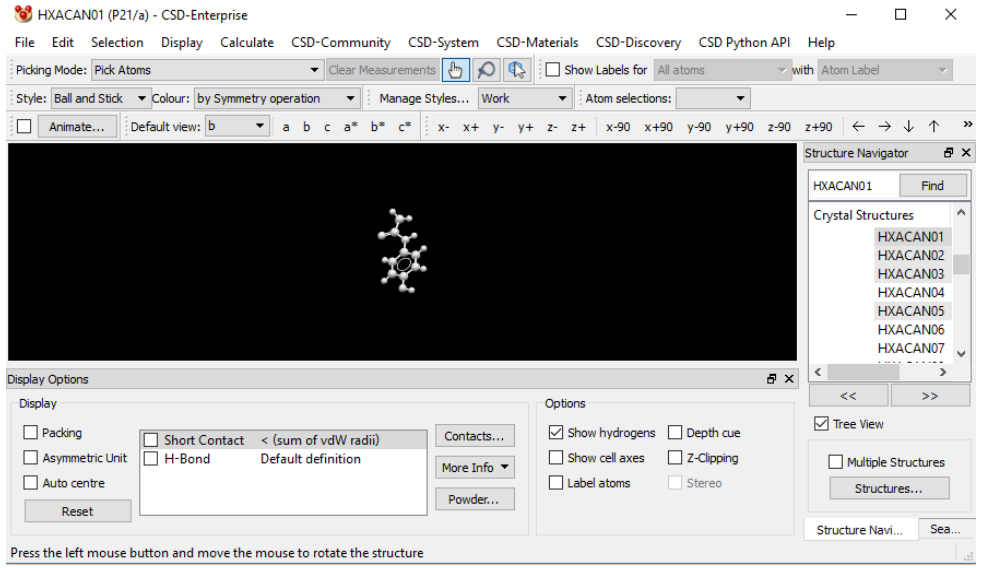

1. Open CIF file in Mercury

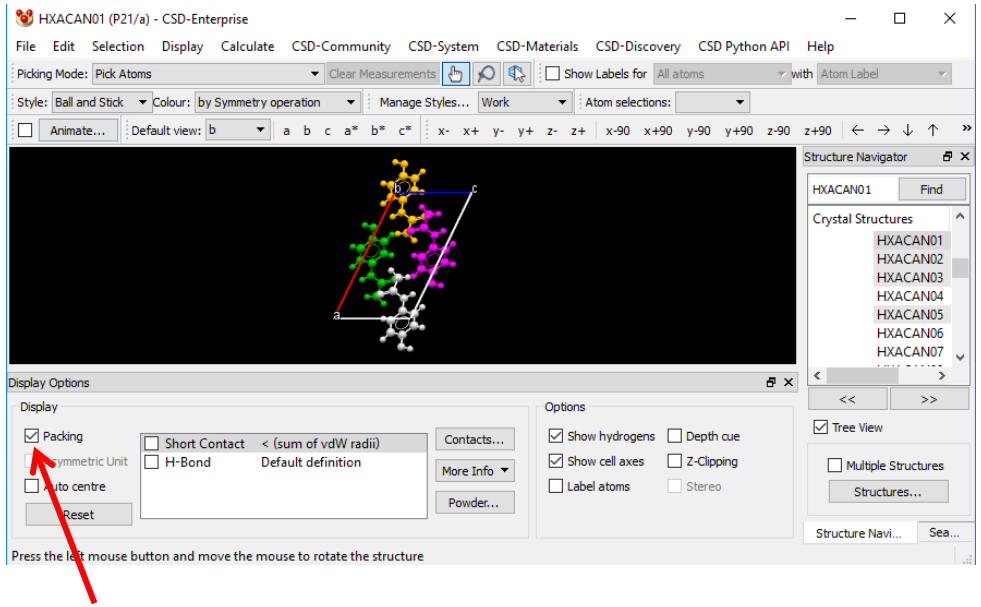

2. Click packing and save as .mol2 file

We designed our input to be the crystallographic unit cell so ADDICT can be extended to cocrystals, solvates and organic salts in the future (these have complex asymmetric units)

30

ADDICT Architecture

Phase 1: Interpret crystallography

- Obtain complete description of physical crystal growth units in the cell

Phase 2: organize energetics

- Calculate energetics
- Create faces, organize interactions, find slice
- Find bond chains and select step edges
- Implement solvent effect

Phase 3: implement mechanistic model

- Calculate Boltzmann step distribution
- Calculate incorporation rates
- Calculate step velocities
- Calculate spiral rotation time and 2D nucleation coverage time
- Calculate relative growth rates

31

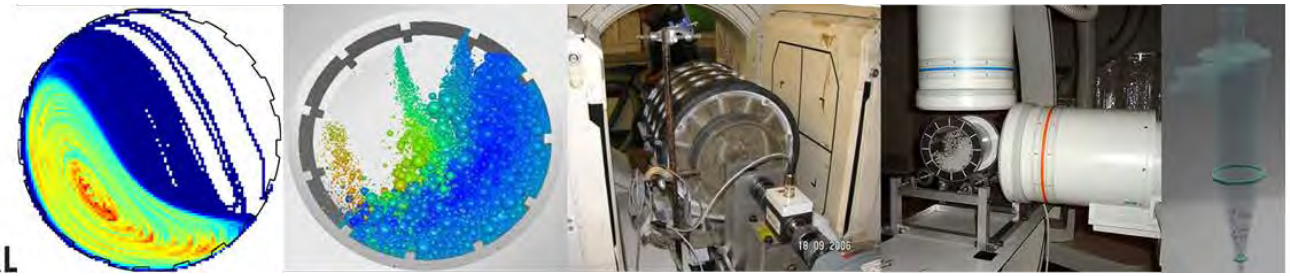

Particle Technology Group

Mixing Rules for Powder Mixing (Phase 1): A PEPT Investigation of a Binary Mixture

By

Indresan Govender, Suren Moodley, Marcelle Pillay, Malcom Rengasamy

International Fine Particle Research Institute

Outline

- Tracking techniques employed by the Particle Technology Group (PTG)
- Experimental Program
- Typical mixing ingredients derived from PEPT data

Bi-planar X-Ray Imaging

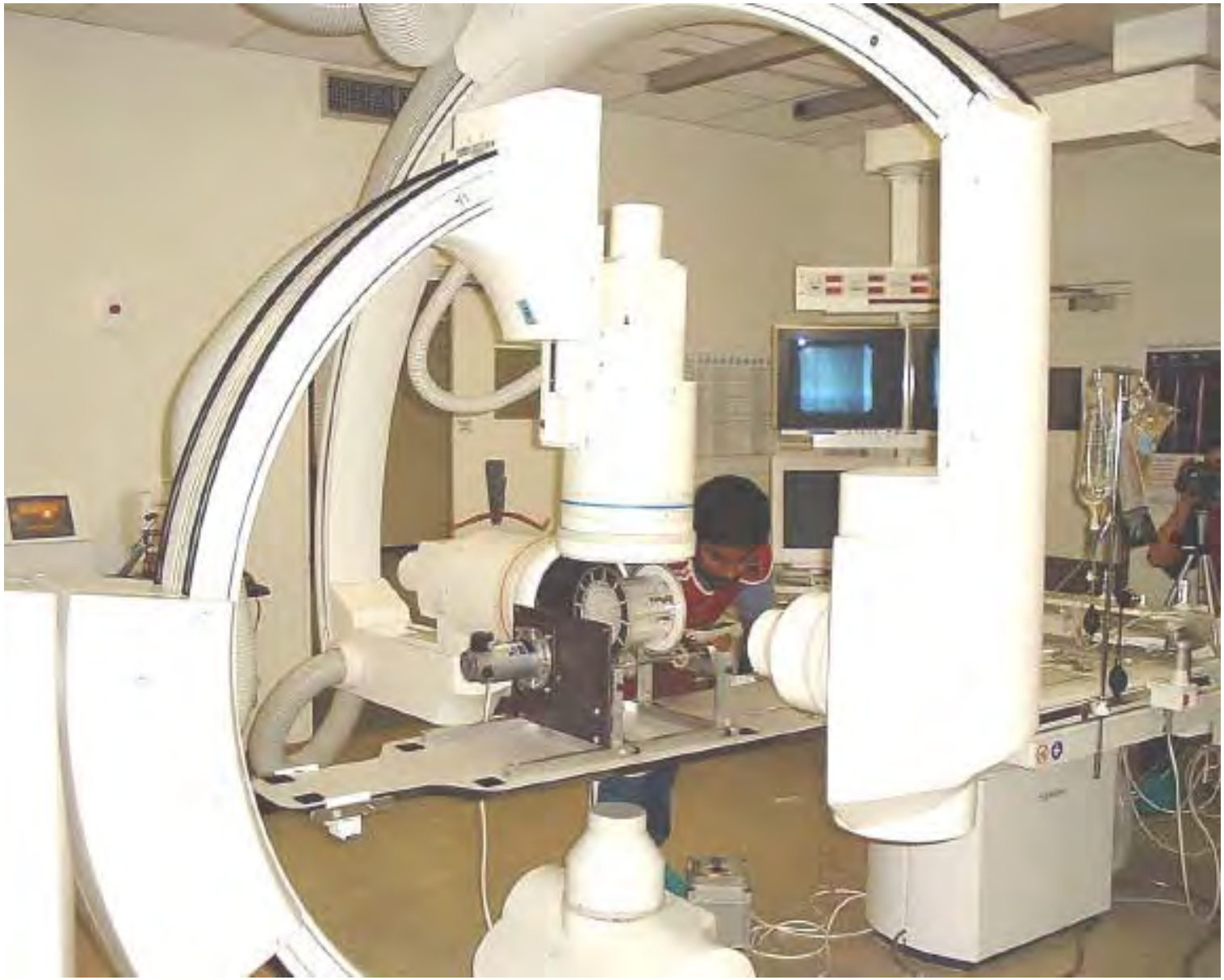

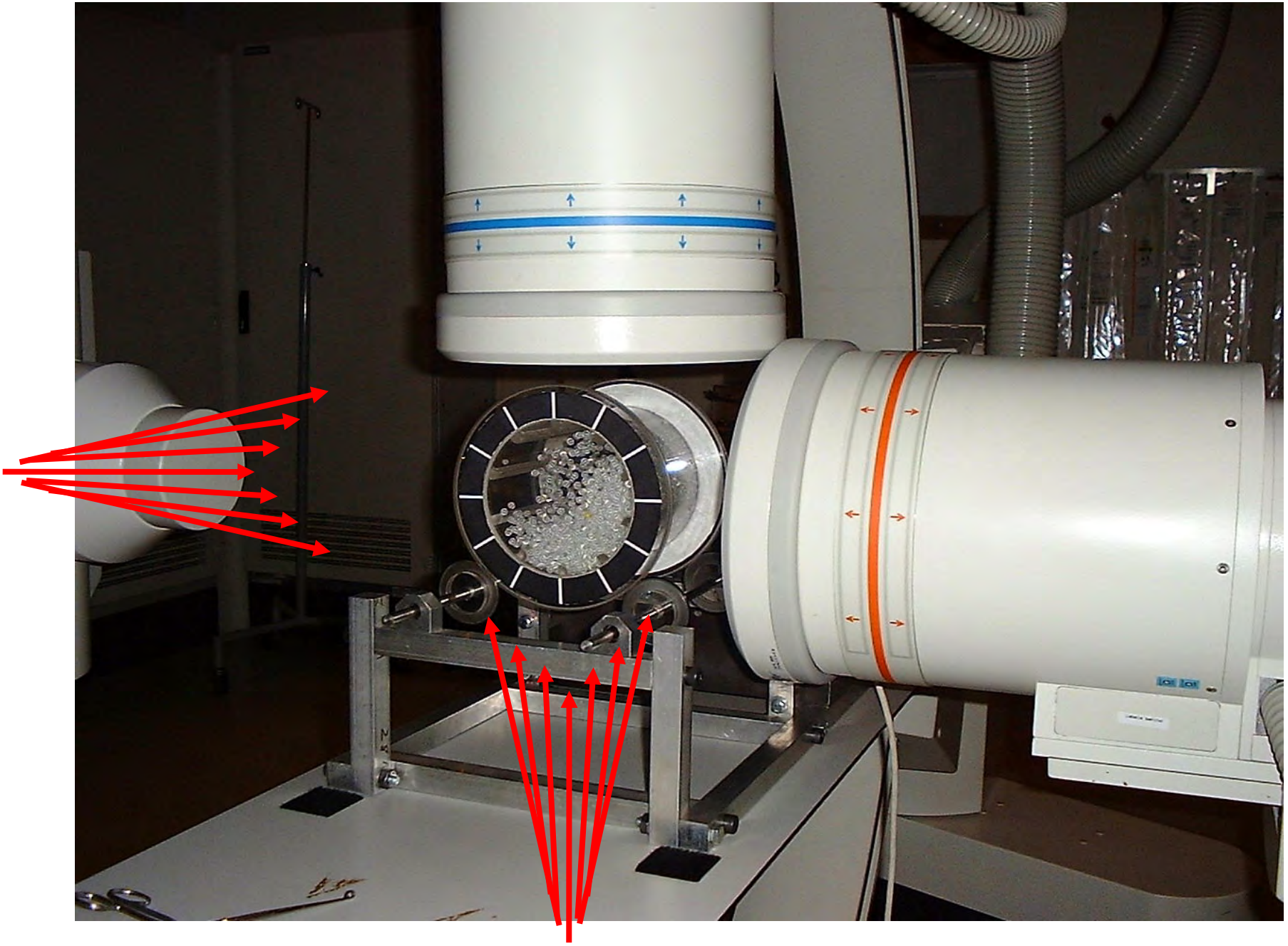

3D reconstruction

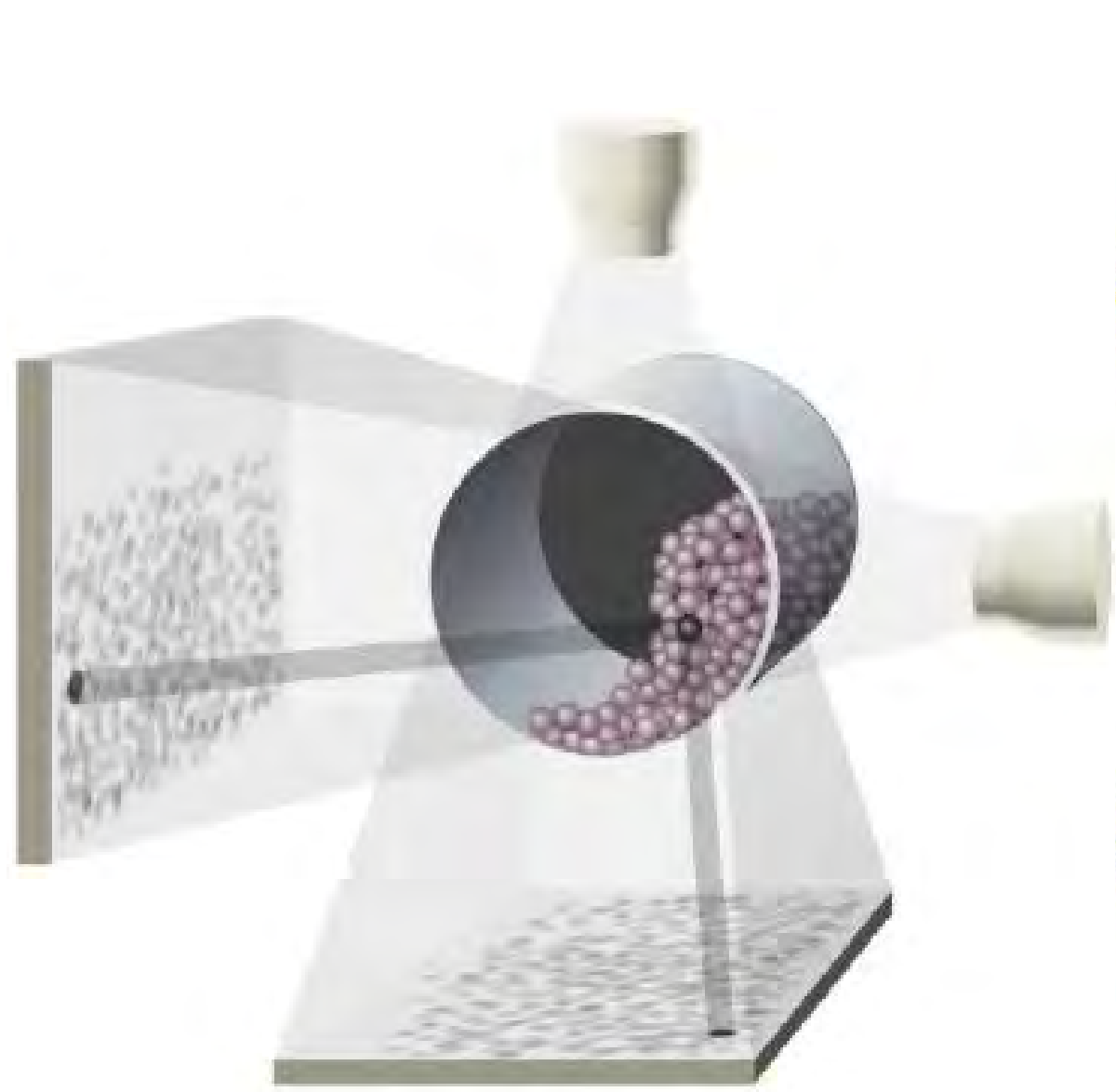

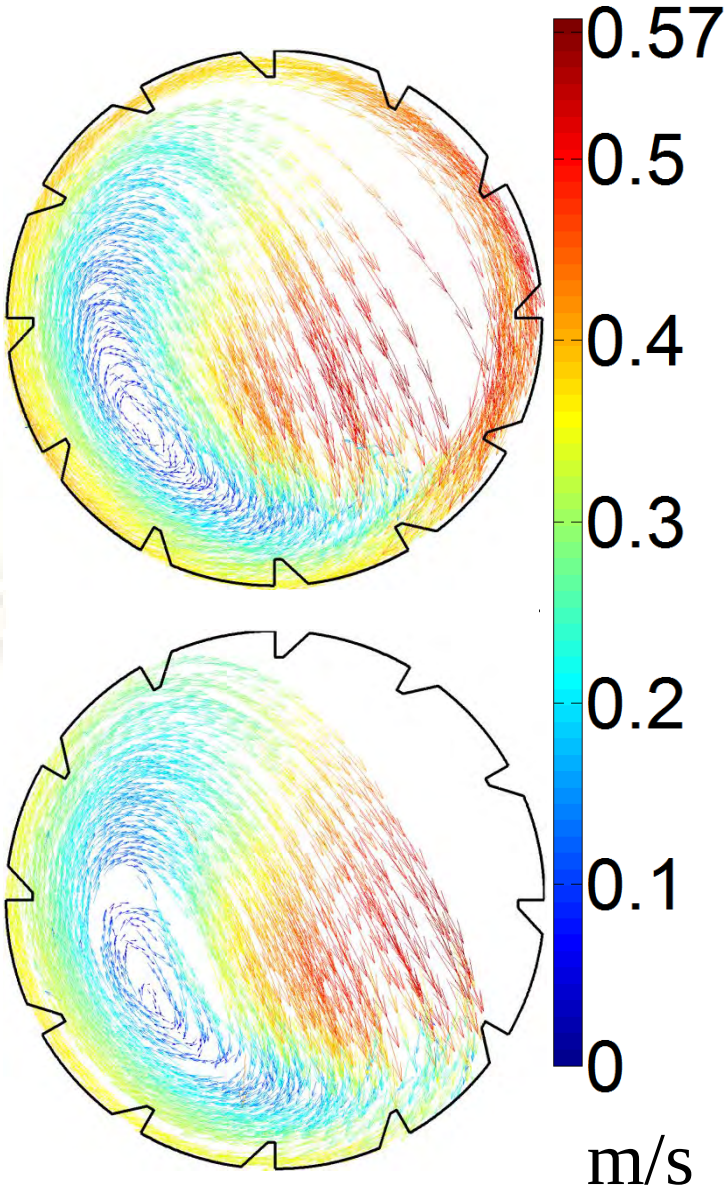

Positron **E**mission **P**article **T**racking

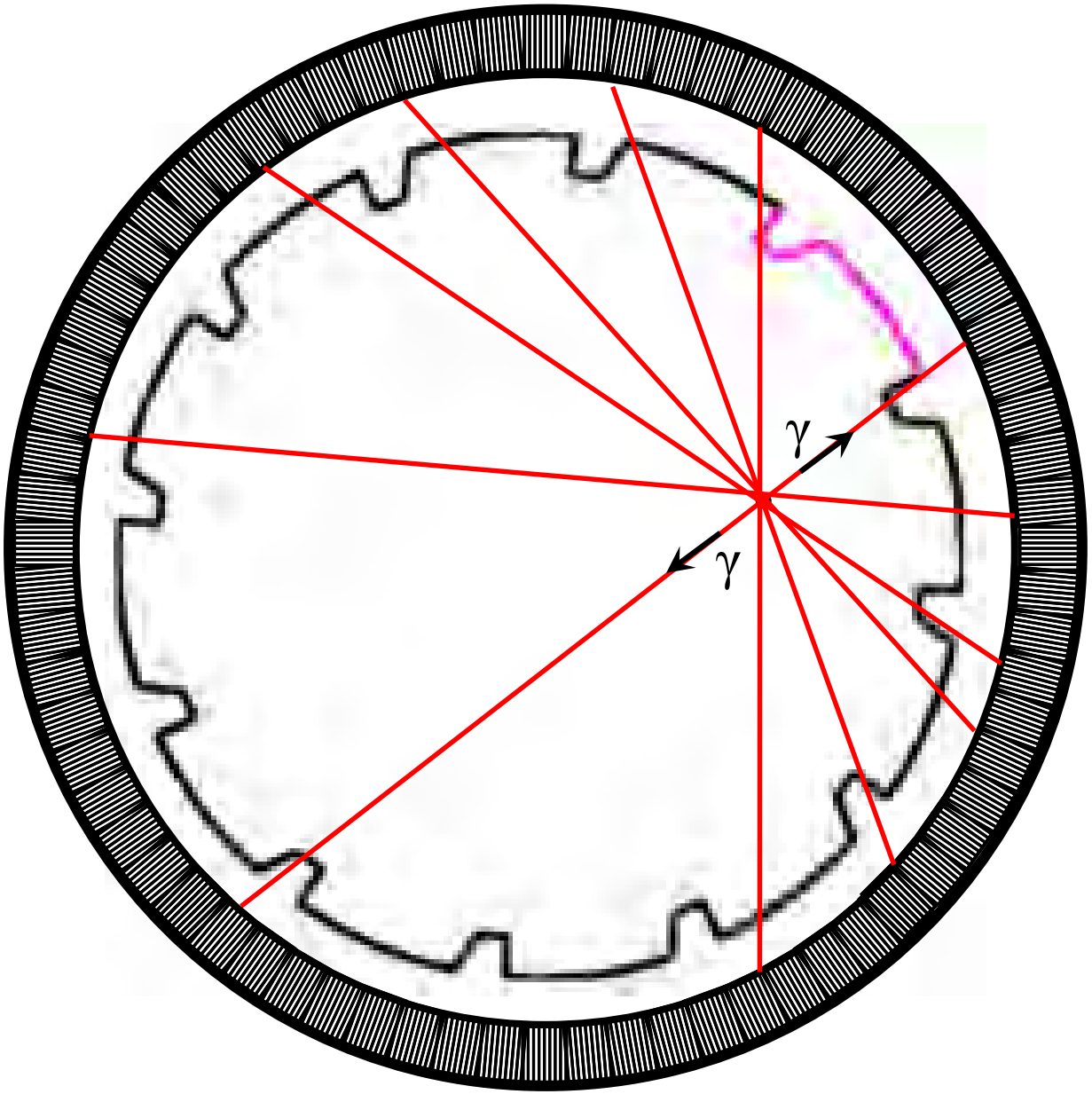

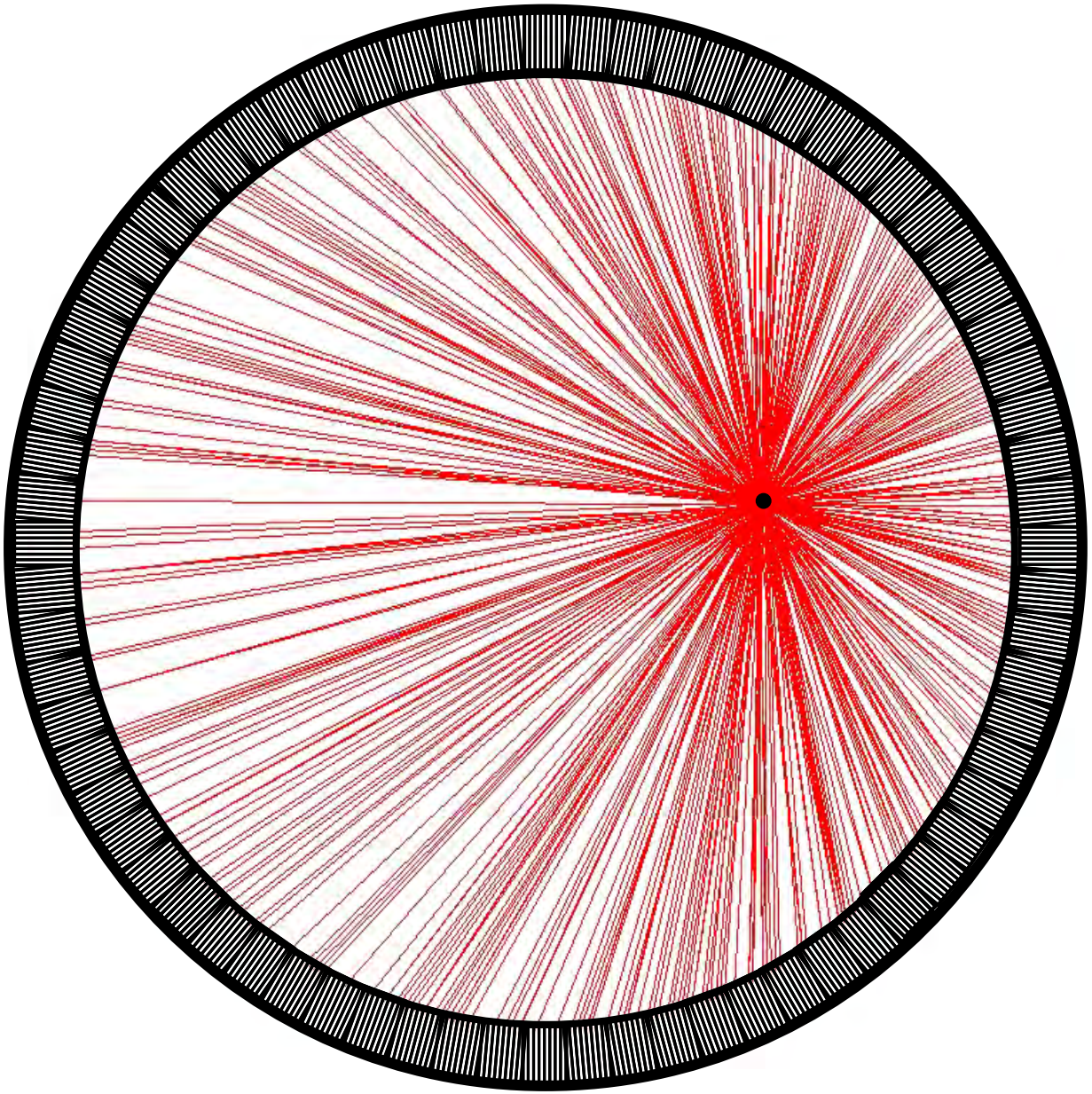

PEPT camera

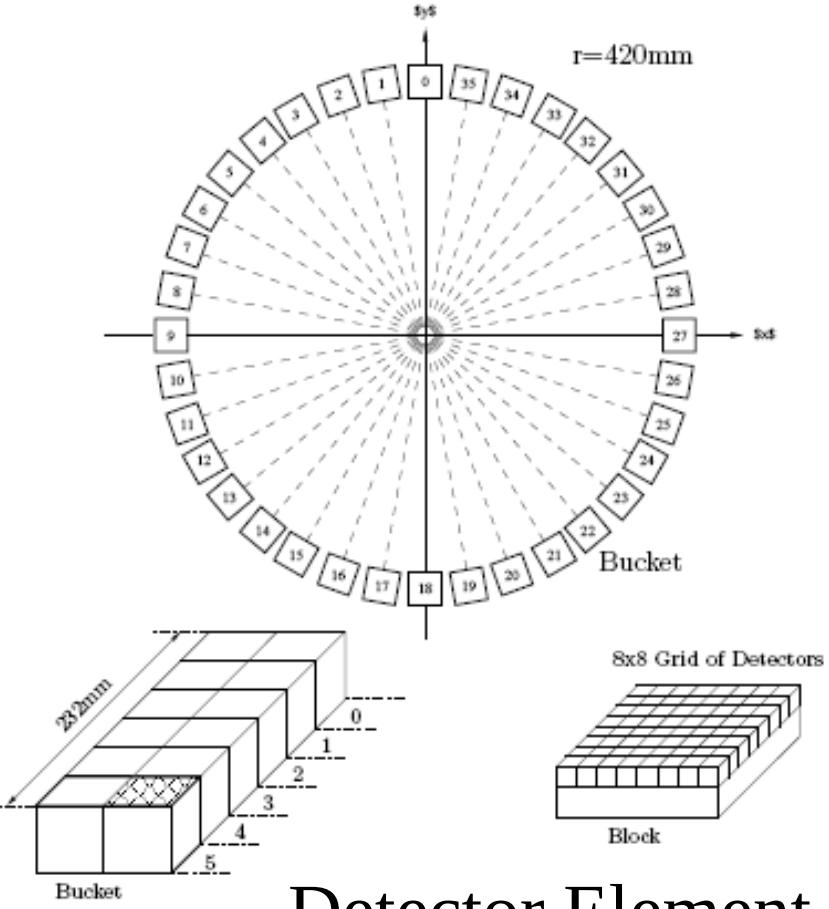

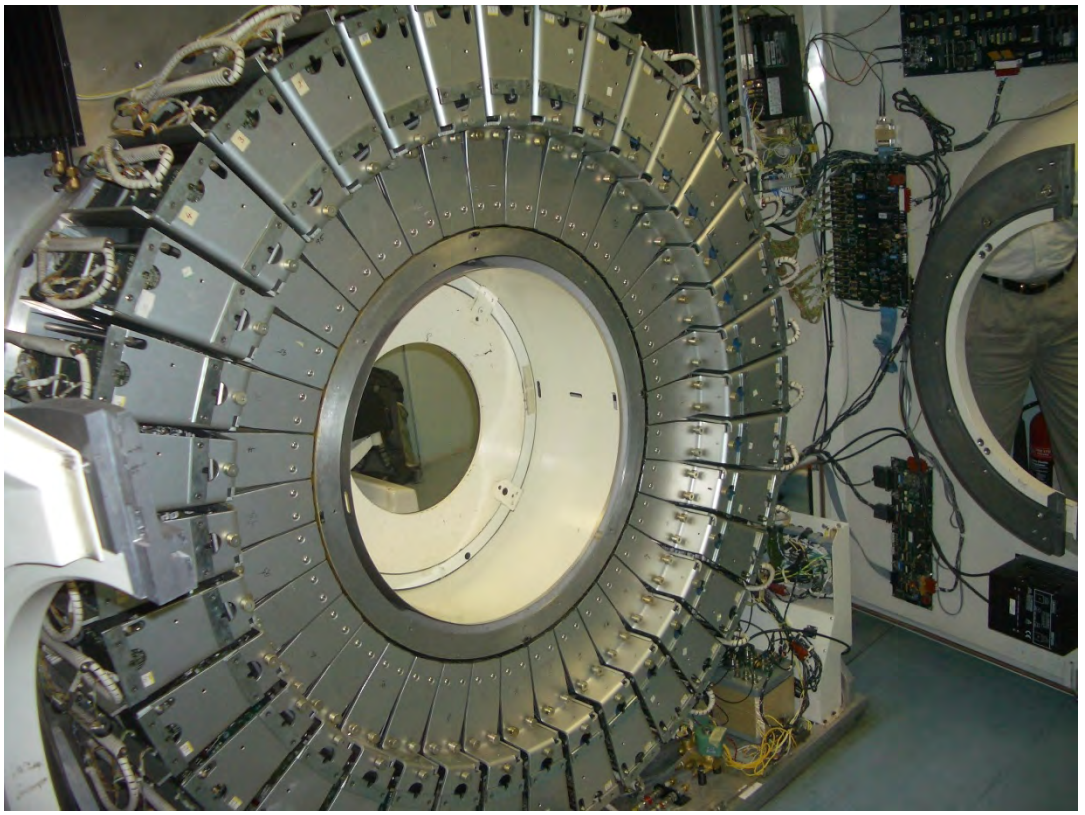

Detector Element size = 4.8mm x 4.8mm

# of detector elements = 36 x 12 x (8x8) = **27648**

Max LoR's per second = 4 Million!

Tracking statistics

Resolution: < 1 millimeter

Frequency: ~ 1 millisecond

Tracer Size: 20 μm (minimum)

Tracer type: anything!

# of tracers: currently 20 (aim for 100)

System size: ≤ (500mm × 230mm)

Cyclonic Flow

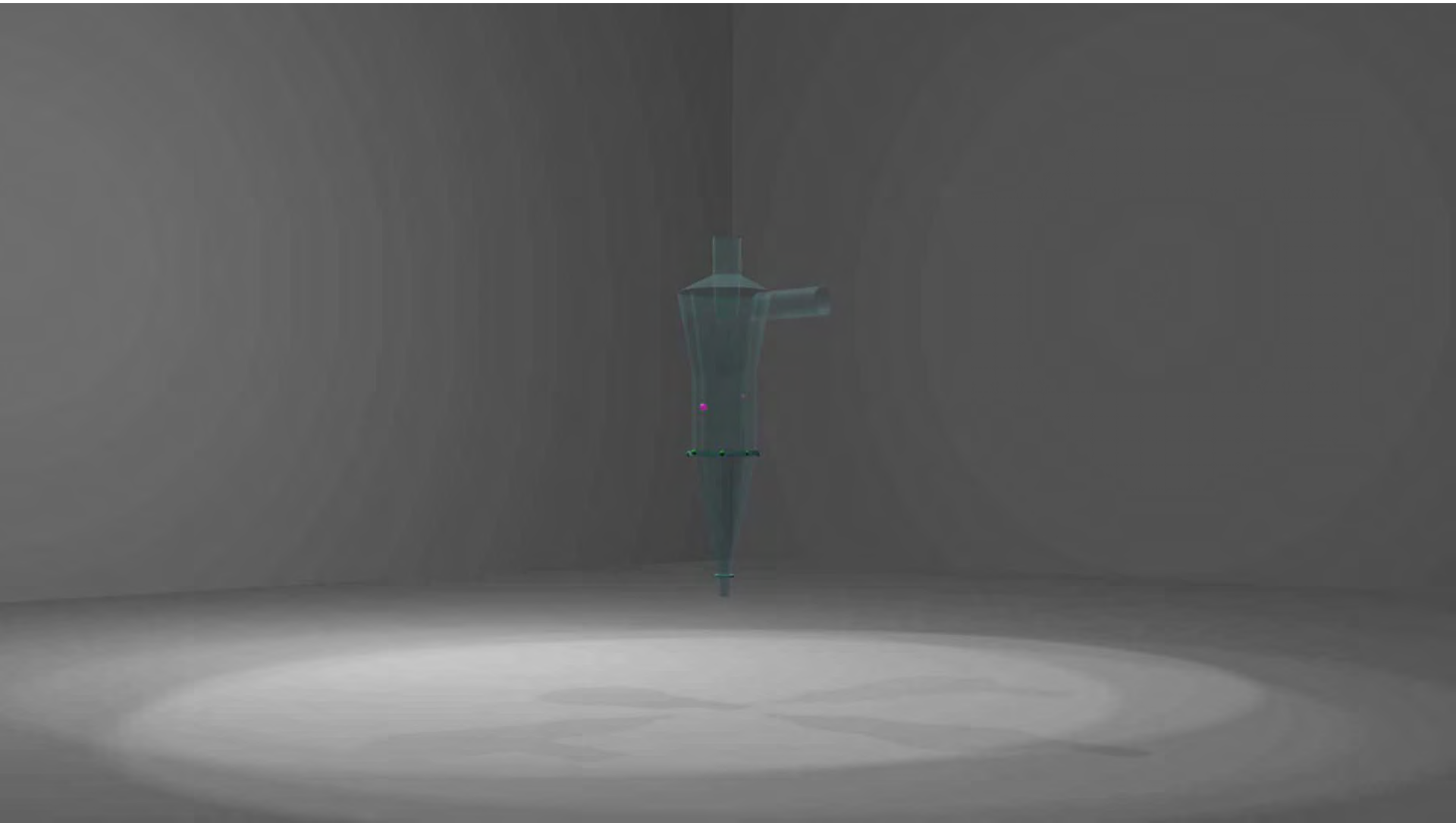

Multiple Particle Tracking

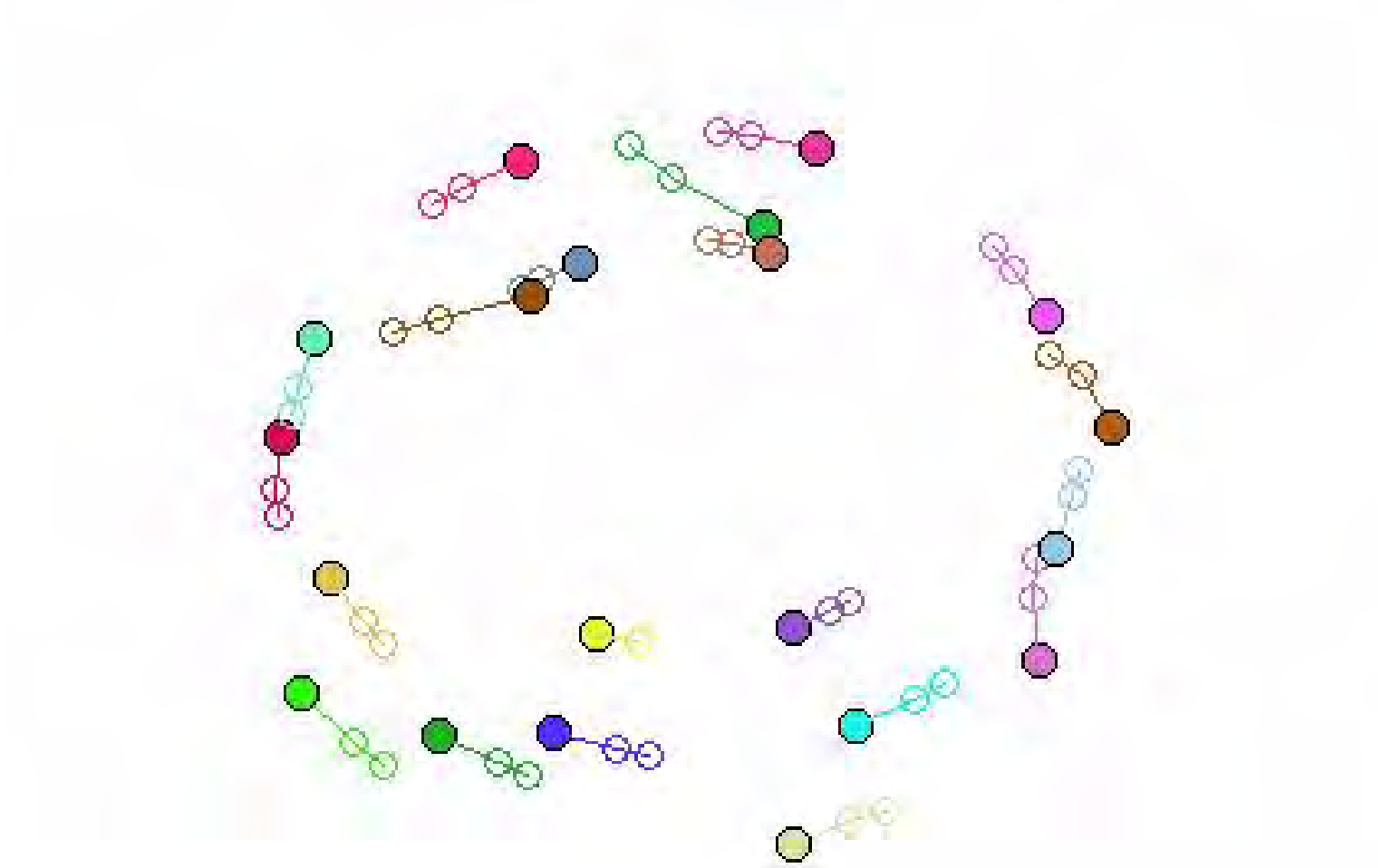

Ergodicity

<u>Under steady state conditions</u>:

- Compute the ***time-averaged*** behaviour (velocity, acceleration) ***per voxel*** from a single representative PEPT tracer.
- ***voxel size*** = length scale of continuum model
- If we have tracked for long enough (usually ~ 2 hrs), then we assume:

Averaged quantities per voxel = Ensemble average

<u>This is the Ergodic Hypothesis (for continuum modelling)</u>

Experimental Program for IFPRI

1. The experimental matrix is large (R672k=$53k US); cross subsidised from other projects with similar interests (DBM; Mintek; SAMMRI)
2. Experimental program:
   a) 56 runs (4 runs per day) = 14 days of experiments + 3 days for repeats of failed days
   b) Data pre-processing—from back-2-back gamma rays to [x, y, z, t]—takes around 2-4 weeks (depends on data & student quality)

3. Provisional analysis performed with two 4th year Chemical Engineering students (Malcom and Marcelle) & a PhD candidate (Suren)
4. Experimental program completed to date:
   a) Binary mixture of 3mm & 5mm plastic beads = equal by mass
   b) Load (%): 10, 20, 30, 40
   c) Speed (% crit): 40, 60, 70, 80, 90, (100, 110)

Experimental Rotating Drum

Lifter Bar profile

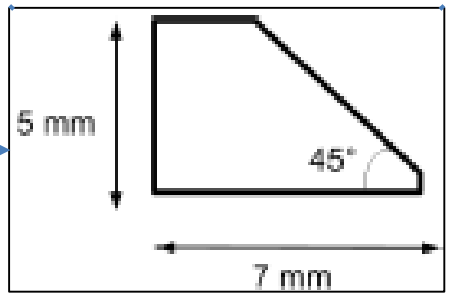

Typical Mixing Ingredients from PEPT

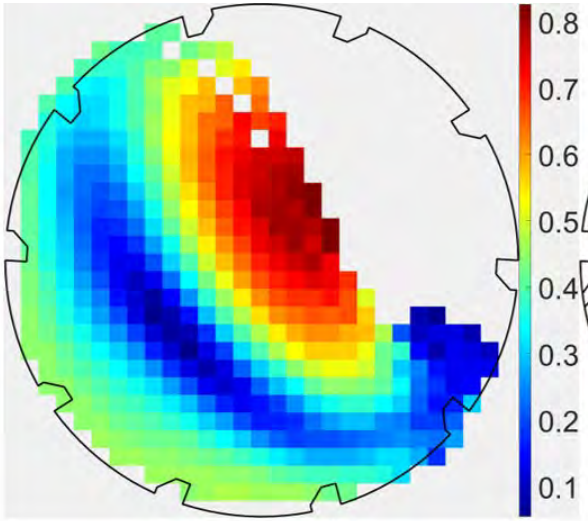

Speed (m/s)

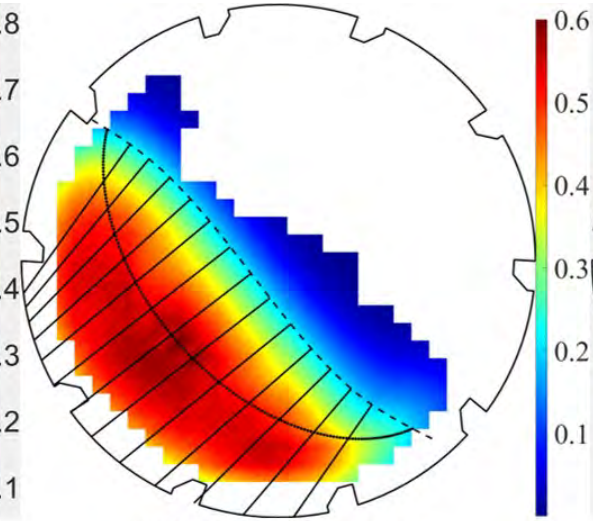

Solids Fraction (-)

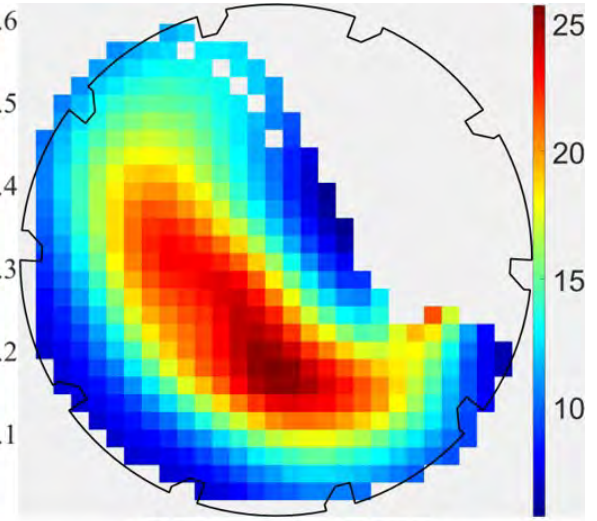

|Shear Rate| (1/s)

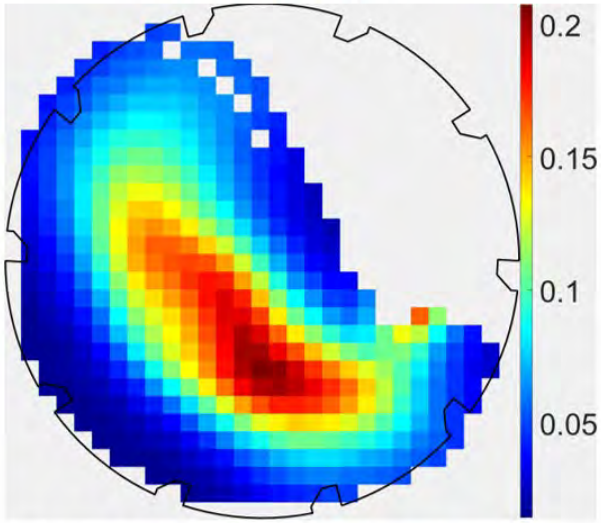

|Granular Temperature|

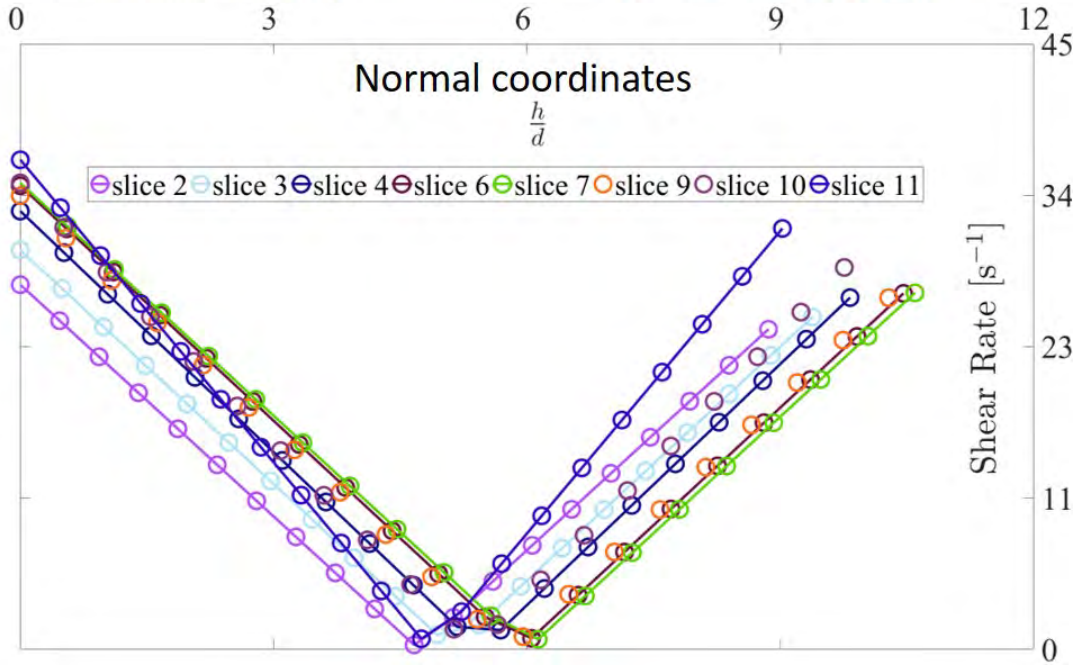

Thank You!

IFPRI

International Fine Particle Research Institute

3D printing “Perfect Particles”

Prof Karen Hapgood
School of Engineering
Deakin University
Geelong Australia

DEAKIN UNIVERSITY

PART 1 – Agglomerate breakage finale

Three different agglomerate designs

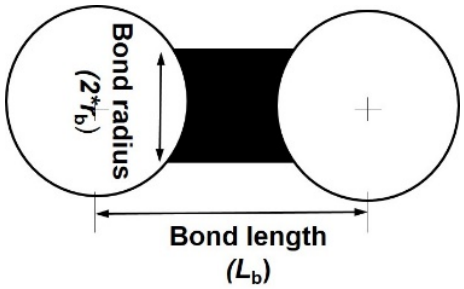

Cubic tetrahedral structure (L_b =4.25 mm, r_b=1.3 mm)	Random structure (ε=49 %, L_b =4.25 mm, r_b=1.3 mm)	Dense structure (ε=44 %, L_b =4 mm, r_b=1 mm)
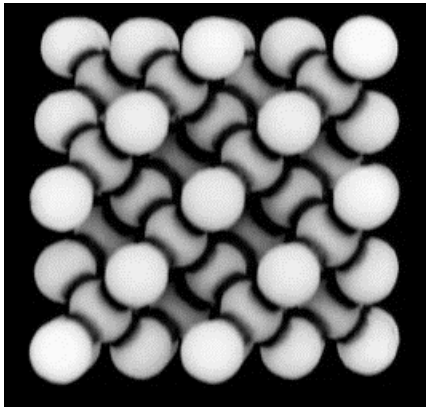	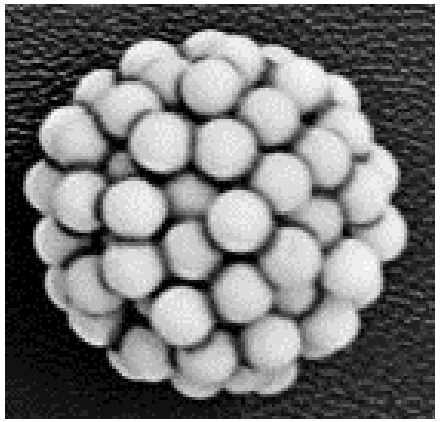	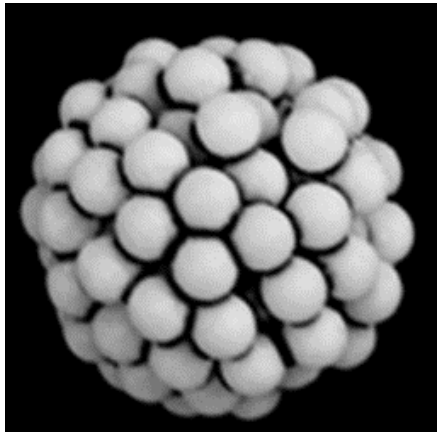

DEAKIN UNIVERSITY

Random spherical agglomerate (ε =44%) Quasi-static compression 0.02 mm/s.

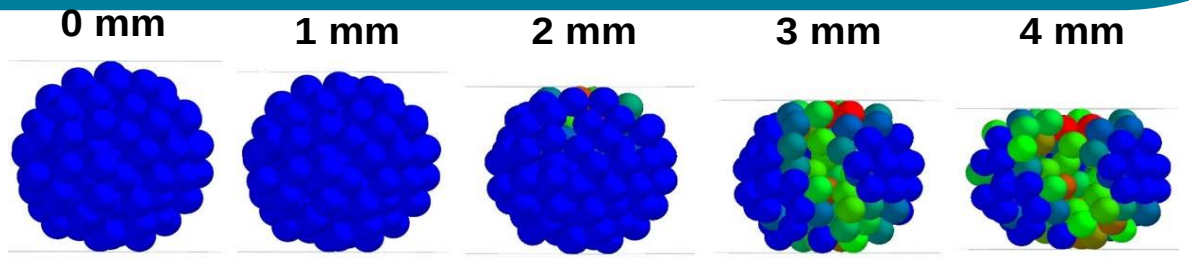

(a) Simulation

(b) Experiment

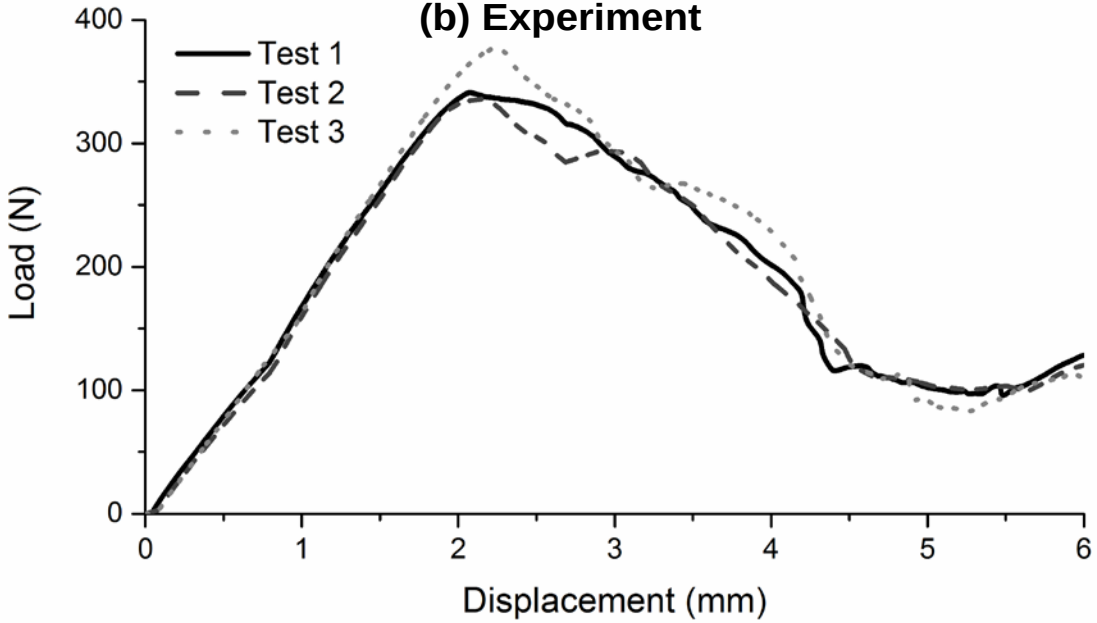

Good qualitative agreement

Good reproducibility

DEAKIN UNIVERSITY

Load-displacement curves – ??

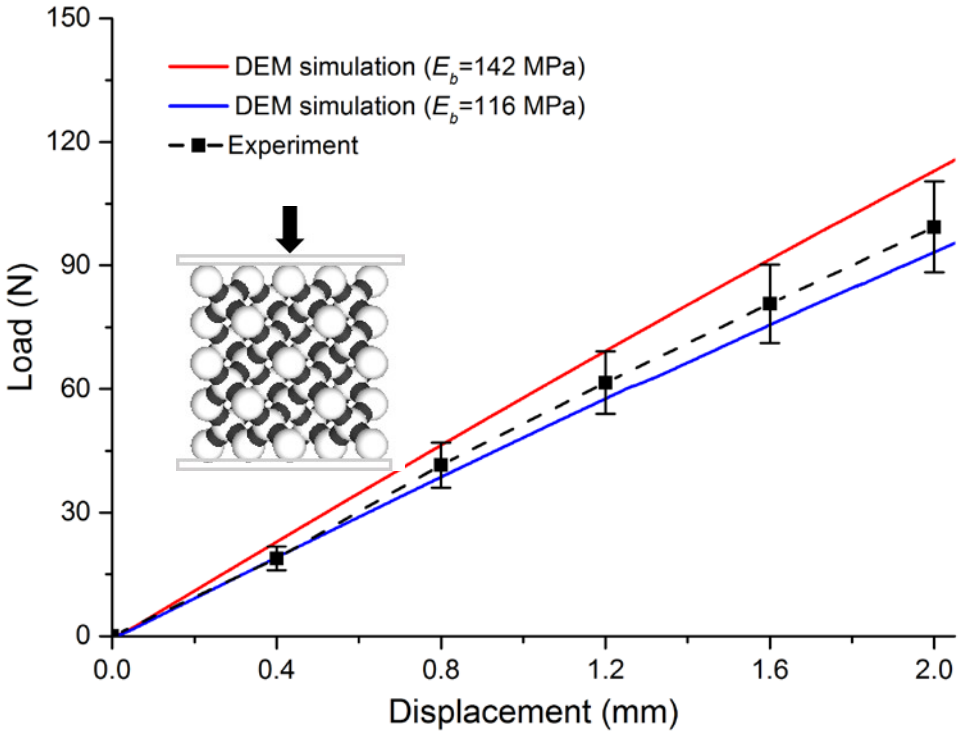

Very good agreement between DEM & experiment for both rigid & strong bonds

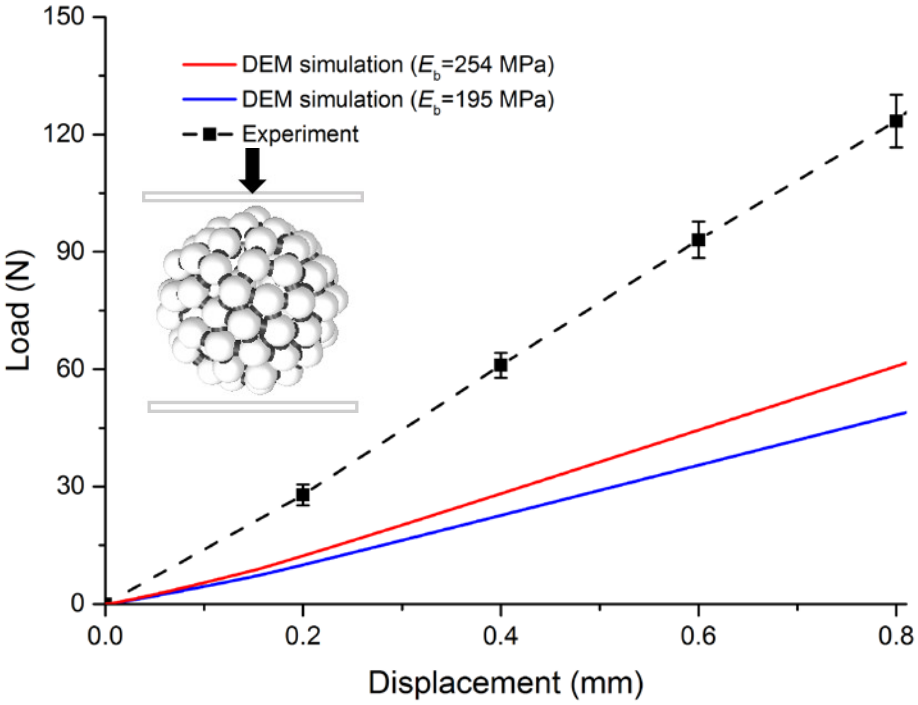

DEM prediction is much lower than the experiments

DEAKIN UNIVERSITY

FEM simulations of doublets

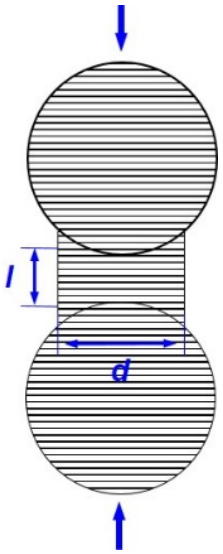

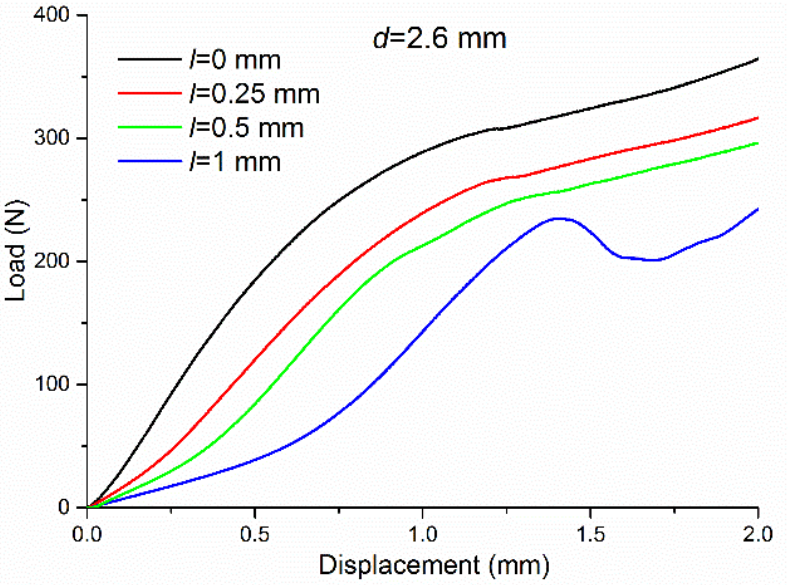

(a) Experimental results

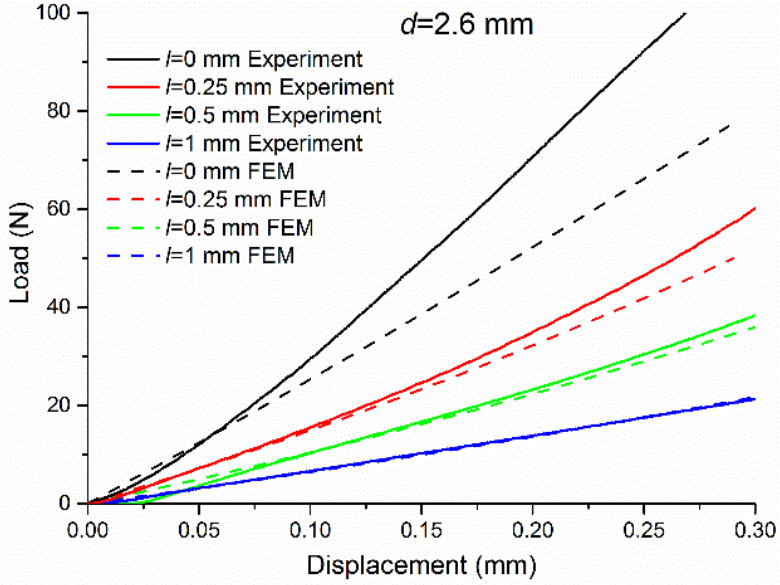

(b) FEM vs Experiment

- Linear elastic range is ~ 0.3 mm bond compression

DEAKIN UNIVERSITY

Load-displacement curves v2

- NEW spherical random structure (ε =49 %)
  - same *average* bond length (L_b= 4.25 mm) as the cubic tetrahedral structure
  - same corrected bond Young's modulus $E_{b,m}$ captures the compressive load at the initial elastic stage (~1 mm deformation).
  - Beyond this point, nonlinear behaviour takes over

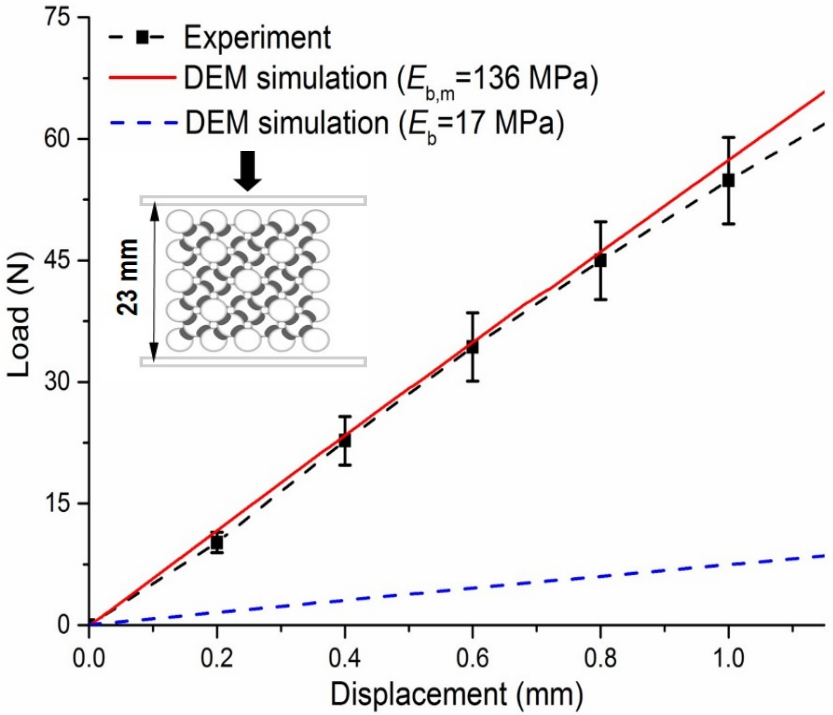

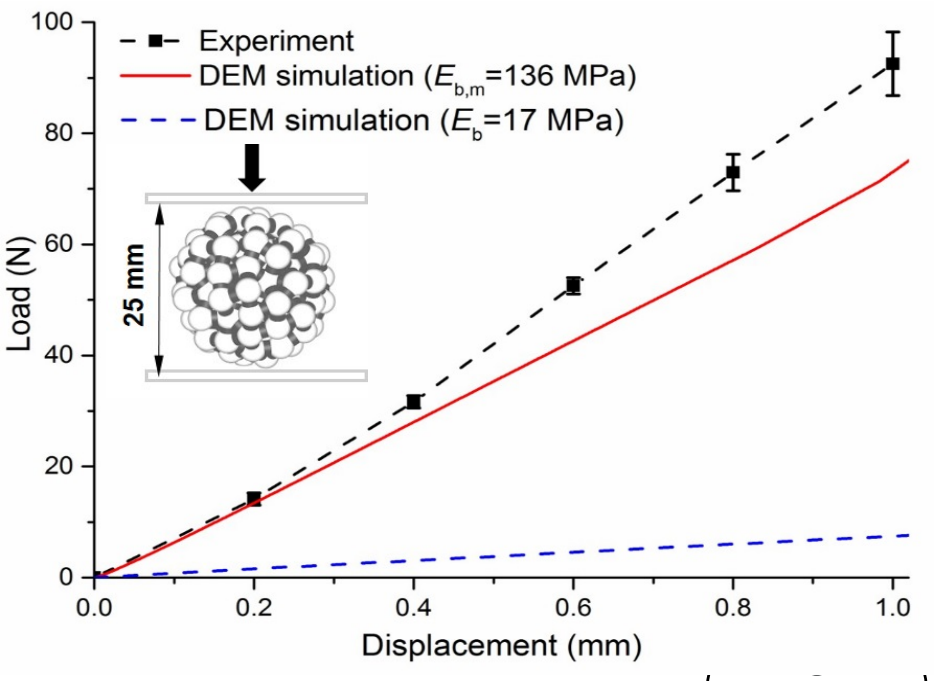

Two issues that require further consideration:

- Non-linear and anisotropic characteristics of 3D printing materials.
- Non-linear contacts between particles when particles are in contact (l=0).

PART 2 – New “perfect particle” applications of 3D printing

New uses for 3D printed particles: Flow of irregular particles

- Testing of original shape and “equivalent” DEM shape in simple flow – how many spheres are required?

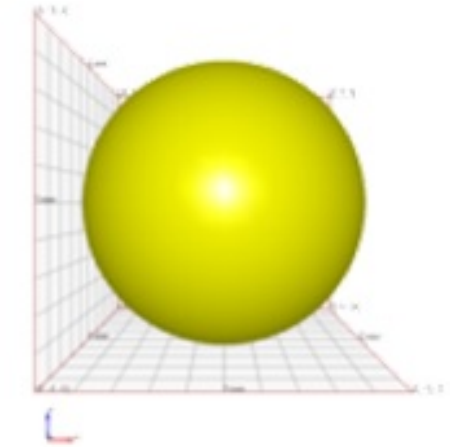

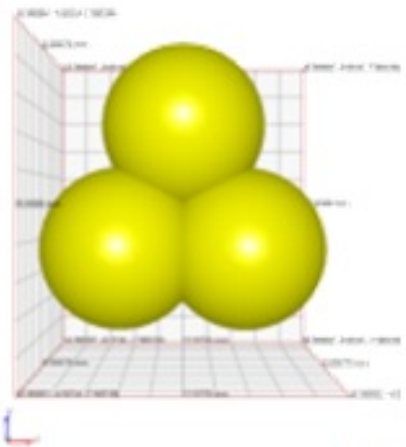

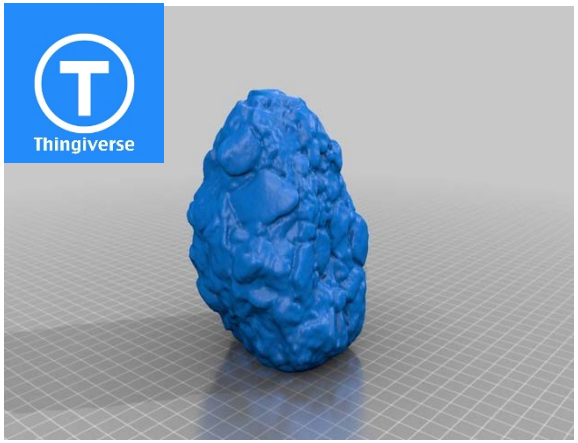

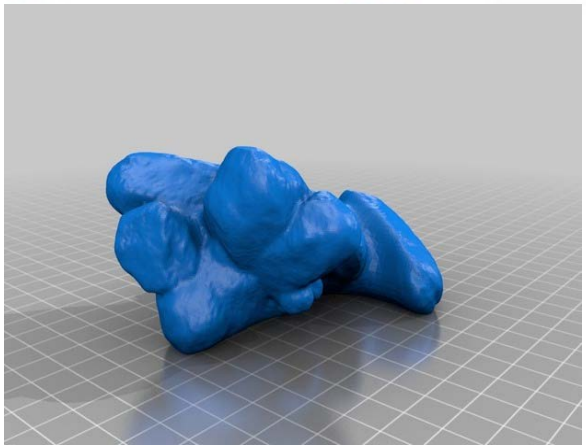

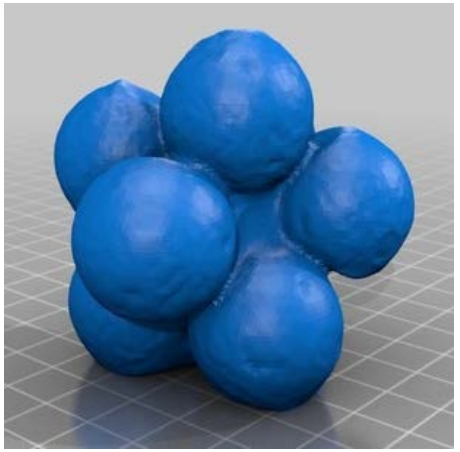

Use 3D printing colours for particle size, shape and density

ROCKY

Spherical	Faceted	Rounded Cylinder	Rounded Polygon	Rounded Polyhedron	Gummy Bear

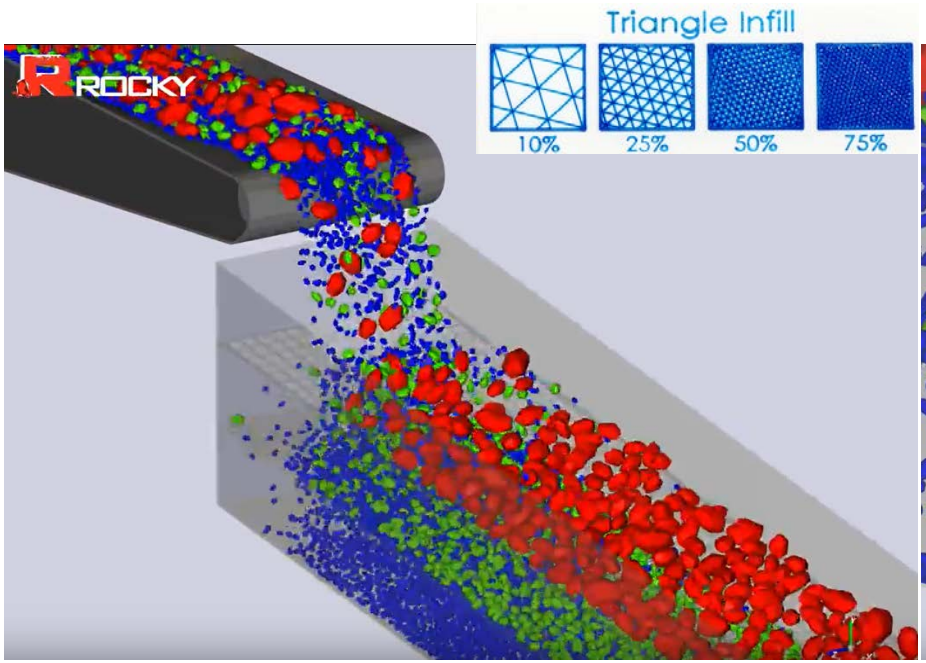

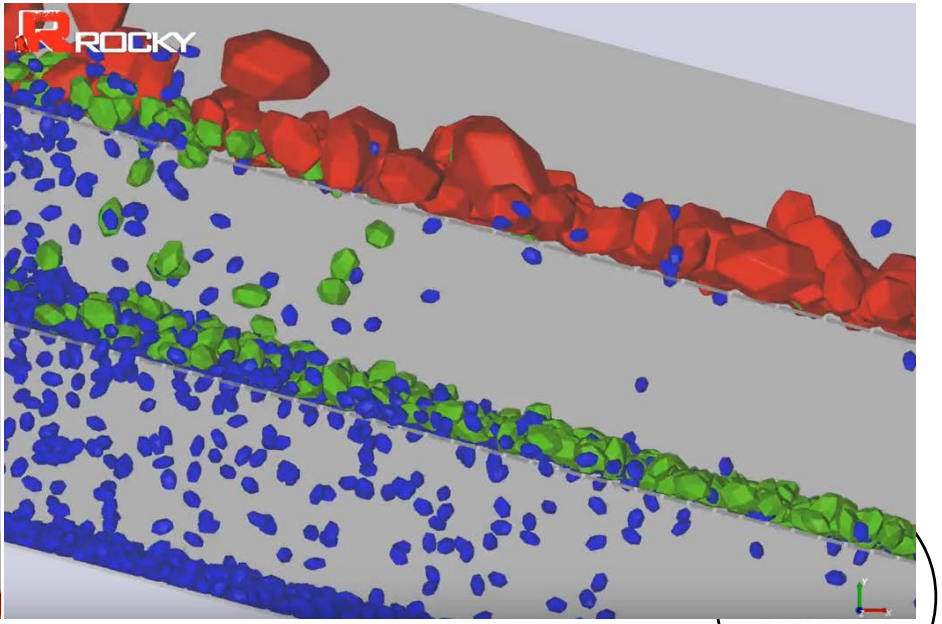

UNIVERSITY

IFPRI

International Fine Particle Research Institute

3D printing “Perfect Particles”

Prof Karen Hapgood
School of Engineering
Deakin University
Geelong Australia

DEAKIN UNIVERSITY

Flowability Assessment of Weakly Consolidated Powders

Colin Hare[1], Ali Hassanpour[2], Azza Mahmoud[1], Alexandros Stavrou[1]

[1]Department of Chemical and Process Engineering, University of Surrey
[2]Institute of Particle Science & Engineering, University of Leeds

The brief

- In traditional flowability measurement devices:
  - Reproducibility of unconfined yield strength is greatly reduced at low stresses.
  - Or inconsistent with observed behaviour.
  - Materials found to be cohesionless may have practical differences.
  - Onset of flow is measured – may not be complete flow description.

- IFPRI seek to develop a theoretical understanding of flow of weakly consolidated & weakly cohesive powders.
  - Development of practical means of making measurement to support theory.
  - Results should be generalisable to broad class of powders.

Stress direction

	Shear cell	Uniaxial compression	Ball indentation (original method)	Ball indentation (critical method)
Consolidation	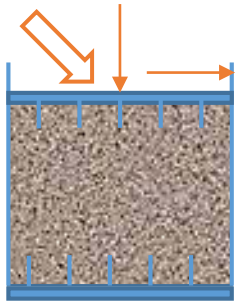	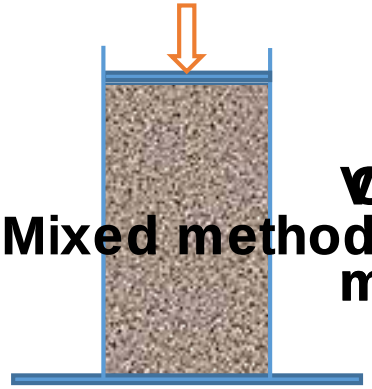	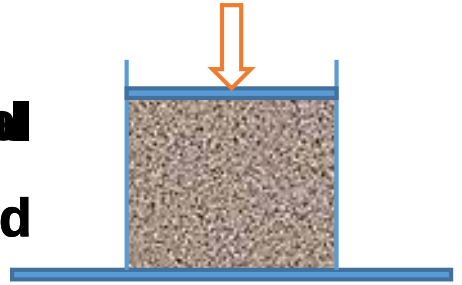	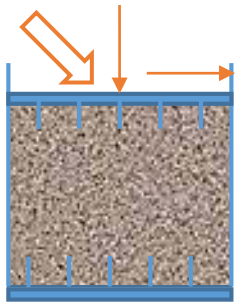
Failure	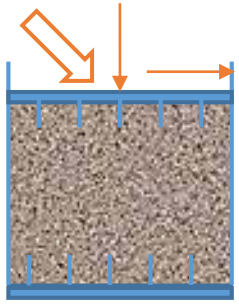	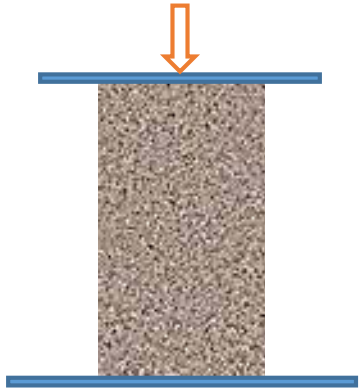	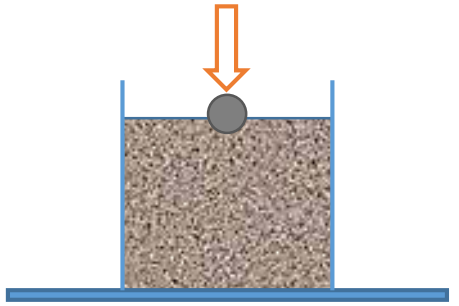	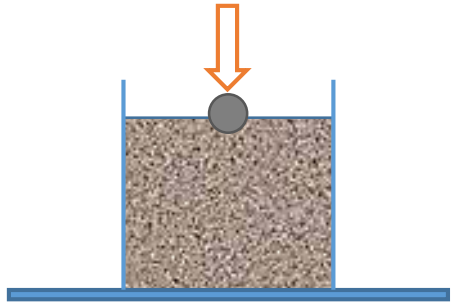
Measurement	Control: σ Measure: τ Determine: σ_1 & σ_c	Control: σ (σ_1) Measure: σ_c (uUYS)	Control: σ (σ_1) Measure: H Determine: C, σ_c	

Mixed method

Critical method

Unconfined yield strength

- Titania

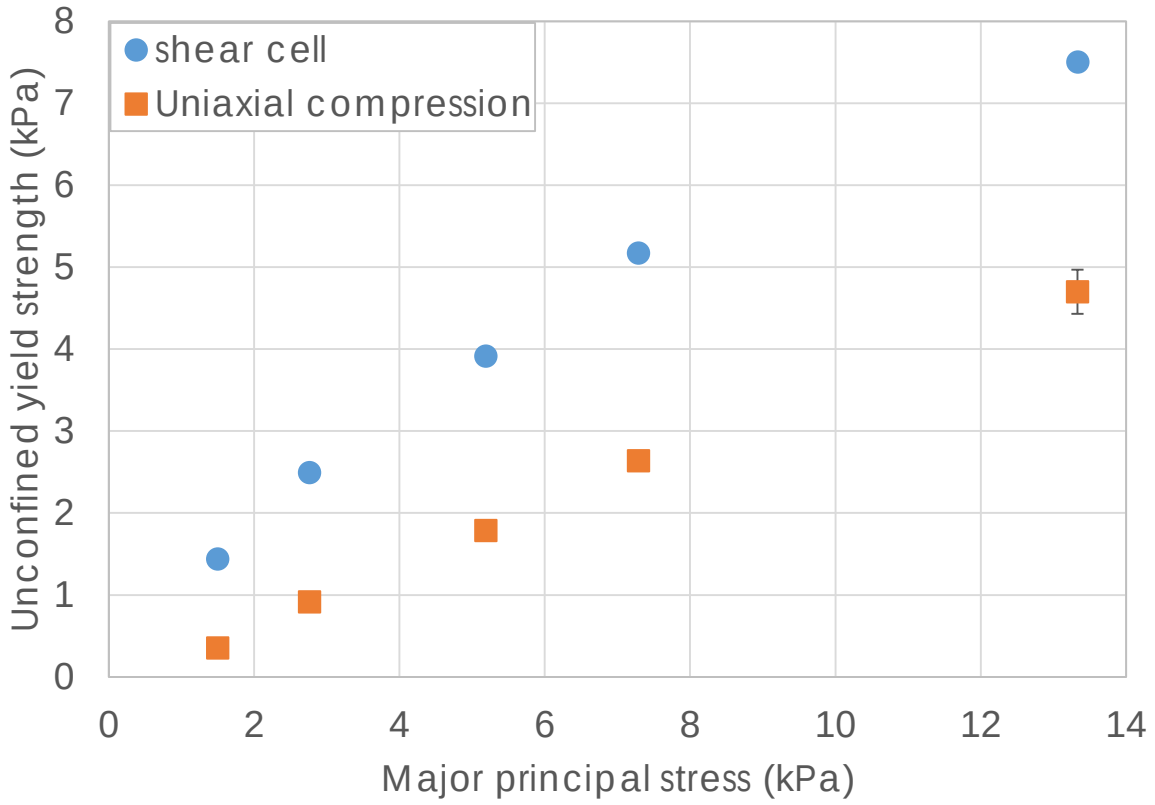

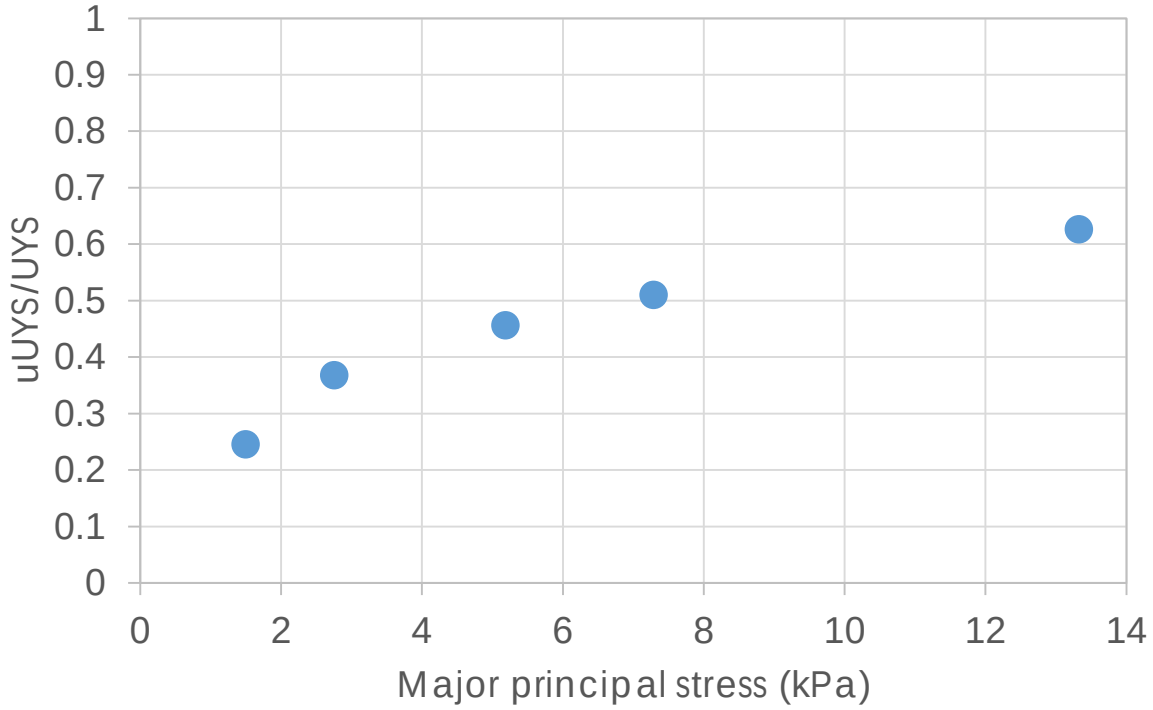

Yield locus

σ_{pre} = 0.5 kPa

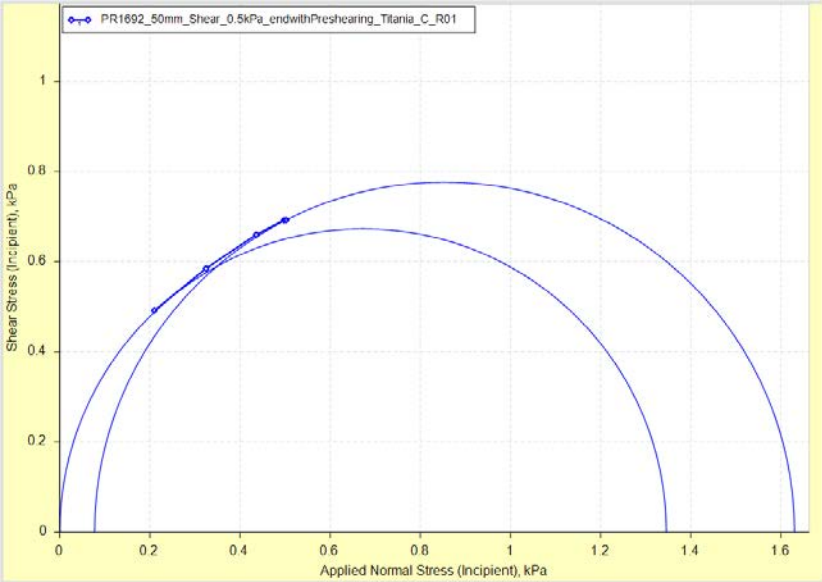

σ_{pre} = 2 kPa

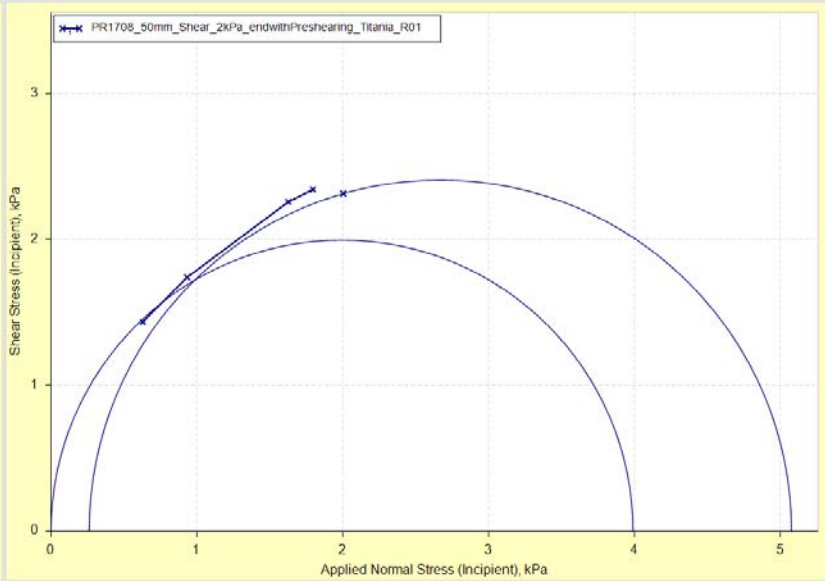

σ_{pre} = 6 kPa

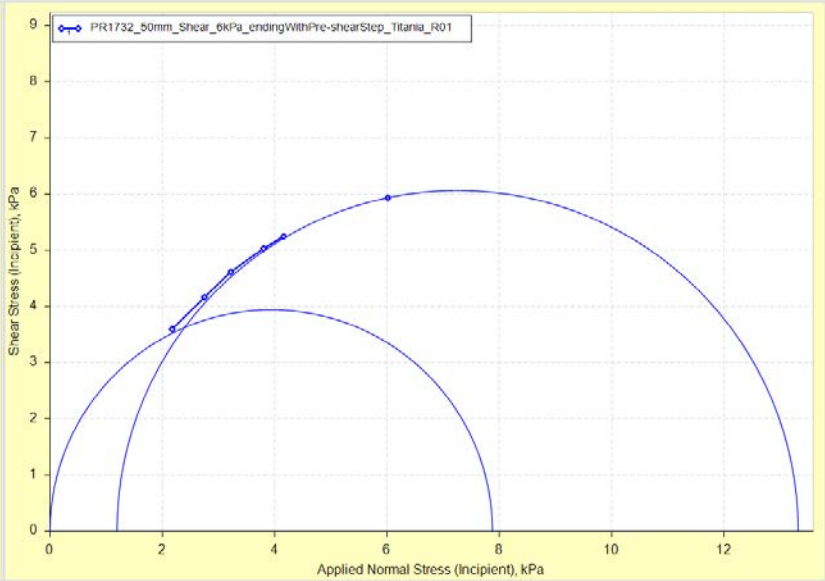

Indenting onto sheared bed

σ_{pre}	0.5 kPa	1 kPa	2kPa	3 kPa	6 kPa
After lid removal					
Reliable indents	0/15	2/15	2/15	4/15	8/15

Indenting onto bed sheared with wall friction head

- Attempted shearing using wall friction head placed at top instead, i.e. no vanes
  - Insufficient grip, measured shear stresses sufficiently reduced

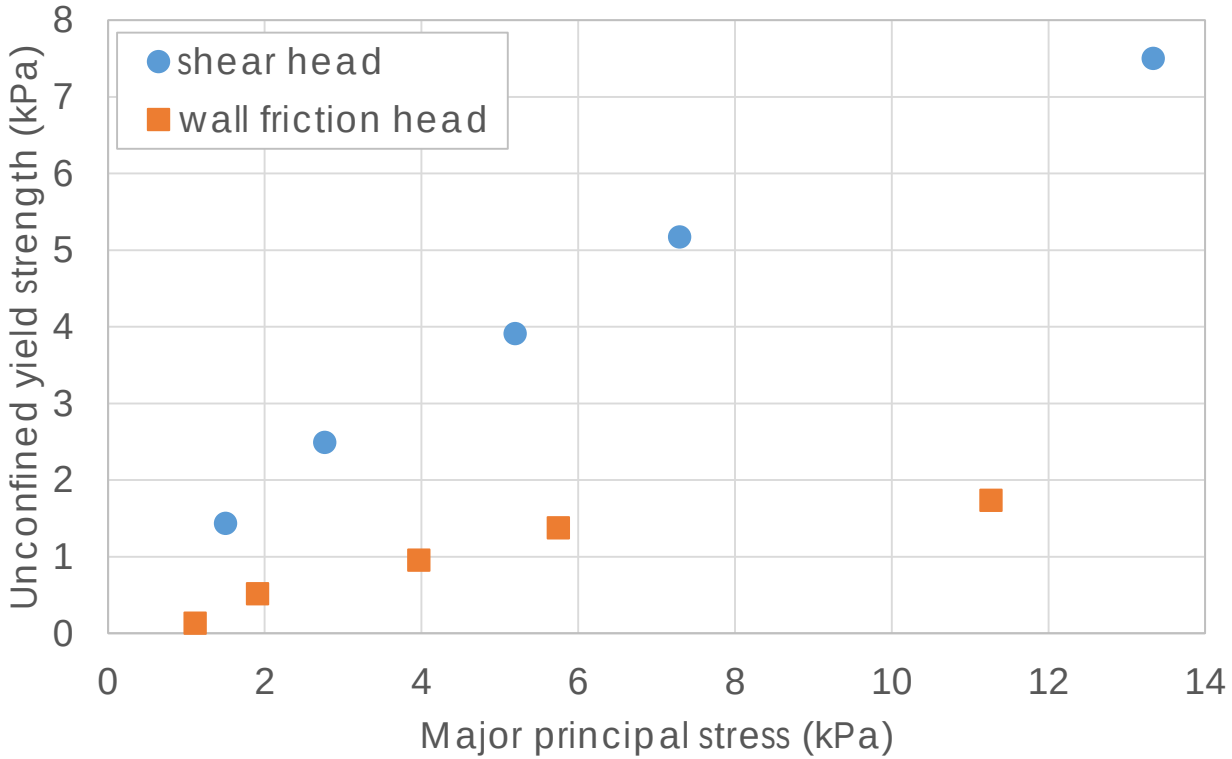

Comparing indentation to shear cell

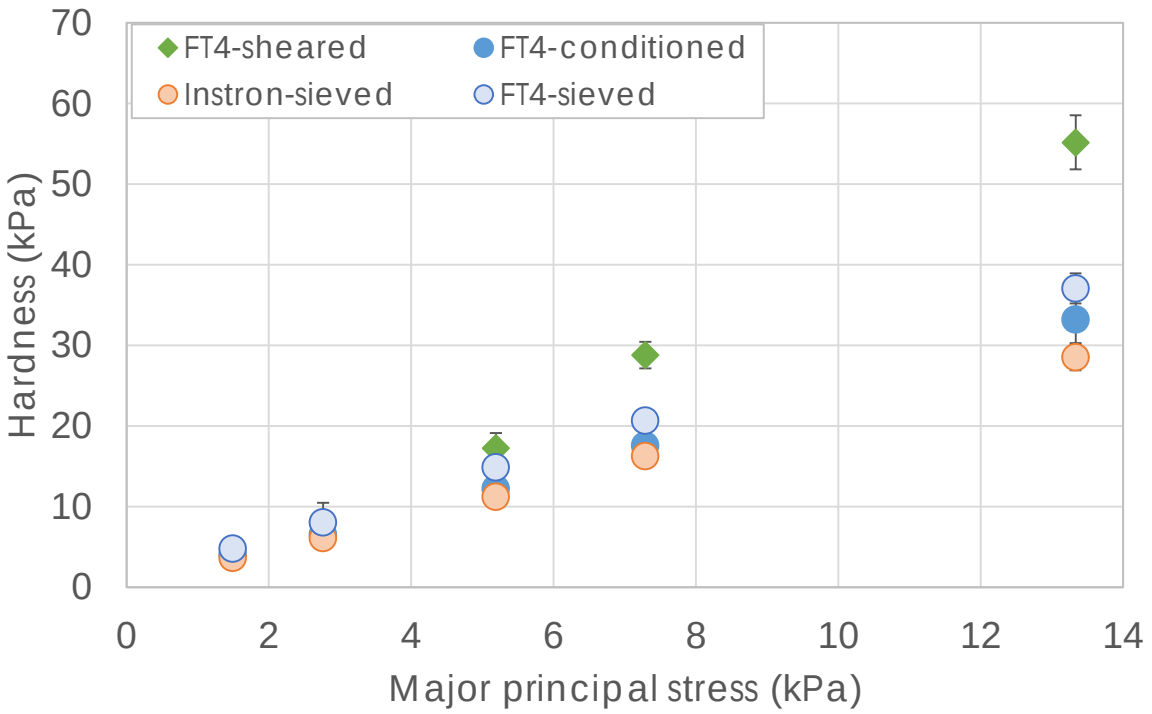

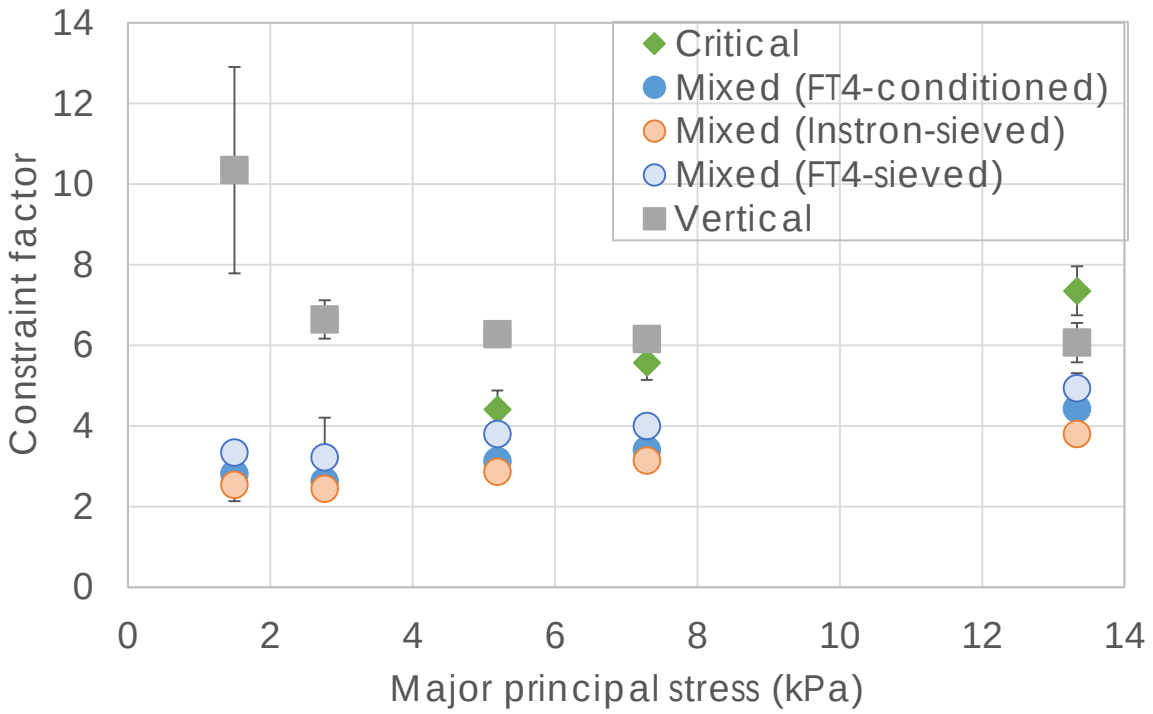

Indentation simulations

- DEM simulations allow internal bed stresses to be assessed
- Elasto-plastic-adhesive model used[1]
- Stress tensors calculated: $\sigma_{ij} = \frac{1}{V}\sum_{1}^{N} F_{ij} \cdot r$
- Deviatoric stress determined:

$$T_D = \frac{\sqrt{(\sigma_1 - \sigma_2)^2 + (\sigma_1 - \sigma_3)^2 + (\sigma_2 - \sigma_3)^2}}{\sqrt{6}}$$

- Hardness calculated

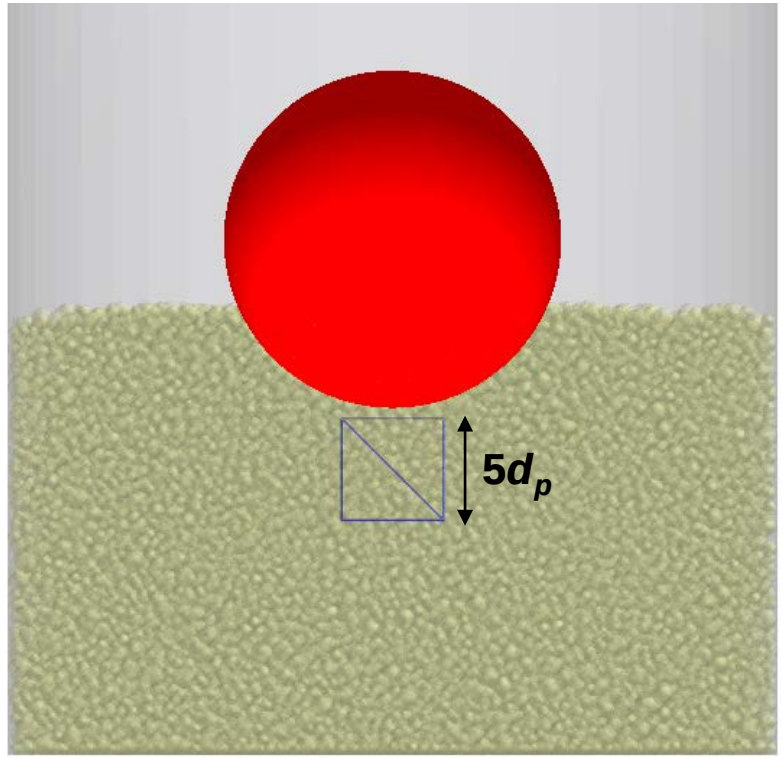

[1]Pasha, M., Dogbe, S., Hare, C., Hassanpour, A., and Ghadiri, M. (2014) A Linear Model of Elasto-Plastic and Adhesive Contact Deformation, *Granular Matter*, 16, 151-162.

Indentation simulations (2)

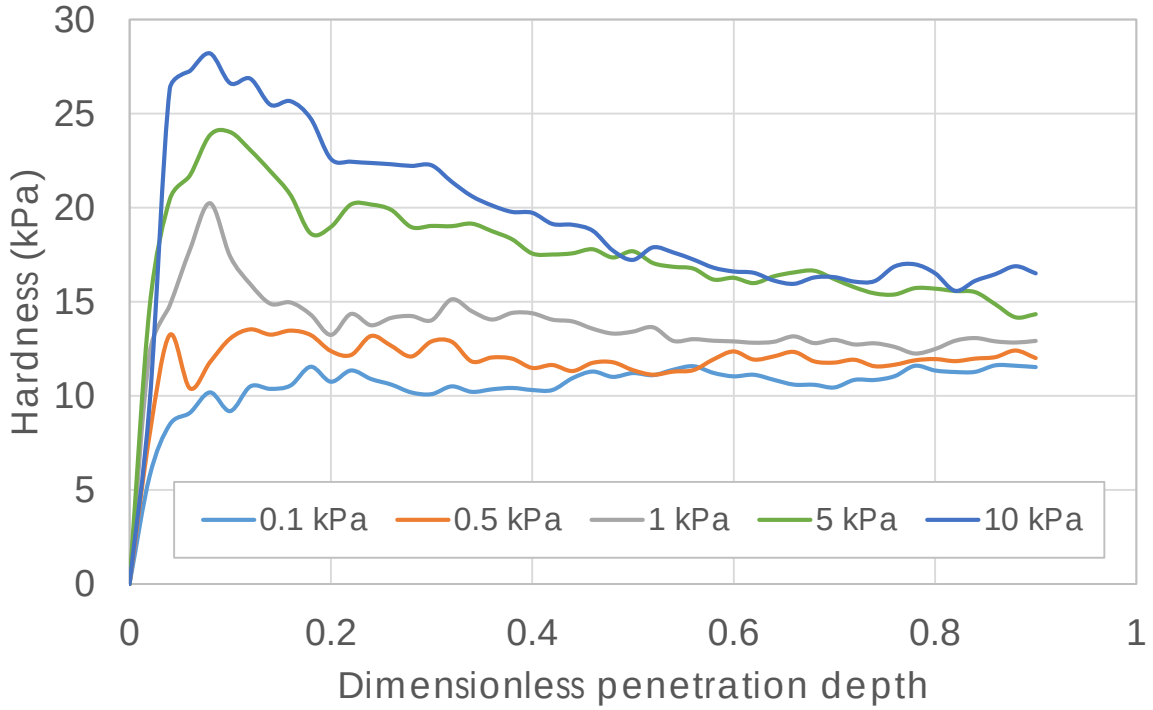

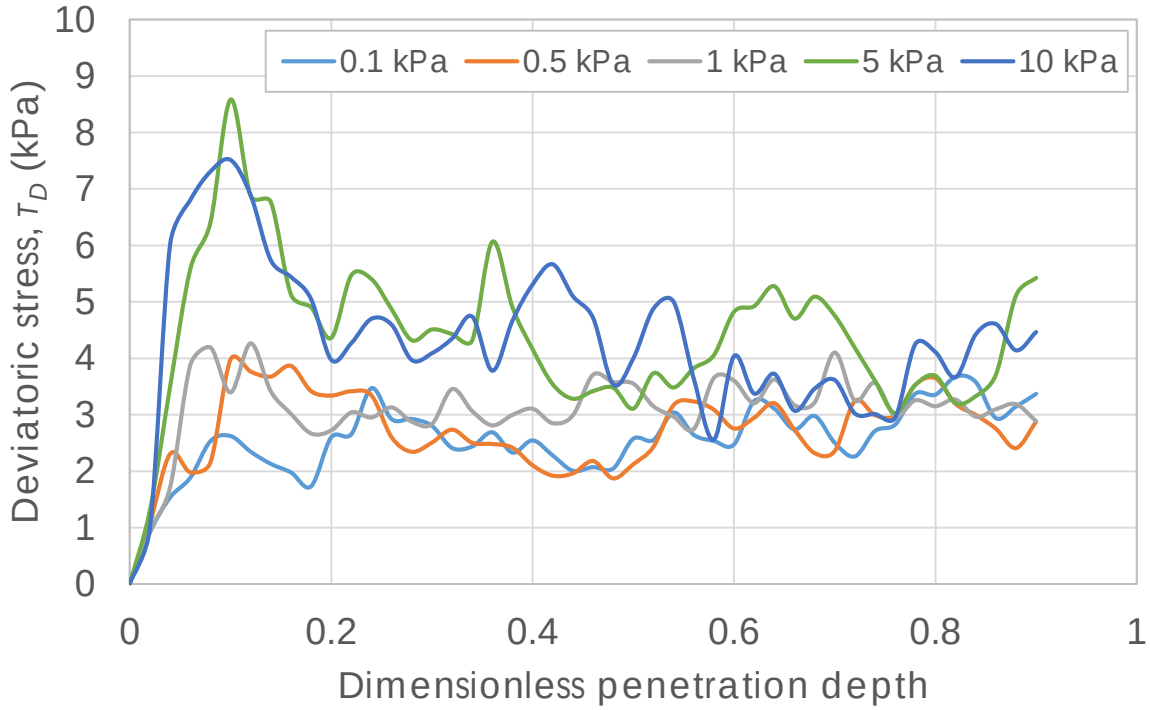

Indentation simulations (3)

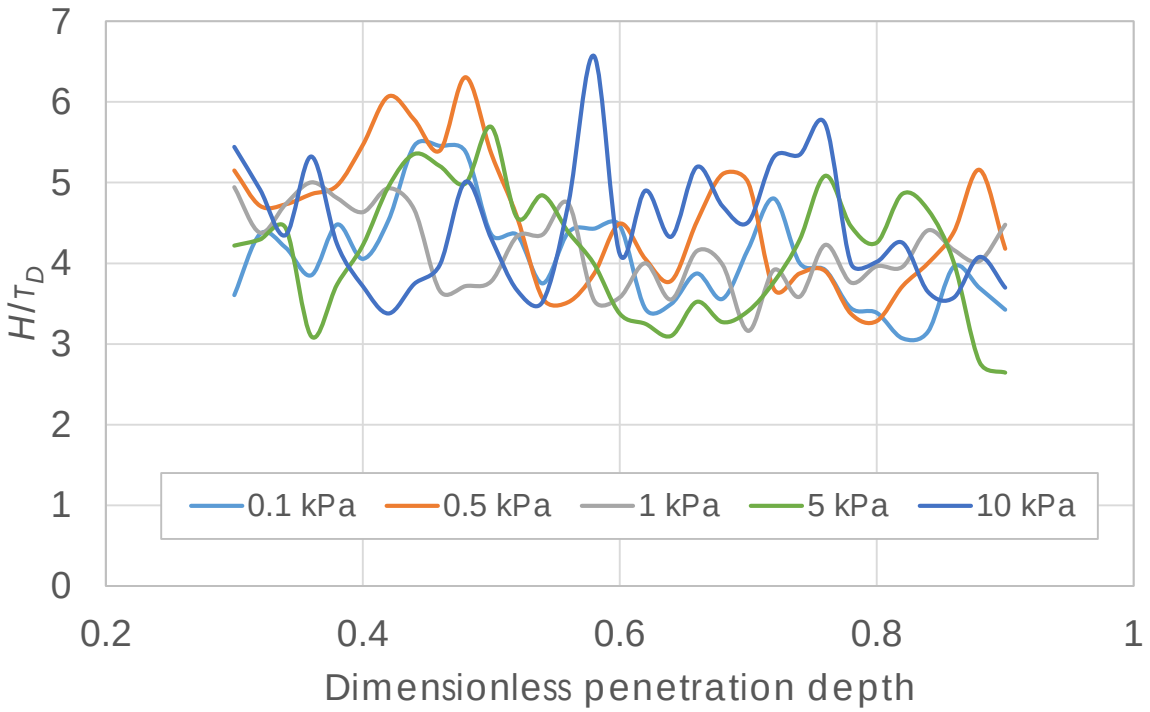

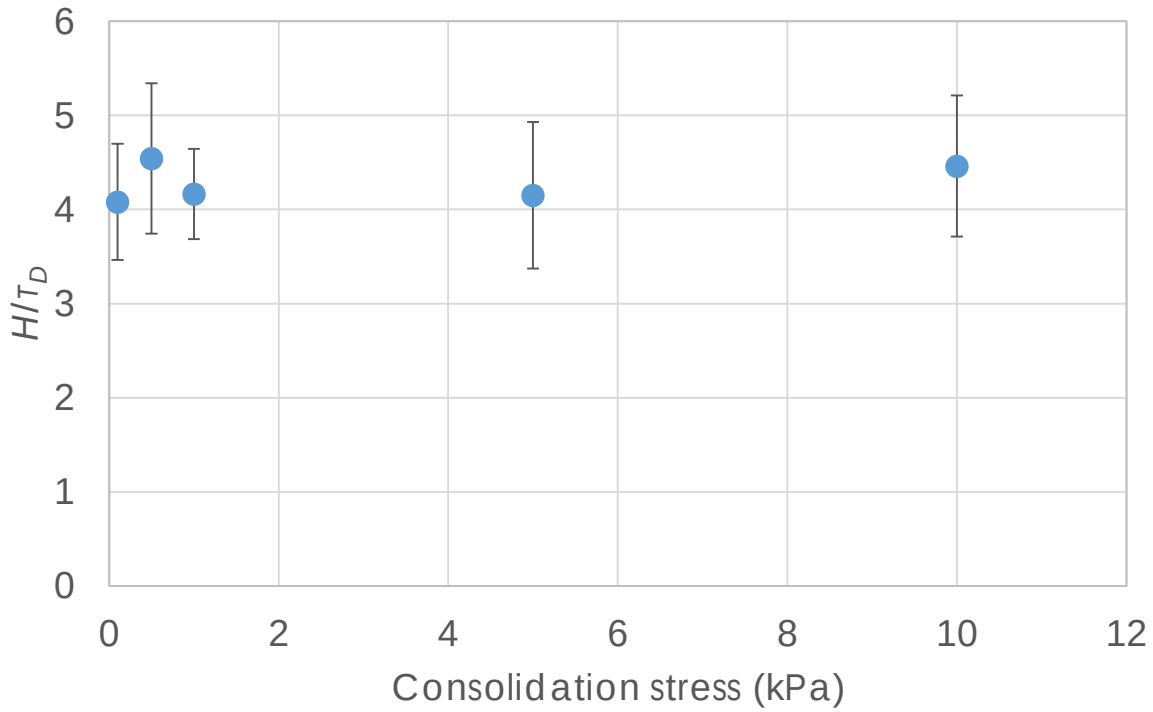

Effect of friction coefficient

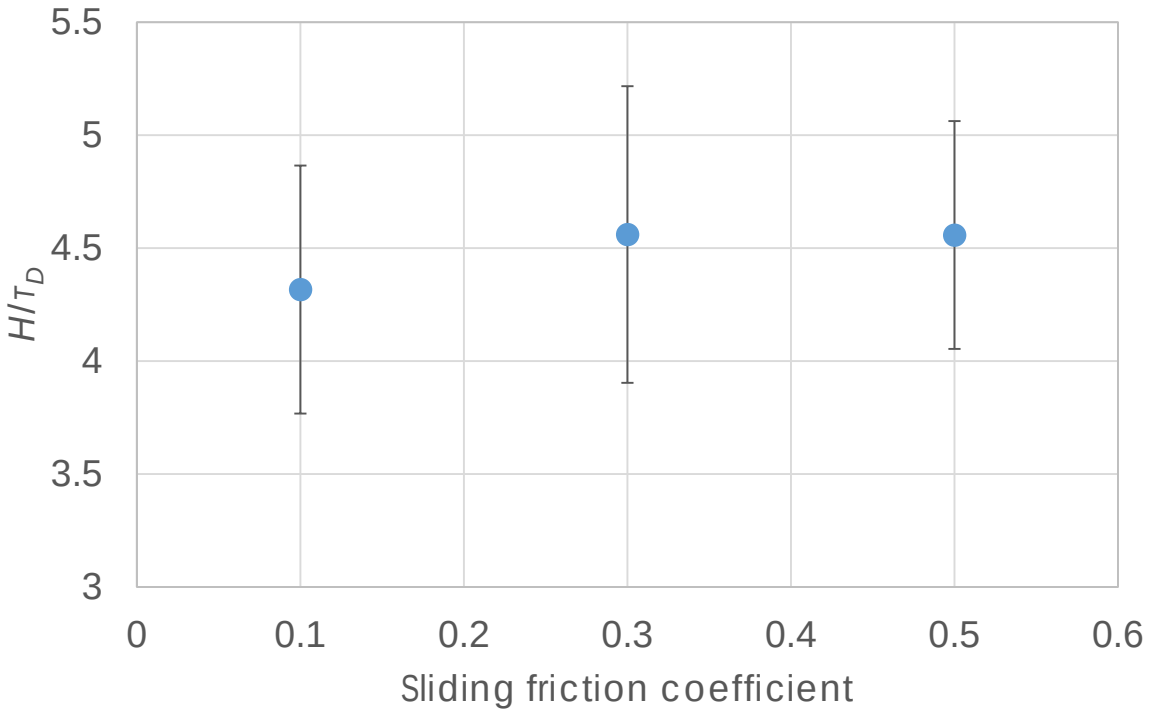

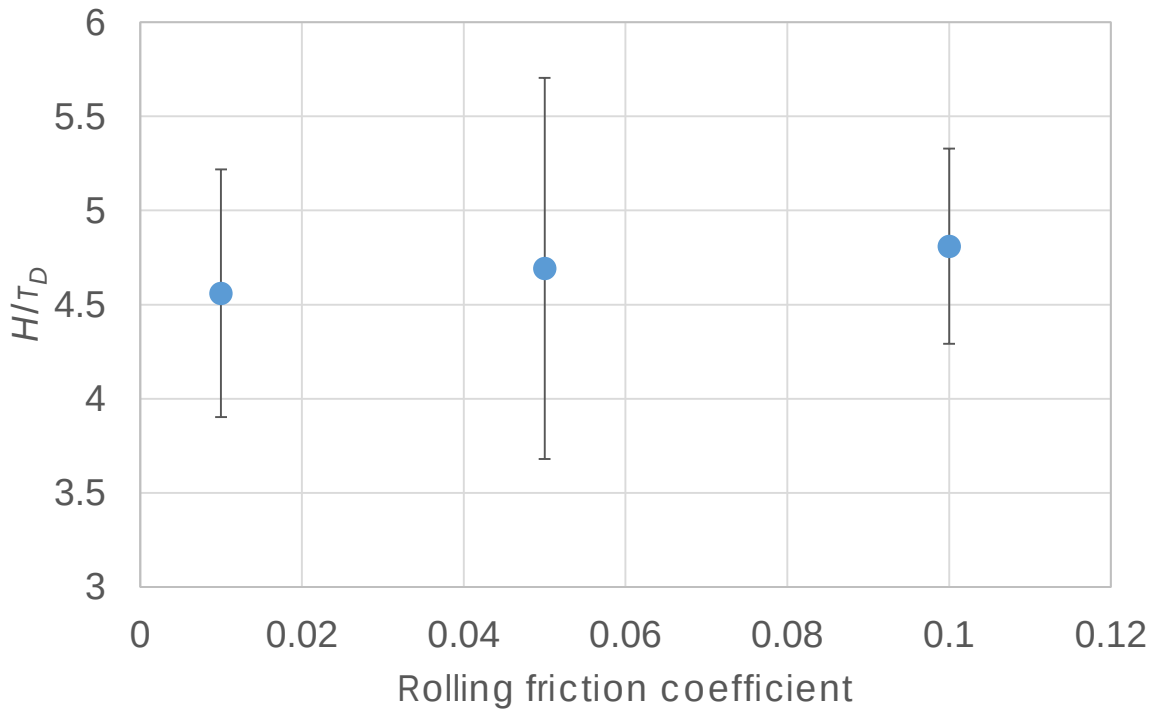

Future Work

- Flowability of various grades of titania to be investigated
  - Using methods applied so far
  - Shearing under constant volume condition
- Most promising techniques applied for other powders
  - Alumina, food powders, pharmaceuticals
  - Investigate optimum approach to estimate yield locus curvature
- Flow field around the ball indenter to be examined
  - Apply for access to Diamond Light Source (Synchrotron) in Harwell (UK)

Exploiting a Framework
for the Development of Segregation Rate Models

J. J. McCarthy

Department of Chemical Engineering
University of Pittsburgh

June, 2018

Quantitative Prediction of Segregation at Process Scale

- Identify critical **material and process parameters** that control the *extent* of powder segregation
- Develop **quantitative models that predict** segregation and possible re-homogenization within a process train
- **Validate** models with appropriate experiments
- Demonstrate that the models are applicable to **full-scale** processes
- In scope:
  - Dense flows
  - Formulated (i.e. multicomponent) mixtures
- Additional considerations:
  - Cohesive powders
  - Particle shape effects

A Unified Model, Based on Rheology

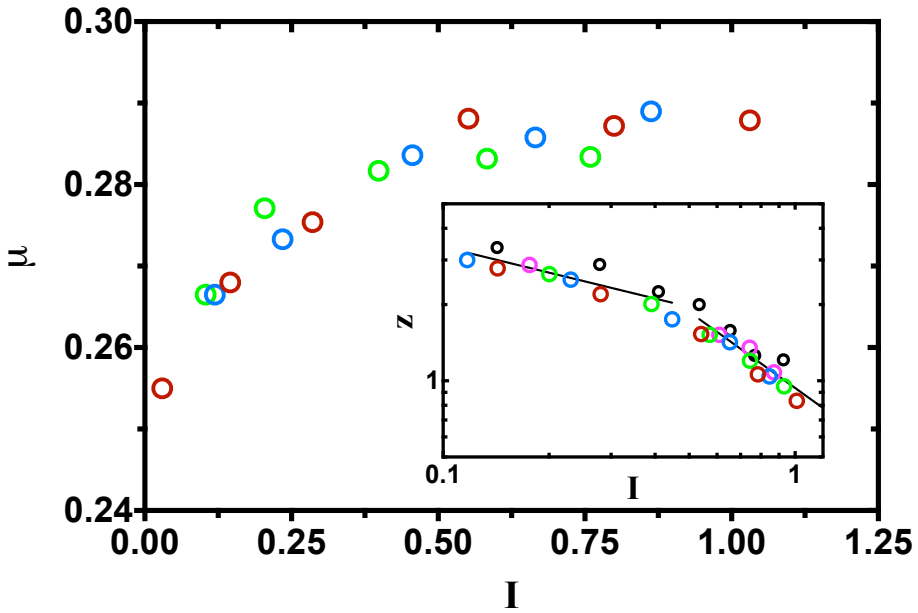

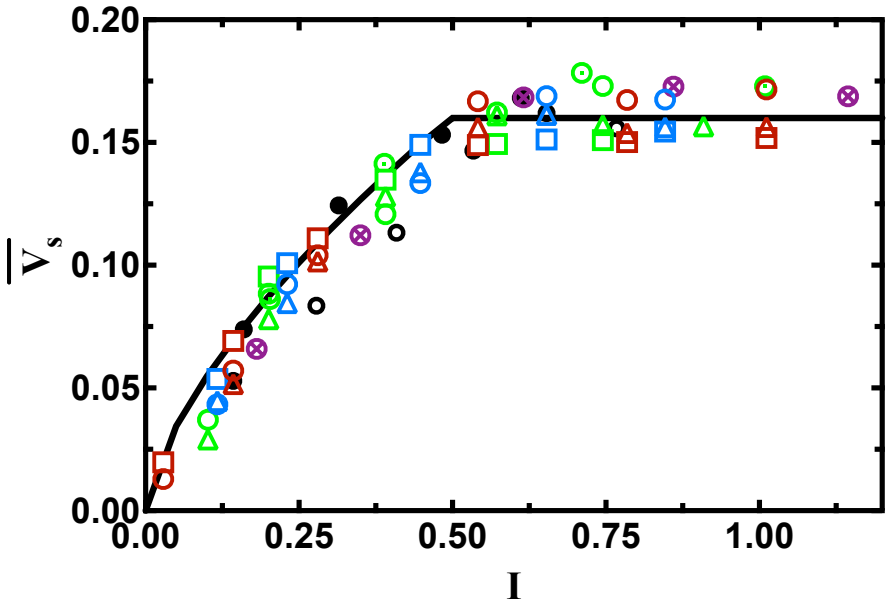

- Segregation saturation occurs at same location as frictional saturation
- Model based on coordination number fits **all** data

This Year in Density

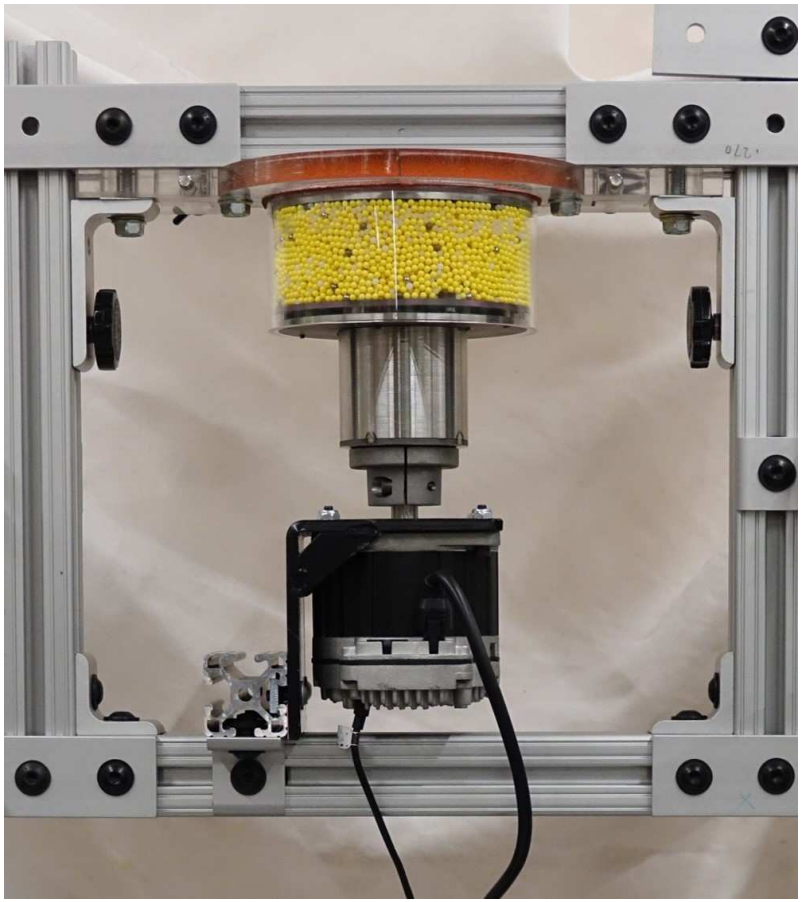

- Experimental apparatus for continuous shearing
- Run with tracer particles that are visually tracked

Experimental Validation

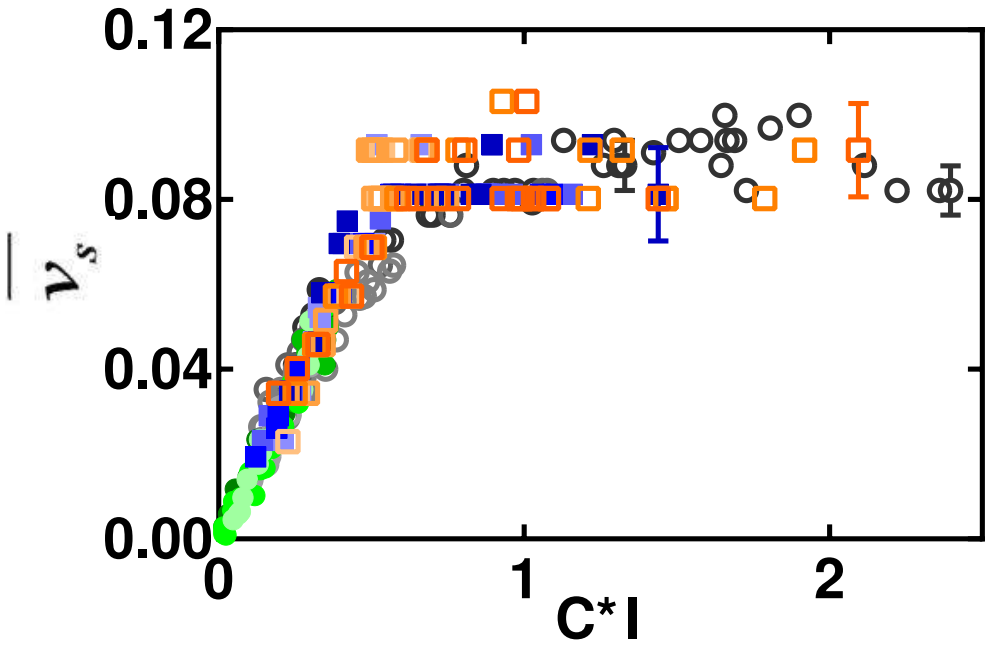

- Inhomogeneous shear means that the inertia number, I, varies with height
- With one experiment we can measure v_s vs I for a range of conditions
- Results confirm novel segregation saturation model

Capturing Size Segregation

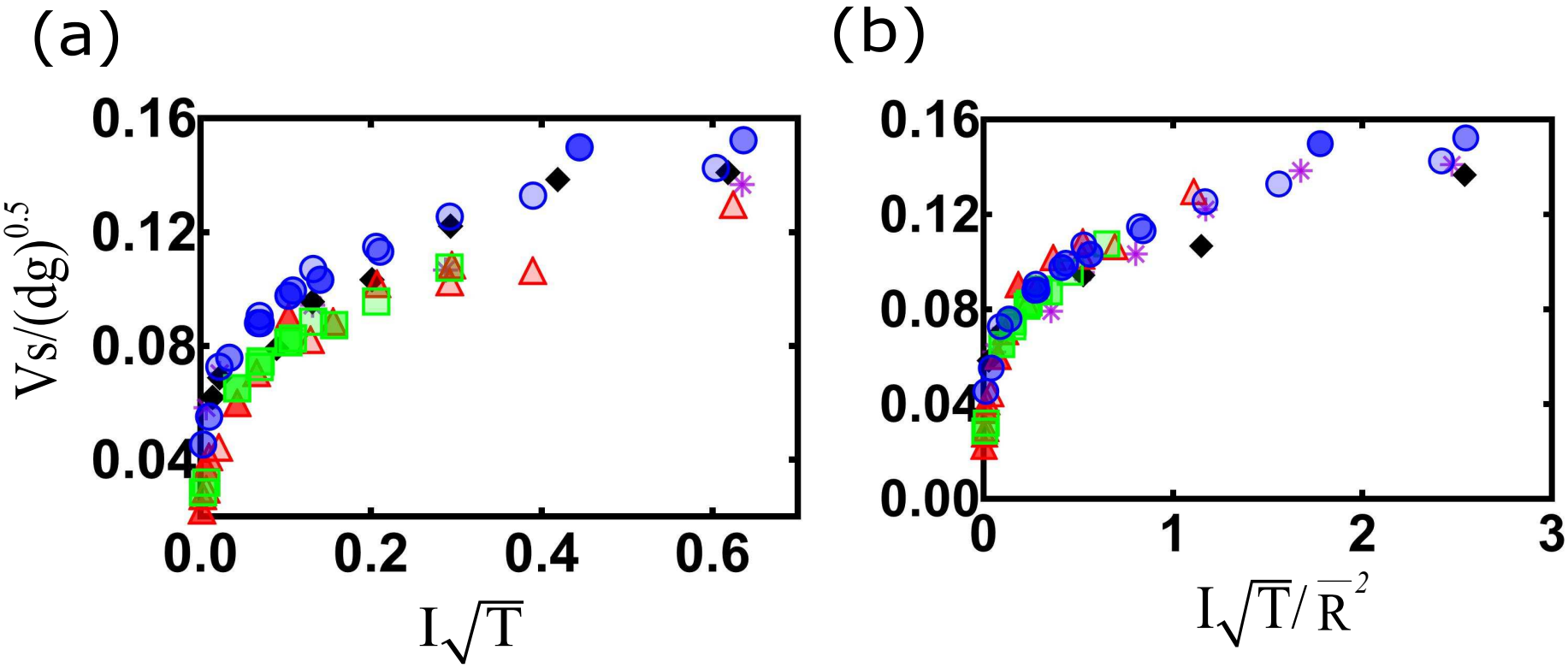

- Size segregation involves a more complex interplay between segregation and rheology
- Combining I and T captures both creation of voids, as well as exploration of space (finding the holes)
- Novel observation: size ratio squared!

Cohesive Segregation

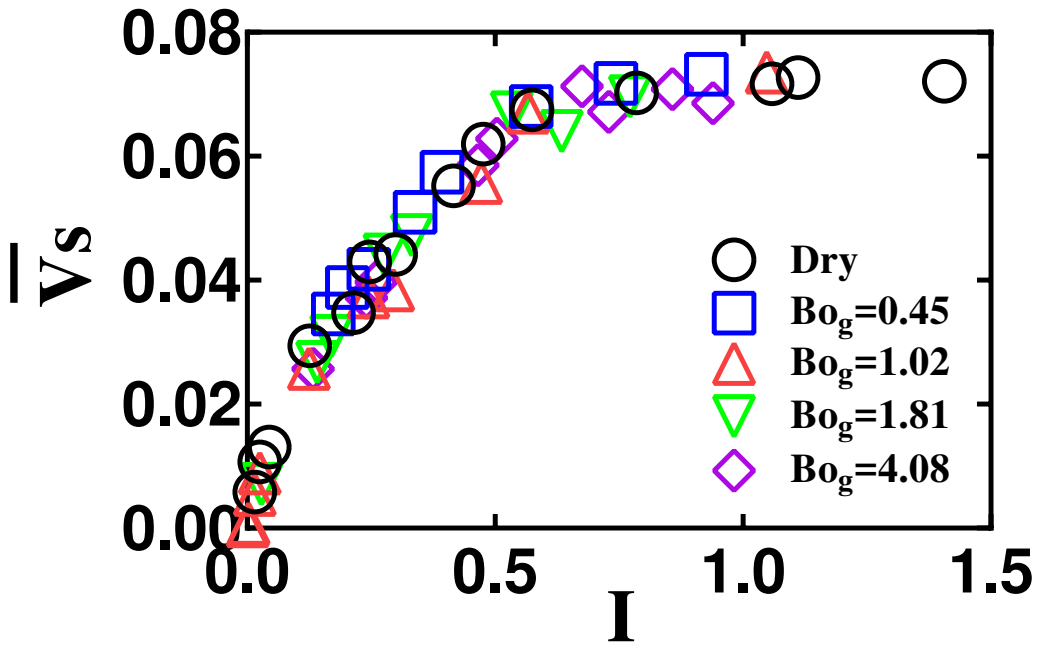

- $\bar{v}_s = \frac{z_{adj}(\bar{\rho}-1)}{6\beta\sqrt{\bar{\rho}}} I$ works for **both** cohesive and non-cohesive systems

Cohesive Segregation Works: How?

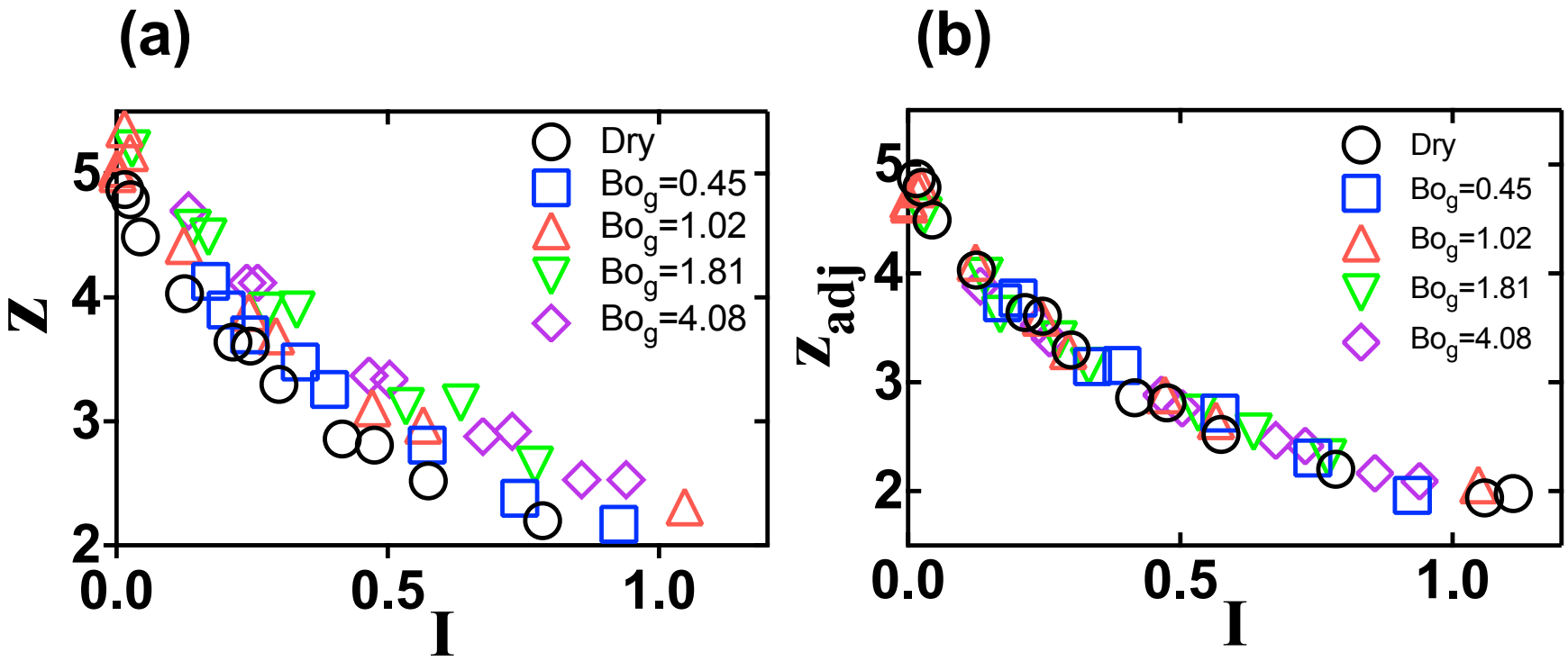

- $z_{adj} = z \cdot (1 - \frac{F_c}{F_z}) = z \cdot (1 - \frac{4\gamma}{\alpha P d_p})$

Experimental Exploration of Shape Segregation

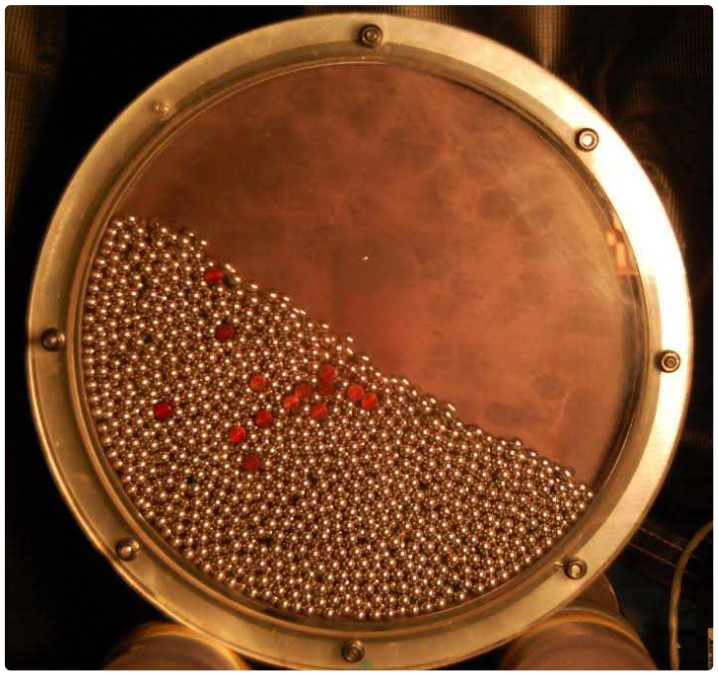

(a)

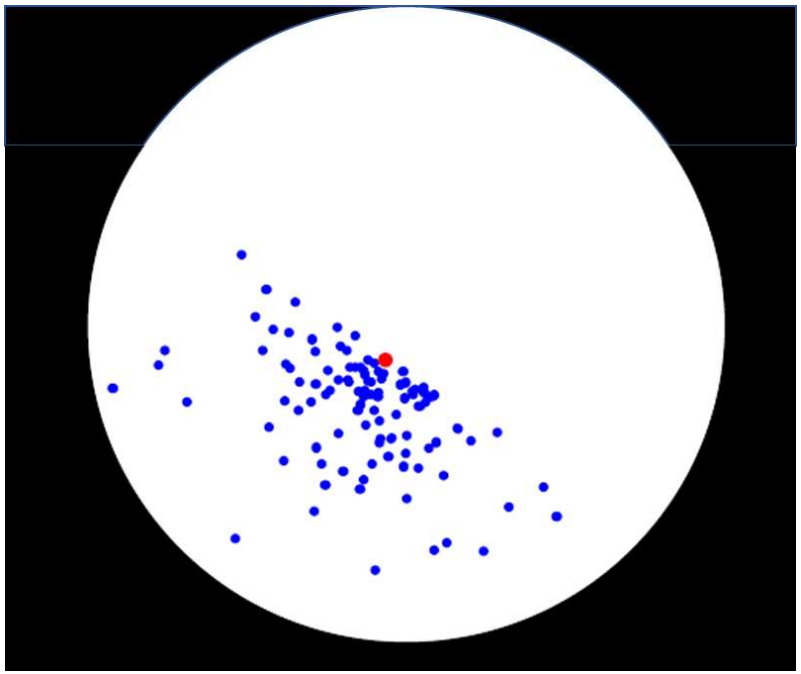

(b)

- Tracking the periodic observed location of tracers allow a measure of segregation based on "distance to center"
- Comparing to sphere-sphere systems $\rightarrow$ equivalent size parameter

Effective Size of Cylinders/Discs

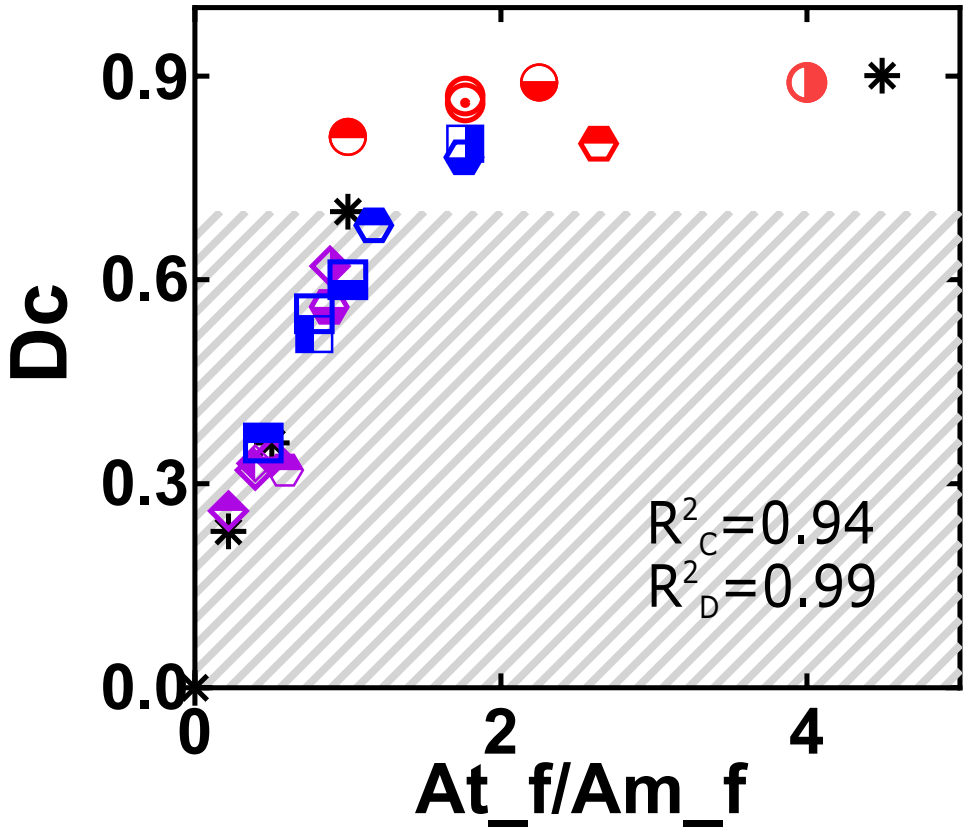

Shape descriptor # Classification #	Shortest L 1D	Average L 1D	"Lay down" A 2D	"Spinning" A 2D	Volume 3D	"Flowing" A 2D
R^2 Cylinder	0.94	0.79	0.77	0.77	0.65	0.94
R^2 Disc	0.74	0.94	0.99	0.57	0.57	0.99

A Holistic Approach for the Model-based Control of Crystal Size, Shape and Purity in Integrated Batch and Continuous Crystallization - Wet Milling Systems

Botond Szilagyi, Zoltan K. Nagy

Purdue University, Davidson School of Chemical Engineering, West Lafayette

Outline

- **Project objectives**
  - *… and main deliverables*

- **Current realizations**
  - *… and how our recent results fit into the project objectives*

- **Short term plans**
  - *… how are we planning to extend the research*

Project objectives

Well-known phrases

- Key unit operation in fine chemical industry
- Its driving force is the supersaturation
- Crystal size and shape: increasing significance
- Distribution - size, shape
- ***Control!***

Physical properties
- Porosity
- Specific surface
- Mechanical properties

Product quality
- Adsorption properties
- Polymorphism
- Dissolution rate

Technological issues
- Efficiency, batch time
- Filterability, drying

PURDUE 3

Project objectives

- **Many technology and economic drivers**
- **70% of all solid products & 90% of APIs involve a crystallization step**
- **Control of crystalline properties (CSD, shape, polymorphic form, purity, etc.) important**
  - **Product effectiveness (dissolution, bio-availability, tablet stability)**
  - **Efficient downstream operations (filtration, drying)**

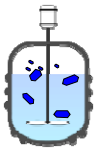

Crystallization → **Downstream processes** → **Final product**

Control of crystal properties is critical for product functionality and operational efficiency

PURDUE 4

Project objectives

- **Crystal size, shape and purity is often not achieved in the crystallizer →innovative technologies are required. We propose the followings:**

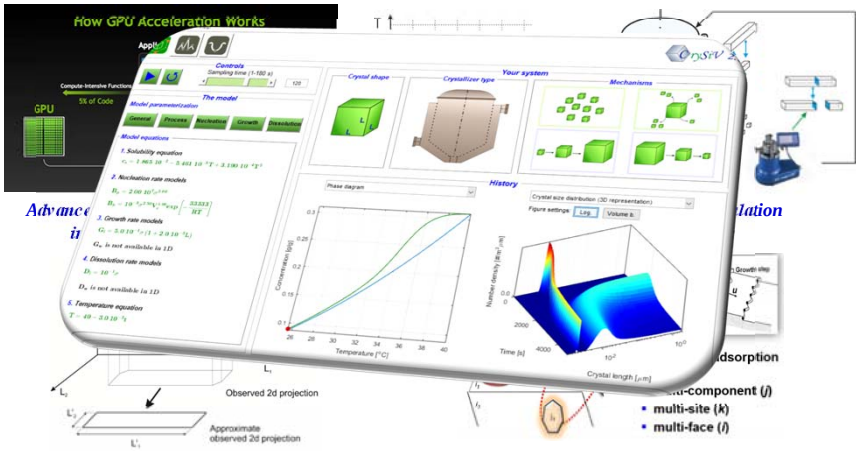

Projection based 2D CSD→CLD, ARD transformation with real time applicability potential for MPC applications

Application additives for purity control and manipulation of crystallization kinetics

PURDUE 5

The CrySiV

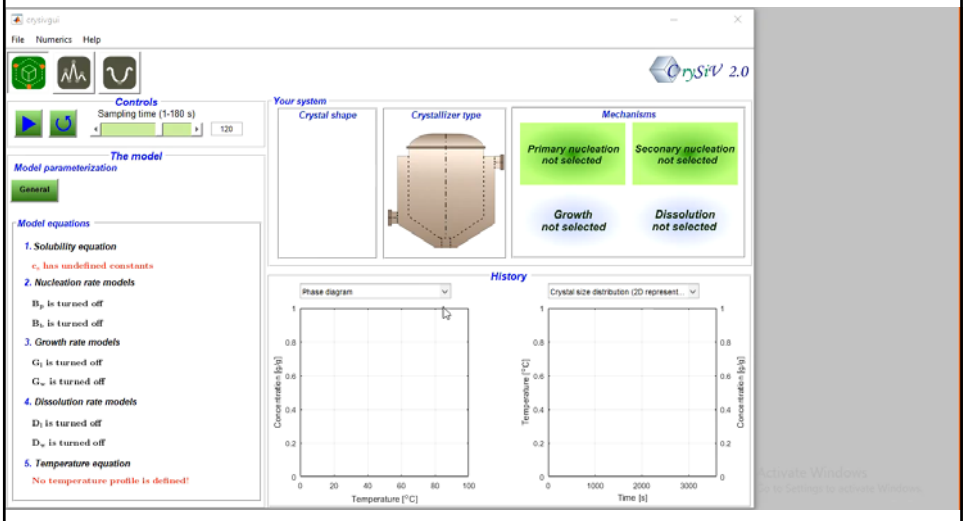

PURDUE 6

Project objectives

Main deliverables:

- A model based optimization case study for the optimization of temperature and GM concentration profiles for crystal shape control using 2D/nD PBM models (3 year)
- Efficient nD PBM-based simulation, optimization and control platform (1 year)
- FBRM-PVM sensor model for quantitative use of these technologies (1 year)
- Simulation case studies for NMPC of CSD and shape for the batch and continuous integrated crystallization-wet milling processes (2 year)
- First proof-of-concept experimental implementation of a full 2D PBM based real-time predictive control of CSD and shape during crystallization in impure media, using in line real-time image analysis (3 year)
- High quality journal and conference publications (2-3 year)

Recent results – Soft-sensor development

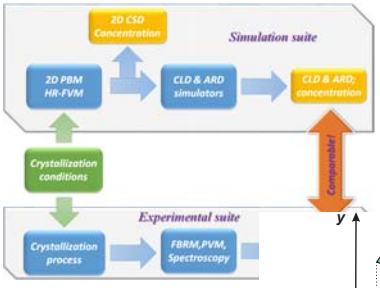

Transformation between CSD and CLD is generally required for practical applications

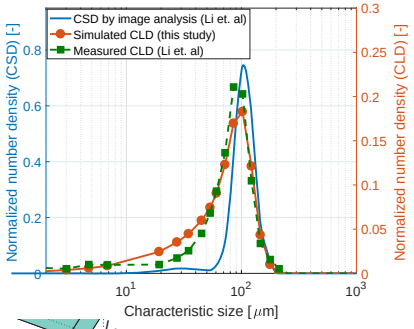

Transformation performance for sphere-like crystals' population

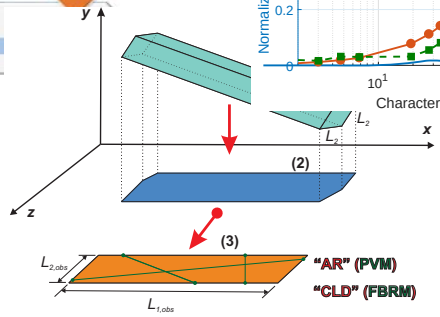

Geometrical model based approximate forward transformation

Recent results – Soft-sensor development

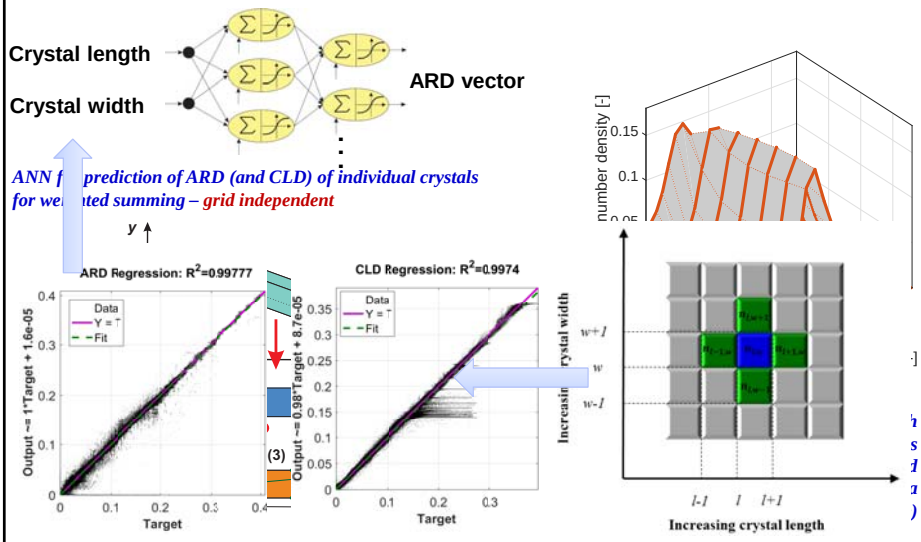

ANN performance for training data

PURDUE

Recent results – CLD based NMPC

KP: vector of unknown kinetic parameters to be estimated

$$SSE(\boldsymbol{KP}) = \underbrace{\frac{1}{I\,J}\sum_{i=1}^{I}\sum_{j=1}^{J}\left(\frac{c_{e,\{i,j\}} - c_{s,\{i,j\}}}{c_{e,\{i,j\}}}\right)^2}_{\text{Concentration fit}} + \underbrace{\frac{\boldsymbol{w}}{I\,J\,K}\sum_{i=1}^{I}\sum_{j=1}^{J}\sum_{k=1}^{K}\left(\frac{CL_{e,\{i,j,k\}} - CL_{s,\{i,j,k\}}}{CL_{e,\{i,j,k\}}}\right)^2}_{\text{CLD fit}}$$

Optimize the objective function: $SSE(\boldsymbol{KP}) \overset{!}{=} min$ **

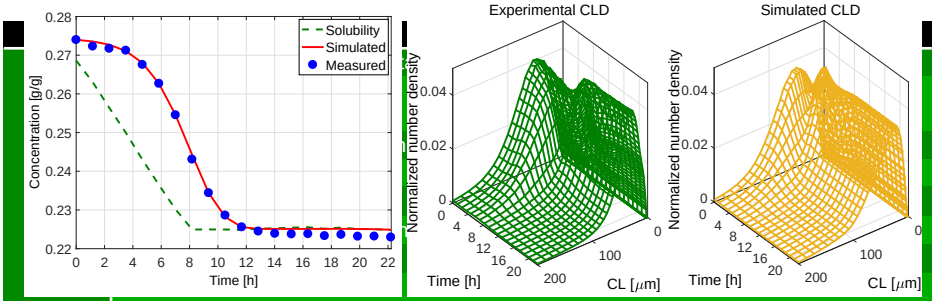

Calibrated model: concentration fit ***Calibrated model: CLD fit***

PURDUE ENGINEERING

Recent results – CLD based NMPC

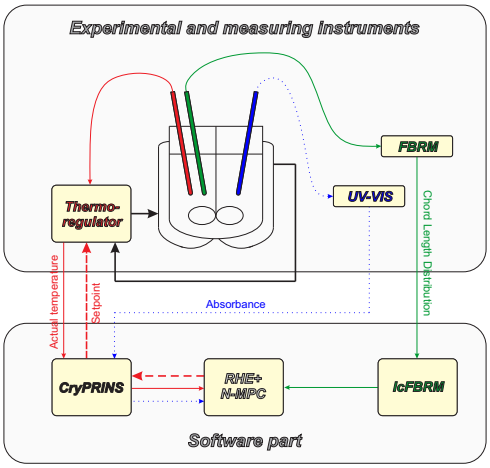

The applied software and hardware infrastructure

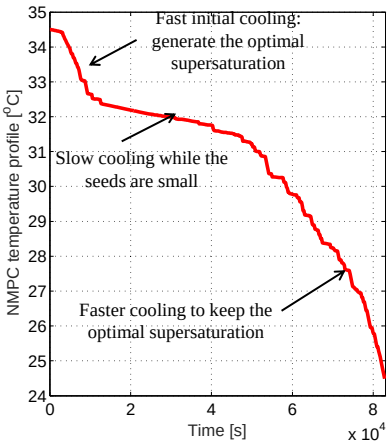

NMPC temperature profile: optimal control

11

PURDUE

11

Recent results – CLD based NMPC

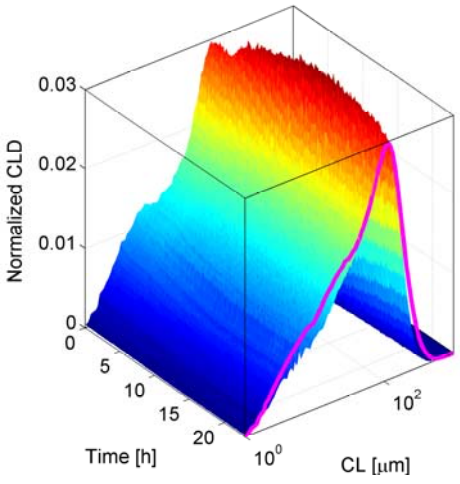

CLD variation during the batch and the target CLD

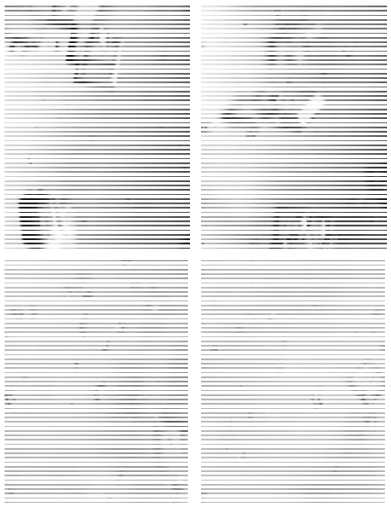

NMPC (top) and the corresponding linear cooling (bottom) crystals (1000 x 1500 microns)

PURDUE ENGINEERING

12

Recent results: crystallizer-wet mill optimization

- Crystallizer: crystallization **only**
  - primary nucleation
  - growth
  - dissolution
- Wet-mill: **breakage + crystallization**
  - fragmentation
  - attrition
  - primary nucleation
  - growth
  - dissolution
- Temperature: controlled in the crystallizer, **energy balance in the wet-mill** (no heat losses)

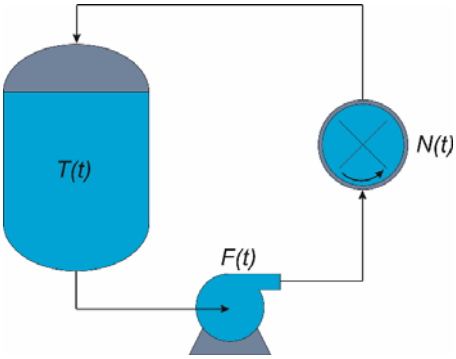

Scheme of the integrated crystallizer-wet mill system with the most important design parameters

PURDUE 13

Recent results: crystallizer-wet mill optimization

- Grid discretization. **Inflation**: min/max cell size, linear transition
- **Non-uniform grid** is always **faster** at the same level of accuracy (~ 1 OM)
- **GPU** brings > **2 OM** speedup under 3 % accuracy

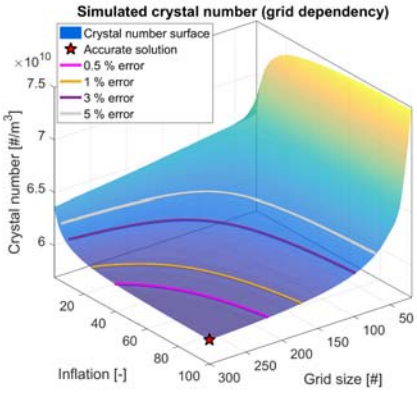

Simulated crystal number as a function of grid size

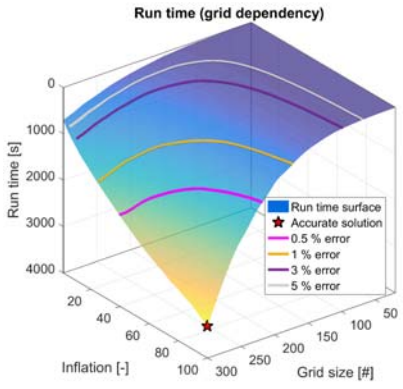

Run time as a function of grid size

PURDUE 14

Recent results: crystallizer-wet mill optimization

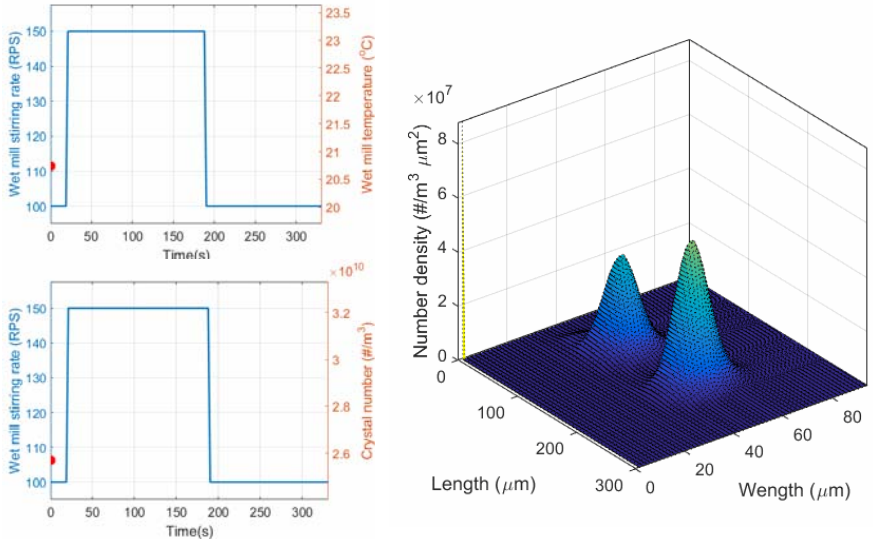

Visualization of the wet-mill dynamics after step-changes in the wet-mill stirring rate

Recent results: crystallizer-wet mill optimization

- **Seeded crystallization. Target CSD not achievable for the crystallizer-only**
- **Mean product size realized well with the integrated system**
- **Integrated system in un-seeded case: in-situ seed generation in the wet-mill and optimal dynamic seeding through the pump**

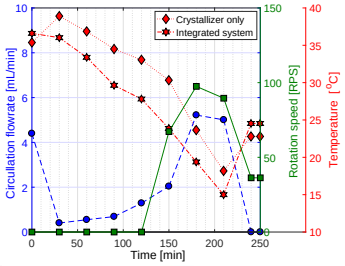

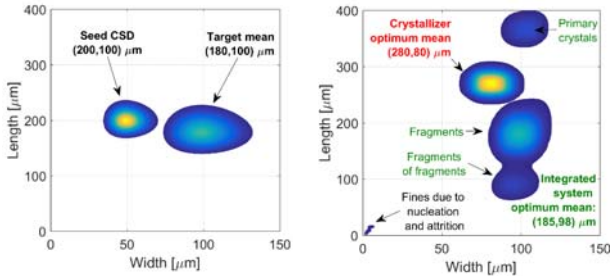

The optimal performance of the two systems for seeded crystallization of rod-like crystals

Short term plans (~1 year)

Continuous MSMPR-wet-mill

… with multiple MSMPR stages for growth and dissolution

2D crystallization

… parameter estimation based on in-situ measurable experimental data

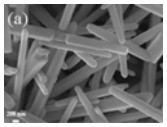

2D MPC implementation

… for model based size and shape control

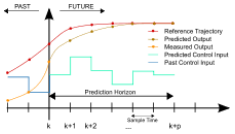

PURDUE

17

A Holistic Approach for the Model-based Control of Crystal Size, Shape and Purity in Integrated Batch and Continuous Crystallization - Wet Milling Systems

Botond Szilagyi, Zoltan K. Nagy

Purdue University, Davidson School of Chemical Engineering, West Lafayette

Thank you for your attention!
Questions?

18

IFPRI 40th Annual General Meeting

Project Reporting:

Milling and Material Grindability

J.Y. Ooi, L.G. Wang, X.Z. Chen, C. Labra, J.F. Chen*, J. Sun

University of Edinburgh, UK

*Queen's University Belfast, UK

Edinburgh, June 2018

Project Overview

- Overall goal is to develop a generic methodology to characterise grindability of particulates in milling, through:
  - Develop grindability measures to characterise the comminution behaviour of particulates
  - Understanding particle dynamics in a mill from computational modelling and experiments
  - Hierarchical verification and validation leading to robust evaluation of milling performance
- Project commenced January 2013
- A summary of key findings for the project is presented

Material grindability in a mill

Material-dependent function

- Density
- Young's modulus
- Hardness
- Poisson ratio
- Yield stress
- Strength
- ……

Mill-dependent function

- Machine type
- Machine size
- Grinding tools
- Operating parameters
- Feed rate
- Solid holdup
- ……

Multiscale strategy

Exp. measurement and DEM simulation

Milling tests and DEM simulation

mill grindability prediction

How will a particle break under a loading event?

“**material function**”

Material characterisation experiments

Material behaviour under indentation, static and impact loading were investigated:

Micro and nano-indentation tests – collaboration with Colin Hare (Surrey University, former Leeds University)

- Micro and nano-indentation & SEM
- Hardness, *H,* Young's Modulus, *E*, Fracture Toughness, K_c

Single particle impact tests

- Single particle impact
- Damage related with velocity and impact angle

In-situ loading test under X-ray micro-CT

- In-situ loading apparatus design and implementation
- Full field breakage behavior from X-ray μCT analysis

Measurement of fracture toughness, hardness, and Young's modulus

Material	H (GPa)	E (GPa)	K_c (MPa.m$^{1/2}$)
Alumina (1.0–1.18 mmm)	0.87	18.36	0.26
Zeolite (1.4–1.7 mm)	0.13	5.95	0.13
Zeolite (2.0–2.36mm)	0.33	8.15	0.43

Significant coefficient of variation in measurement:

H, E: 21 – 54 %

K_c: 27 – 75 %

- key mechanical properties governing breakage
- Provide basis for breakage model development

Breakage vs Impact Velocity and Impact Angle (Zeolite 1.4-1.7 mm)

- Minimal breakage below impact velocity of 15 m/s
- Breakage increases over 15 m/s and increases with increasing impact angle (90° is normal impact)

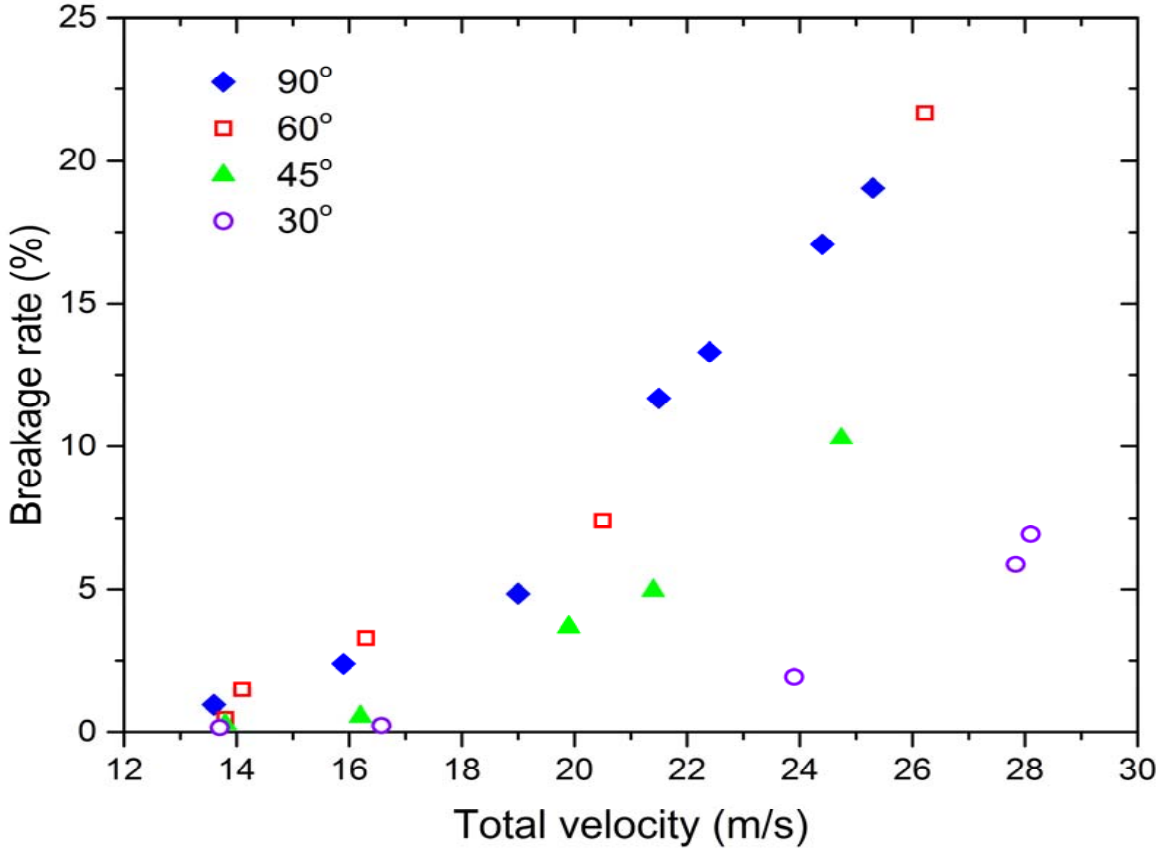

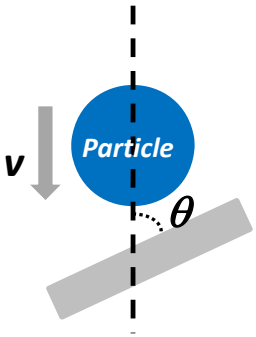

Tangential Velocity Component Contribution

- Results below show breakage at different impact angles for a low normal velocity (~8 m/s) and a higher normal velocity (~14 m/s)
- At low normal velocity, tangential velocity has a negligible effect
- At higher normal velocity (above a certain threshold velocity), breakage ratio increases with increasing tangential velocity

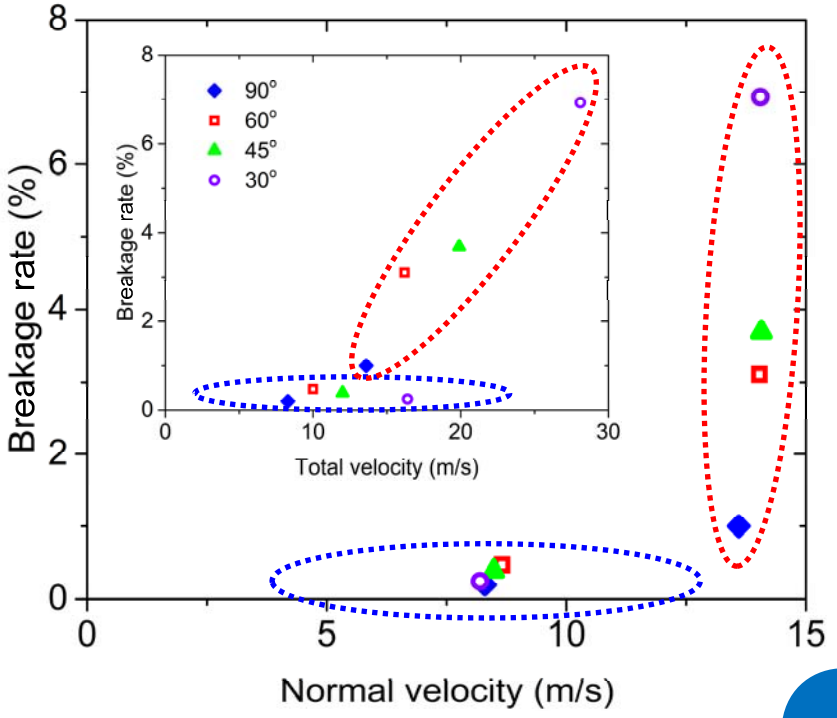

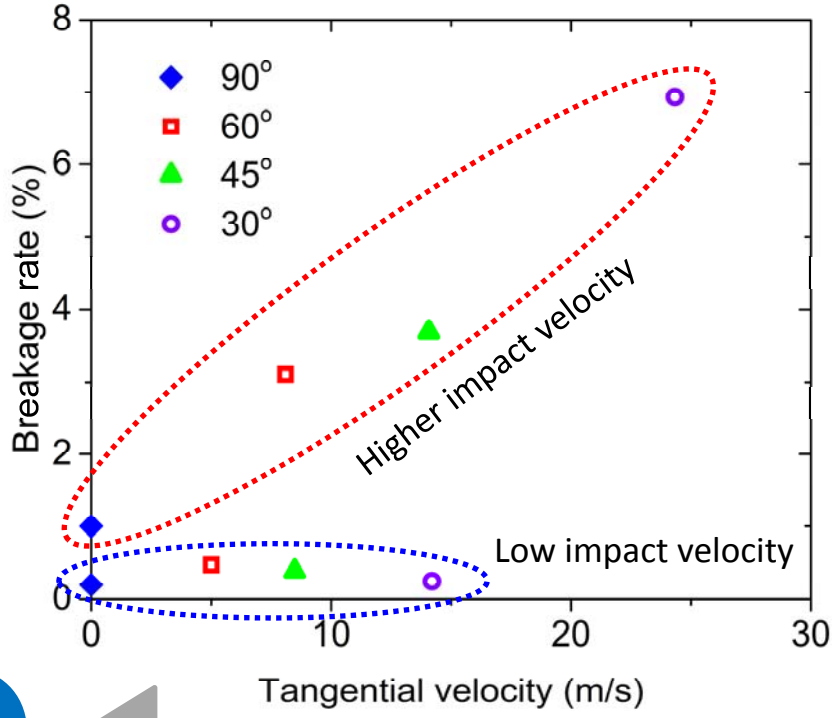

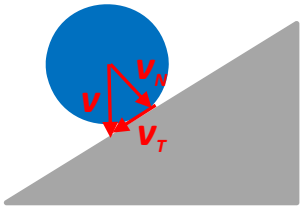

Summary on material characterisation

- key mechanical properties governing breakage measured from indentation tests
- Under impact loading:
  - Normal component of velocity plays a dominant role in particle breakage
  - Tangential component of velocity plays increasingly important role in breakage with increasing impact velocity
  - The role of tangential velocity (or impact angle) should be considered in breakage model development
  - Impact velocity was limited to 30 m/s in the experimental setup. Bonded DEM simulation would be used to inform the higher impact velocity regimes

Bonded DEM simulation

- A bonded particle model based on Timoshenko beam (Brown et al. 2014) was used to simulate particle breakage
- Each bond contact considers forces and moments response under compression, tension, torsion and bending

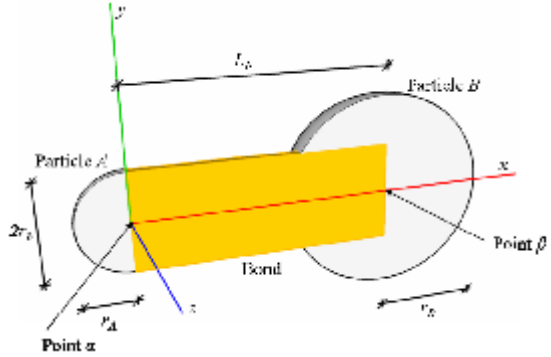

Bond between two particles

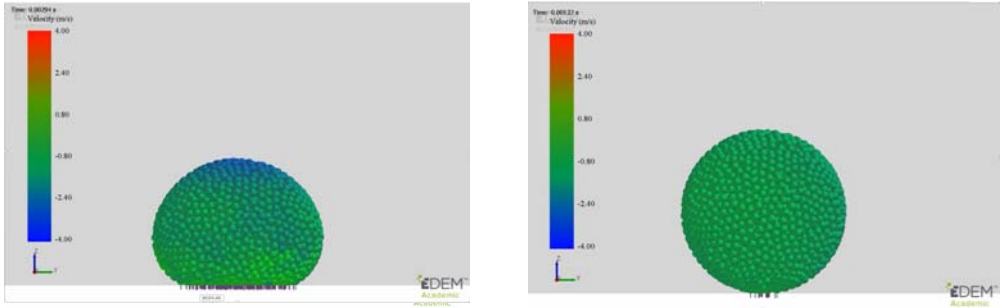

Velocity distribution during impact

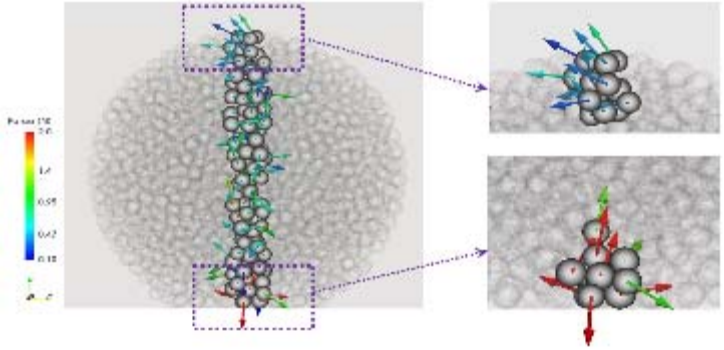

- Help reveal the failure mechanism

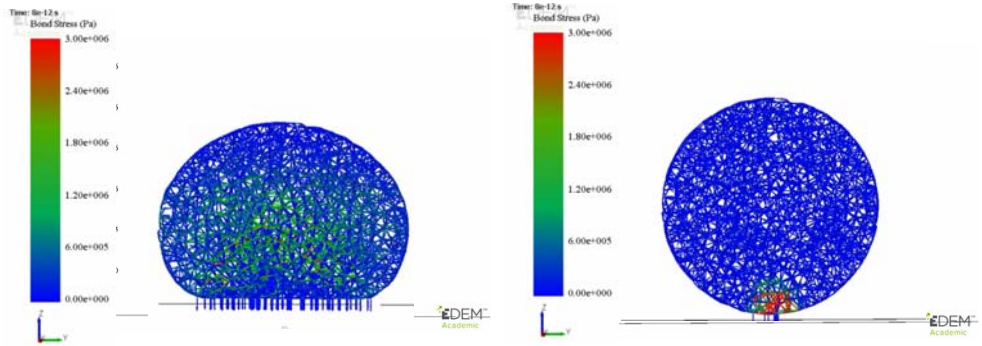

Tensile stress on bond network

- The model used to study various materials

DEM impact simulation - Zeolite

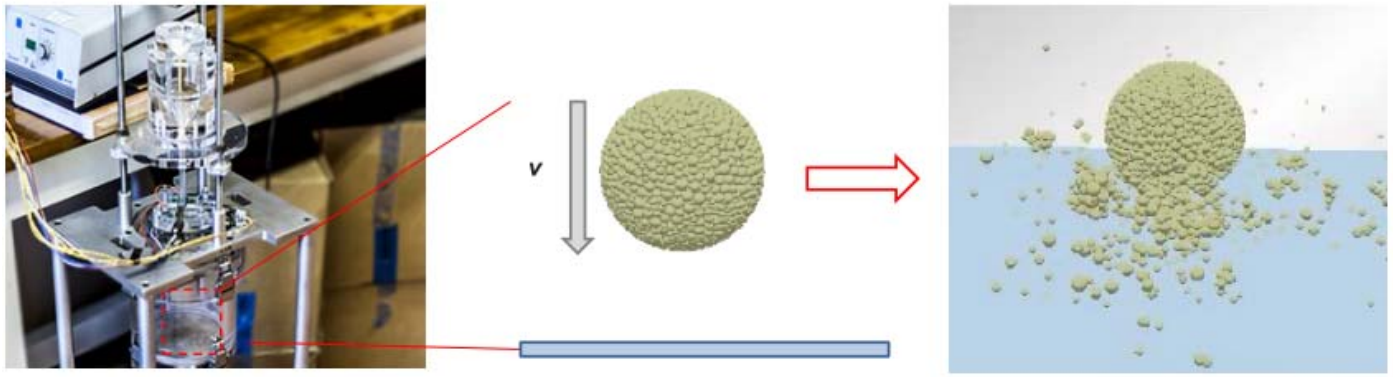

3687 constituent particles for a bonded particle

Single particle impact tester (courtesy: Leeds University)

Edinburgh Bonded Particle Model simulation

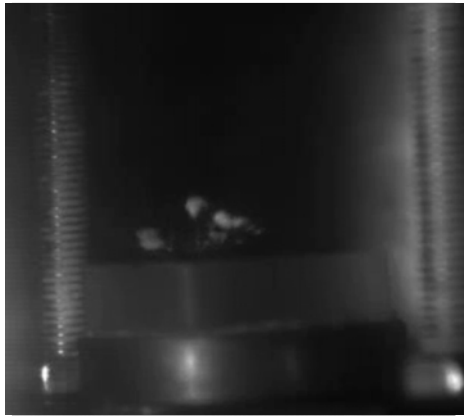

30 m/s

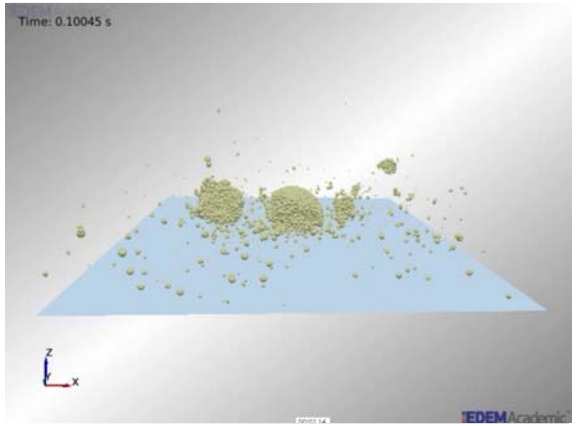

30 m/s

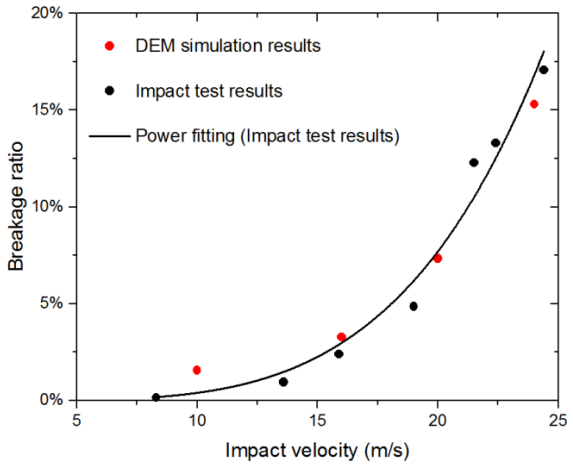

Good qualitative and quantitative agreement with experiment; 2.0 mm zeolite particle

DEM impact simulation - Alumina

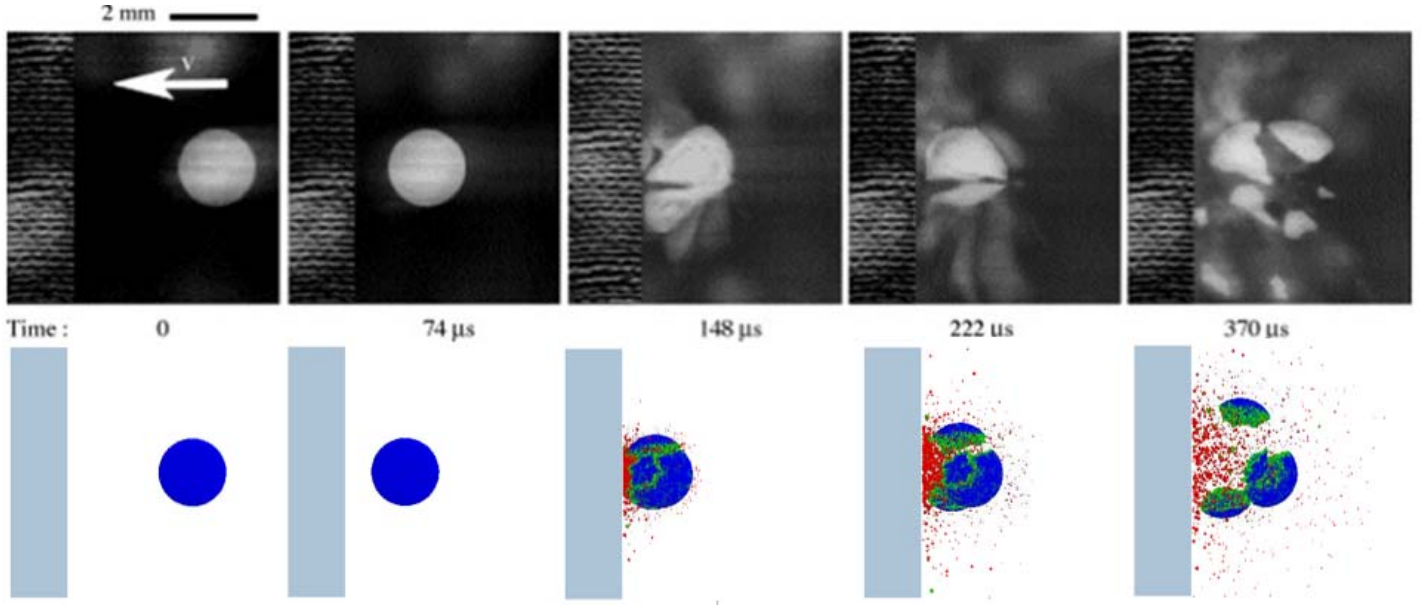

- Comparisons between the simulation and the experiment of Antonyuk *et al* 2006

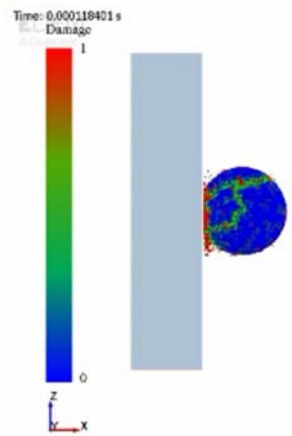

Alumina: Impact velocity :23m/s

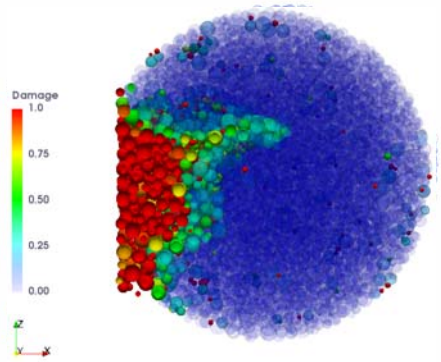

Diametrical slice

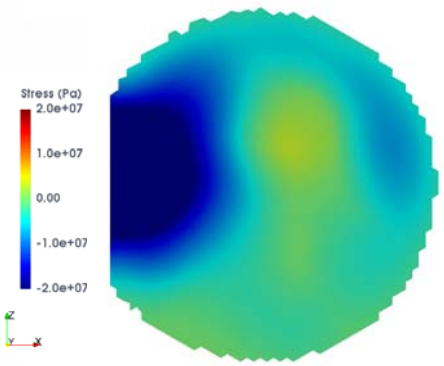

Min. principal stress

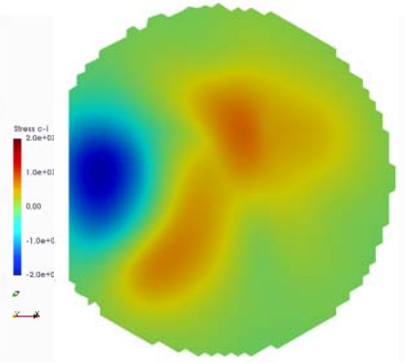

Max. principal stress

- Cone crack initiated with secondary crack propagation leading to fragmentation (23 m/s)

Impact DEM simulation- Alumina

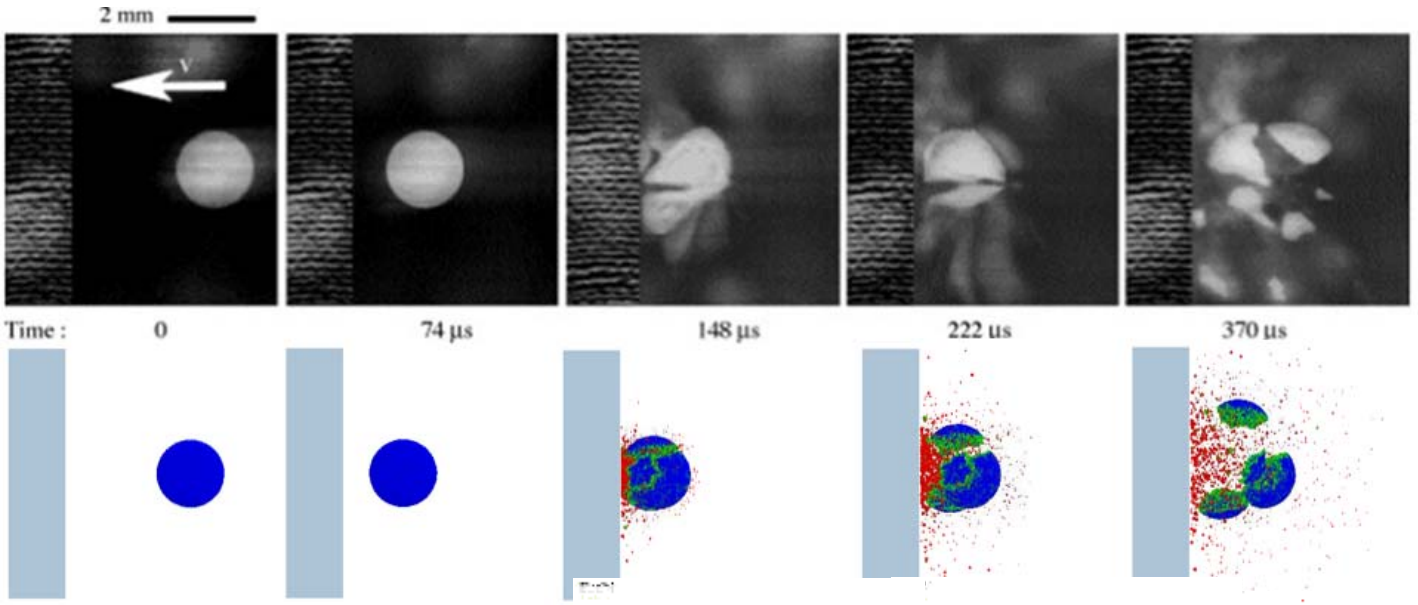

➢ **Comparisons between the simulation and the experiment of Antonyuk *etal* 2006**

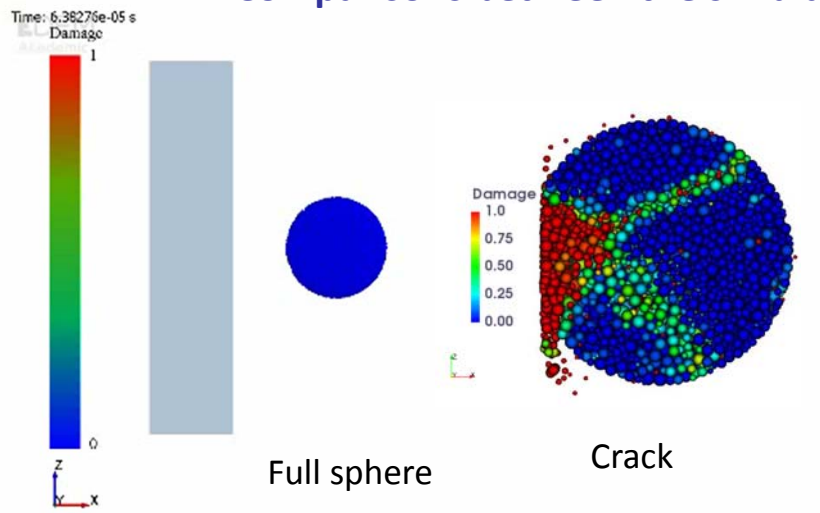

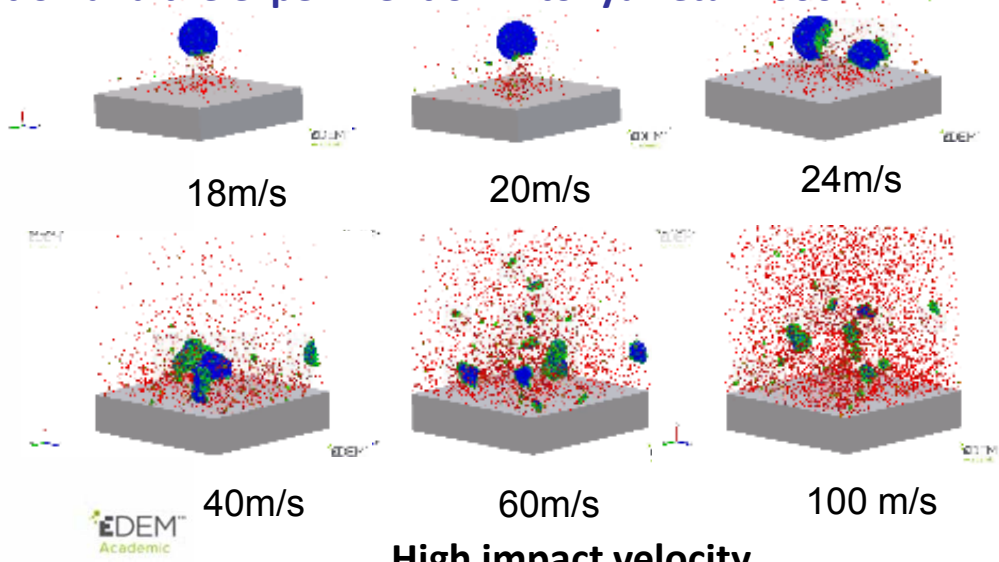

Alumina: Impact velocity :23m/s

High impact velocity

Development of a single particle breakage model to include the effect of impact angle

Model Considering Lateral Cracks under Normal Impact

- Assume: lateral crack responsible for chipping mechanism;
- Most existing models based on crack length from static or quasi-static analyses;
- Only Evans et al. (1978) used radial crack length under impact loading;
- Based on lateral crack length from impact damage (dynamic) analysis, a new model is developed for breakage ratio ε:

$$\varepsilon = \frac{V_{det}}{V} = \frac{\pi {c_l}^2 h}{\frac{4}{3}\pi R^3} = \frac{3{c_l}^2 h}{4R^3} \propto \frac{\rho^{1/4} R^2 H^{1/2}}{k_c^{5/2}} v^{9/2}$$

V_{det}=detached vol., V=total vol., c_l=lateral crack length, h=crack depth, R=radius, H=Hardness, v=impact vel., k_c= fracture toughness

- Close agreement between proposed model and impact test data

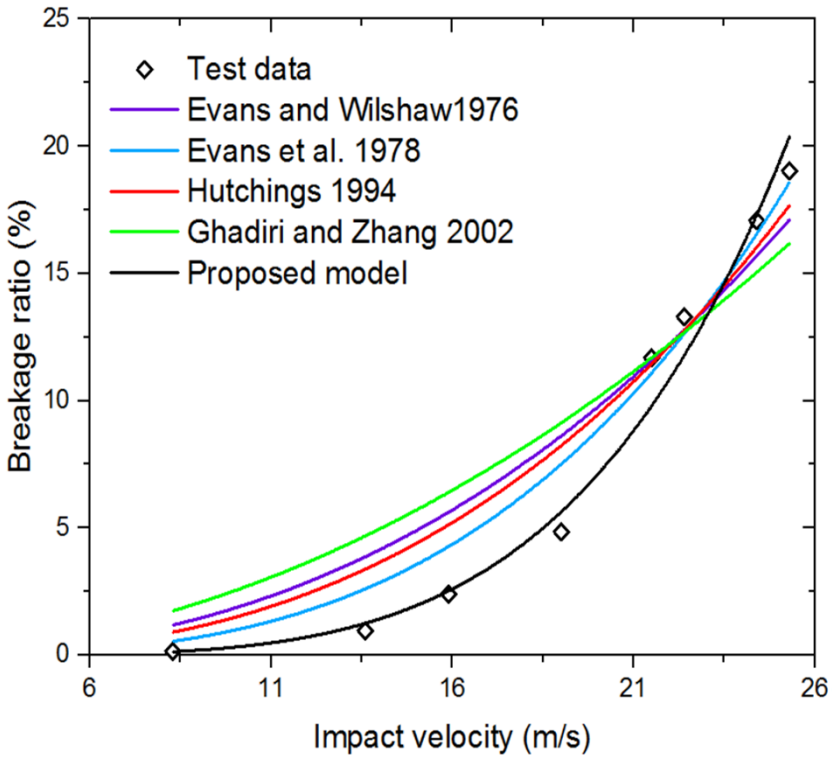

Model Considering Oblique Impact

- All previous models only considered the normal component of the impact velocity: the tangential component is ignored
- Experimental evidence has shown the significance of tangential component
- The effect of the incidence angle may be considered using the following equivalent velocity:

$$v_{eq} = \sqrt{(sin^2\theta + \alpha^2\mu^2 sin^2\theta cos^2\theta)}v$$

where v_{eq} is the equivalent velocity, v is the total velocity, θ is the incident angle (=90 deg when normal), μ is the dynamic friction coefficient between particle and impact surface, α is a coefficient.

Comparison with Test Data

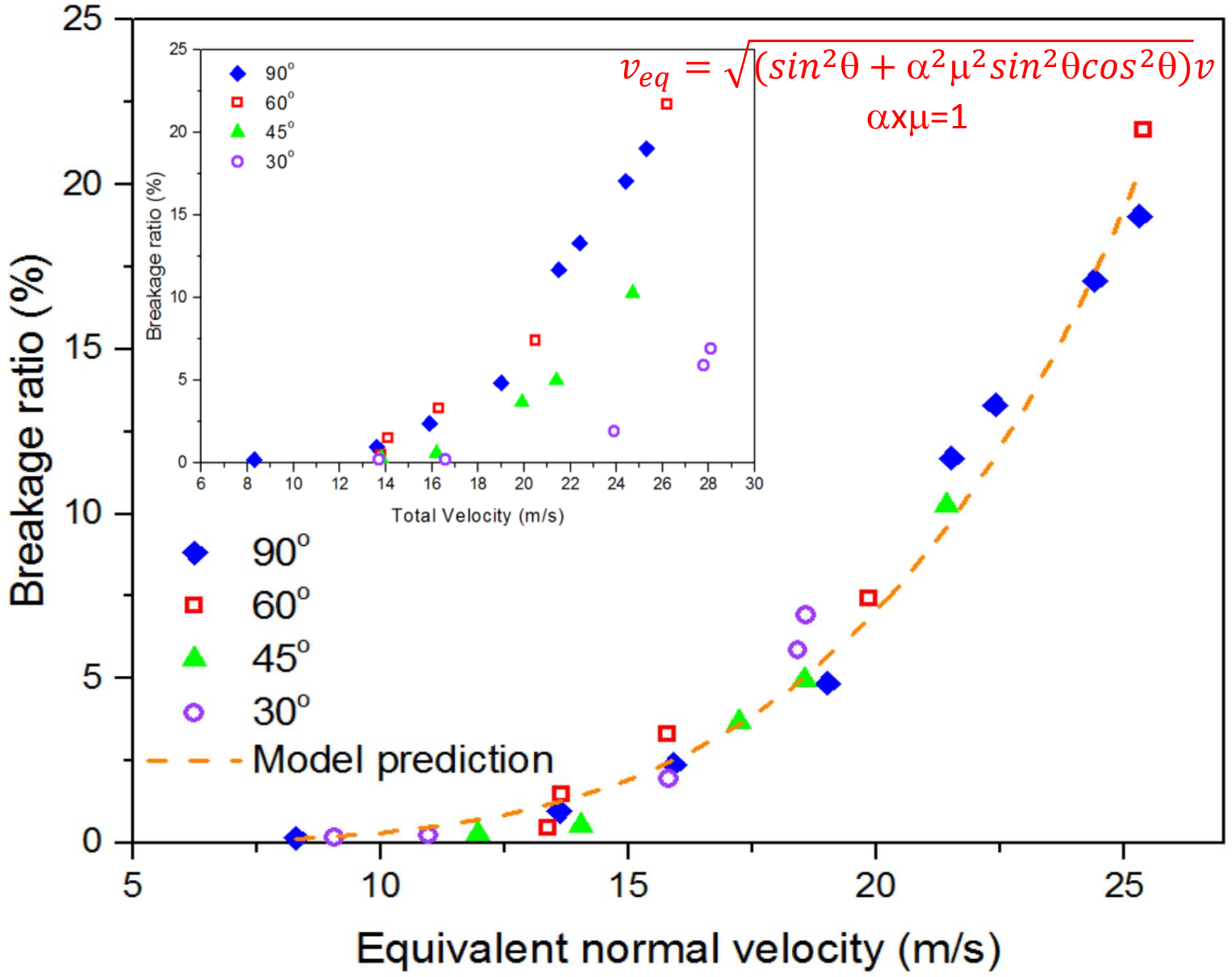

Model Assessment: Fragmentation

Data source: Salman et al. (2003) Impact breakage of fertiliser granules

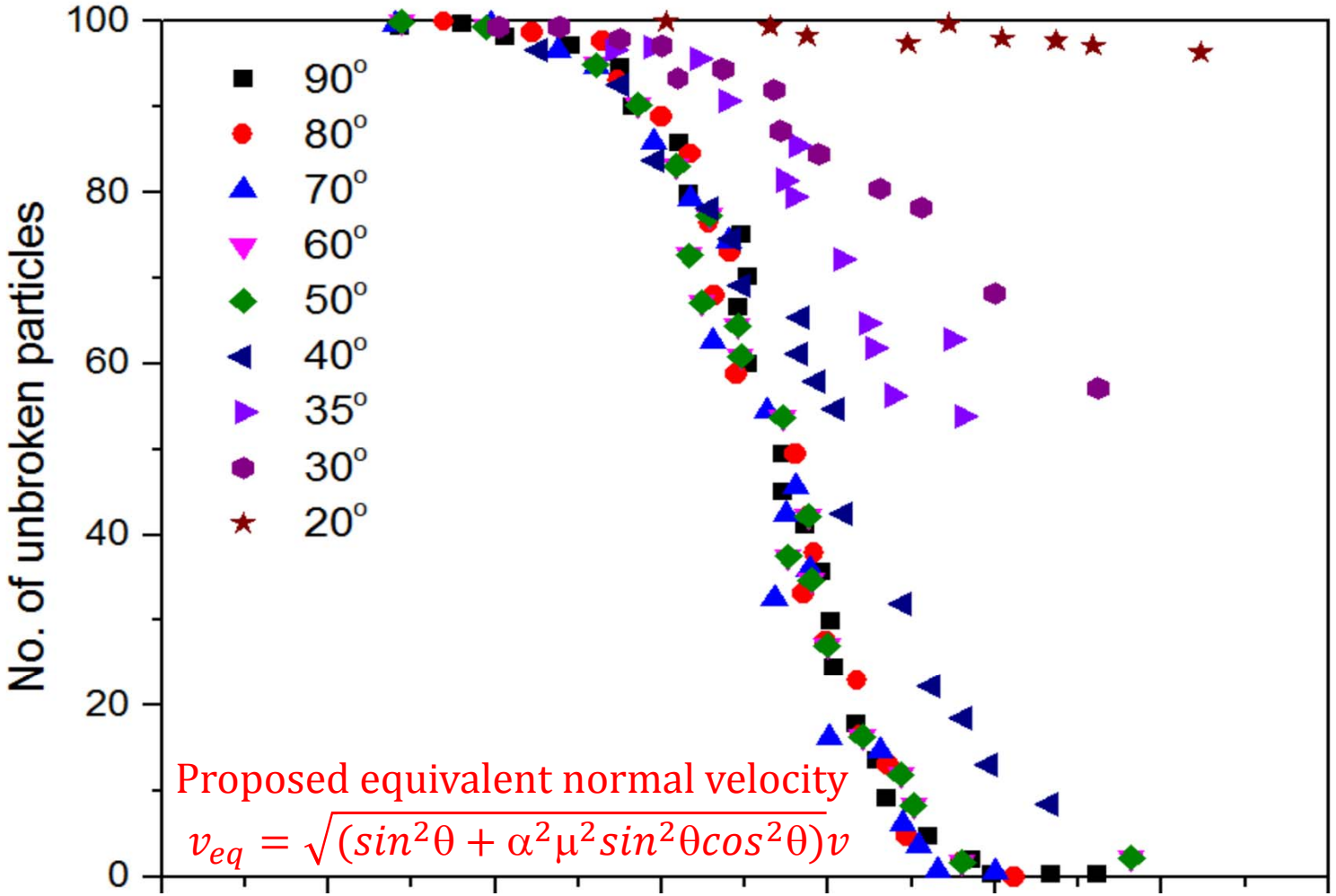

The equivalent normal velocity proposed successfully predicts the breakage under various oblique impact for both chipping and fragmentation (First model to consider impact angle!)

Model Assessment: Fragmentation

Data source: Salman et al. (2003) Impact breakage of fertiliser granules

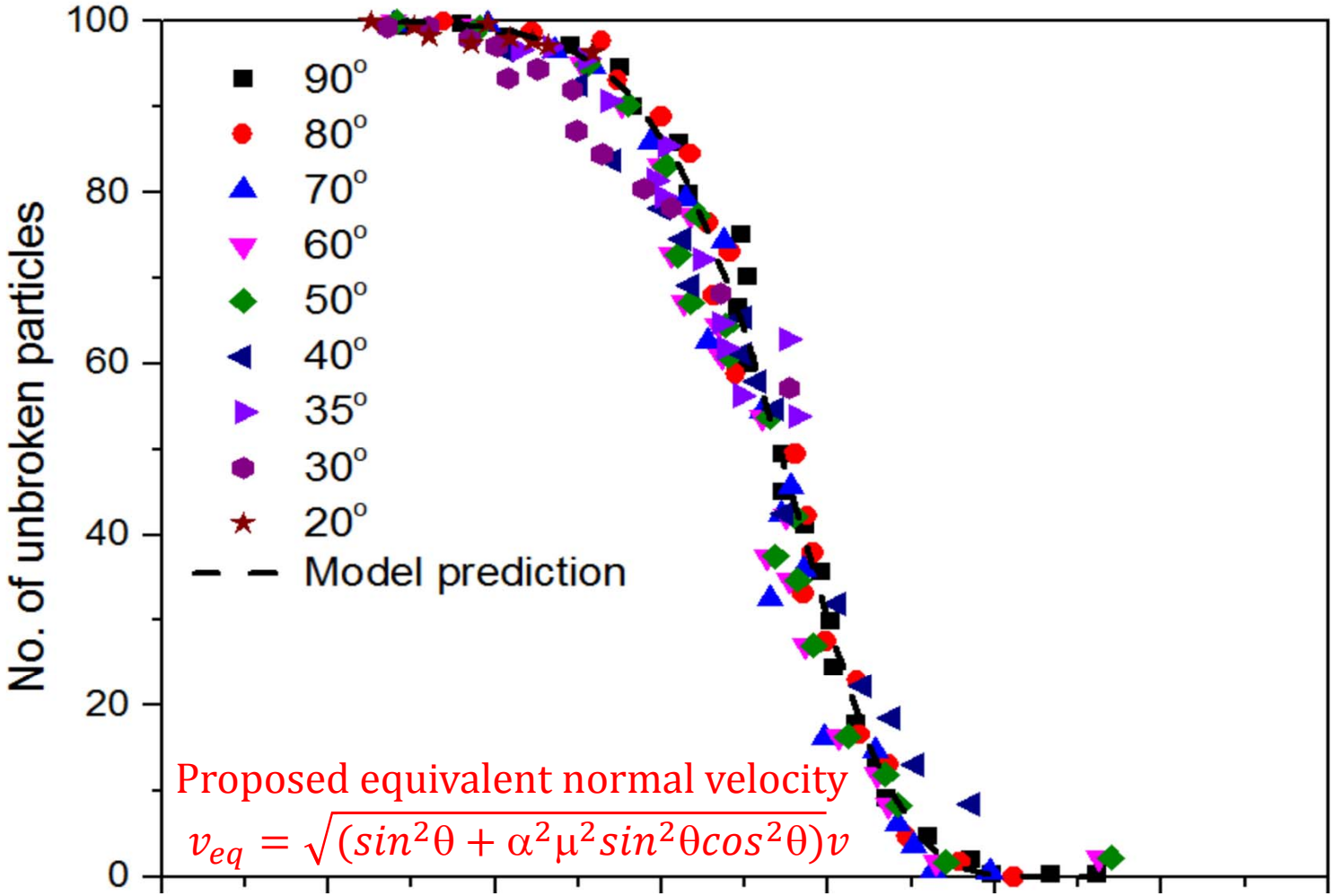

The equivalent velocity proposed successfully predicts the breakage under different oblique impacts involving chipping and fragmentation (First model to consider impact angle)

What are the loading events giving rise to particle breakage in a mill?

“**mill function**”

Milling Process and Test Materials

Pin impact mill was chosen to be studied

- High velocity impacts: 100UPZ mill
- Four rotary and stationary rings
- For fine and ultrafine grinding
- Collaboration with Hosokawa

Two test materials explored: brittle and semi-brittle response with nearly isotropic and reasonably well defined properties

Test conditions:
Rotatory speeds: 8k, 12k,16k, 18k rpm
Feed rates: 9, 14 ,19, 24 kg/h

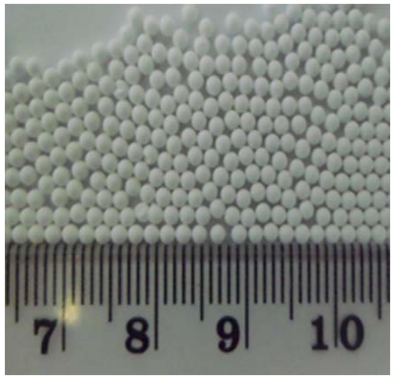

Alumina oxide

Zeolite 4AK

DEM simulation of impact pin mill

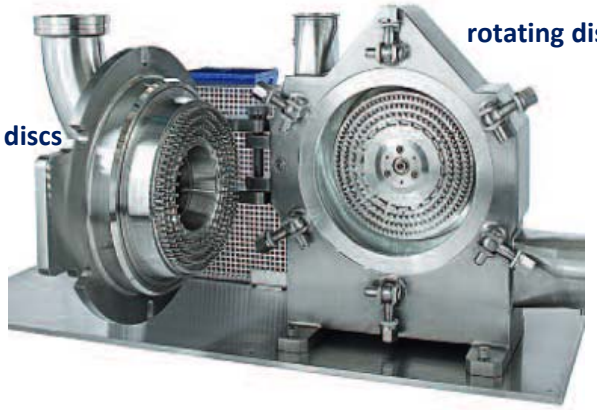

pin mill UPZ100 from Hosokawa

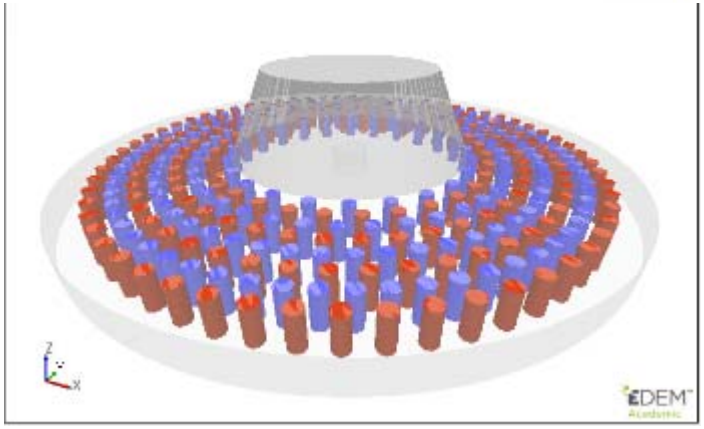

DEM implemented full scale model

Simulation parameters for Alumina particle

Parameters	Value
Particle density (kg/m^3)	3370
Particle diameter (mm)	1.1
Particle Poisson's ratio	0.3
Particle Young's modulus (GPa)	15
Coefficient of restitution	0.82
Coefficient of static friction	0.37
Coefficient of Rolling friction	0.1
Pin density (kg/m^3)	7850
Pin Poisson's ratio	0.25
Pin Young's modulus (GPa)	81

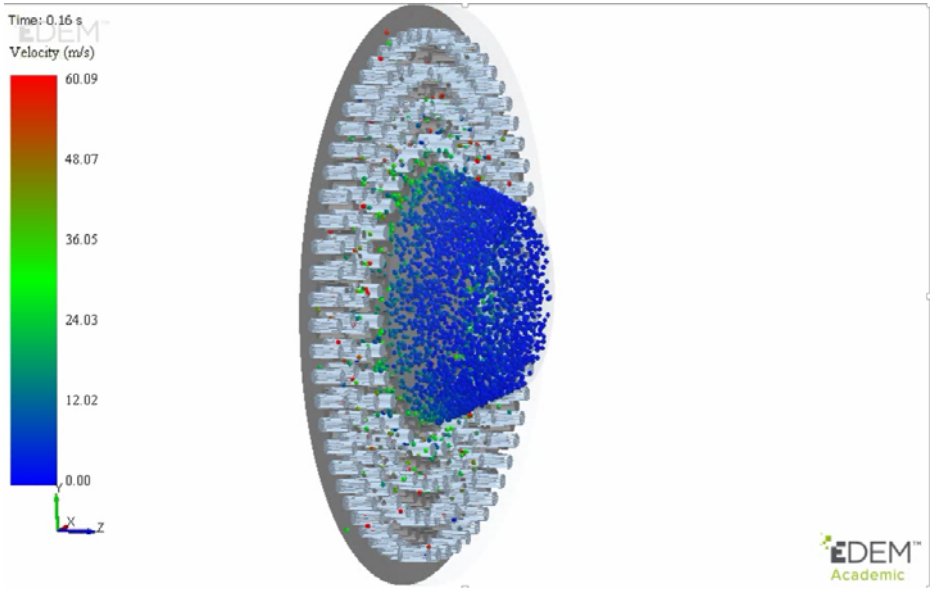

- Parameters from lab characterization and calibration
- Pin region is the active region

Results on feed rate and rotary speed

Experiment product size distribution

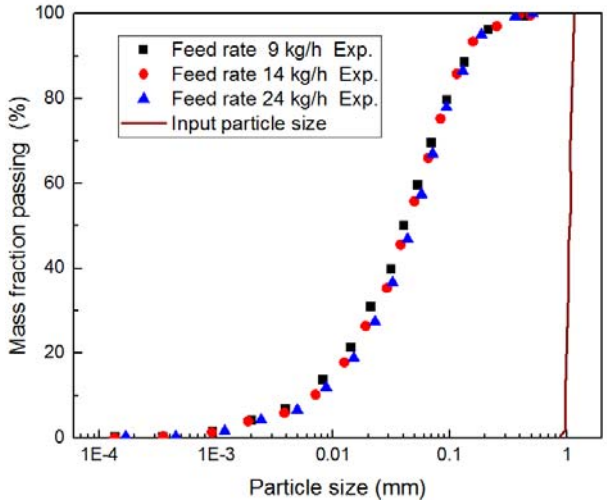

Alumina milling tests at different feed rates under 8000RPM

Computed Impact velocity distribution

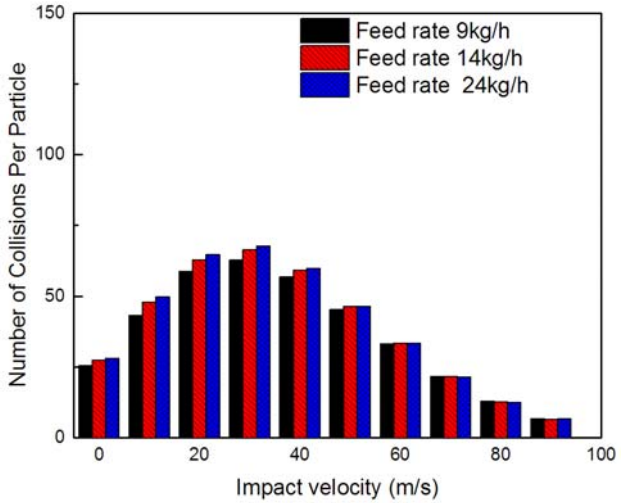

DEM simulation: different feed rates under 8000RPM

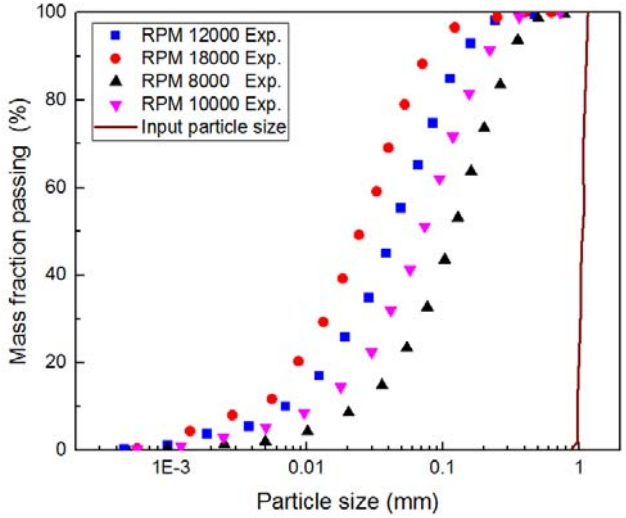

Alumina milling tests at different feed rates under 8000RPM

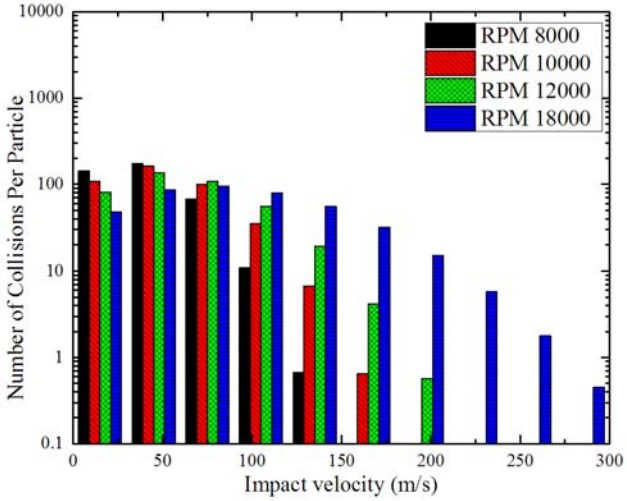

DEM simulation: different rotation speeds under 24kg/h

➢ Impact velocity distribution from DEM is the most useful indication of mill environment

Computed impact statistics

Average variables/RPM	8000	10000	12000	18000
Residence time (ms)	86.2	71.3	61.8	44.6
Impact per particle (-)	175	179	184	183
Impact velocity (m/s)	46.3	58.4	69.5	104.3
Normal velocity (m/s)	33	41.5	49.1	72.7
Tang. velocity (m/s)	26.7	33.7	40.3	61.4
Normal force (N)	36	47.3	58.1	93.5
Tang. Force (N)	4.4	5.7	7.1	11.5

- Although tangential impact velocity is comparable with normal impact velocity, tangential force can be much smaller – friction mobilisation

Linking material function and mill function to achieve a prediction

Multiscale DEM-PBM upscaling

Motivation of DEM-PBM coupling

- DEM provides particle scale data to inform Population Balance Model (PBM) prediction of an industrial mill

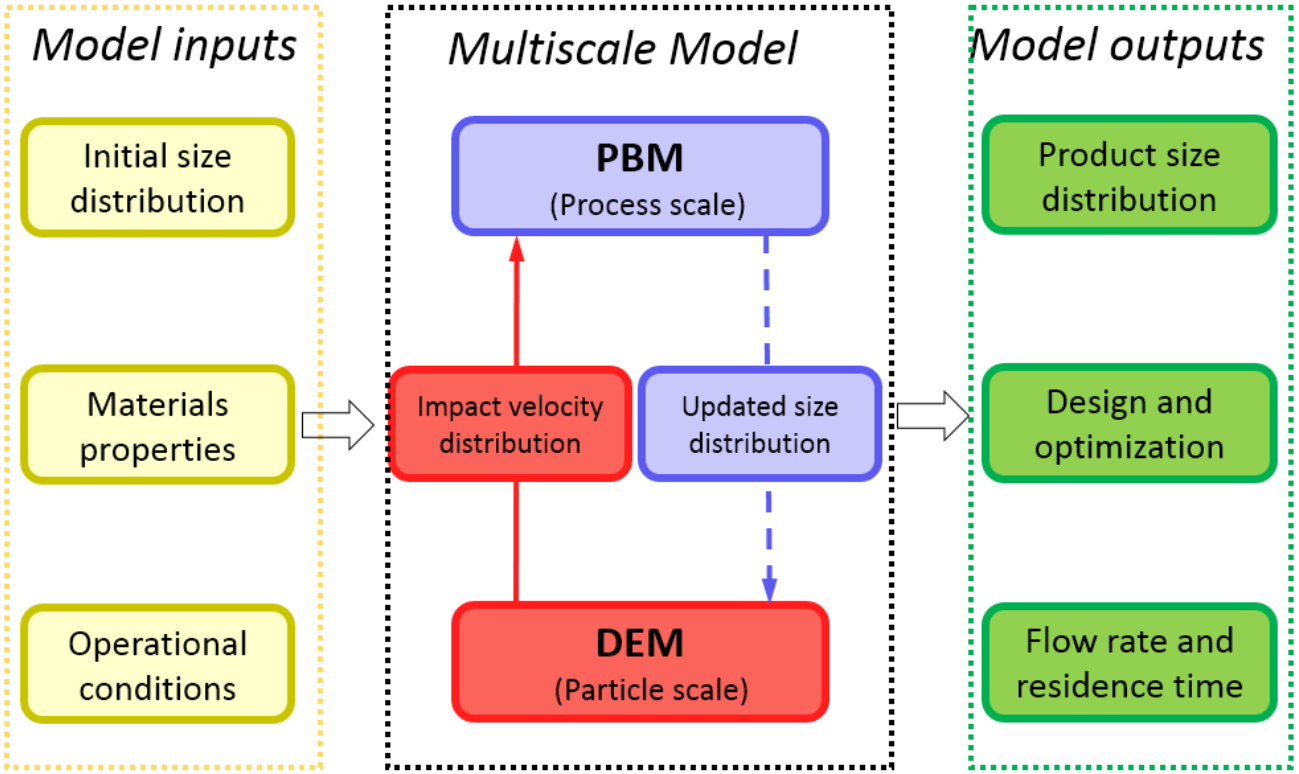

DEM-PBM upscaling strategy

Population balance model

$$\frac{\partial M_p(x,t)}{\partial t} = -S_M(x)M_p(x,t) + \int_0^\infty S_M(y)M_p(y,t)b_M(x,y)\,dy$$

Breakage rate

$$S_M(x) = Sc_M\left[1-\exp\left(-f_{mat}x\left(W_{m,kin}-W_{m,\min}\right)\right)\right]$$

Breakage Distribution

$$B_M(x,y) = \frac{1}{2}\cdot\left(\frac{x}{y}\right)^q\cdot\left(1+\tanh\left(\frac{x-x'}{x'}\right)\right)$$

Red variables: obtained from DEM

- ✓ Impact energy $W_{m,kin}$
- ✓ Impact frequency Sc_M

Blue variables: fit from 12000 RPM

- o Threshold energy $W_{m,\min}$
- o Material properties f_{mat}, q

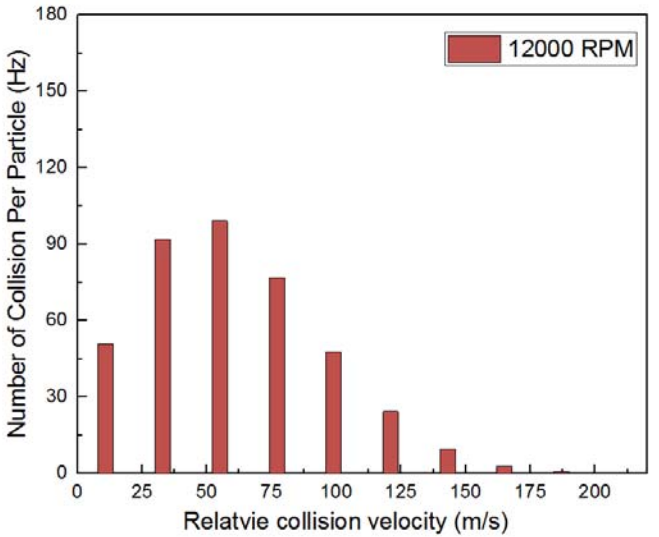

Impact velocity distribution from DEM

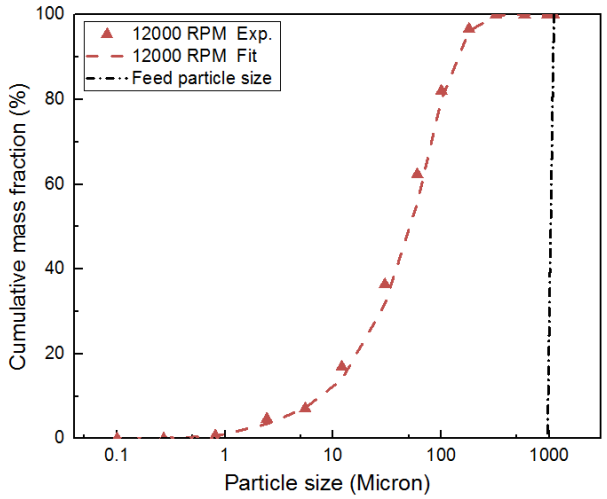

Using milling data to calibrate material parameters subject to the milling dynamics

DEM-PBM upscaling prediction

Population balance model

$$\frac{\partial M_p(x,t)}{\partial t} = -S_M(x)M_p(x,t) + \int_0^\infty S_M(y)M_p(y,t)b_M(x,y)\,dy$$

Breakage rate

$$S_M(x) = Sc_M\left[1-\exp\left(-f_{mat}x\left(W_{m,kin}-W_{m,\min}\right)\right)\right]$$

Cumulative breakage Distribution

$$B_M(x,y) = \frac{1}{2}\cdot\left(\frac{x}{y}\right)^q\cdot\left(1+\tanh\left(\frac{x-x'}{x'}\right)\right)$$

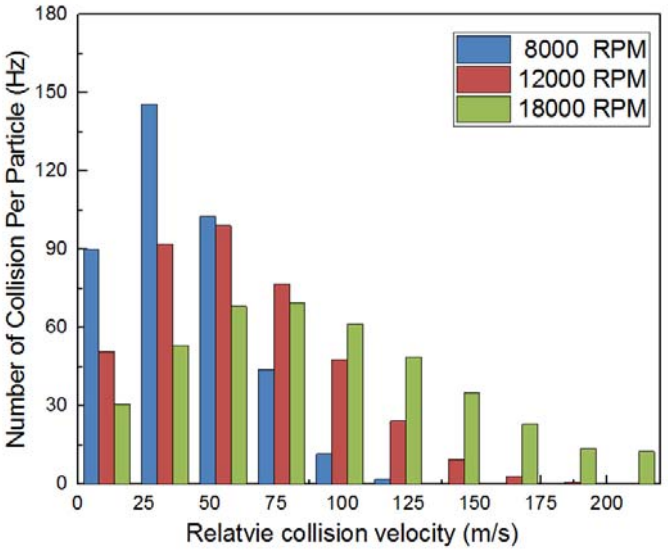

Impact velocity distribution from DEM

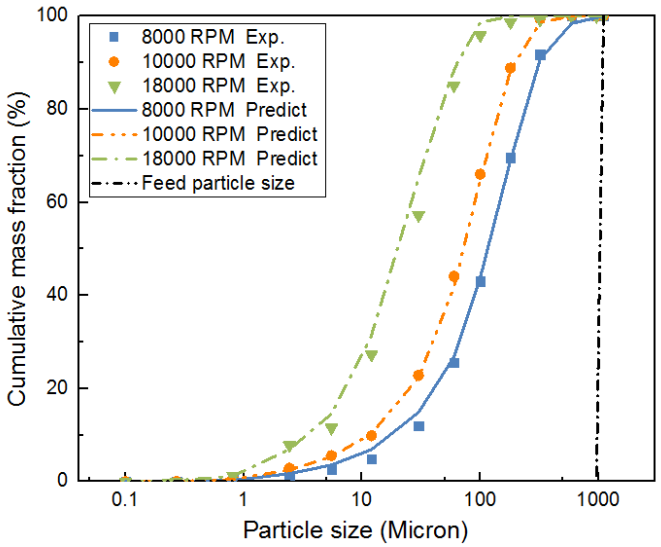

Product particle size distribution predictions

- The PSD of the other three rotation speeds were well predicted

High feed rate prediction

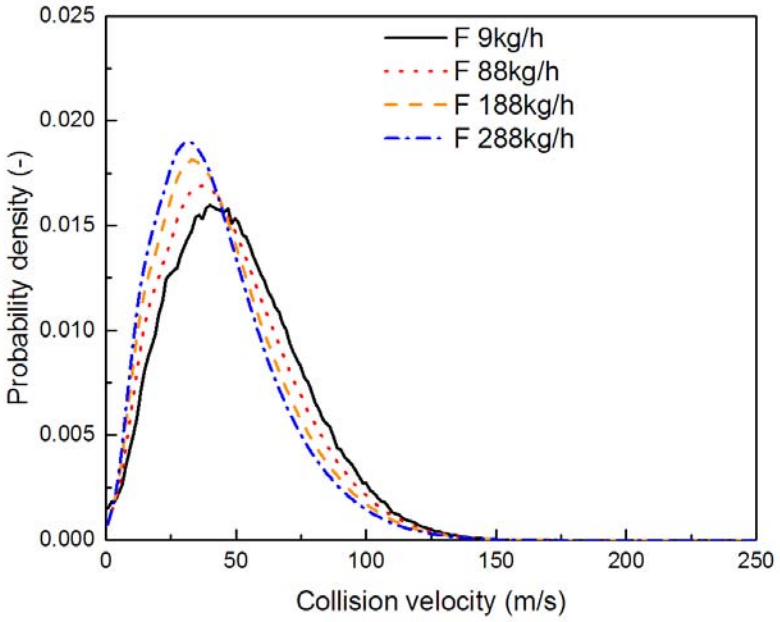

Impact velocity distribution from DEM

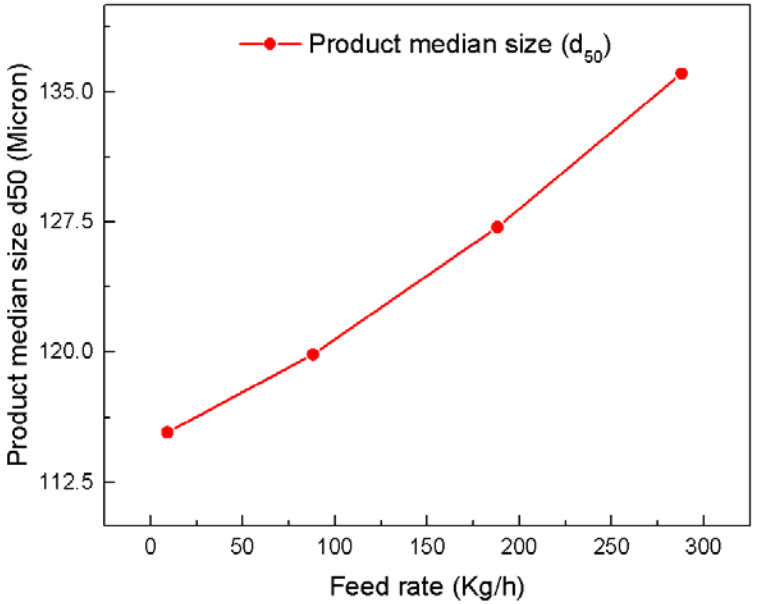

DEM-PBM coupling predictions

- For alumina particles:

  Increasing the feed rate from 9kg/h to 288kg/h, DEM predicts a decrease of the average impact velocity by 14%, leading to an increase of product median particle size (d_{50}) by 19%.

- Further confirmation from experiments would be useful

Summary of DEM-PBM strategy

1. Identify key loading events controlling breakage in the mill

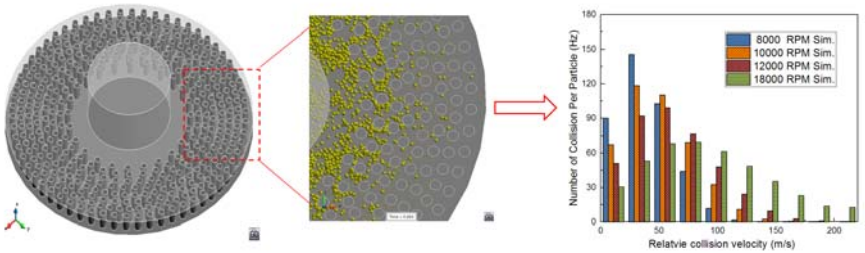

2. Establish how will particles break under these loading events

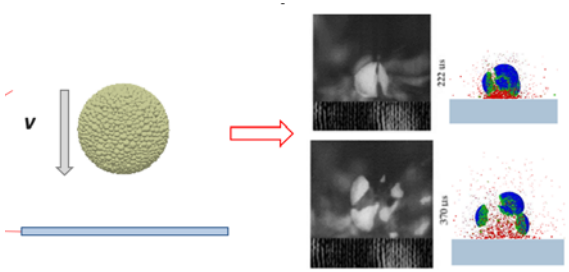

a. Experiments and DEM to determine material properties

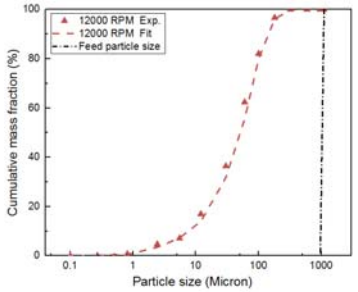

b. Control milling test to calibrate model parameters using system approach

3. DEM-PBM coupling to link material function and mill function to predict milling performance

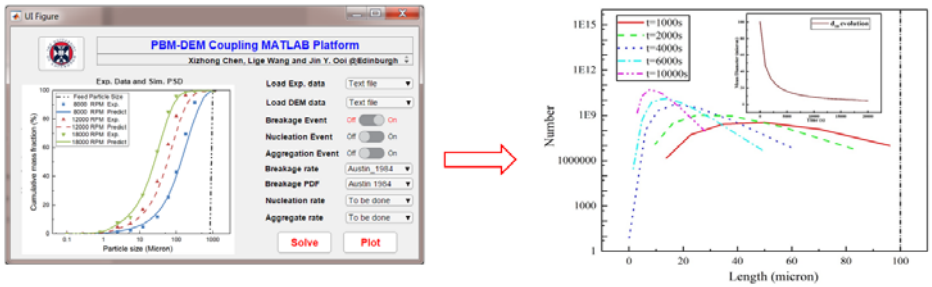

Mill function estimation

Scaling-up

Material function estimation

procedure

DEM-PBM coupling for PSD prediction

Conclusions and looking forward

- Static, indentation and impact loading tests were deployed to characterise particle properties
- A new model of particle breakage under impact loading was proposed including the effect of impact angle
- Chipping and fragmentation of particle under impact were captured using the bonded DEM simulation
- Pin mill test data at four rotary speeds and feed rates provides data for validation
- DEM modelling of UPZ100 pin was implemented to evaluate particle dynamics during milling
- A multiscale framework of DEM-PBM coupling was developed to predict the milling behaviour of impact pin mill
- Further two-way coupling refinement is progressing
- Extending the strategy to other granular processes

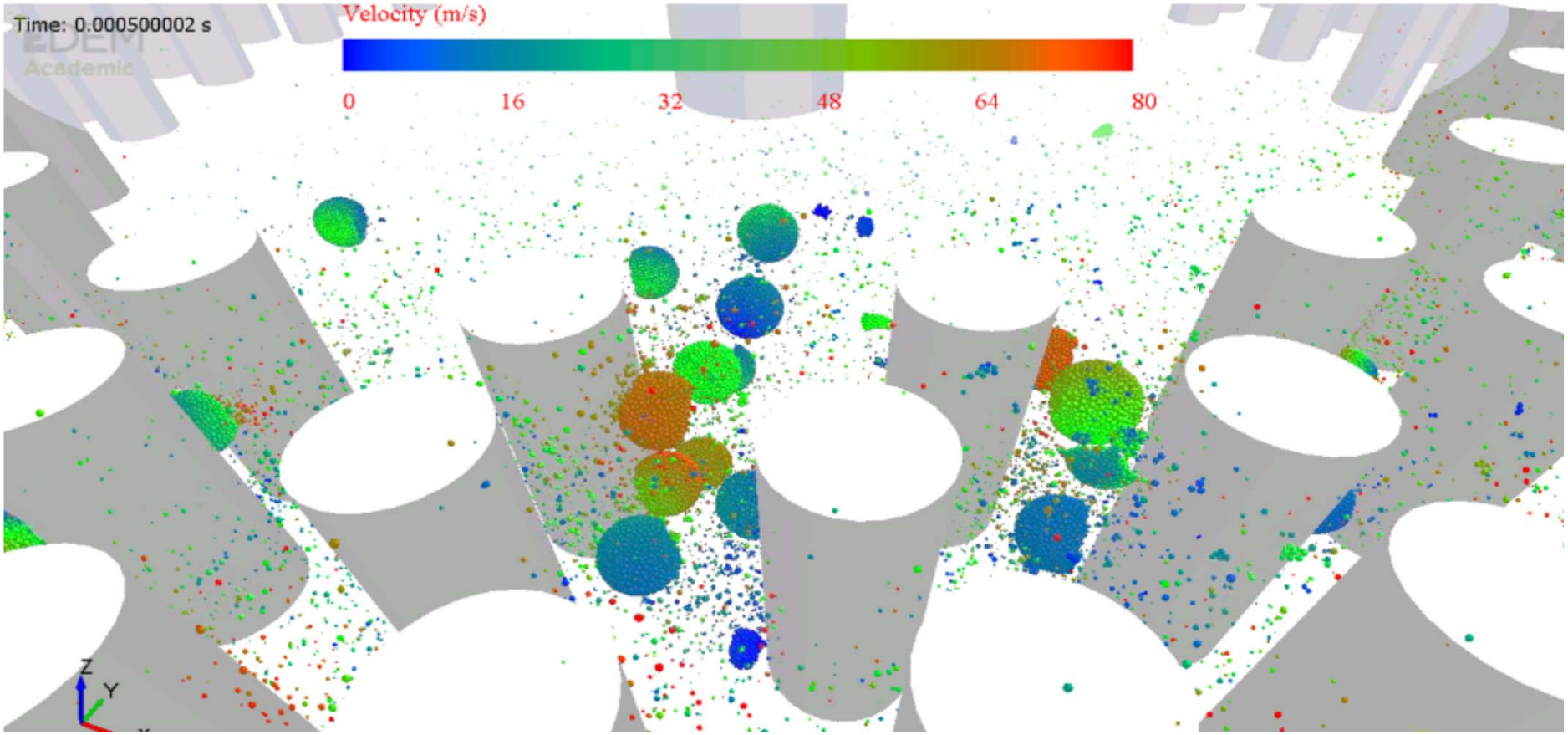

Thank you!

Acknowledgements:

International Fine Particles Research Institute; Hosokawa Micron Ltd. UK;

Leeds University, UK; DEM Solution Ltd. UK; Process System Enterprise, UK

TECHNISCHE UNIVERSITÄT
BERGAKADEMIE FREIBERG
The University of Resources. Since 1765.

INSTITUTE OF MECHANICAL
PROCESS ENGINEERING
AND MINERAL PROCESSING

DETAILED INSIGHT INTO MICROSCOPIC FILTER CAKE PHENOMENA USING 3D-TOMOGRAPHY

M. Mohammadfoghi, E. Löwer, T. Leißner, U.A. Peuker

Research Framework

PARTICLE PROPERTIES

- particle shape
- particle size
- particle-particle interaction

FILTER CAKE PROPERTIES

- integral porosity
- pore size
- trapped liquid areas

PROCESS RELEVANT PROPERTIES

- dewatering behavior
- moisture content
- specific cake resistance

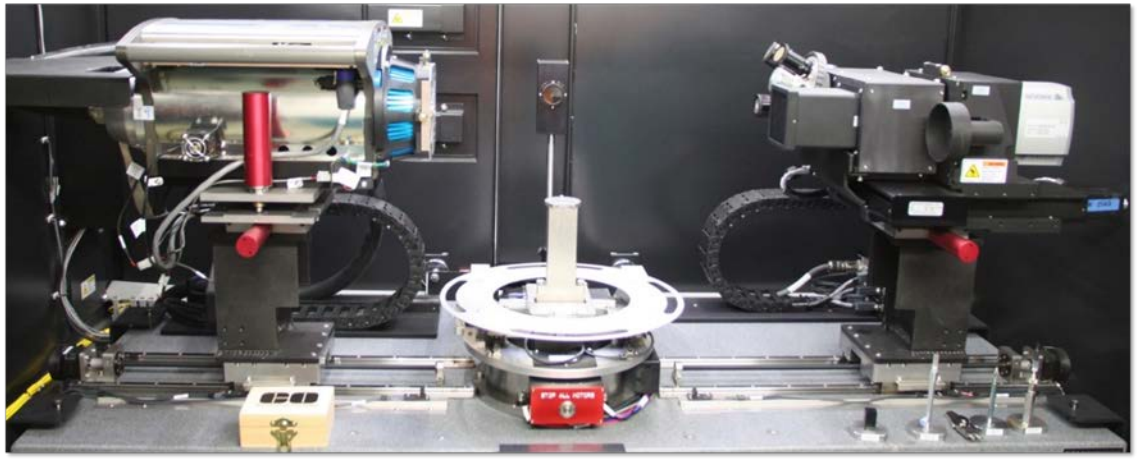

Measurement tool (Xradia Versa 510)

Measurement Method

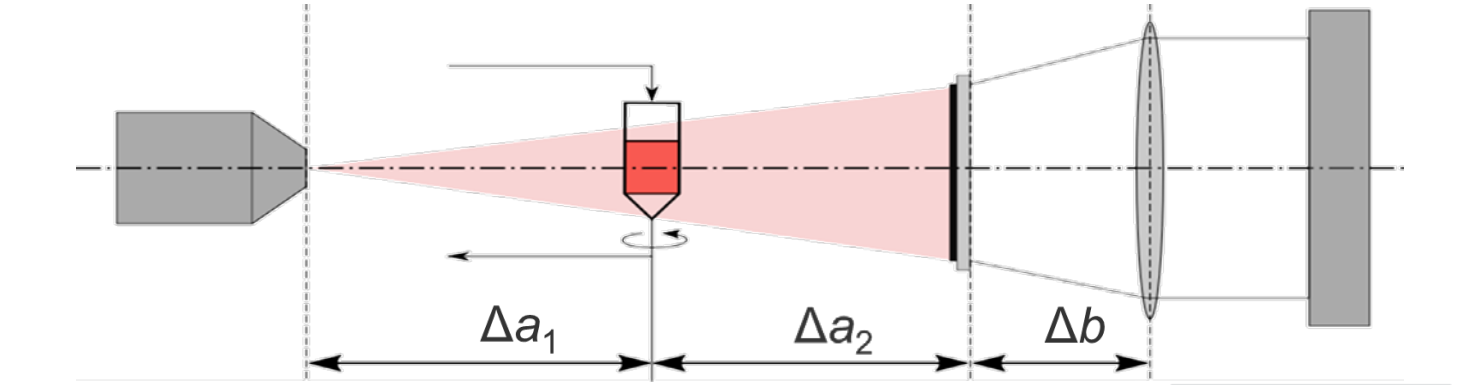

voltage/power:
20-160 kV/1-10 W

Sample size:
5 x 5 x *h* mm³

magnificiation:
$\frac{\Delta a_1 \Delta a_2}{\Delta a_1} \Delta b$

Voxel size:
(0.7-5 µm)³

IN-SITU MEASURING SET-UP

DOWN-SCALE: $A_{\mathrm{VDI}}/A_{\mathrm{insitu}} = 100$

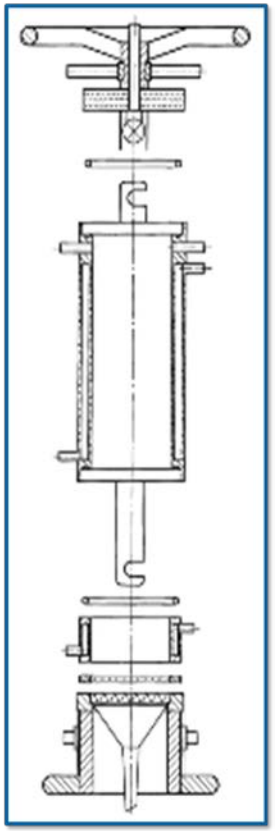

VDI 2762

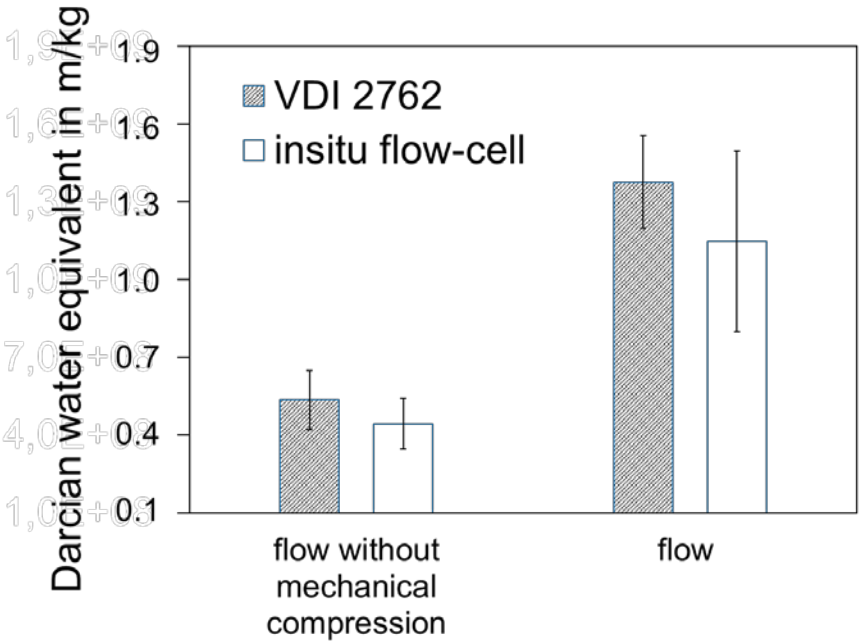

insitu flow-cell

PARTICLE PROPERTIES

compact particles

crushed Al_2O_3

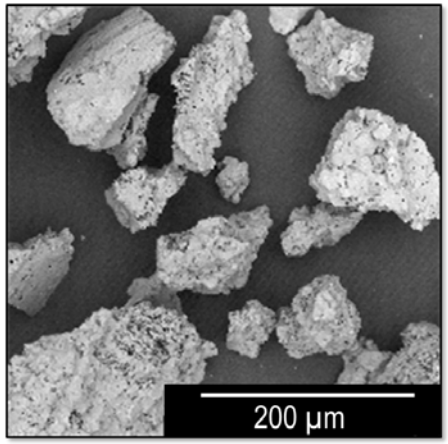

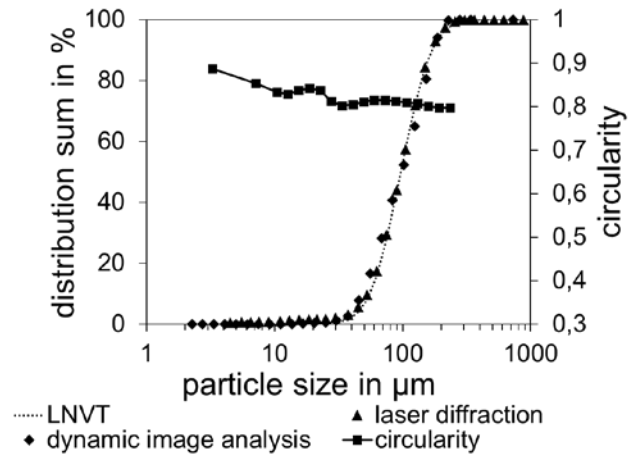

needle-like particles

wollastonite $CaSiO_3$

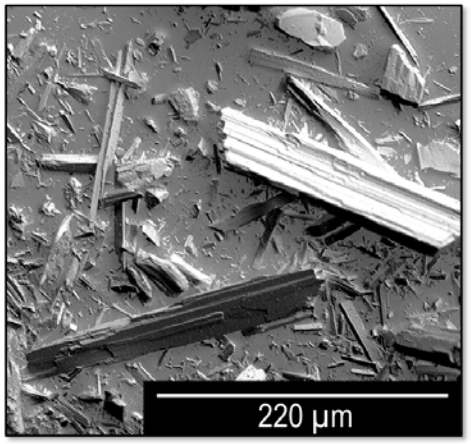

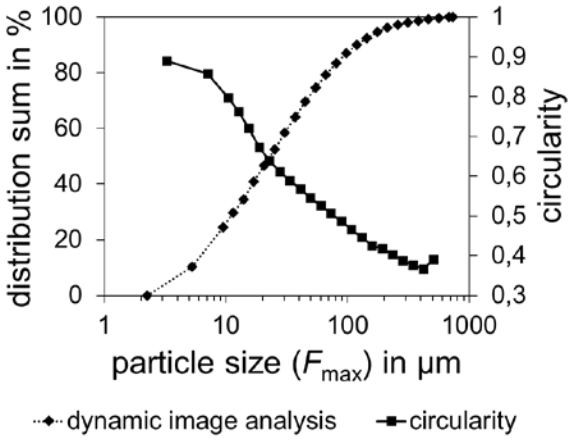

FILTER CAKE PROPERTIES

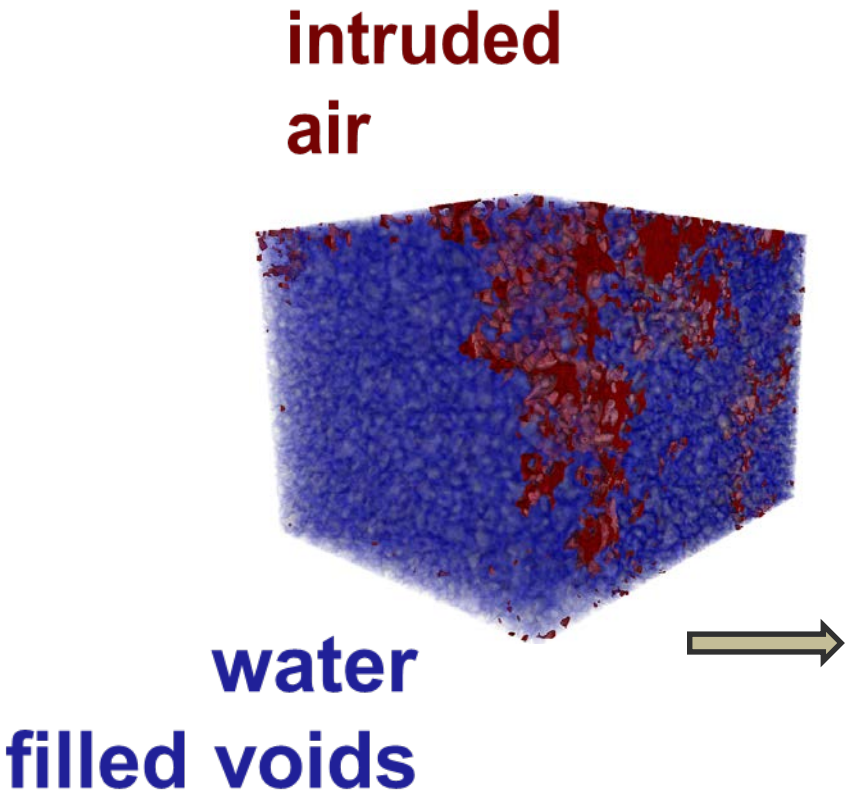

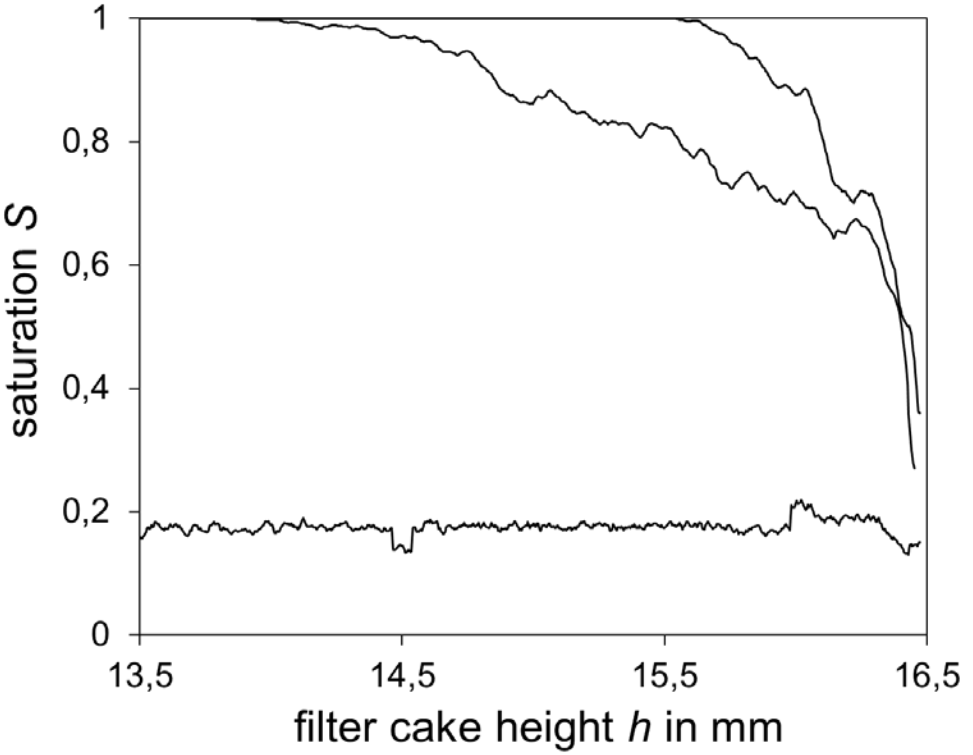

DATA GENERATION FROM 3D-IMAGE ANALYSIS

Parameter, e.g. porosity, contact number, liquid distribution..

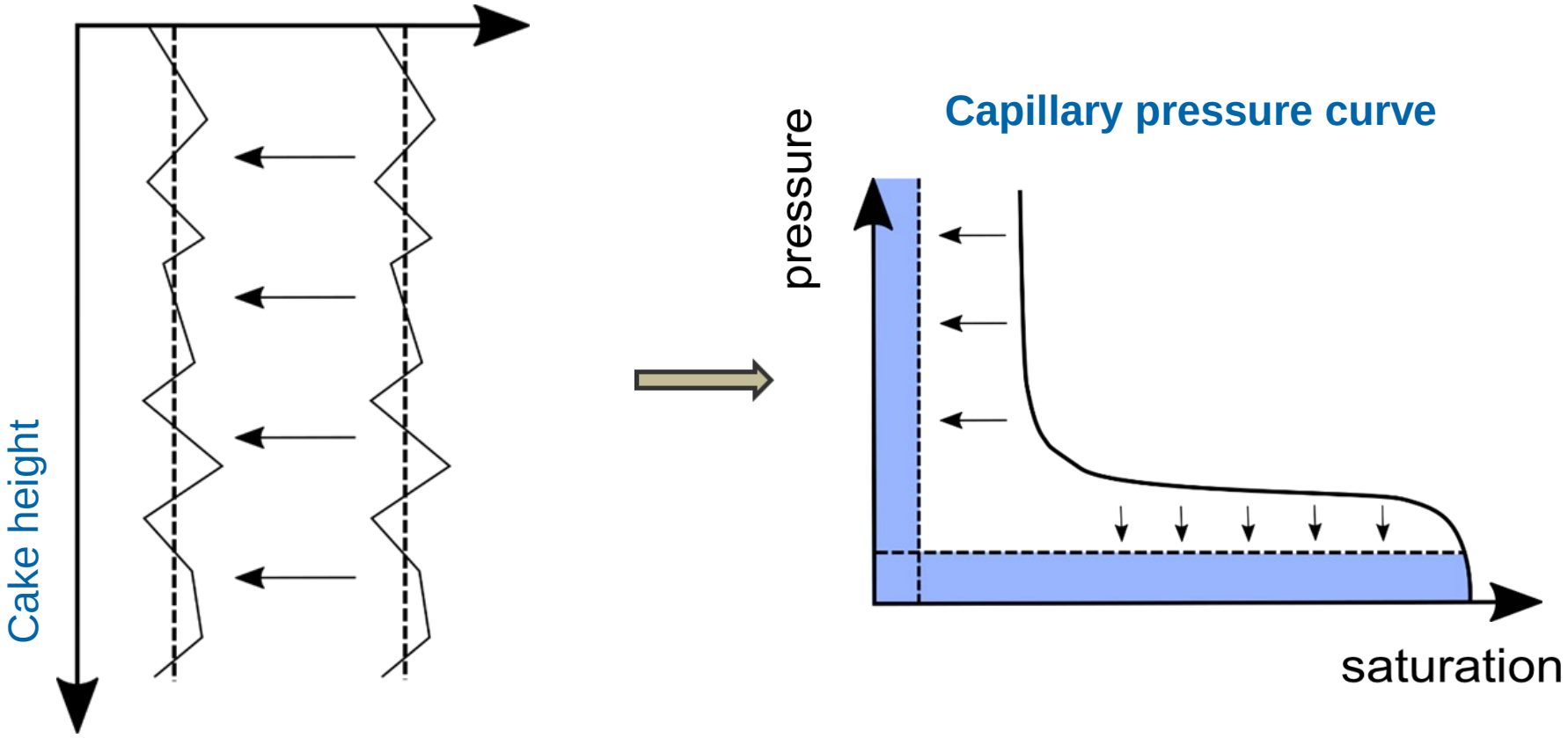

Conclusions

Down-scale of filtration test rig has been achieved

3D – Computer Tomography images are now available

- Resolution between solid and liquid phase is sufficient
- Resolution between solid, liquid and gas phase has to be triggert

3D – image analysis is a powerful tool to characterize particles & particle structures:

- Quantitative determination of property distributions (full set of data)
    - Distribution in z-direction (filtration direction)
    - Distribution in x-y plane (filtration plane parallel to filter cloth)
- Application of expert software packages
- Programming of own subroutines on the basis of statistical and mathematical models.

Looking forward to quantitative results

The long-term stability of colloidal gels
in gravity and under external shear

Wilson Poon
Xuemao Zhou, Joost de Graaf, Michiel Hermes
Jujie Jiang, John Royer

Reminder of story so far

Colloidal gel

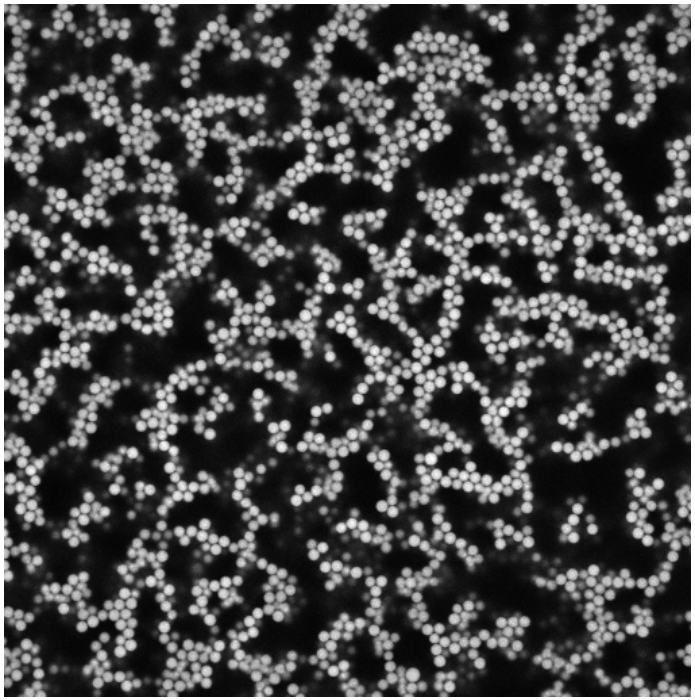

Space-spanning network of attractive particles …
… stabilises against sedimentation/creaming …
… but still has low enough yield stress to flow in use

Key control parameters

$\frac{U_0}{k_{\mathrm{B}}T}$

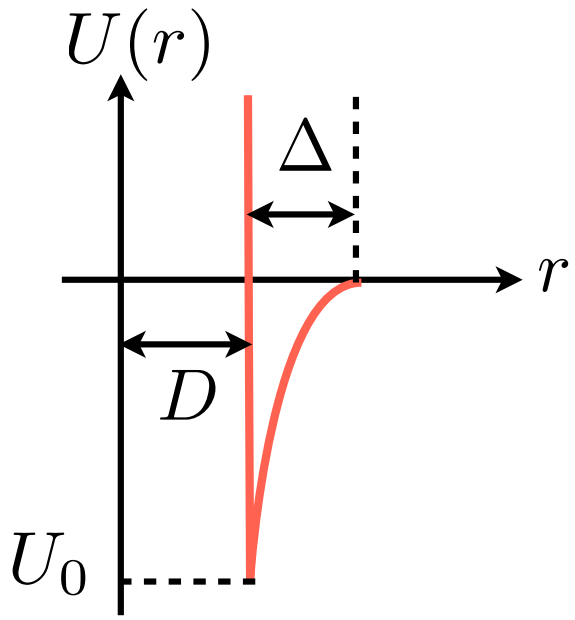

$\frac{\Delta}{D}$

$$\text{Gravitational Péclet no.} = \frac{\text{time to diffuse ownsize}}{\text{time to sediment own size}}$$

$$\mathrm{Pe_g} = \frac{4\pi}{3}\frac{\Delta\rho g a^4}{k_B T}$$

Two generic collapse mechanisms

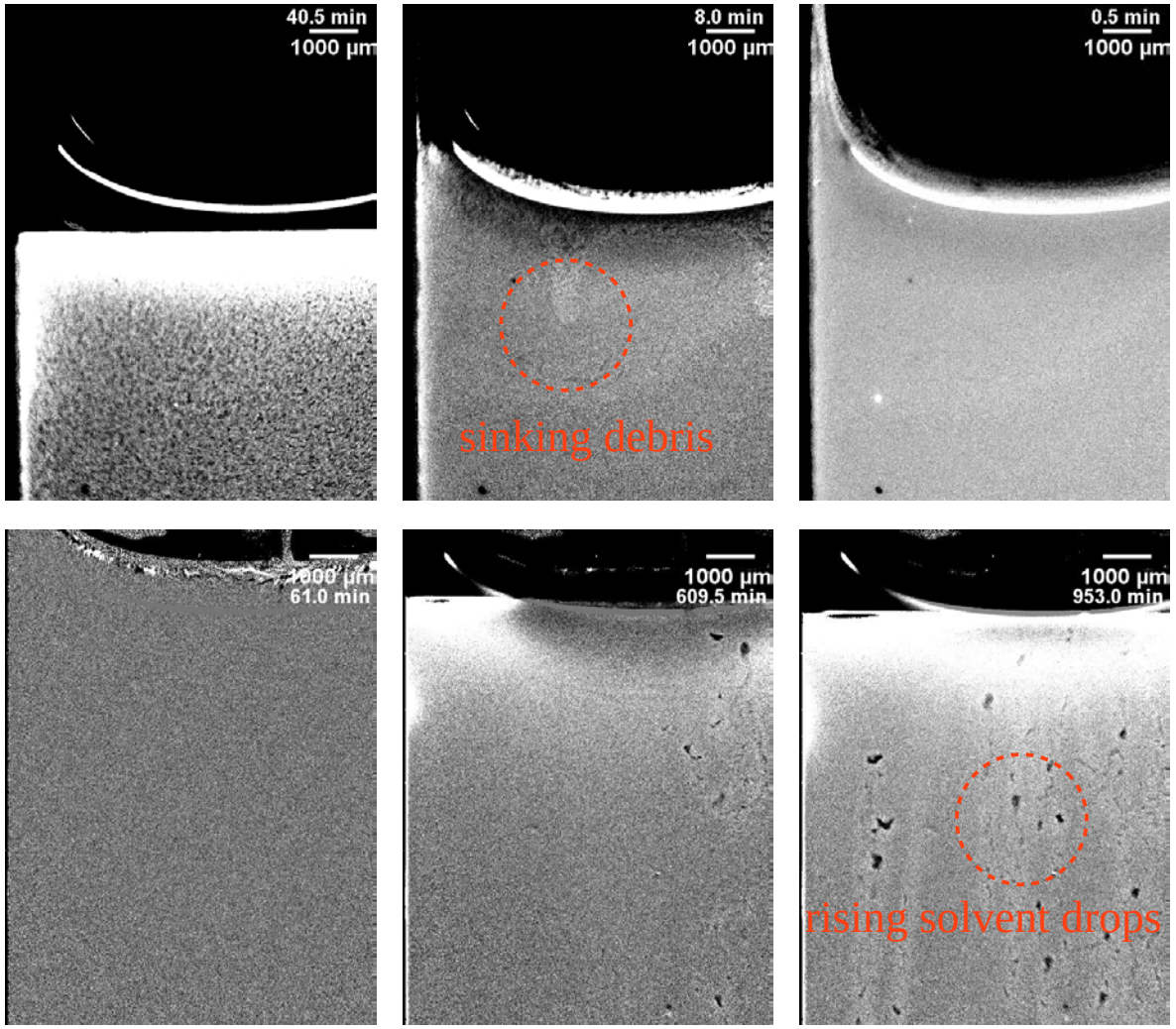

$$\mathrm{Pe} = 2.25, U_0/k_\mathrm{B}T \approx 10, \Delta/D = 0.05T$$

Accumulation of ‘debris’ on top

We’ve figured out how to eliminate this!

Gel too weak to support ‘debris’

→ Crashing ‘debris’ → fast collapse

Gel strong enough to support ‘debris’

→ Solvent bubbles → slow collapse

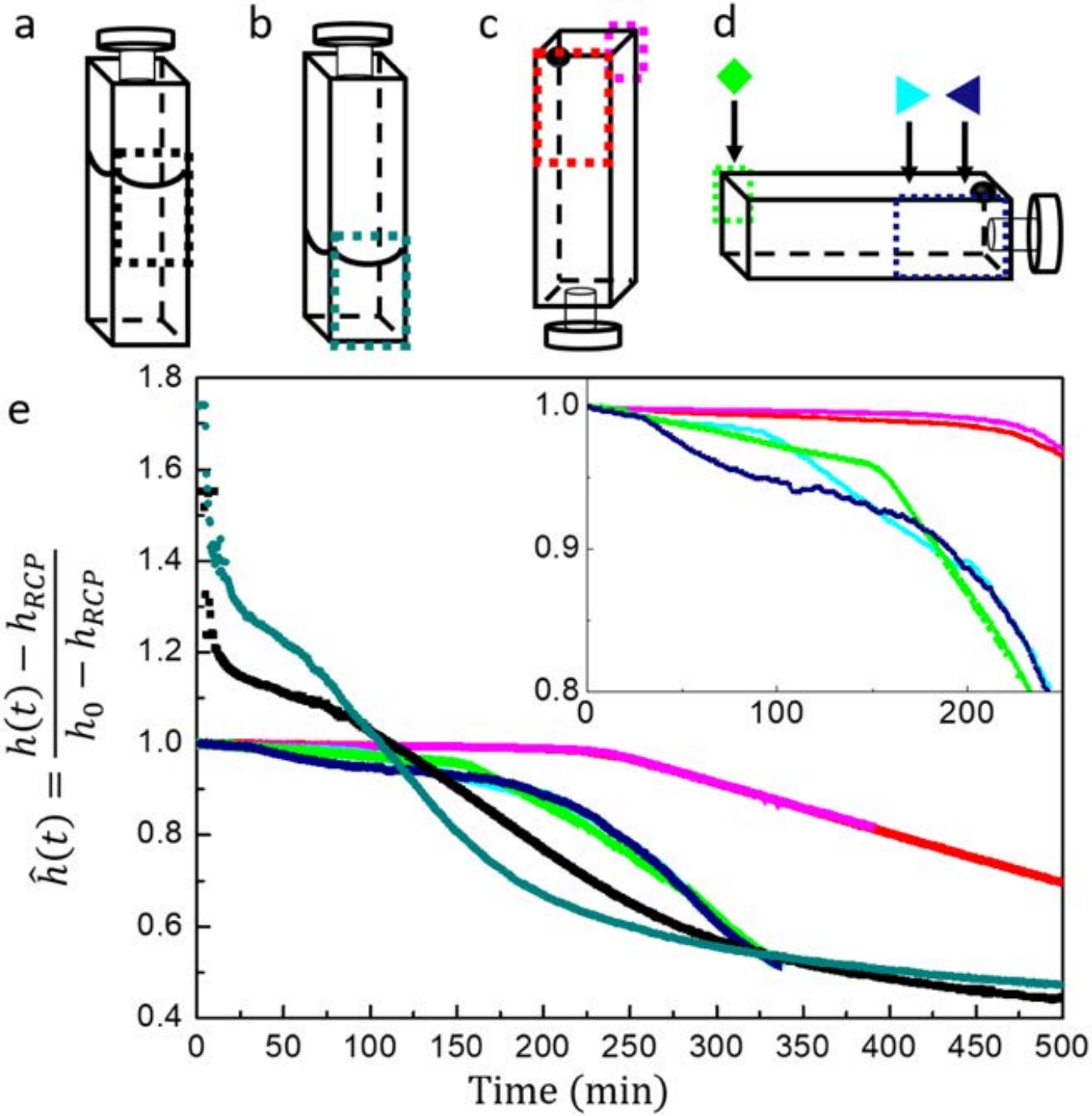

$$\mathrm{Pe} = 2.25, U_0/k_\mathrm{B}T \approx 18, \Delta/D = 0.05, \phi = 0.23$$

New experiments: manipulating the meniscus

Apparatus to obtain meniscus of either curvature

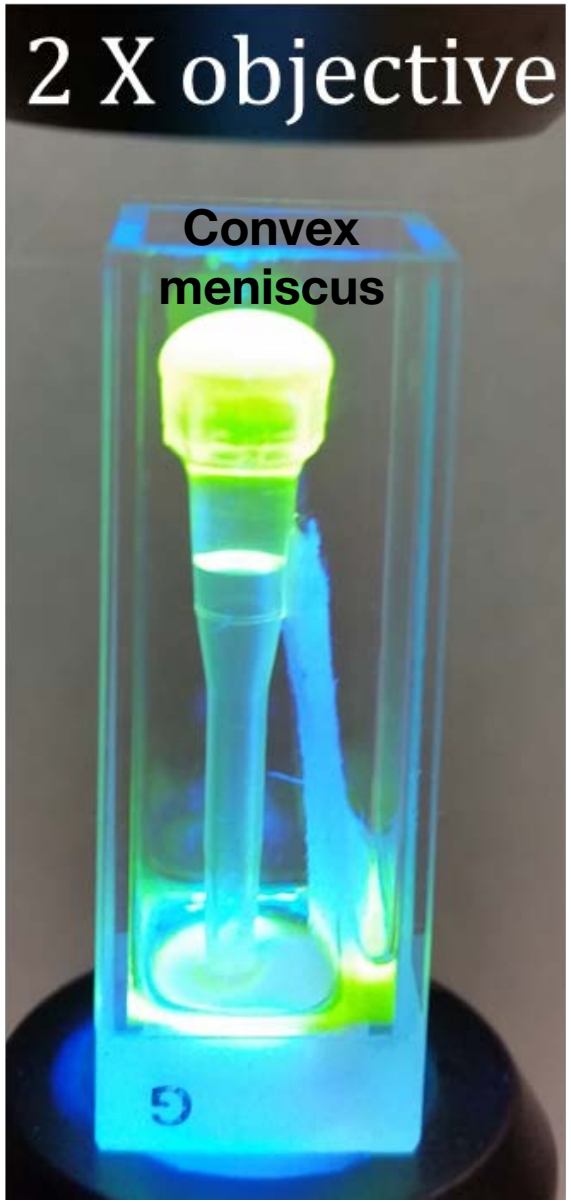

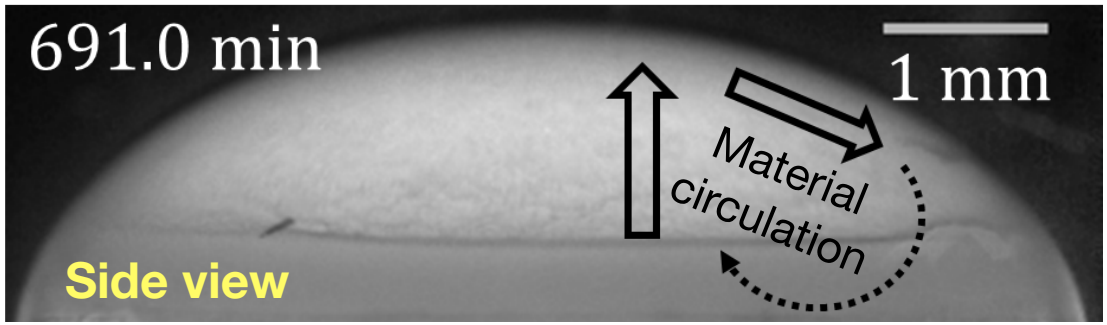

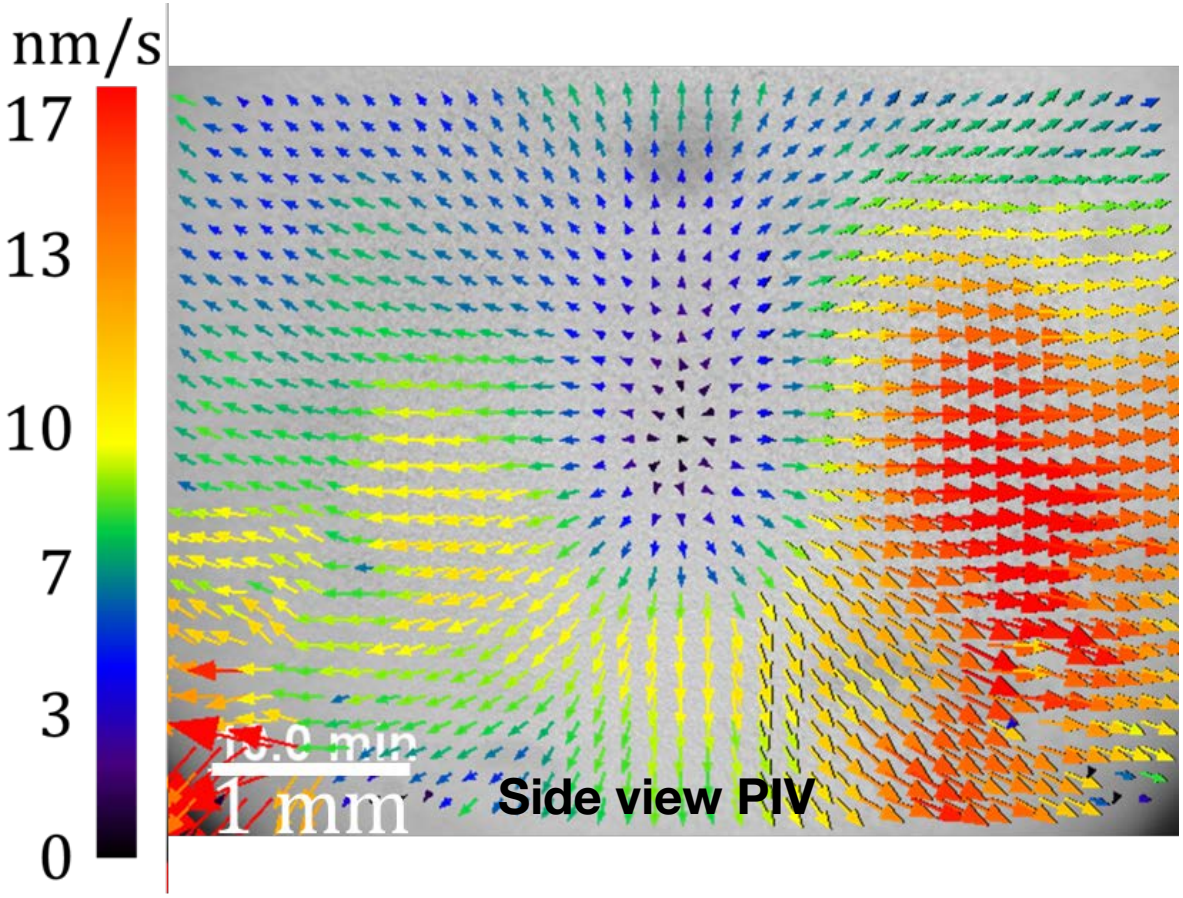

Unbalanced tangential force at *any* curved meniscus

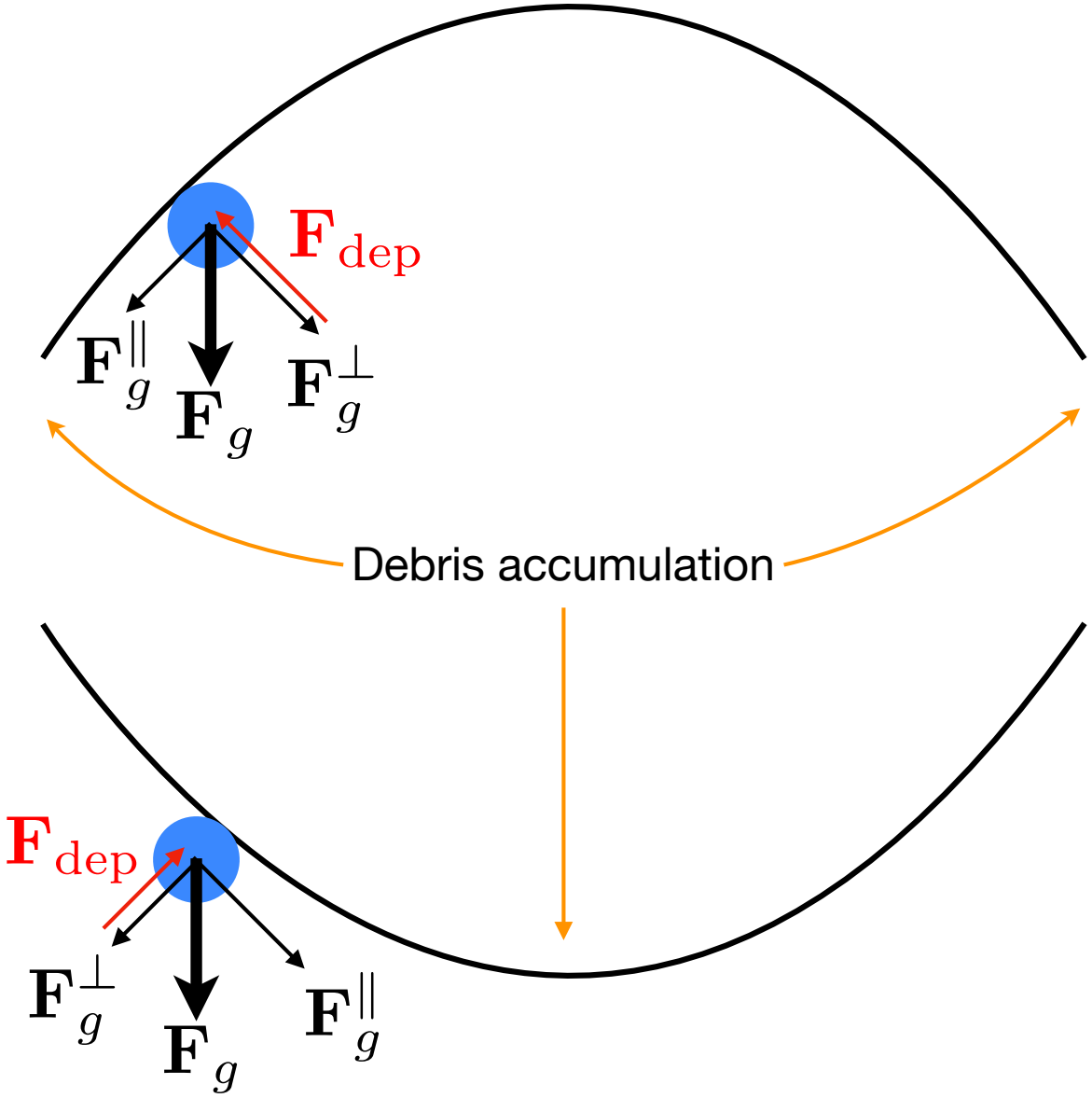

New simulations: effect of percolation

$$p \sim t^{\beta+1} \qquad v = \frac{dp}{dt} \sim t^{\beta}$$

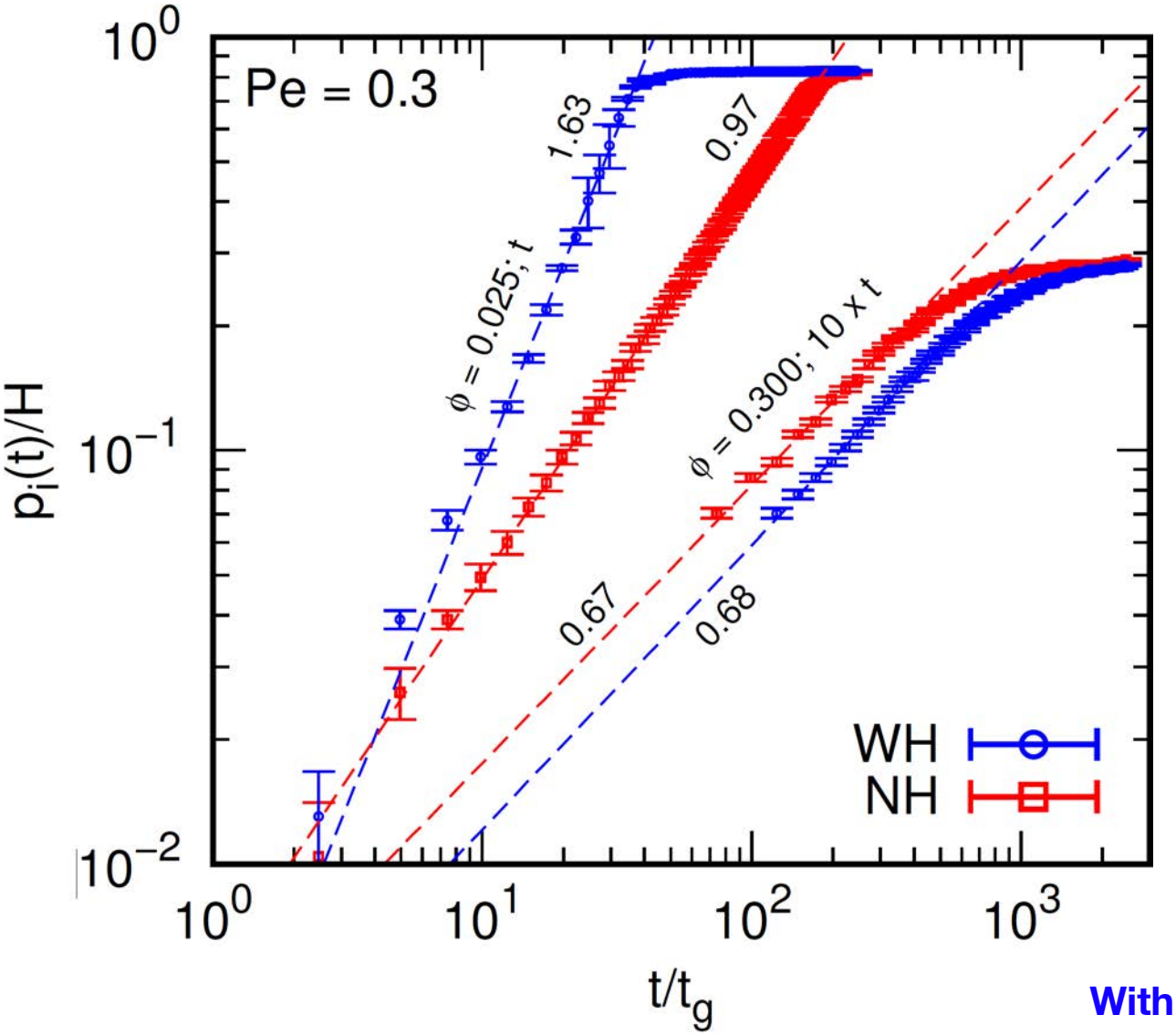

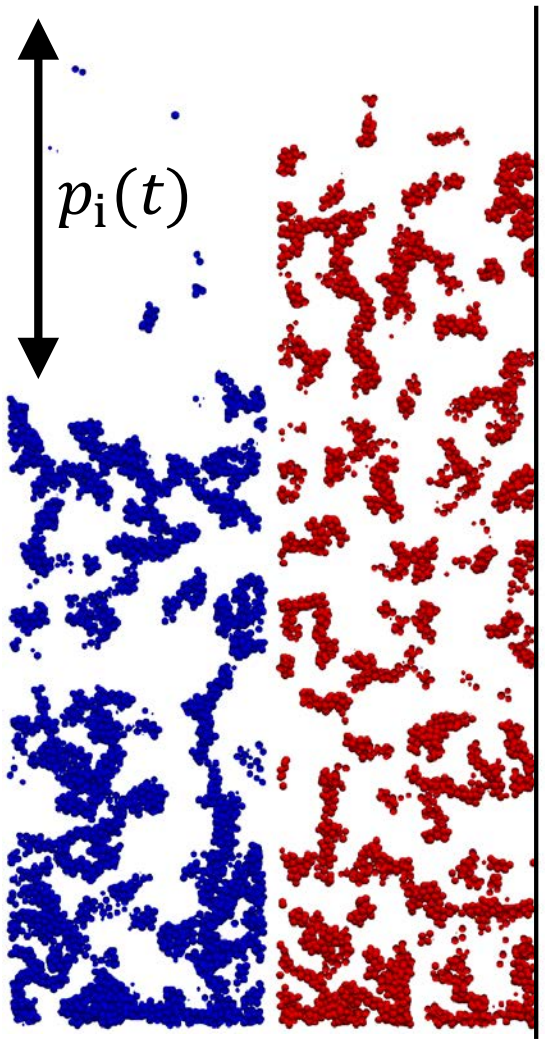

With hydrodynamics No hydrodynamics

$$v \sim t^{\beta}$$

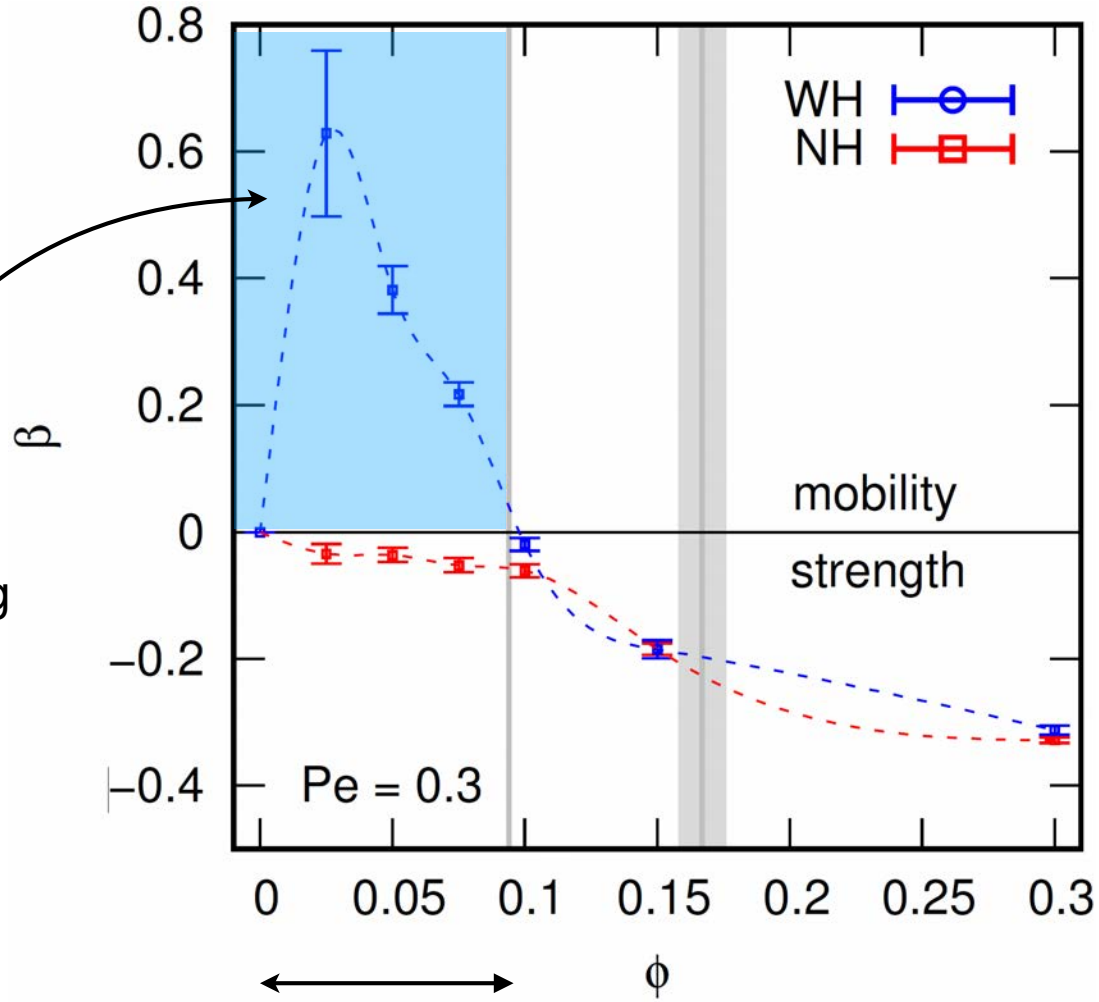

Hydrodynamics causes accelerating interface via strong back flow

No pre-existing percolating cluster

New model system: big particles in small particle gel

$d \sim 4$ μm

$d \sim 0.5$ μm

Granular particles in colloidal gel

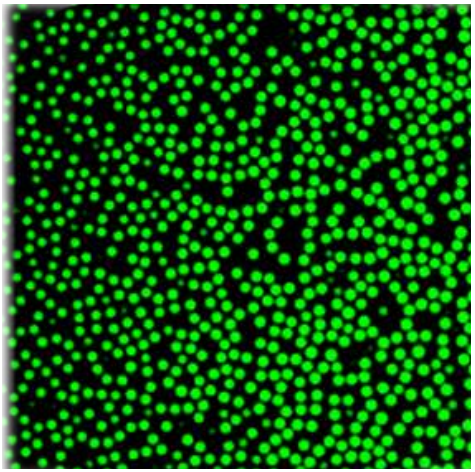

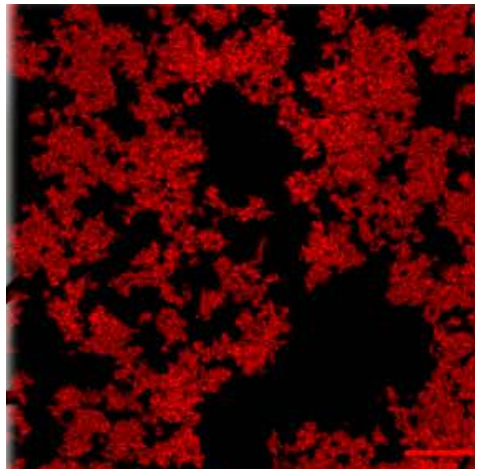

water +
glycerol

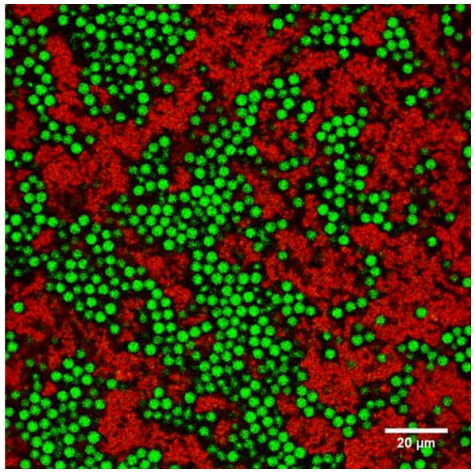

Hydrophilic silica

Hydrophobic silica

Rigorous shaking: background gel rejuvenates to suspend big particles

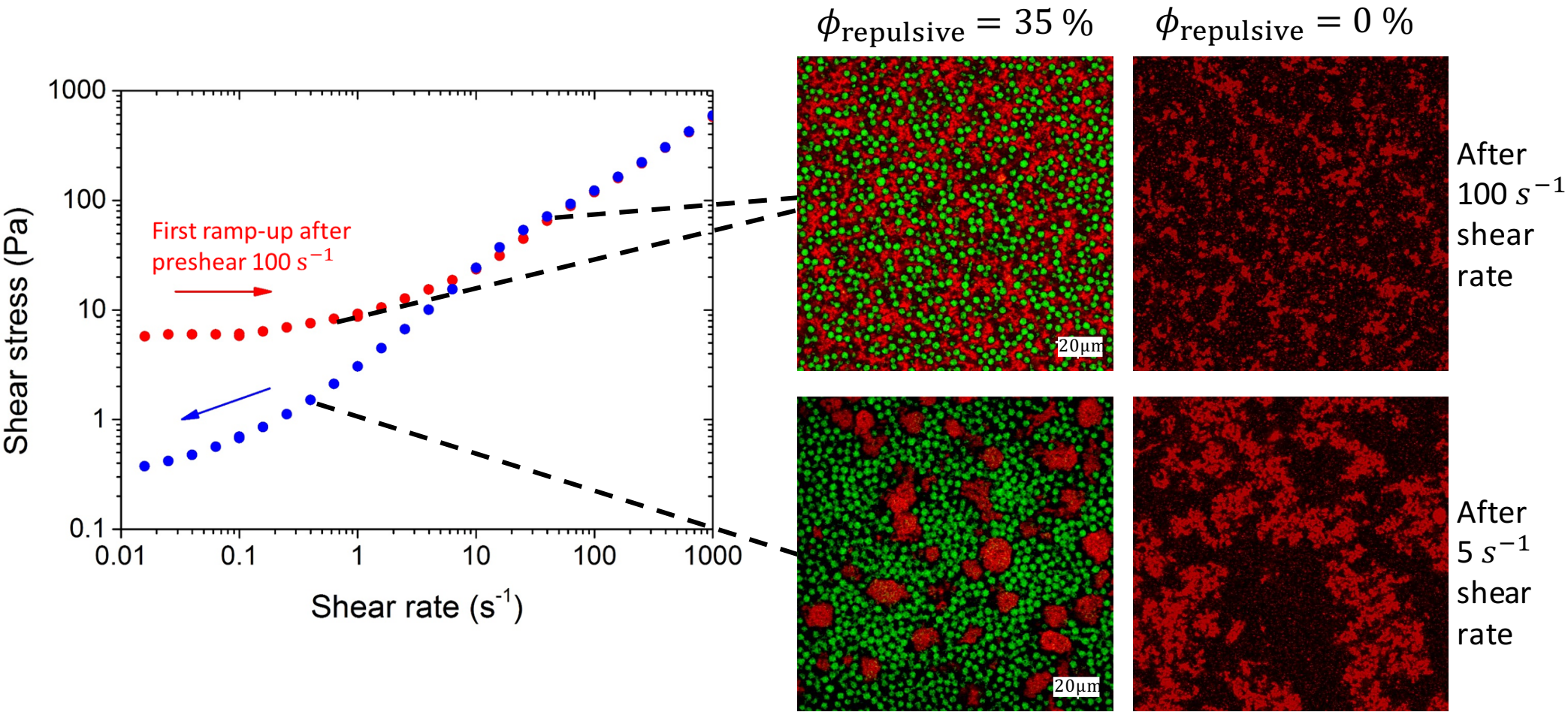

Moderate shaking: background gel breaks up to form compact drops …

Not seen in rheometer! [N. Koumakis et al., Soft Matter **11**, 4640 (2015)]

… stable resuspension of big particles fails!

There will be a dramatic movie here of the processes shown in the previous slide!

Self-Assembled Monolayers as Nucleating Surfaces to Study Early Formation Pathways of Crystal Polymorphs

Jiazhen Xu, Ethan Susca, Detlef Smilgis, Lara A. Estroff and Uli Wiesner

Materials Science and Engineering

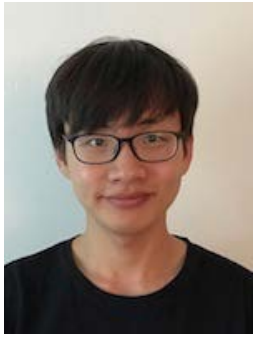

Jiazhen Xu

ubw1@cornell.edu

IFPRI 40th Annual General Meeting, Edinburgh, Scotland, June 24-28, 2018

This work made use of the Cornell High Energy Synchrotron Source (CHESS), a national user facility supported by the National Science Foundation (DMR-1332208).

Research Project Brief

- Fund project to understand and control crystallinity, polymorphism, and particle morphology in the *early formation stages* of crystals.
- Use advanced techniques like cryo-TEM, synchrotron derived pair-correlations, solid-state C^{13} NMR, and in-situ AFM, to visualize these stages.
- High level objectives of this project:
  - *identify appropriate model system(s)* to study, adapt and apply characterization techniques to describe early particle formation stages;
  - collect data that is relevant for the development of molecular dynamic simulation or other computational physics models.

Proposed Approach

- Here: Use of self-assembled monolayers (SAMs) to study the relationship between nucleation event and polymorph selection.

- Advantages: (i) Enables establishment of scientific correlations between chemistry of nucleation surface and observed polymorph and (ii) may provide access to polymorphs not accessible via solution methods.

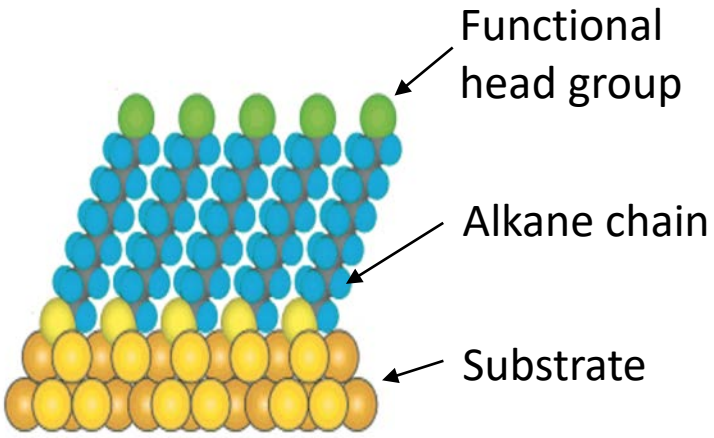

J.C. Love et al., *Chem. Rev.* 2005, **105**, 1103−1169.

Model system

Acetaminophen (ACM): Two polymorphs

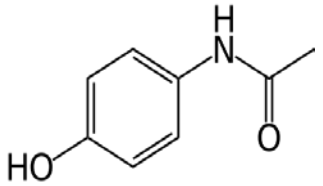

Monoclinic (Form I)

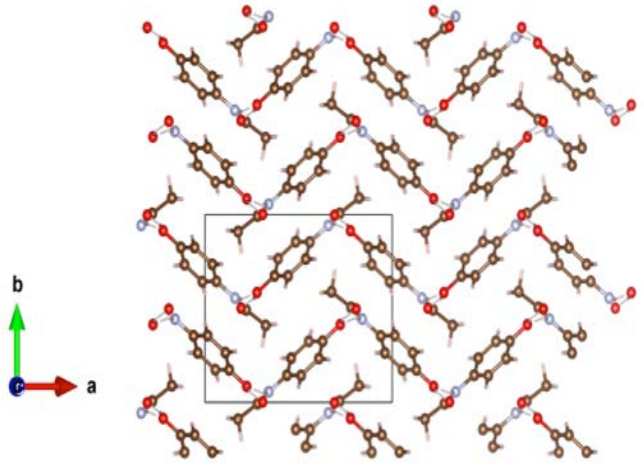

(001) face shown

Example solution grown crystals:

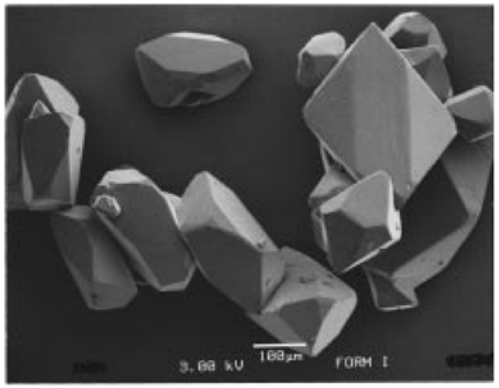

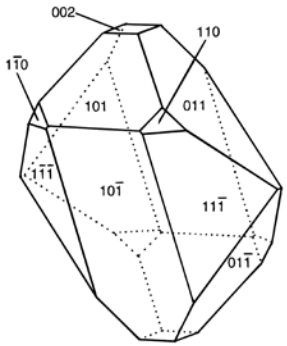

G. Nichols and C.S. Frampton. *J. Pharm. Sci.* 1998, **87**, 684.

Orthorhombic (Form II)

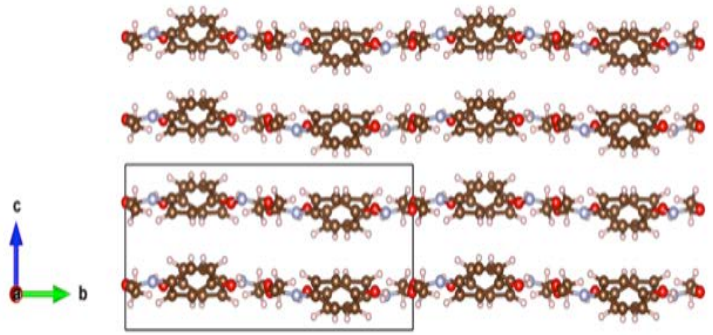

(200) face shown

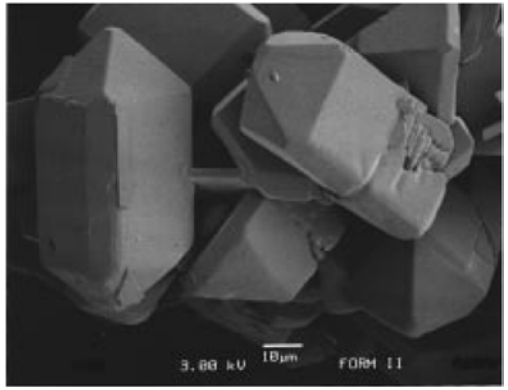

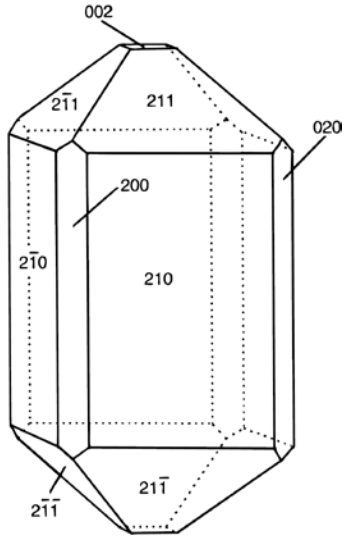

Note: indices h and k are switched from our convention in this schematic

Two substrate chemistries: Au and SiO_2

Thiol-gold chemistry

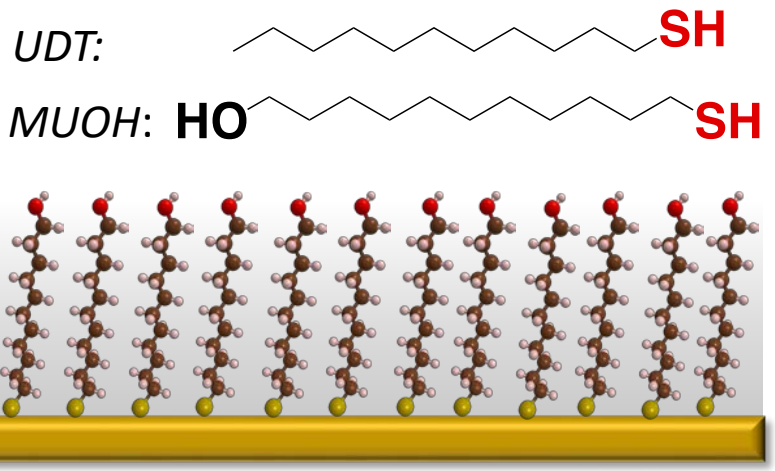

- Highly ordered SAMs
- Poor solution stability
- More expensive

Silane-SiO_2 chemistry

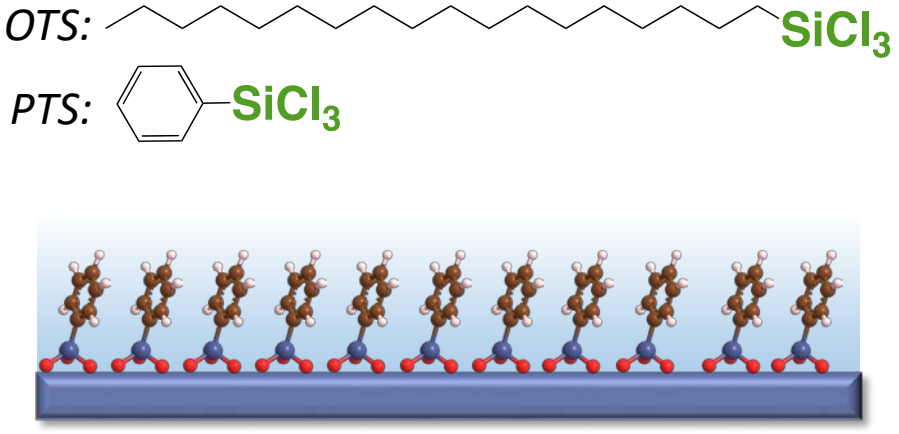

- Less ordered than Au SAMs
- Very good solution stability
- Works on Si-wafers and glass

Experimental set-up: droplet experiment & WAXS

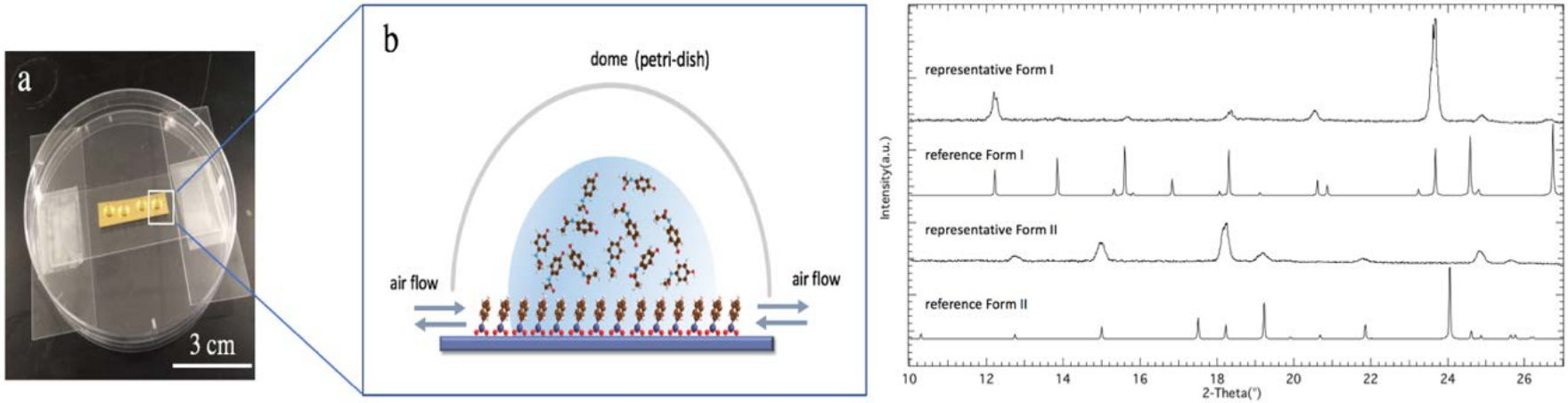

- Very simple and reproducible experimental set-up
- Dome allows to control evaporation rate
- Simple control of droplet volume allows multiple experiments on same substrate
- Wide-angle x-rays used to check for crystal polymorph

Summary of Results of Previous Years

Solvent Effects on the polymorph control: hydrophobic surfaces

Solvent	*SAM chemistry*	*n*	*Form I*	*Form II*
Ethanol 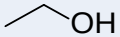	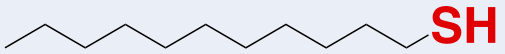	20	**80%**	20%
	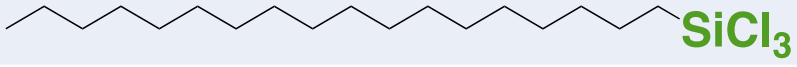	18	**94%**	6%
	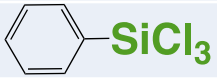	14	**93%**	7%
Deionized water	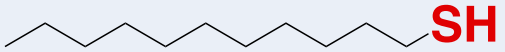	9	**93%**	7%
	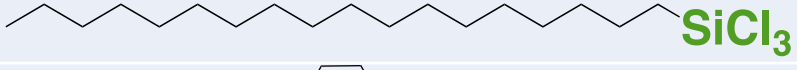	18	**89%**	11%
	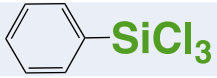	10	**90%**	10%
1,4-dioxane 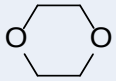	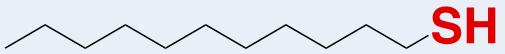	12	**100%**	0
	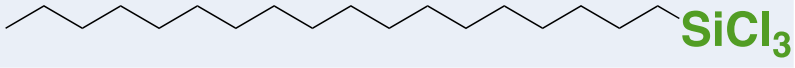	10	**90%**	10%
	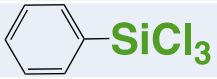	10	**70%**	30%
DI water/dioxane 20:80	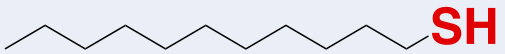	11	9%	**91%**
	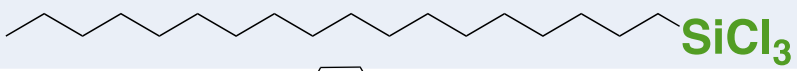	11	0	**100%**
	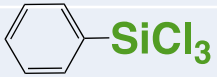	9	0	**100%**

Pure solvents result in Form I polymorph.

Water/dioxane mixture results in Form II polymorph.

Both solvent and substrate work together to control crystal polymorph

Solvent \ Substrate	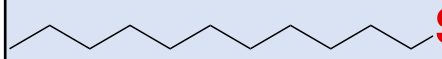 SH on Au			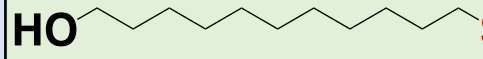 HO SH on Au		
		Form I	Form II	n	Form I	Form II
DI water	9	**93%**	7%	17	**100%**	0
DI water/ dioxane 20:80	11	9%	**91%**	10	0	**100%**

- In water containing systems, polymorph selection is independent of substrate chemistry, whether hydrophobic or hydrophilic.
- However, for pure organic solvents, polymorph switches from Form I to Form II when surface chemistry is changed from hydrophobic to hydrophilic.

⇨ Therefore, solvent and surface chemistry must be considered in concert when predicting or designing crystallization process.

Substrate can dictate crystallographic orientation: Form II

Solvent	*SAM chemistry*	*n*	*Form I*	*Form II*
DI water/dioxane 20:80	SH	11	9%	**91%**
	$SiCl_3$	11	0	**100%**
	$SiCl_3$	9	0	**100%**
	HO SH	10	0	**100%**

X-ray diffraction: ACM on PTS

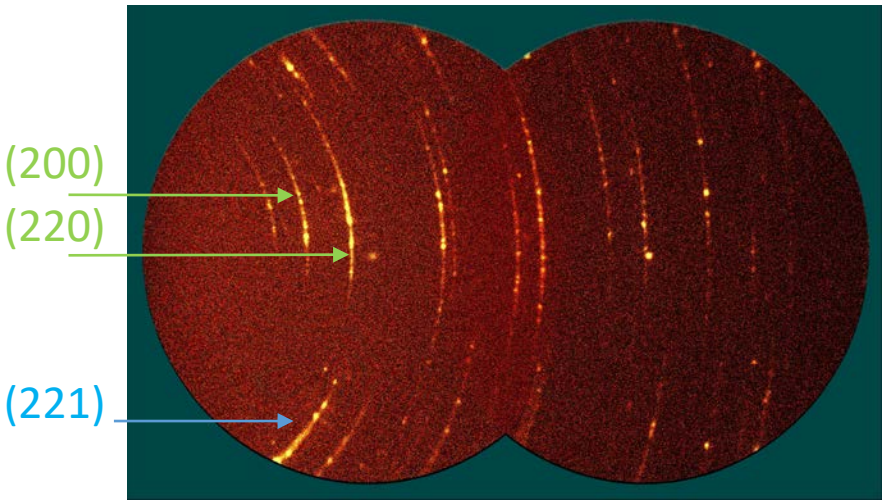

ACM on –OH:

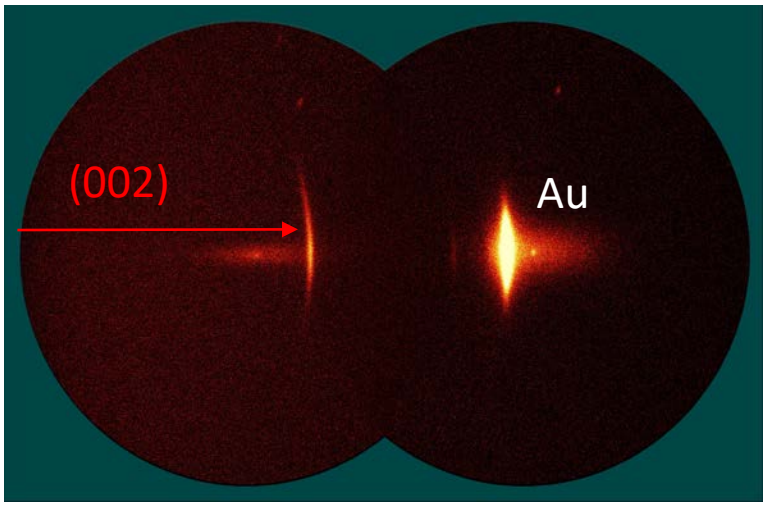

PTS:

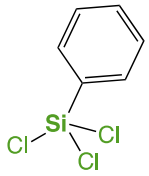

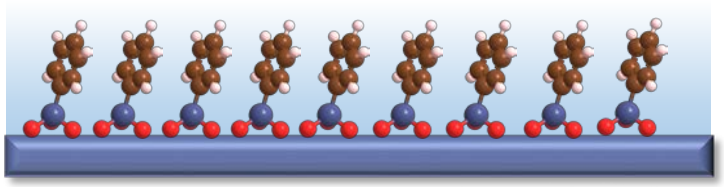

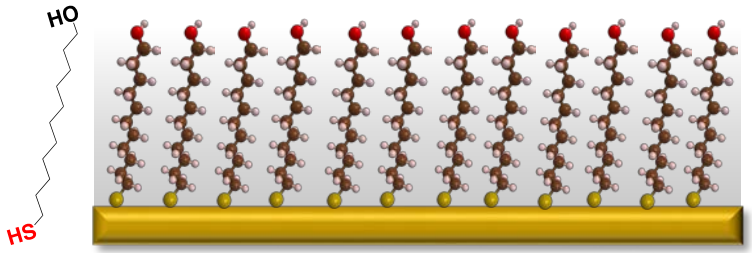

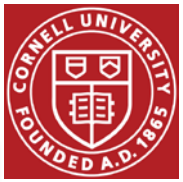

Molecular Interpretation: Form II

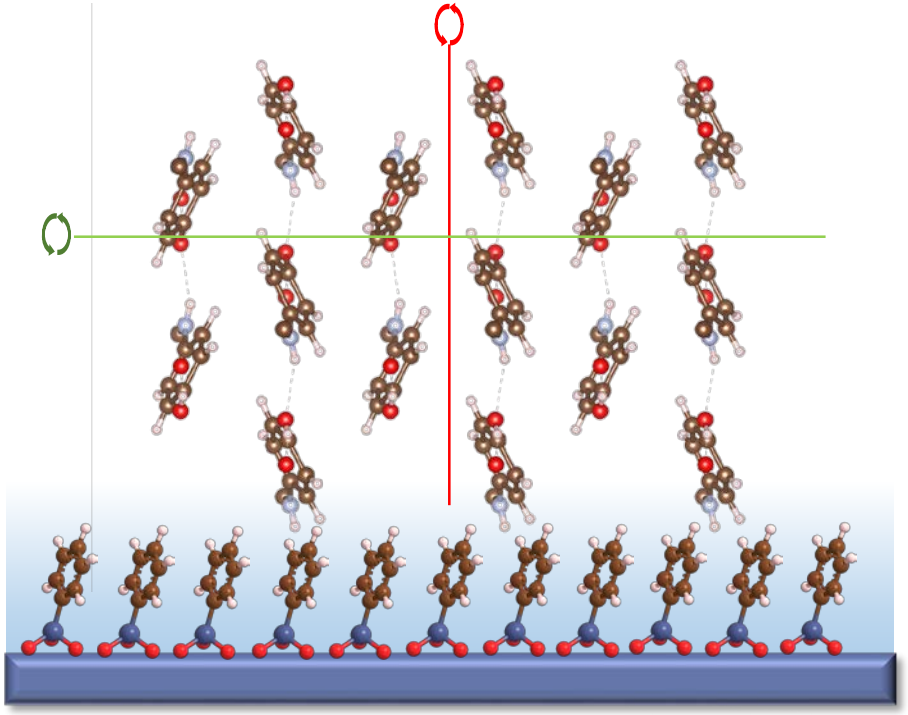

(2 0 0) II to substrate

- PTS SAMs promote the crystals to nucleate with phenyl rings oriented perpendicular to substrate
- Powder-like arcs in XRD indicate rotational variation around the (200) and similar planes
- The absence of (002) plane in XRD suggests cleavage planes (red) are always perpendicular to the substrate

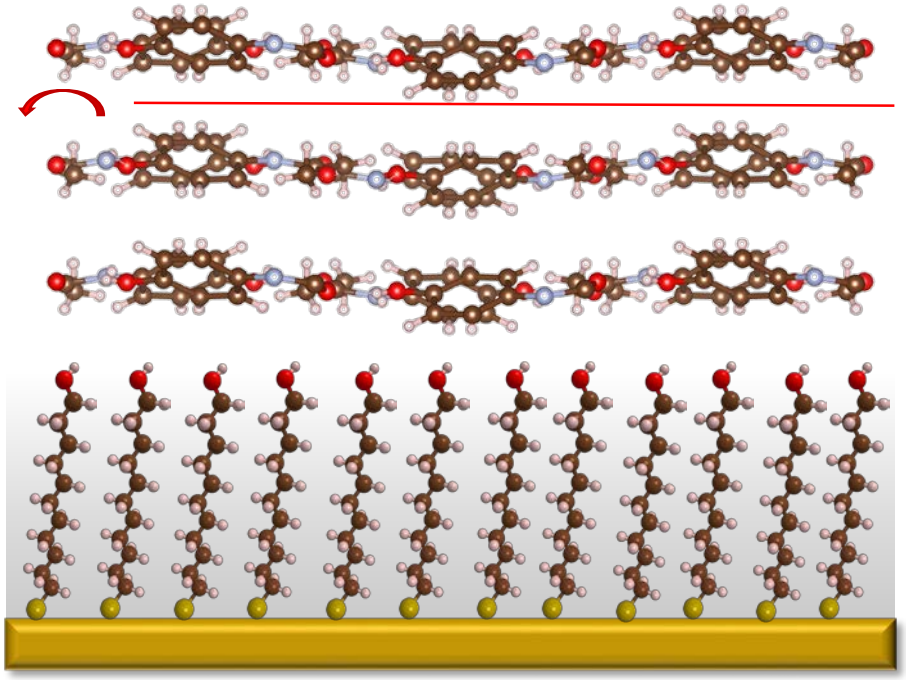

(0 0 2) II to substrate

- Alcohol terminated SAMs exclusively promote crystallization with (002) planes parallel to substrate
- Azimuthal spread of the (002) peak suggests some tilt in the orientation

New Results of In-situ Synchrotron Work

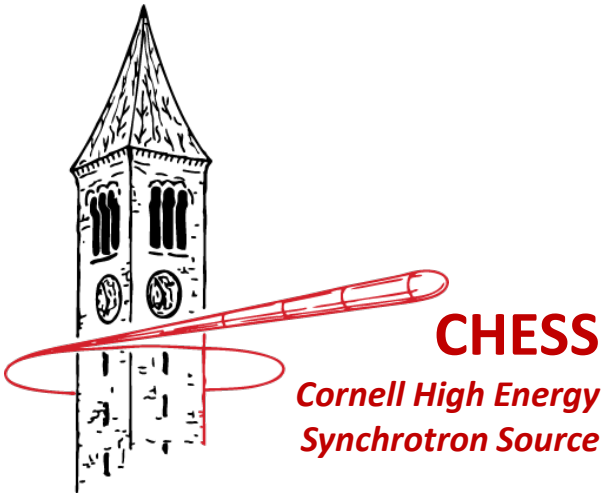

Sample preparation: Form 2 formation in water/dioxane on PTS

- 200µL of concentrated ACM in water/dioxane solution was deposited on PTS at 50°C in 10µL increments creating long, narrow continuous ‘thin - film’

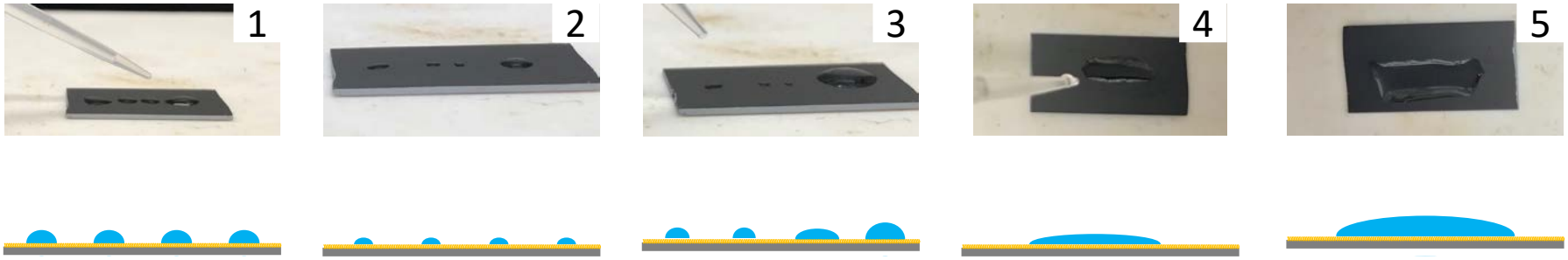

1-2: Solvent evaporation concentrates solution
3: Add additional solution to make larger droplets
3-4: Repeat 1 & 2 multiple times
4: Connect solution droplets to form large single droplet
5: Continue to add solution to create a long narrow shape

In-situ parallel WAXS observation of form 2 formation

- Water/dioxane solvent transforms to amorphous ‘long-lived glassy’ state, which is a reliable precursor for form 2
- Add form 2 seed crystal to one end of film to determine growth direction

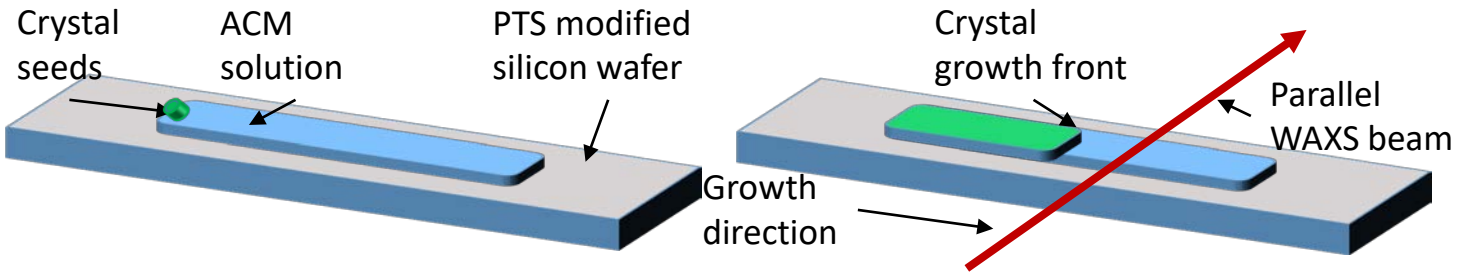

optical micrographs

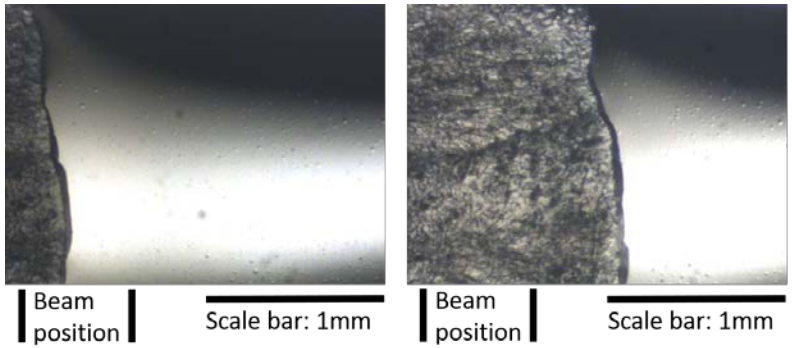

In-situ synchrotron WAXS patterns: ca. 10 sec runs

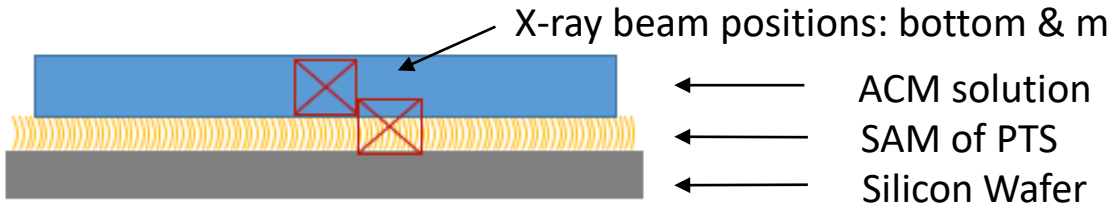

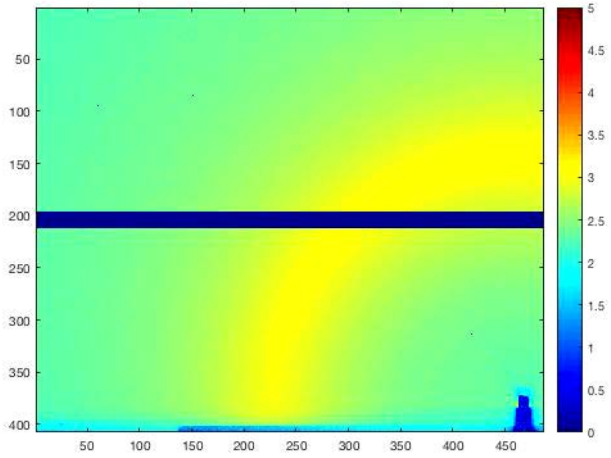

middle

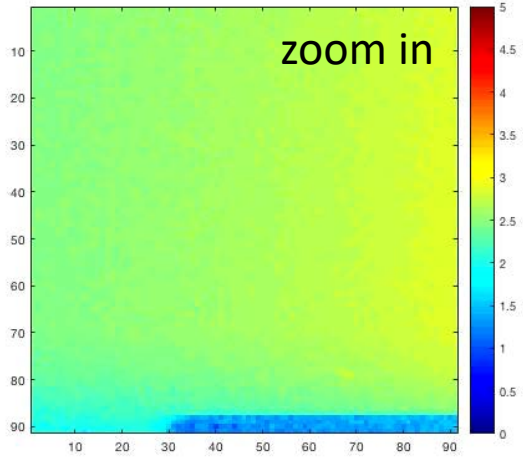

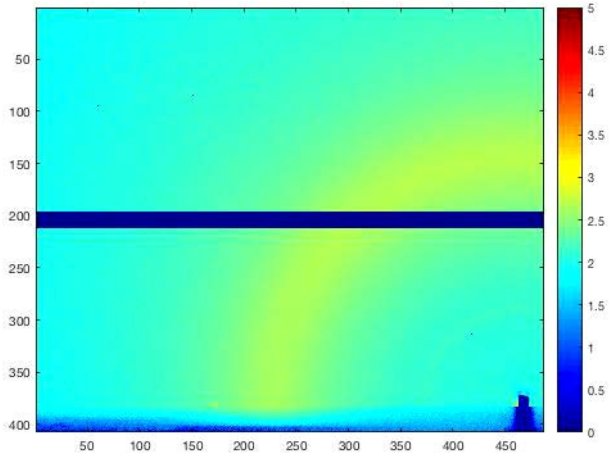

bottom

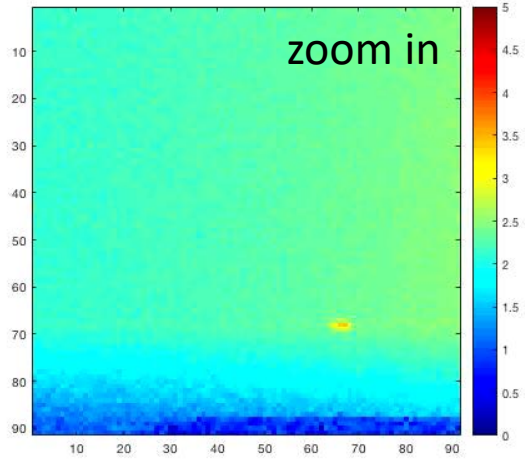

wider azimuthal spread of signal suggests crystals grow up from substrate - solution interface

Final film morphology from SEM

- Central branches are parallel to growth direction
- Secondary branches spread off parallel with twinning-like boundaries between central branches
- Secondary branch growth is inhibited by the parallel central branches?
- Voids are formed between branches
- Twinning system?

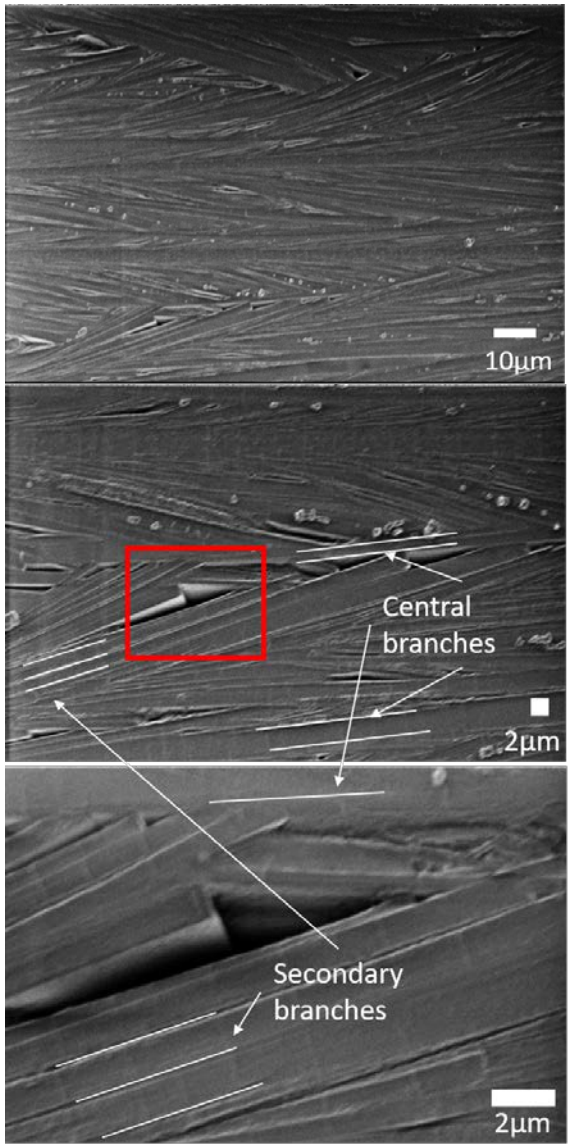

Sample preparation: Spontaneous nucleation & growth of form 1

- Experimental Setup: 10µL water droplet on PTS at 50°C
- Nucleation happens spontaneously at position of beam (rare)

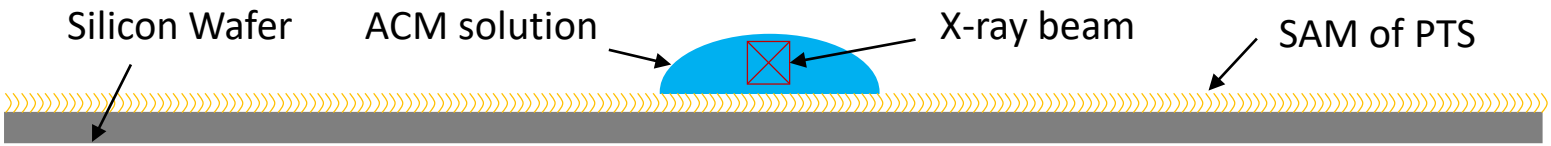

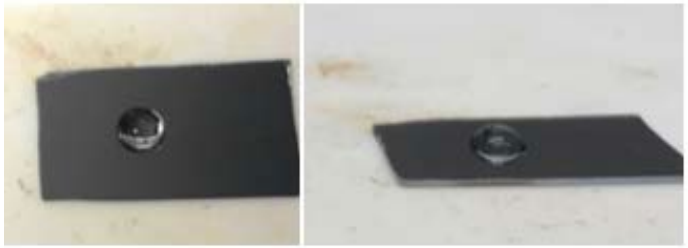

Scale bar: 1mm

Beam position

In-situ synchrotron WAXS patterns: ca. 10 sec runs

optical micrographs

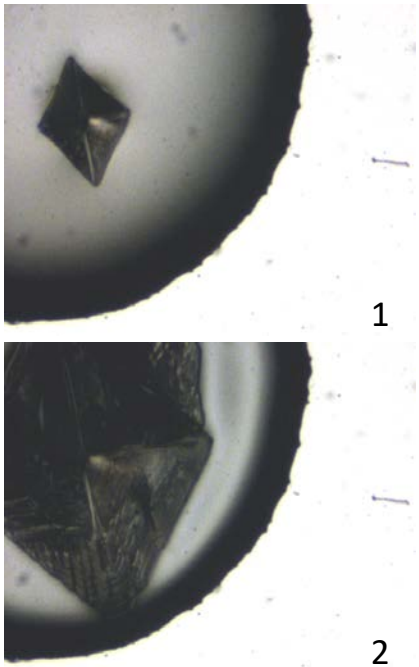

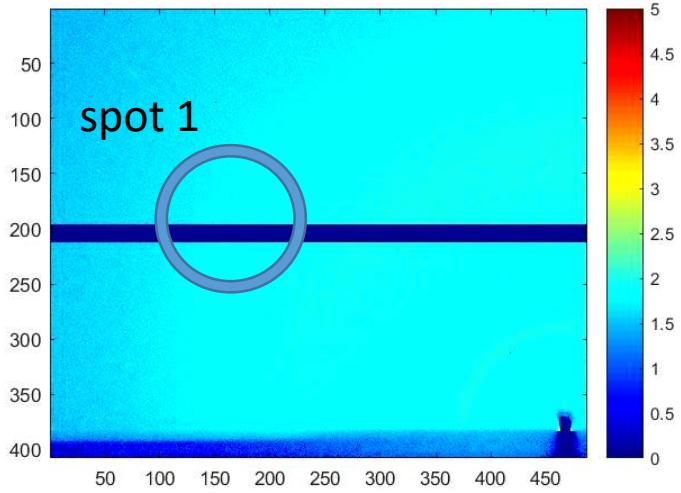

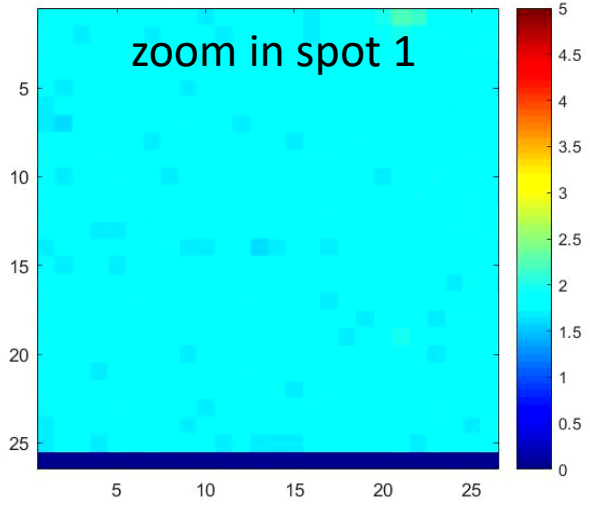

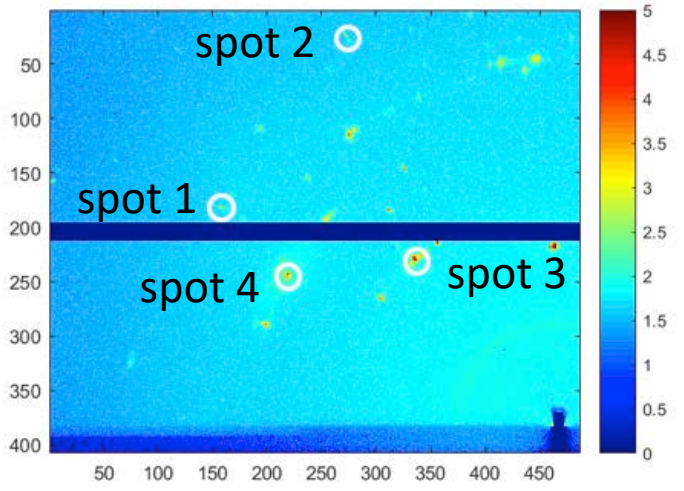

Looking at individual frames

Spot 1

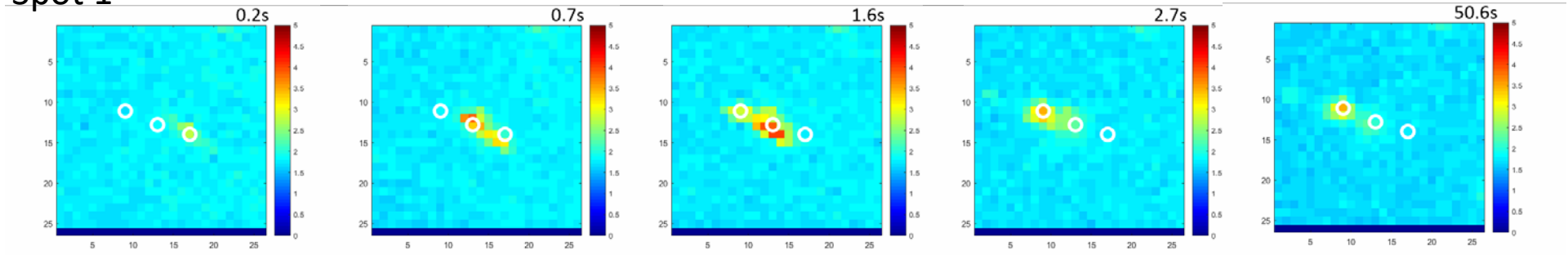

Spot 2

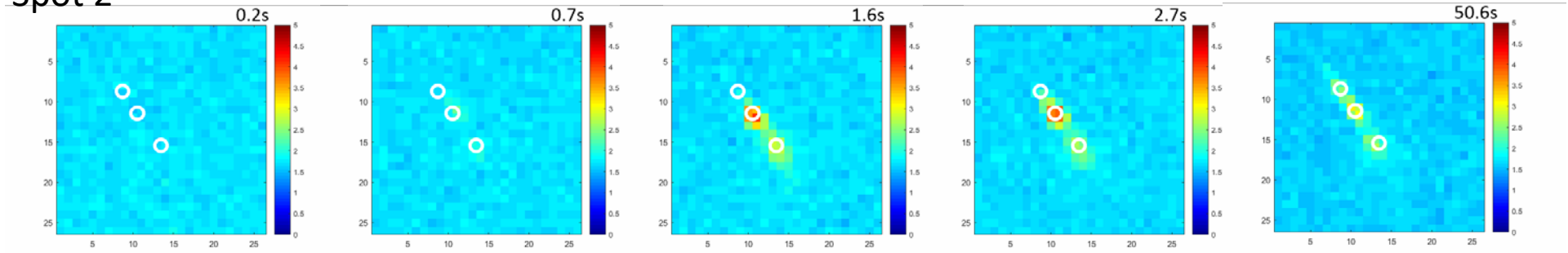

Spot 3

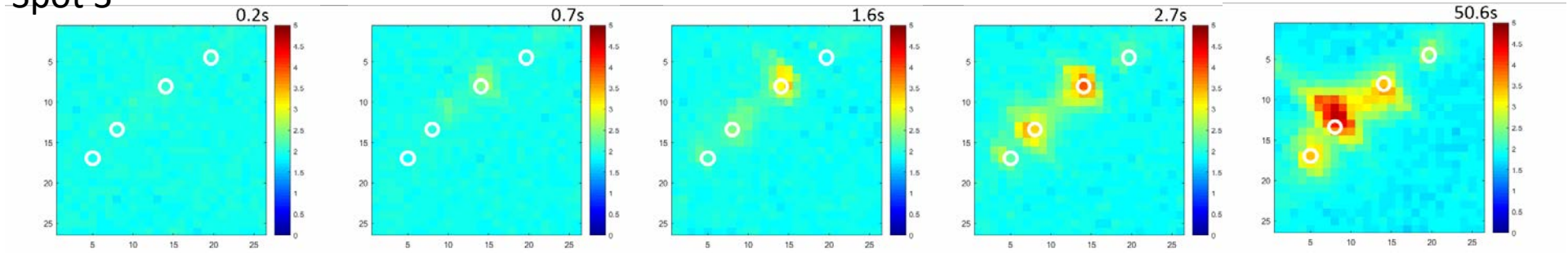

Spot 4

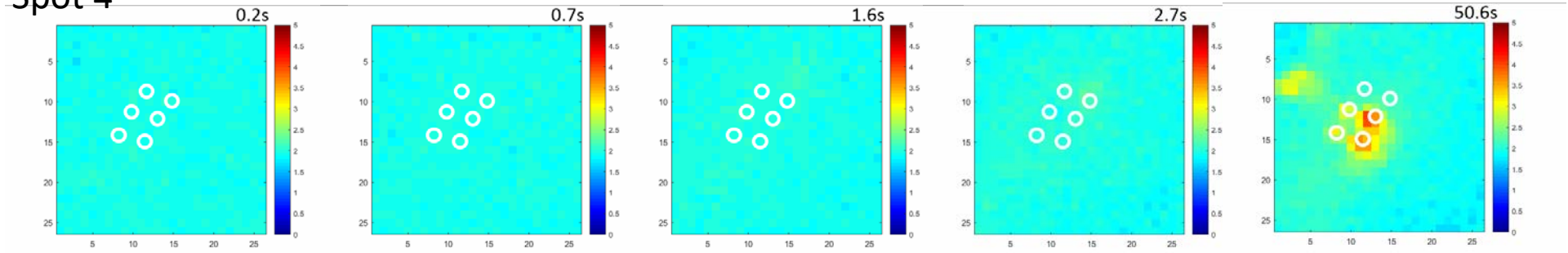

Conclusions

- In-situ synchrotron work provided first insights into early ACM crystal formation stages
- Studies of ACM form II on PTS SAMs in dioxane/water revealed growth upwards from substrate-solution interface
- Studies of spontaneous nucleation of ACM form I on PTS SAMs in water revealed unusual peak shifts at the earliest time points hinting at possible early structural transformations (versus simple rotations).
- These results warrant further in-depth studies of these early formation stages

Future directions: In-situ WAXS & blade coating

- Continuing with in-situ GIWAXS performed at CHESS:

CHESS

Cornell High Energy Synchrotron Source

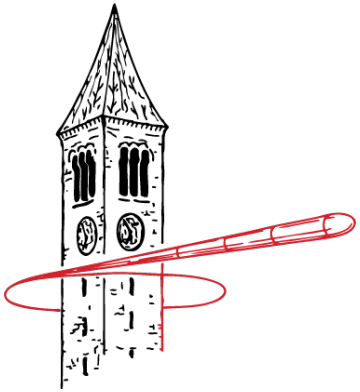

- Introducing blade coating as an alternative method:

Fig.6. Photographs of fully automated doctor blading set up (left) housed in an atmosphere controlled chamber (right).

- Introducing other model systems:
  e.g. 5-methyl-2-[(2-nitrophenyl)amino]-3-thiophenecarbonitrile (ROY)

Die Filling of Aerated Powders

Anastasiya Zakhvatayeva, Charley Wu

IFPRI AGM, Edinburgh, UK, June 24-28, 2018

Charley Wu
Chemical and Process Engineering
University of Surrey,
Guildford, GU2 7XH
@charleywu
C.Y.WU@surrey.ac.uk

UNIVERSITY OF SURREY

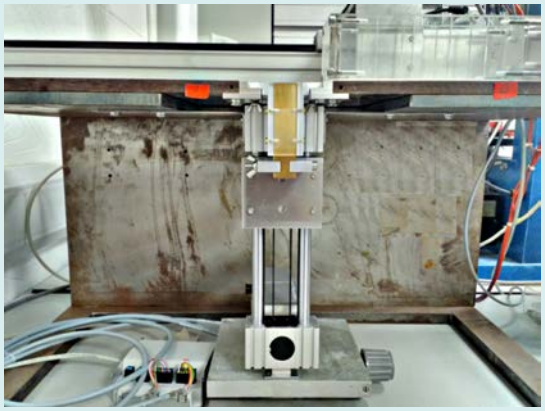

“Future Work” from AGM 2017

Task 2 – Assisted die filling
(Month 13 - Month 24).

Task 2.1 – Suction filling: system development and detailed experimental investigation

Task 2.2 – Paddled hopper/shoe: system development and preliminary investigation

Further CMA study –correlation with other flow measurements;

Further Rotary die filling study – Moist/cohesive powders

Objectives & Tasks

- *The goal is to understand die filling behaviour of aerated powder blends.*
- *The objectives are*
  1) *to explore fine powder mixtures during die filling processes;*
  2) *to identify the critical material attributes and critical process variables*
  3) *to develop a design space for fine powder mixtures to achieve controlled/specified properties during die filling (such as mass variation, content uniformity, mass flow rate).*

Task 1 – Rotary die filling
(Month 1-Month 12).

Task 2 – Assisted die filling
(Month 13 - Month 24).

Task 3 – Segregation during die filling
(Month 24 - Month 36).

CONTENTS

UNIVERSITY OF SURREY

(1)

Rotary vs Linear die filling

(2)

CMA for die filling

(3)

Suction filling

Linear vs rotary

1. Comparison of the die filling behaviour of seven commonly used pharmaceutical excipients.
2. Two die filling systems used: linear and rotary.
3. An investigation in die filling efficiency at various speeds is presented, which takes into account such characteristics as particle density and morphology, as well as powder rheological properties.

Name	d_{50} (µm)	True density (kg/m^3)
Lactose monohydrate	83	1540
Dicalcium phosphate (DCP)	202	2300
Mannitol (Pearlitol 200SD)	123	1469
Microcrystalline cellulose:		
Avicel PH101	88	1581
Avicel PH102	105	1570
Avicel DG	79	1786
Celphere CP102	182	Missing/1600

Properties of studied powders

Air sensitivity index

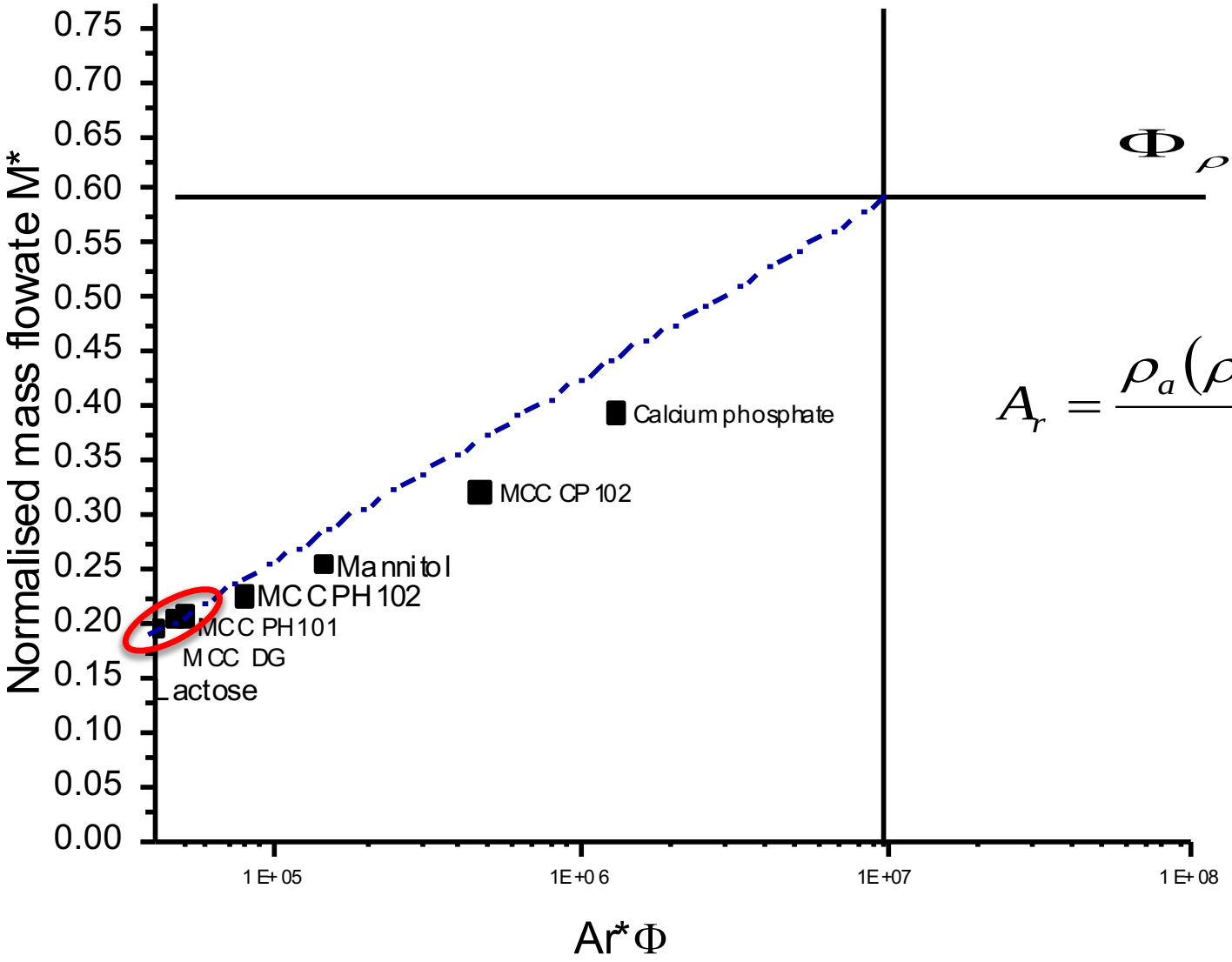

$$\Phi_\rho = \frac{\rho_s}{\rho_a}$$

$$A_r = \frac{\rho_a(\rho_s - \rho_a)gd_p^3}{\eta^2}$$

Morphology

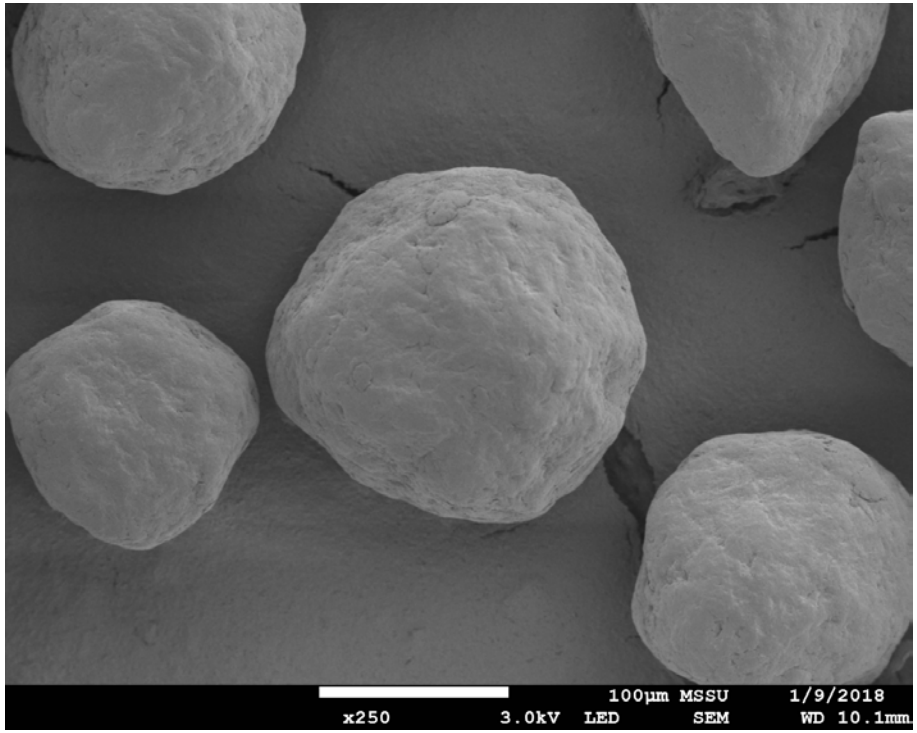

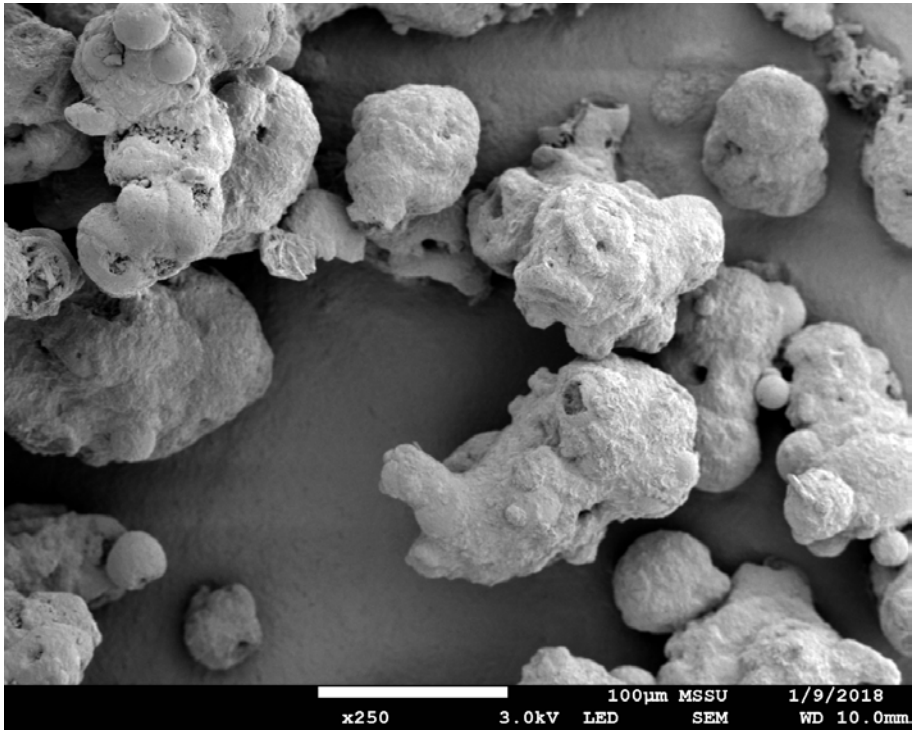

MCC CP102

Mannitol

Aspect ratio values are respectively 0.920 and 0.865, which is confirmed by their high flowability (s90,3).

Morphology

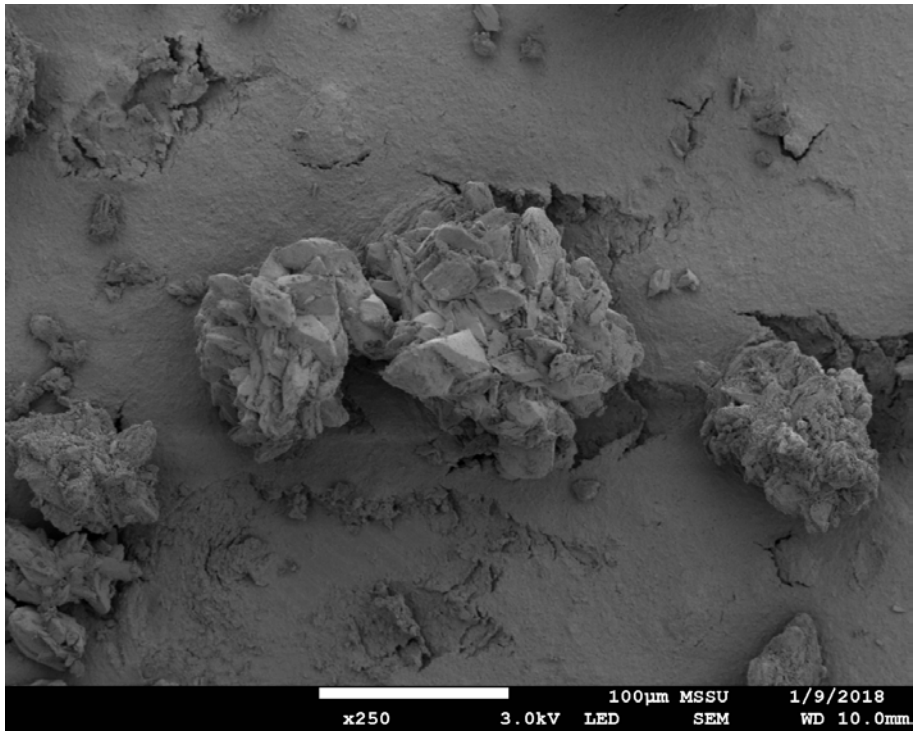

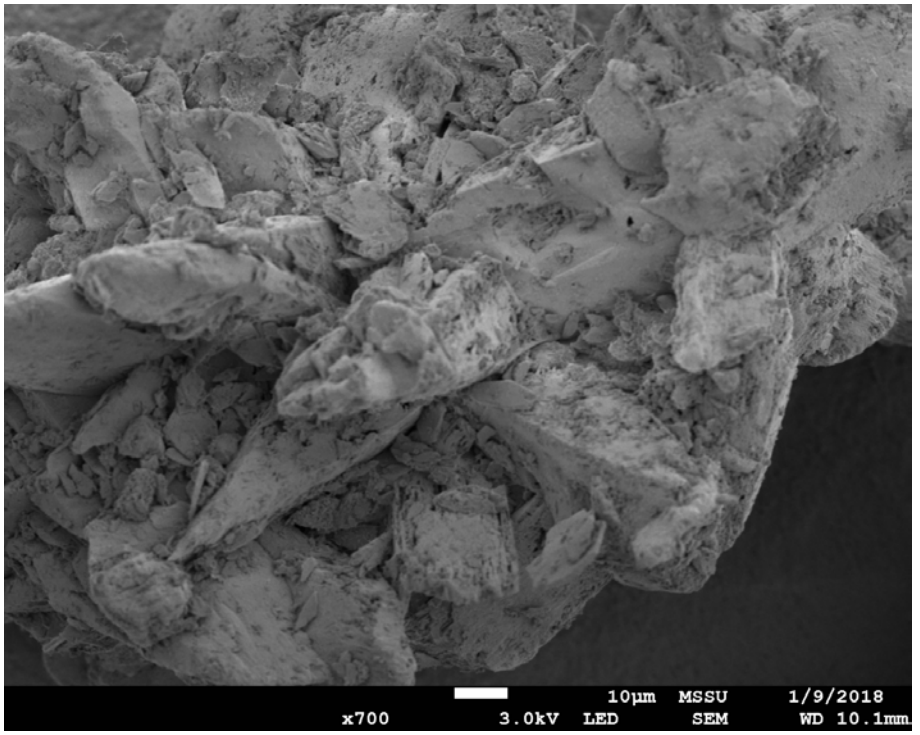

Calcium phosphate is an inorganic crystalline compound, with an aspect ratio very similar to those of mannitol (0.874).

Morphology

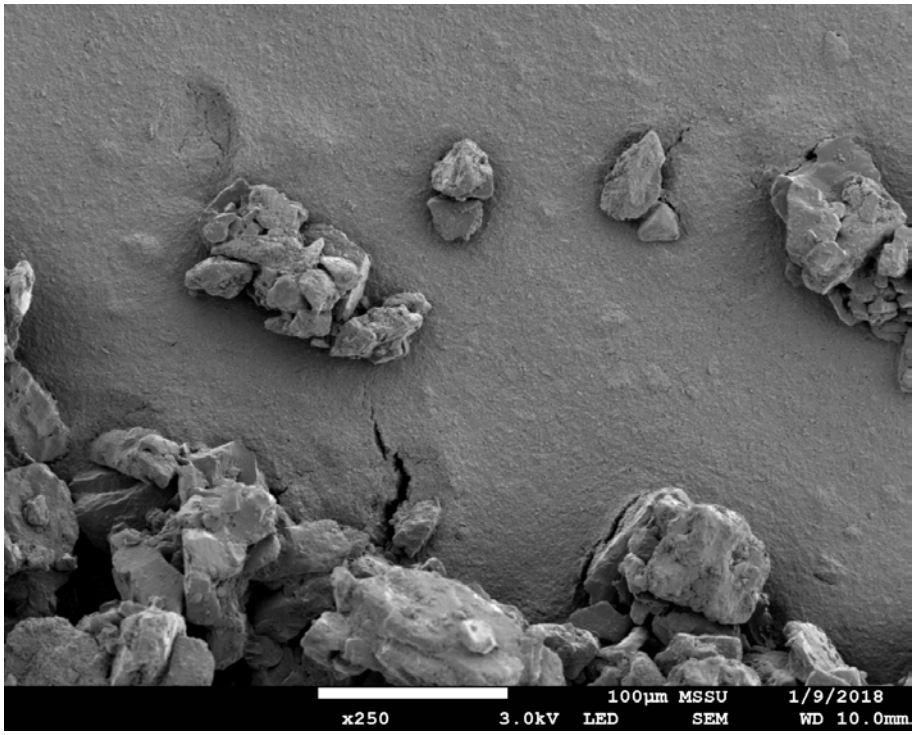

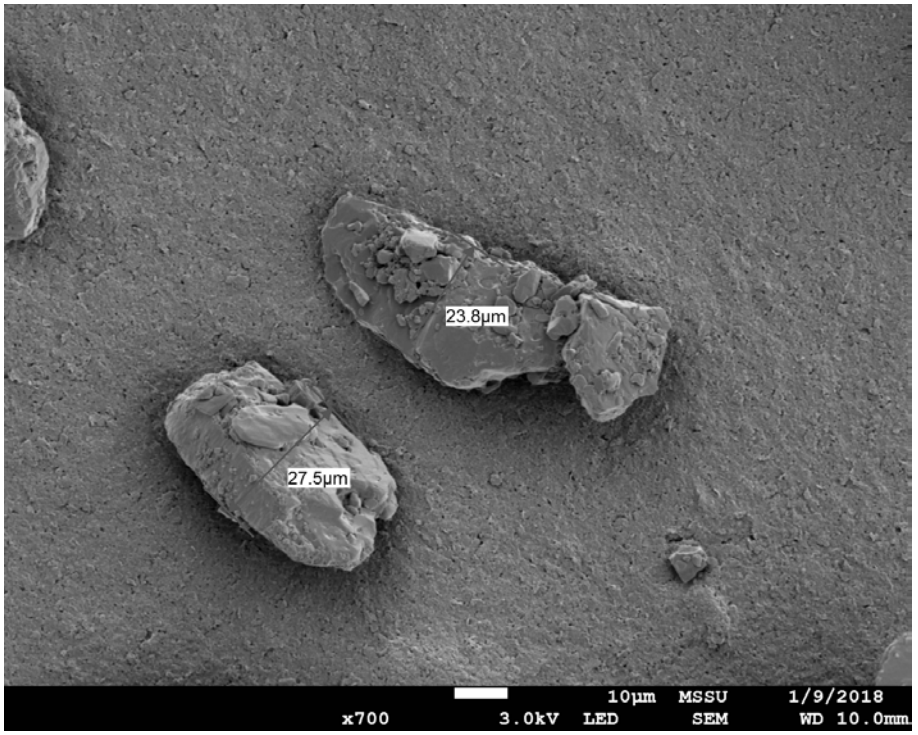

Lactose exhibits a very broad distribution of sphericity values, due to the fact that particles tend to agglomerate very easily.

Morphology

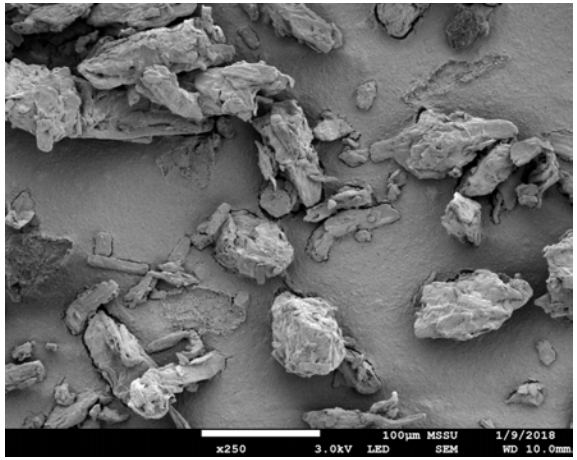

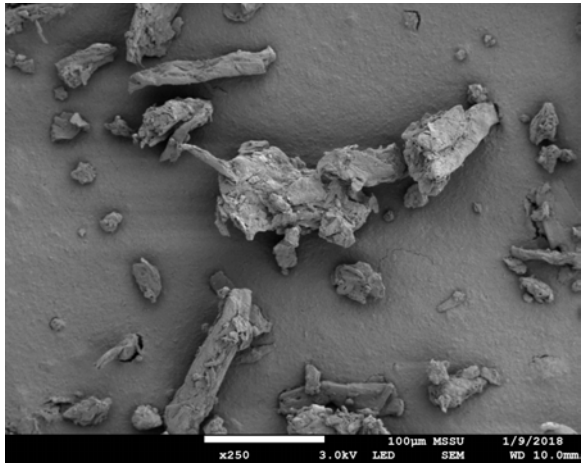

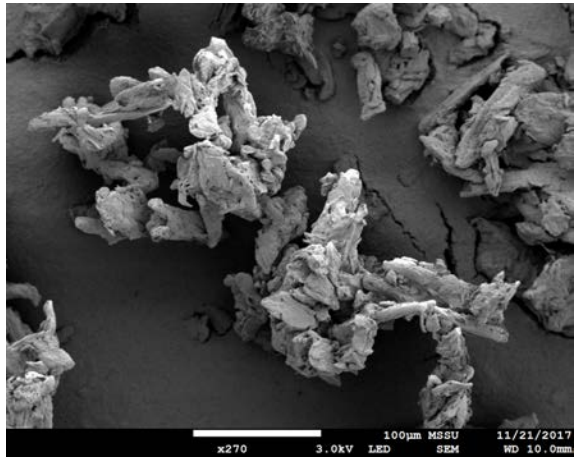

The powders that appear among the most critical in terms of flow, are characterized by highly irregular, oblong shape particles.

In the pictures from left to right: MCC PH102, MCC DG, MCC PH101

Weight fraction as function of speed

Free-flowing materials

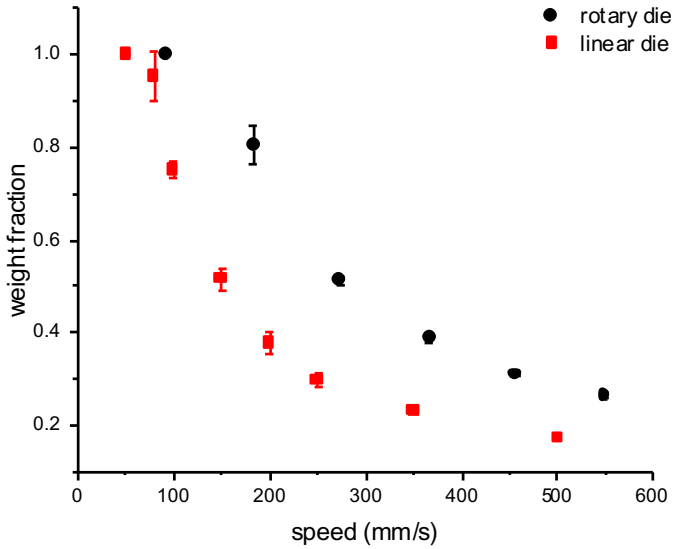

MCC CP102

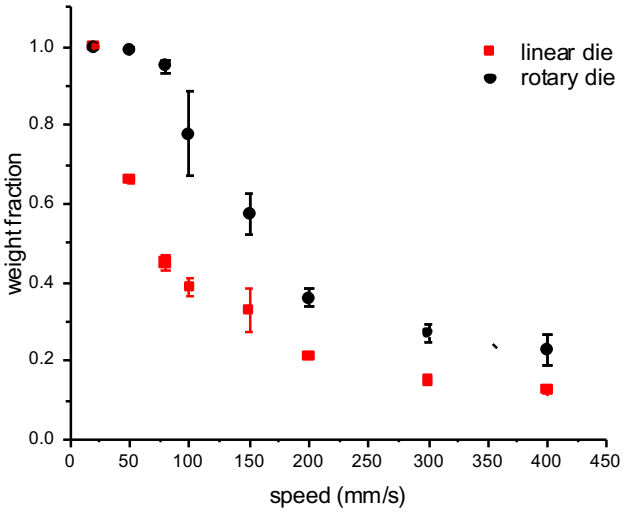

Mannitol Pearlitol 100SD

Weight fraction as function of speed

Free-flowing materials

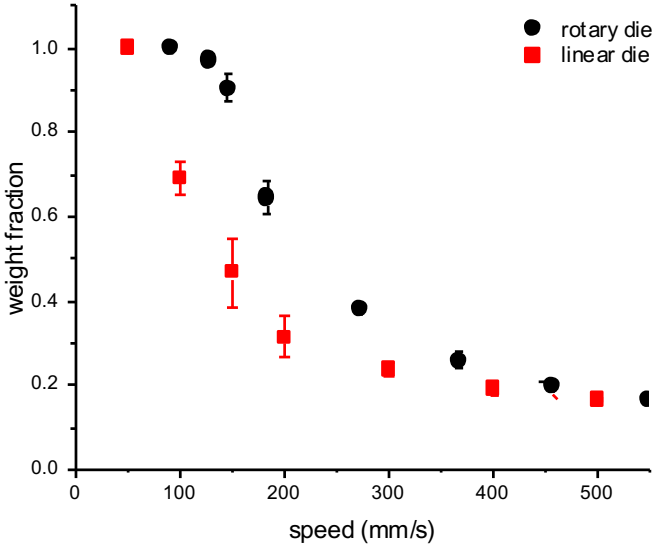

Calcium phosphate

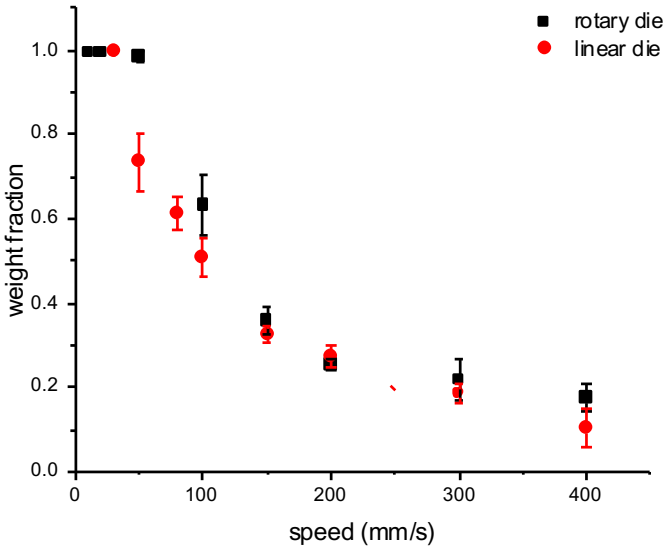

MCC PH102

Weight fraction as function of speed

Easy-flowing materials

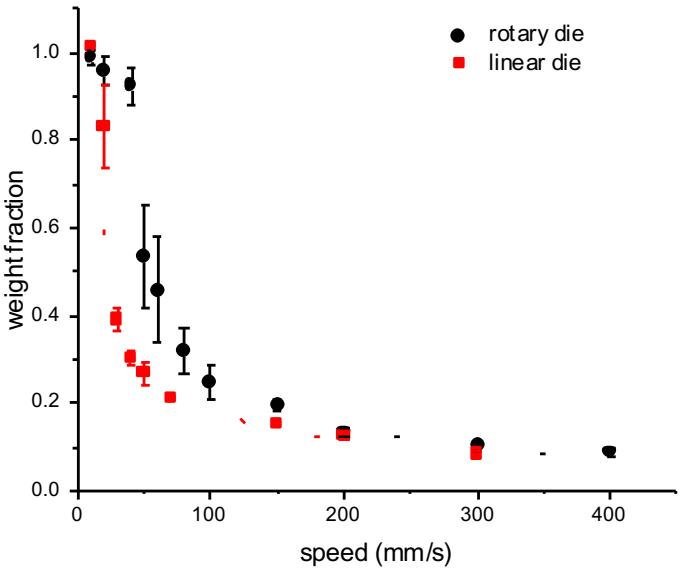

MCC PH101

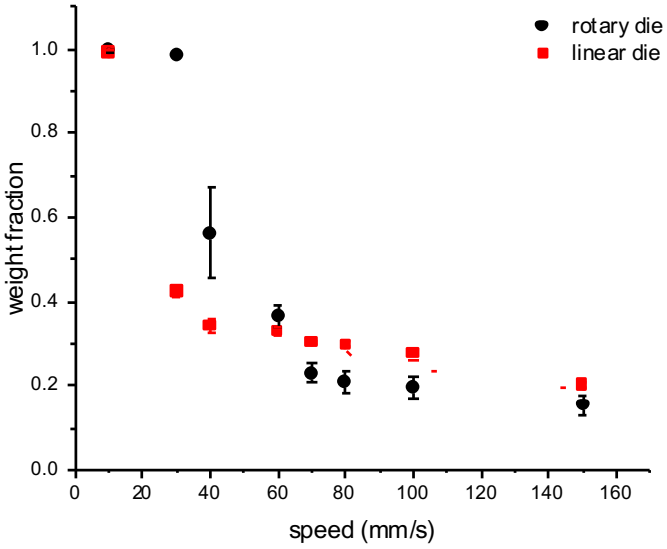

MCC DG

Weight fraction as function of speed

Cohesive material

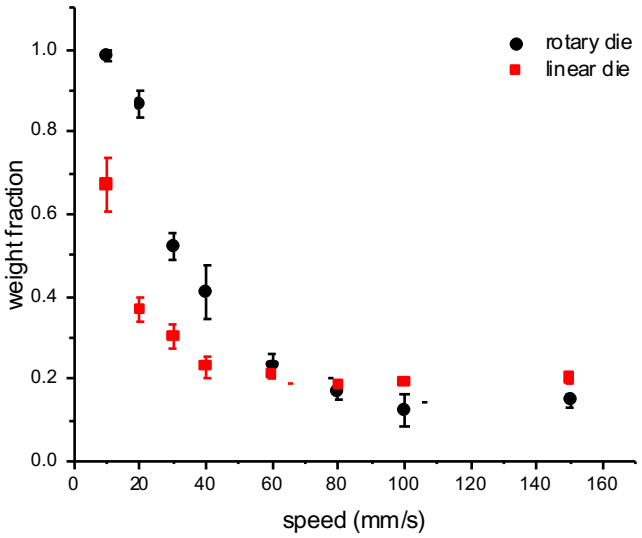

Lactose

Identification of CMAs for die filling

Comparison of flow index as a function of d50 size parameter
Flow index evaluation performed using the Flodex device.

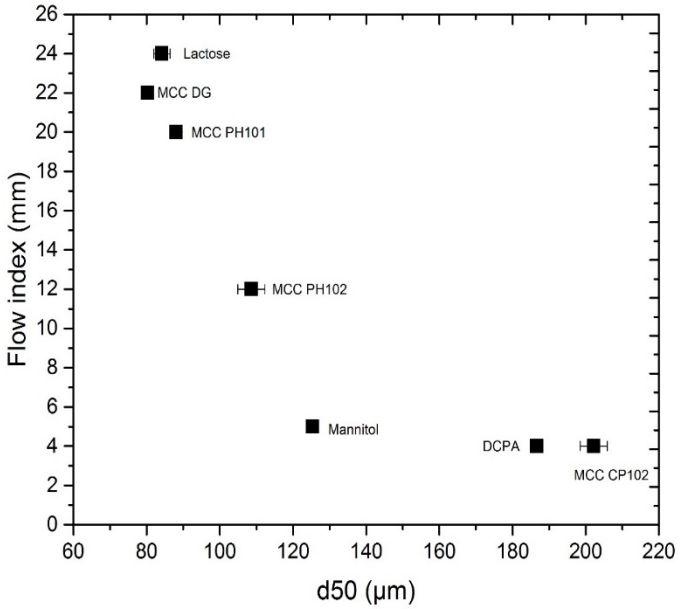

Critical velocity values as a function of the average particle size, expressed as d_{50}.

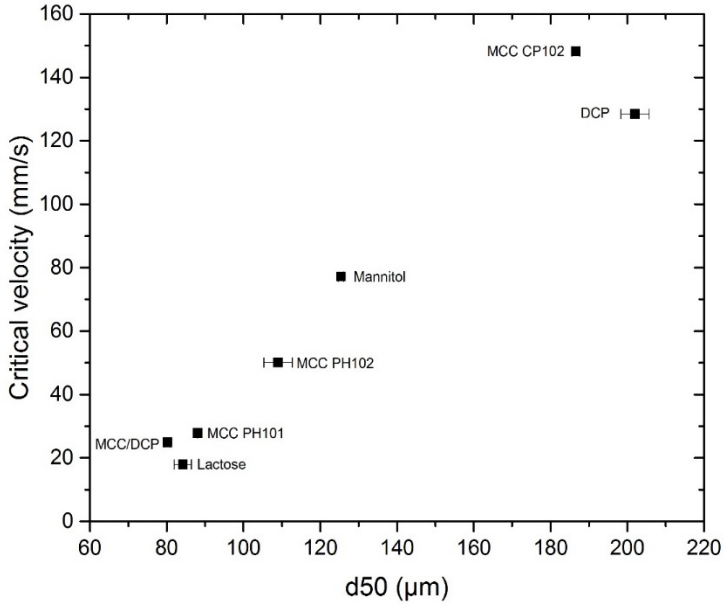

Identification of CMAs for die filling

Critical velocity values as a function of the Specific Energy.

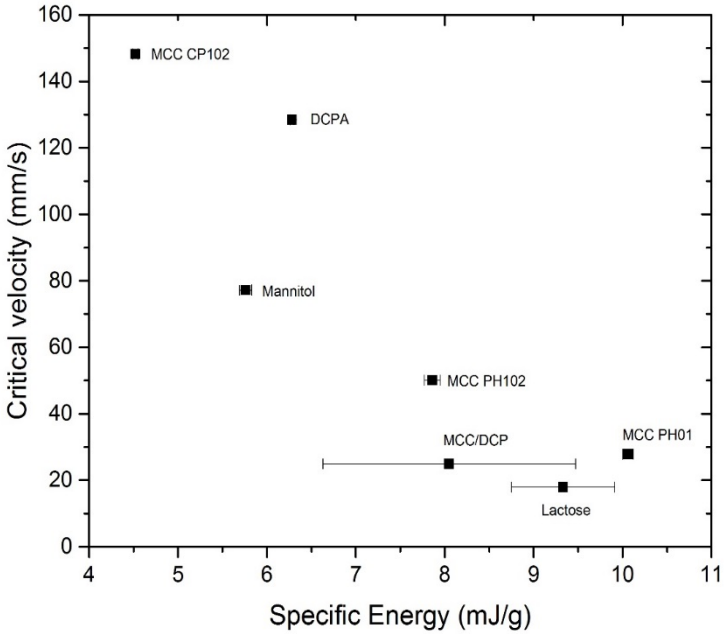

Critical velocity values as a function of the Average Pressure Drop.

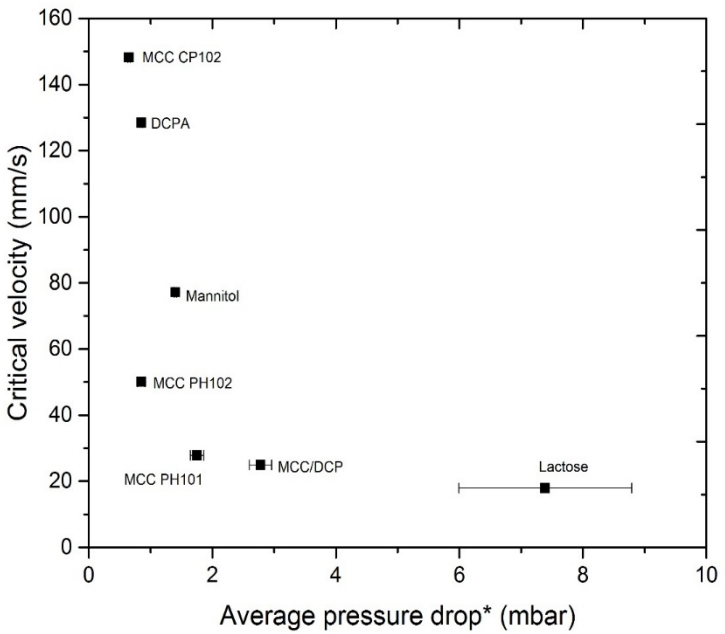

Identification of CMAs for die filling

Critical velocity values as a function of the cohesion assessed at 3 kPa of consolidation stress

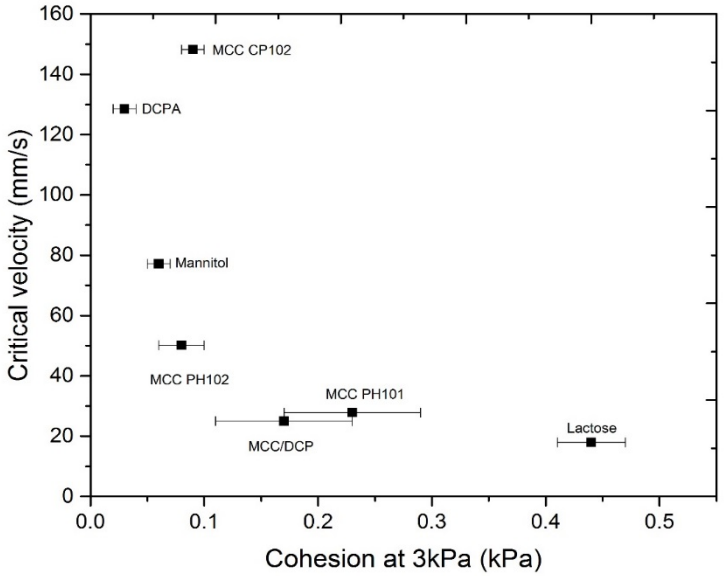

Critical velocity values as a function of the flow function assessed at 3 kPa of consolidation stress.

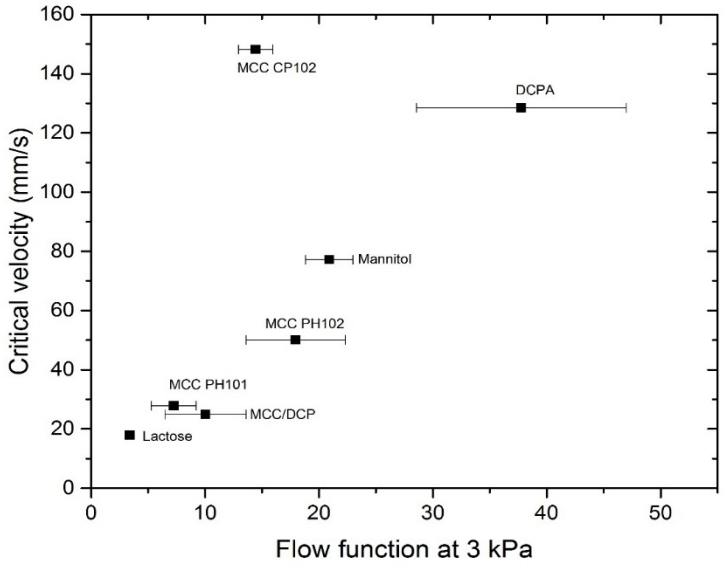

Suction Filling

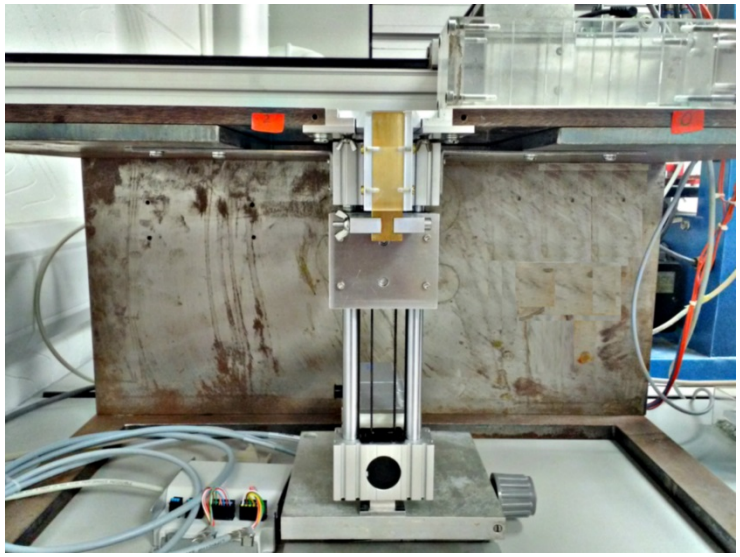

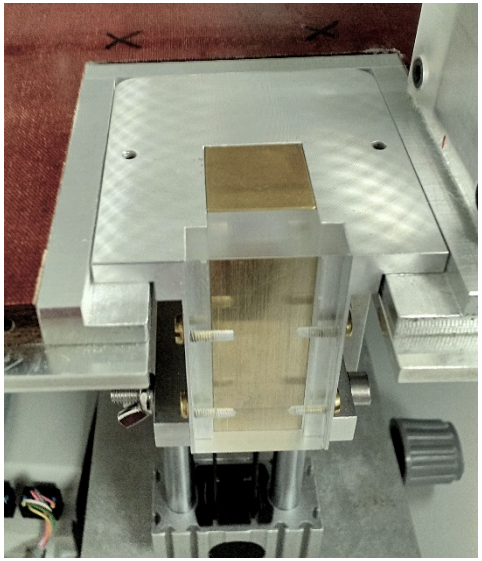

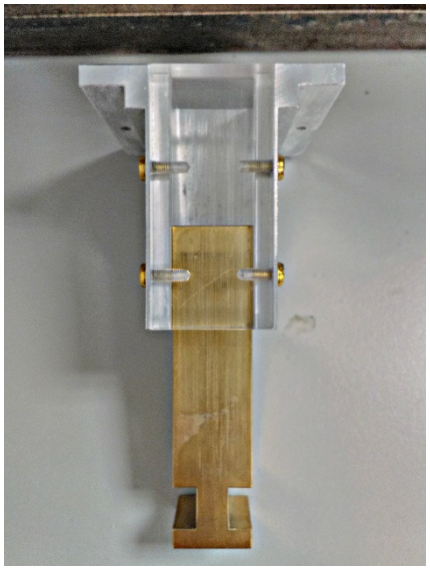

Suction Filling

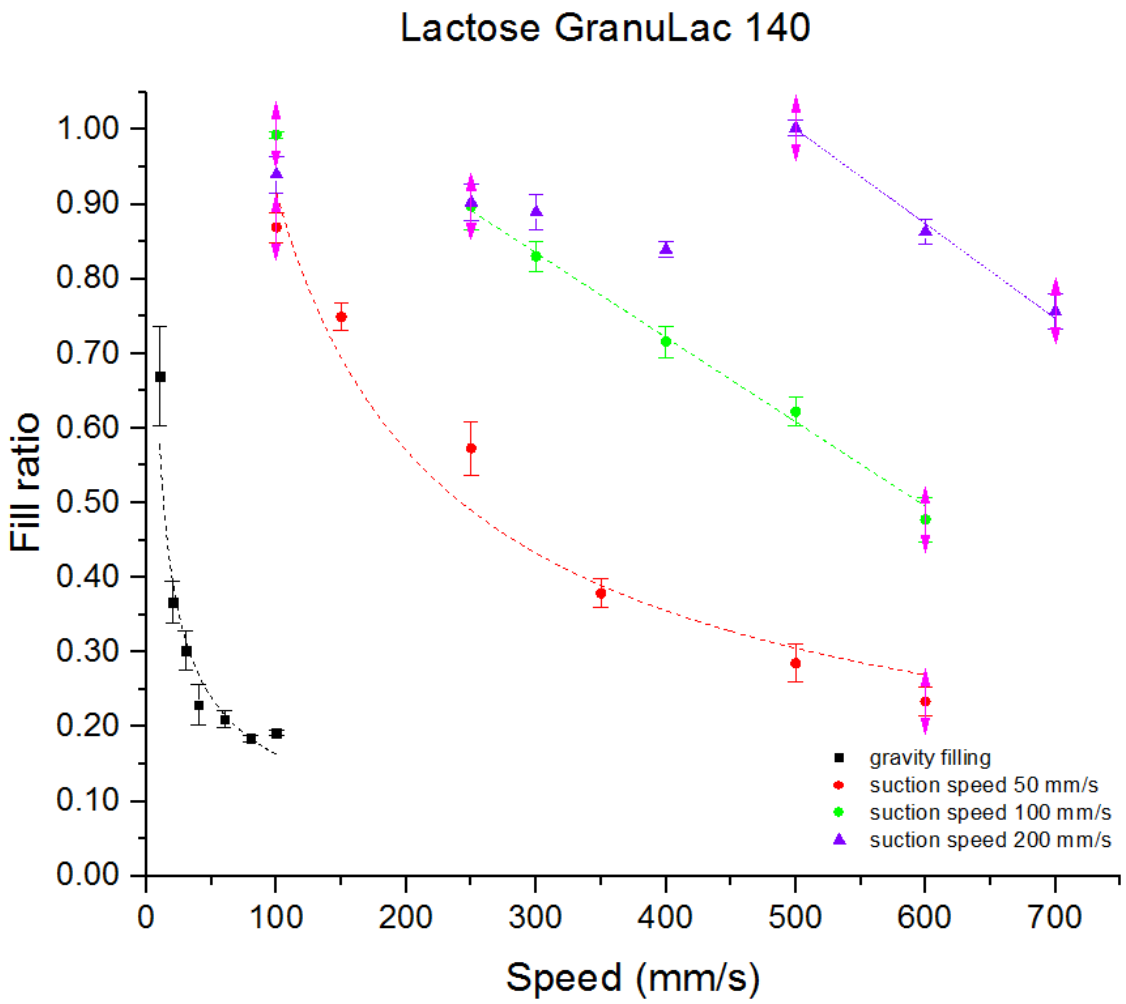

Summary and Future Work

- *Further confirmed that active (rotary) die filling can lead to higher filling efficiency than passive (linear) filling.*
- *Strong correlation between die filling performance and material properties identified.*
- *Efficiency of die filling can be further improved with suction filling.*

Task 2 – Assisted die filling
(Month 13 - Month 24).

Task 2.1 – Suction filling: system development and detailed experimental investigation

Task 2.2 – Paddled hopper/shoe: system development and preliminary investigation

Task 3 – segregation (Using APIs)

Relating Compaction Performance to Process Conditions with Emphasis on Powder Mixtures

Antonios Zavaliangos
Department of Materials Science and Engineering
Drexel University

IFPRI
International Fine Particle Research Institute

Annual General Meeting 2018

Drexel UNIVERSITY

Strength of compacted mixtures

INDUSTRIAL IMPORTANCE

- **Knowledge of mixture rules can reduce dramatically the complexity of multicomponent formulations**

CONNECTION TO FUNDAMENTALS

- **To address strength of binary mixtures compacted at high relative density, we must also understand basic concepts of strength for simple materials and find ways to connect individual granule parameters with the compact properties**

PERSONAL INTEREST

- **Explore the possibilities of Discrete Element Method for compaction to high density as a natural platform to address strength despite the inherent shortcomings of the method**

Rule of mixtures for mixtures?

- **From a fundamental point of view powder compacts are quasi brittle materials**
- **Strength of quasi-brittle materials is related to fracture toughness**
- **No rule of mixtures in fracture toughness**
  No bounds in fracture toughness

DEM for single materials before DEM for mixtures

- Both compaction and strength have to be modeled and there is a causality relationship there.
- Traditional DEM don't "work" because they come from the low pressure-density regime
- Force displacement laws for high densities need to be developed
- Cohesion models need to be developed and checked

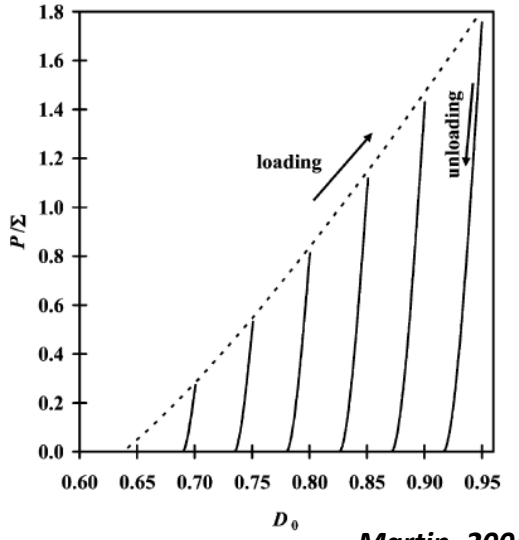

Martin, 2004

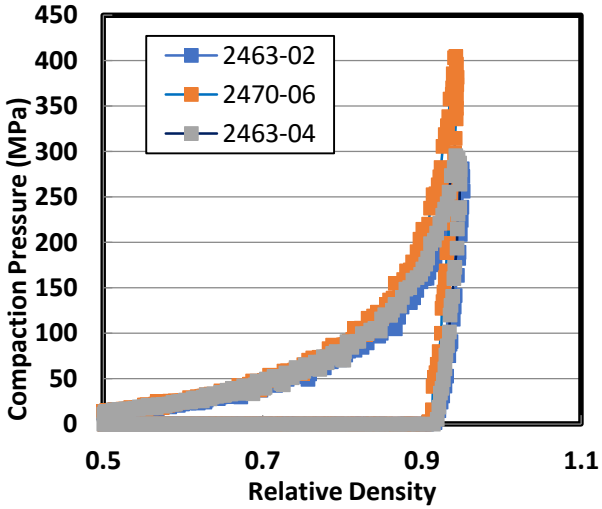

The need for modification of DEM

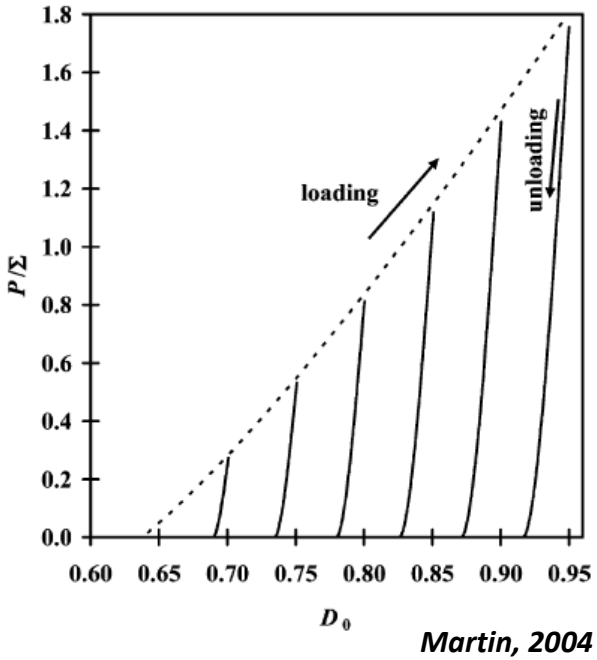

Martin, 2004

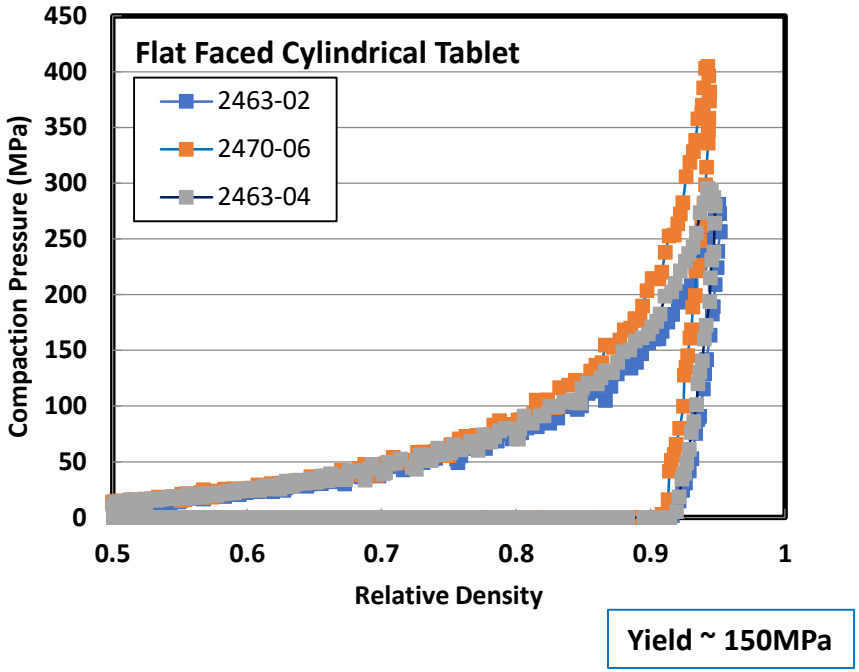

Yield ~ 150MPa

Pressure density curve predicted by model is not realistic

Inelasticity in unloading increases with density but is higher than model predictions

Compaction to large densities

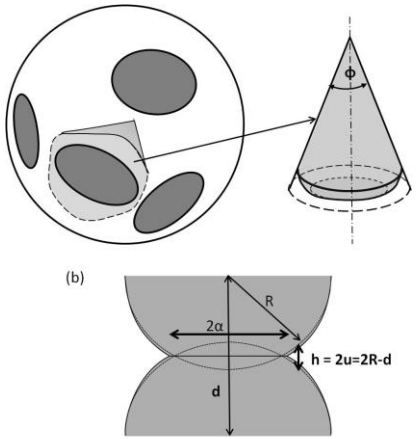

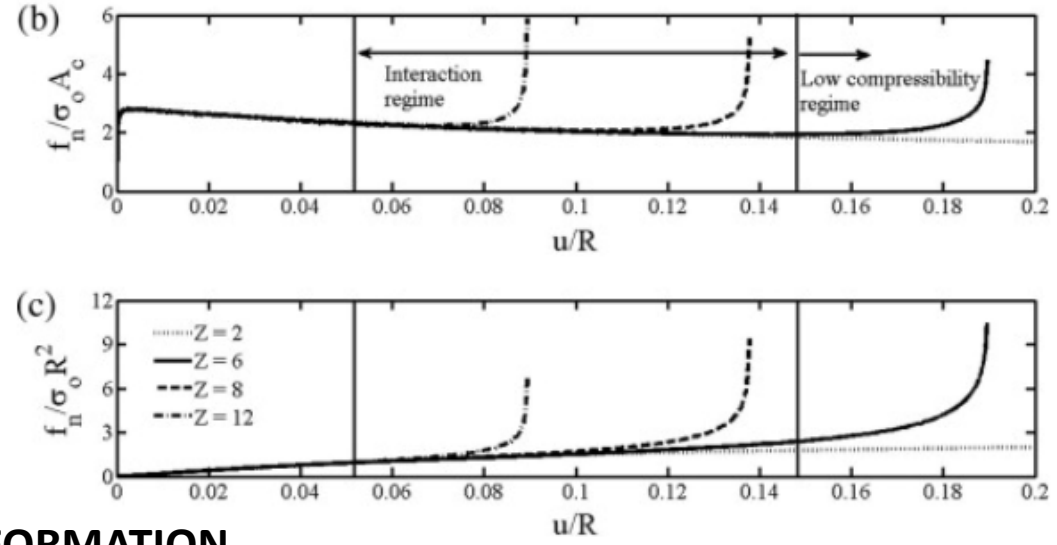

REGIMES OF INTERPARTICLE DEFORMATION

1) **Small deformation regime** : contacts are independent
2) **Contact interaction regime** – each contact "feels" the presence of its neighbors
3) **Low compressibility regime** –porosity almost closed and deformation is nearly elastic

Transitions depend on coordination number.

F-δ is depends not only on coordination number but on "triaxiality" of particle loading also

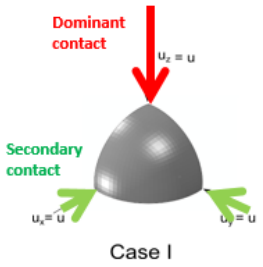

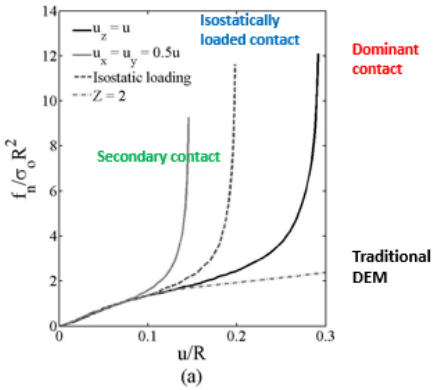

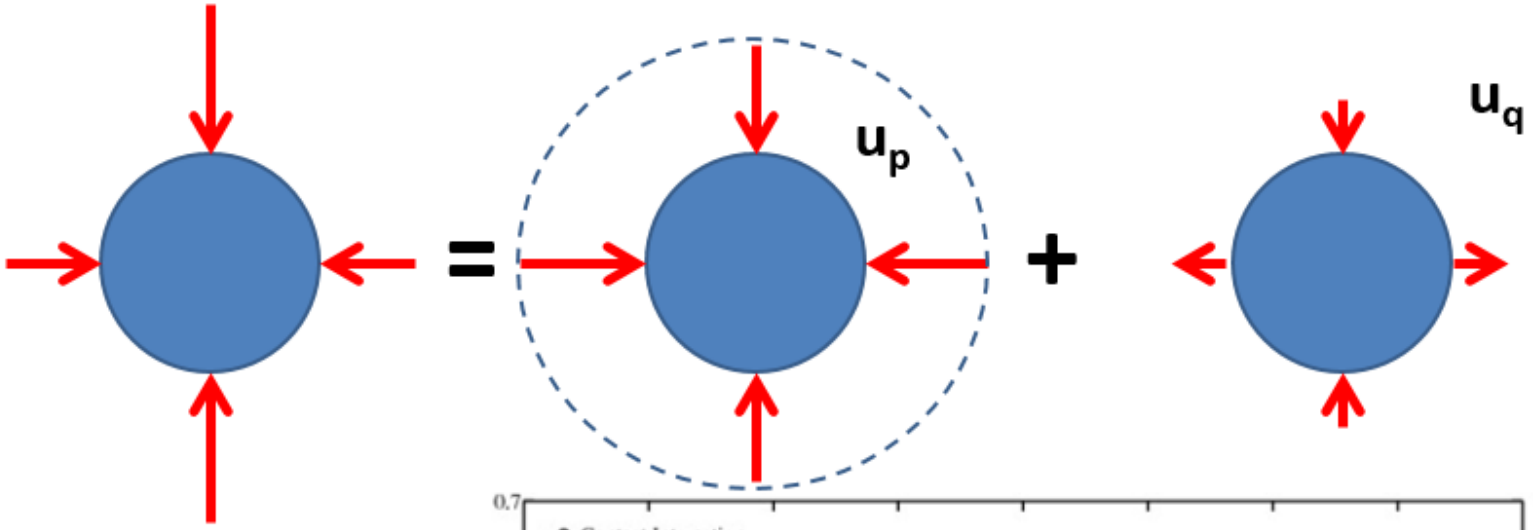

Force displacement law depends on

1. mode of loading
2. deformation of all contacts on the particle

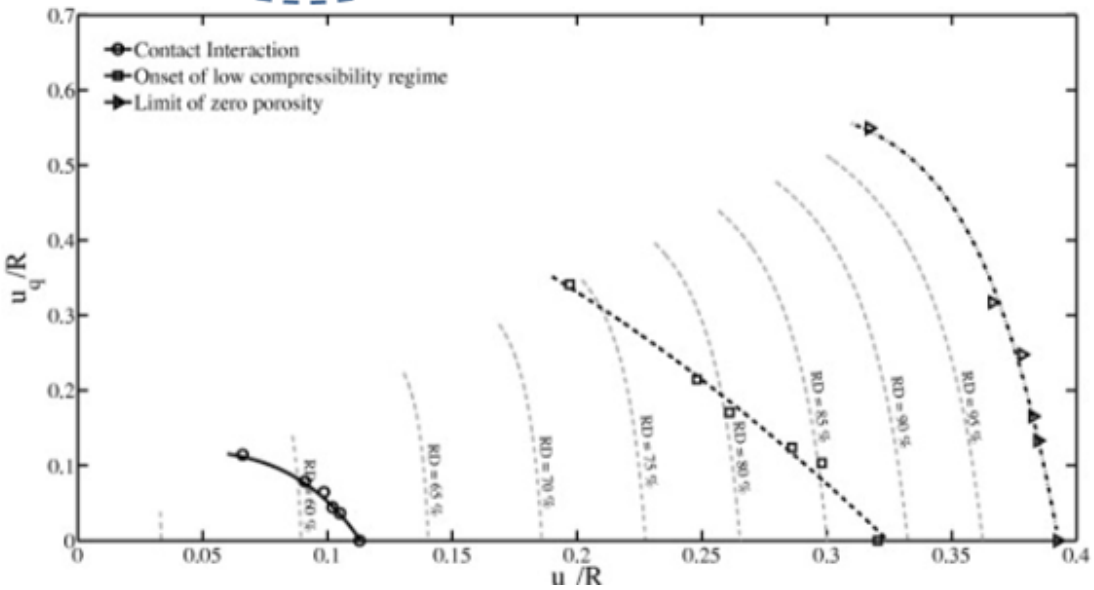

International Journal of Solids and Structures
Volumes 60–61, 15 May 2015, Pages 17–27

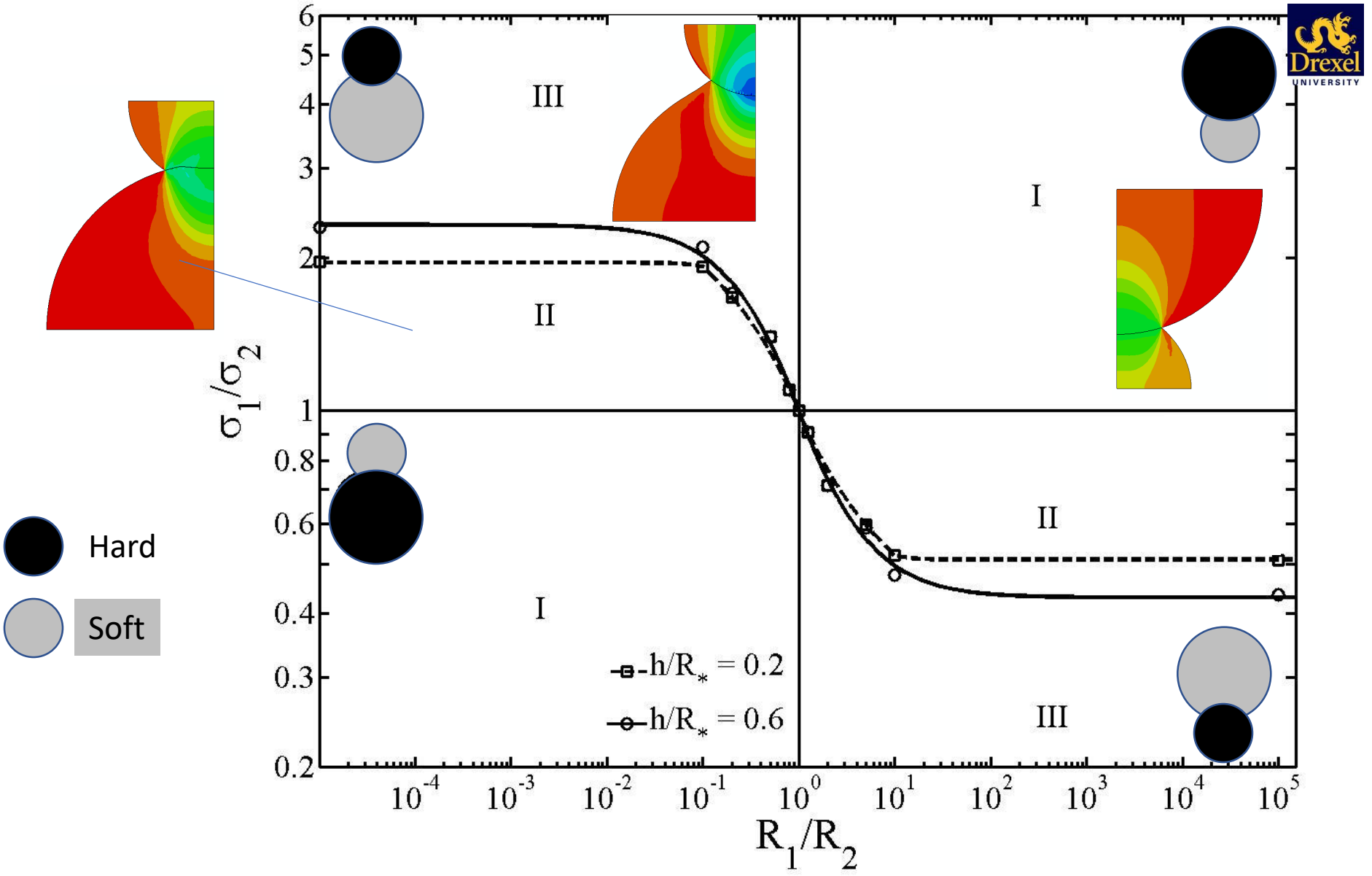

Mode = I and III hard sphere indents soft sphere
II has a mixed history=starts as III and turns into I,
in other words finally the harder sphere deforms.

Force-displacement law in Mode I has a strong dependence on the ratio of sizes

A simplified model

Takes into account contact interaction in a heuristic way

The transition from the commonly used Storakers model (linear force-displacement) to the highly constrained elastic regime is part of the model calibration

A simple cohesion model is included that makes the maximum tensile force supported by a contact proportional to the maximum compaction force that this contact has seen (in the plastic regime)

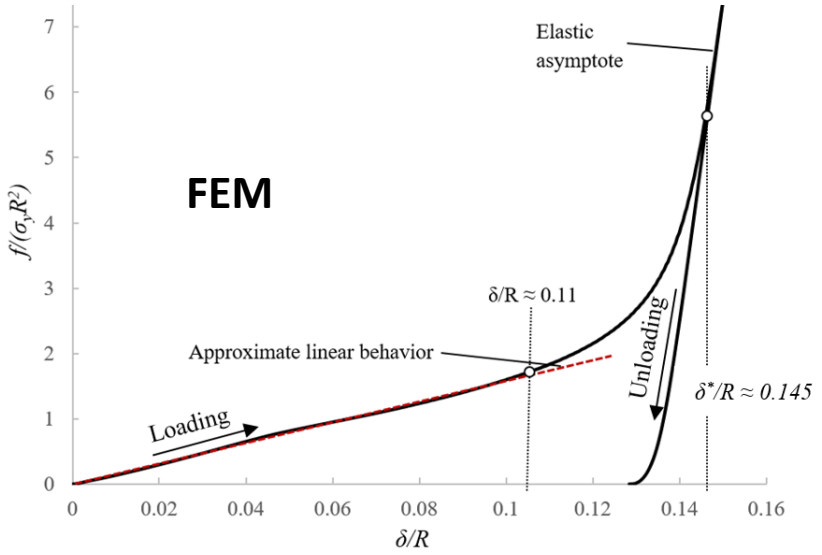

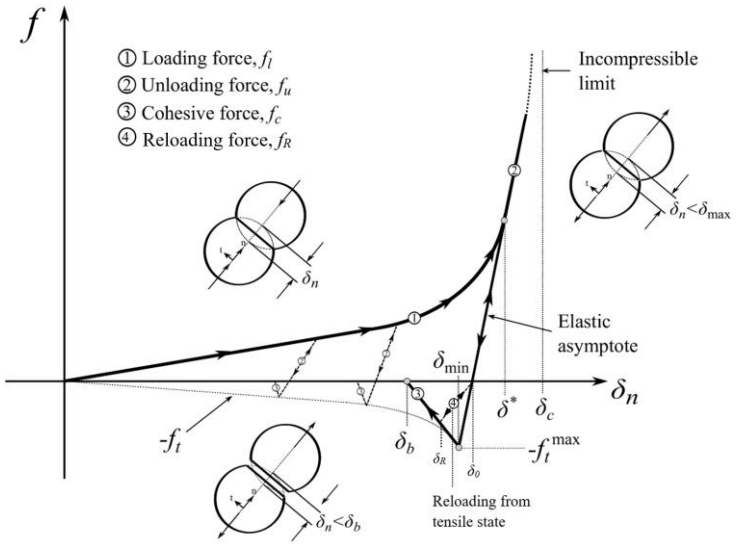

Study of the die compaction of powders to high relative densities using the discrete element method

Powder Technology 330 (2018) 357–370

F-δ law – Model parameter identification

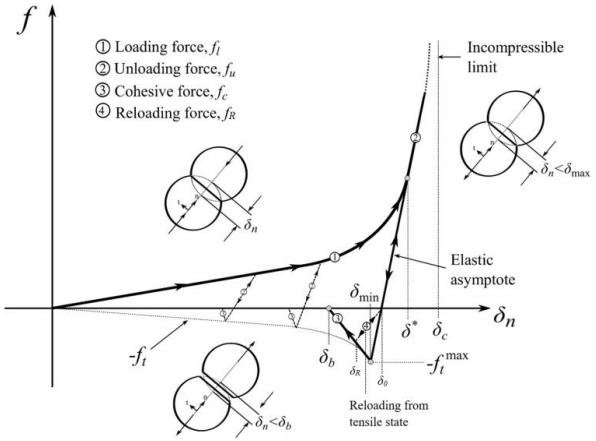

Problem is broken into 2 parts: Compaction and Strength

1. **Key response variables of the model are selected**
2. **The model is approximated by a response surface constructed for each by a number (34 here) of DEM runs**
3. **Model parameters are selected so model response "matches" with experimental data**

5 parameters of the F-δ law + interparticle friction to be determined experimentally

Bayesian optimization is used to minimize need of new runs for new materials.

Key variables:

- **Elastic & Plastic "work" for axial and radial stress at a single"high density"**
- **Strength at 3 densities**

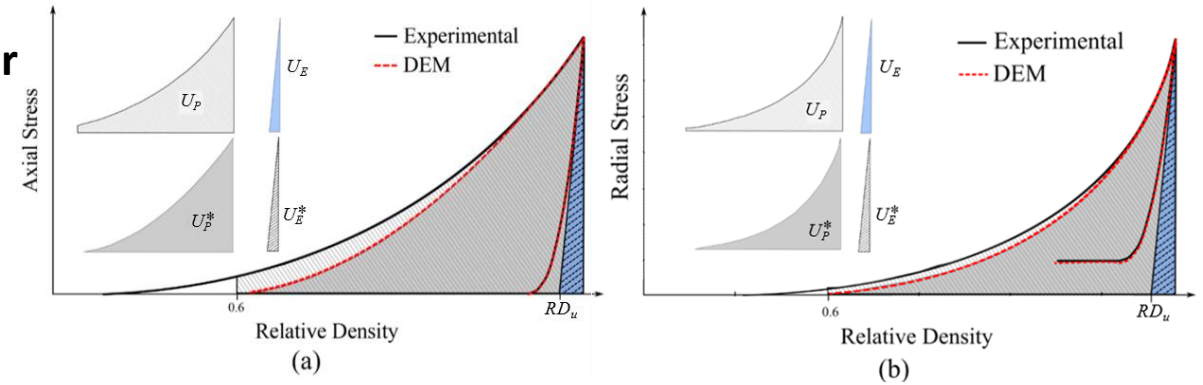

Model performance

CALIBRATION

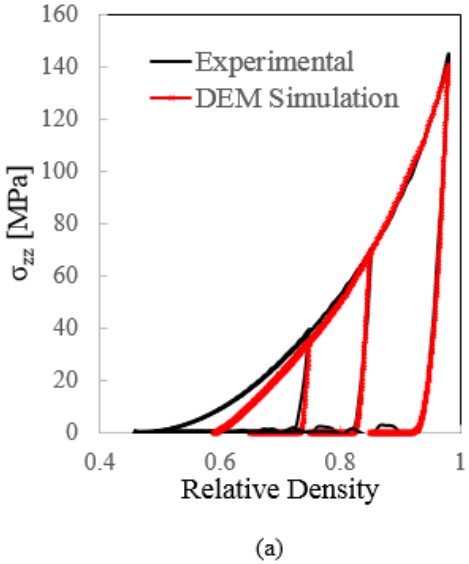

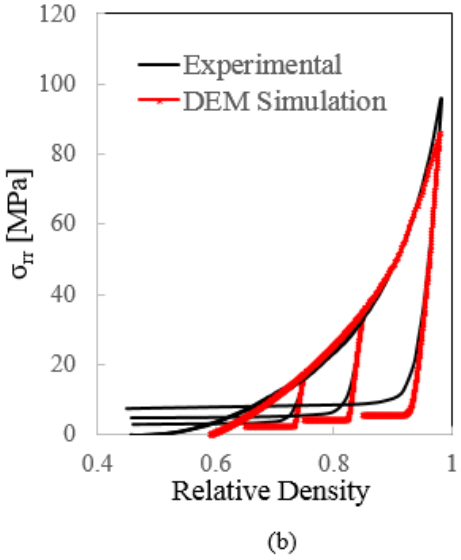

VALIDATION

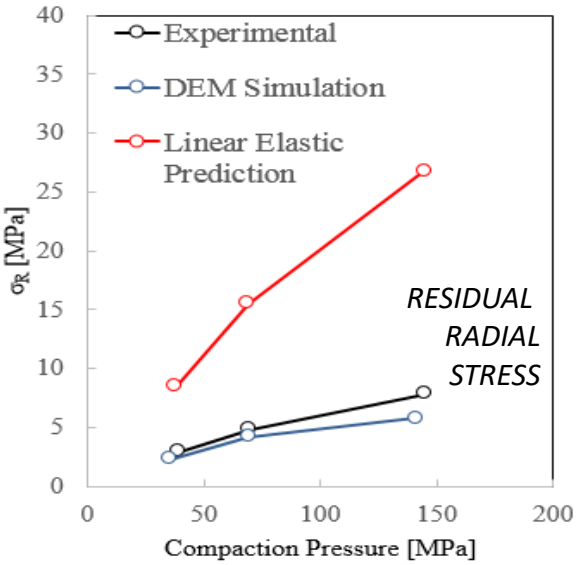

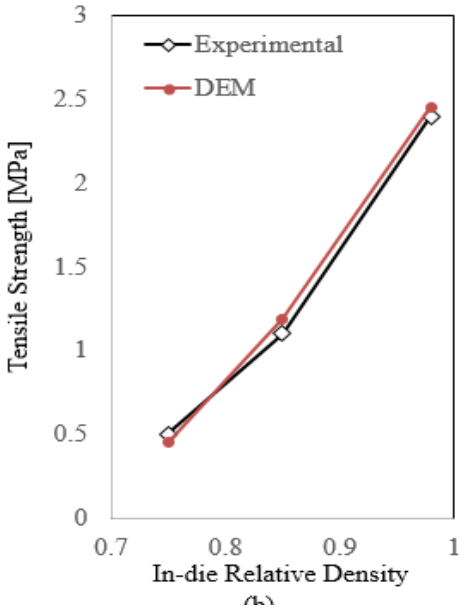

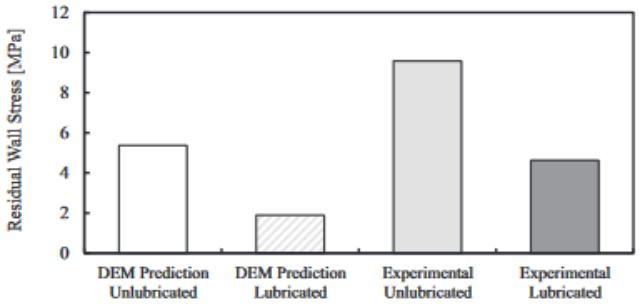

- **Much better prediction of residual wall stresses**
- **Predicts**
  - **connection of the interparticle strength & residual wall stress**
  - **connection of axial expansion post-compaction with interparticle strength**

  as experimentally observed is with excipient versus excipient+MgSt system.
- ***Underpredicts*** **the axial expansion.**

Additional predictions

Improved strength in triaxial unloading in line with Hiestand experiments

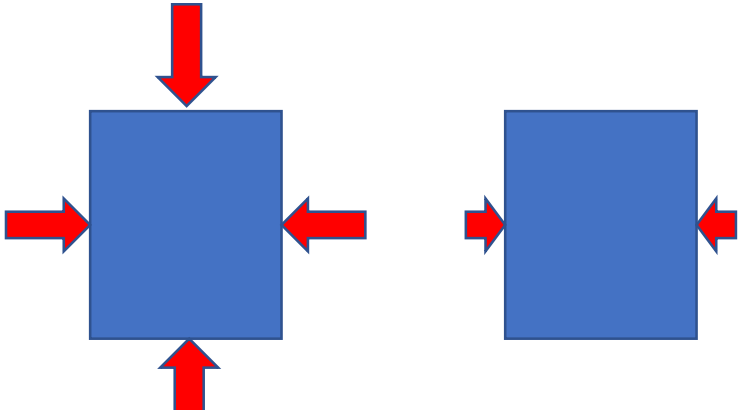

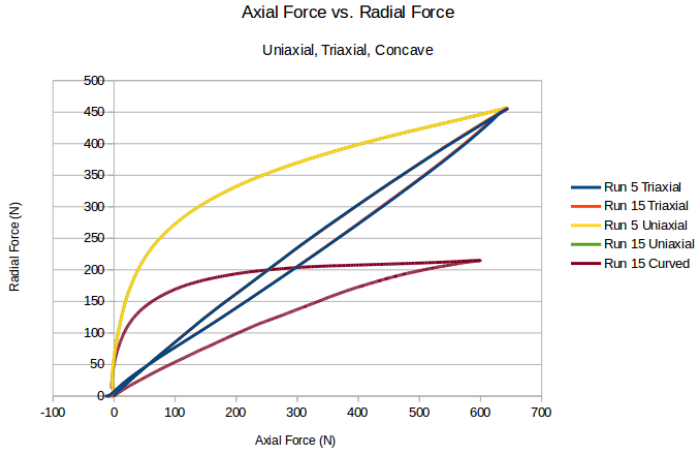

Fundamental highlights of the sticking phenomenon

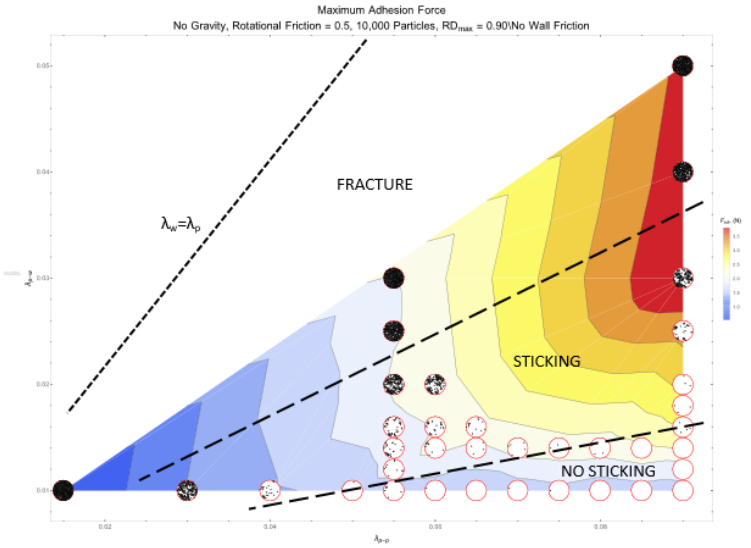

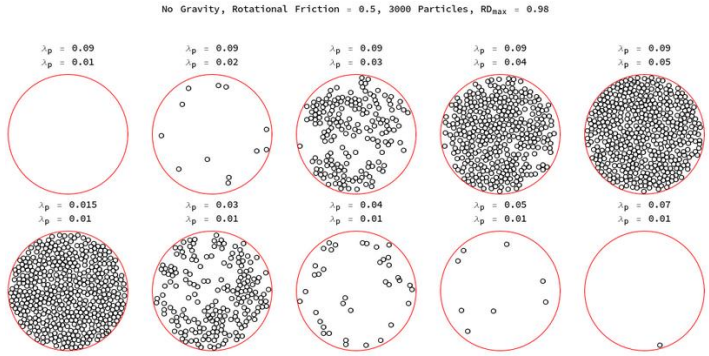

Strength and damage

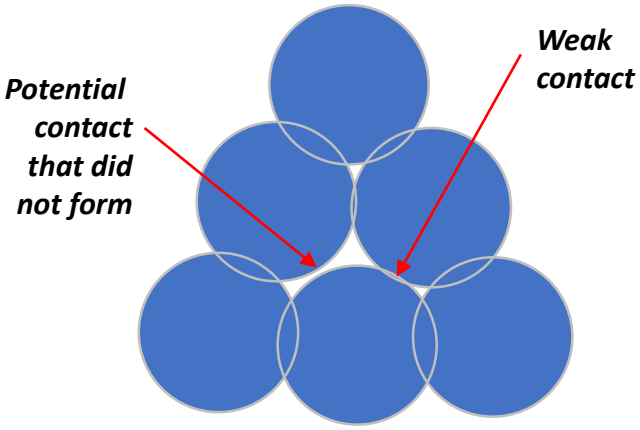

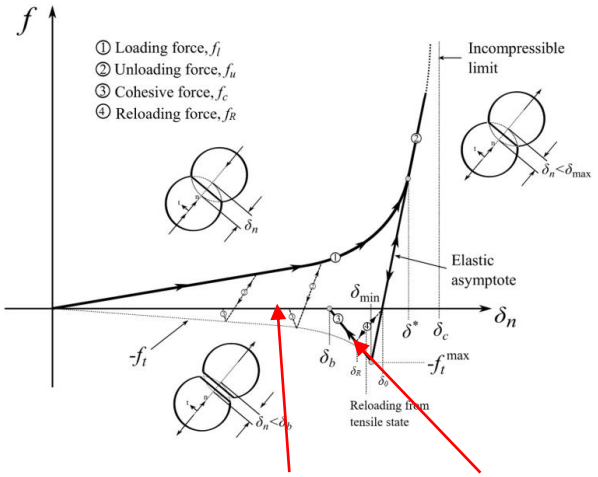

- Contacts that did not form
- Weak contacts pressed at F << average force
- Broken contacts (during unloading)

Fully damaged (broken) contact

Beginning of contact damage

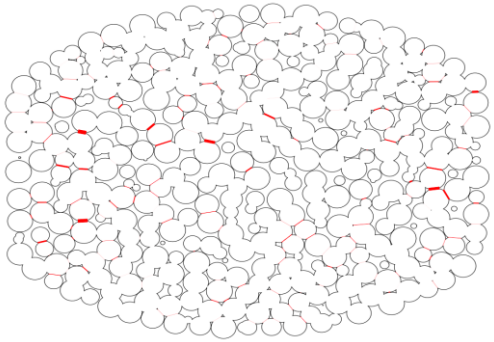

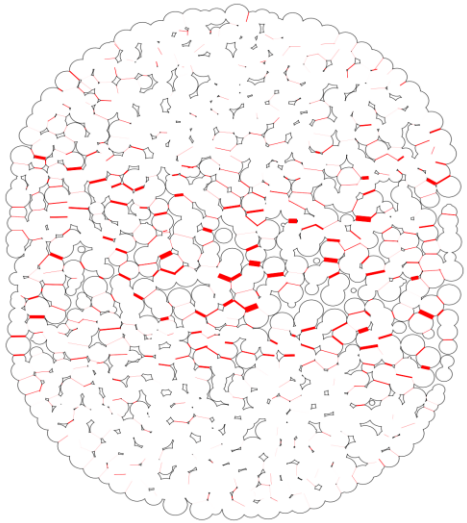

$$D_2 = 1 - \frac{\sum(\min(\delta, \delta_{min}) - \delta_b)}{\sum(\delta_{min} - \delta_b)}$$

An anisotropic damage definition needs to be used.

MIXTURES: Is A+B = A+B?

- **Non-interacting mixtures**
  phases are clearly defined geometrically
  geometric boundaries are subject to change during compaction
- **Chemically interacting mixtures**
  Usually start on particle boundary,
  reaction zone may develop with time (e.g., Al + graphite powder)
- **Physically interacting mixtures**
  Physical transport of species across prior particle boundaries typically by diffusion.
- **EVEN IF MIXTURES ARE NON-INTERACTING** it is possible that A+B ≠ A+B because the process of mixing may affect quantities such as particle size, surface quality etc.

The role of interparticle properties

Simulations were done with 5,000 monosized particles in a cylindrical die with frictionless walls

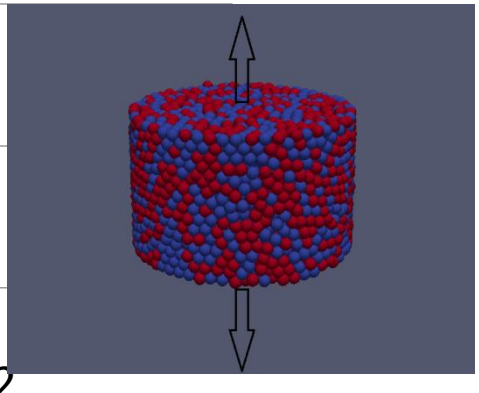

Note the prediction for AB=0 (i.e. the dissimilar contacts have no strength)

Mixtures of pharmaceutical excipients with different mechanical properties

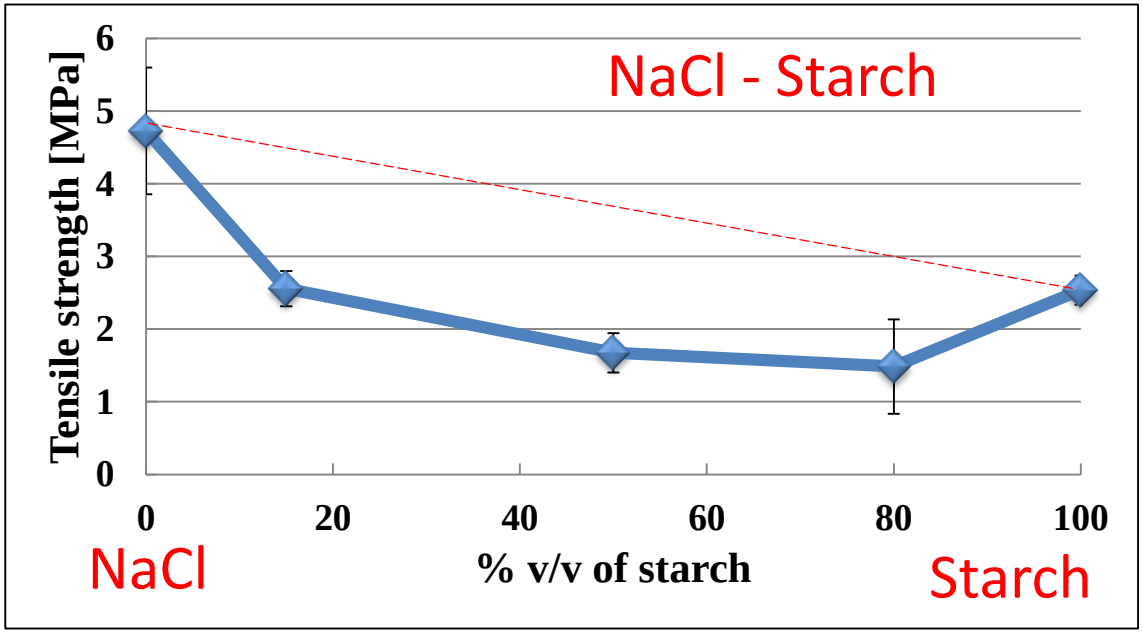

- Particle size distributions (106 – 180 µm)
- Powders are equilibrated at 20°C and 60% RH
- Post-compaction samples are stored for 24 hours at 20°C and 60% RH

Our experiments

- The same procedure as v.d. Voort was followed
- We confirmed that the strength of mixtures is lower than strength of NaCl or starch alone

In prior work

It was argued that this can only be possible if

Veen, v., v.d. Voort, et al., Int. J. of Pharmaceutics, 2000. **203**: p. 71-79

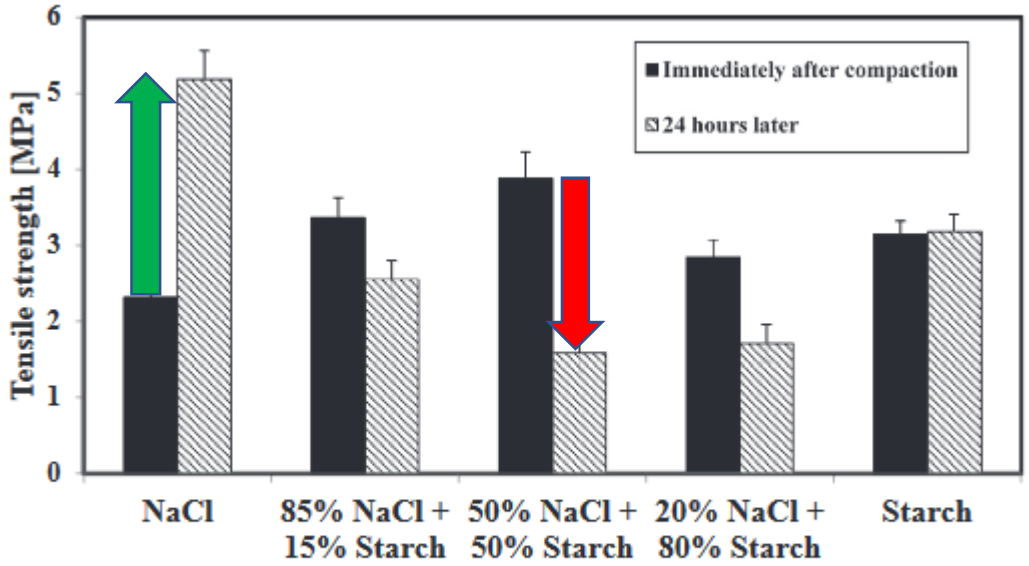

Figure 5. Comparison of strength for NaCl, starch, and their mixtures immediately after compaction and 24 h after storage at 20°C and 60% RH. The results show samples

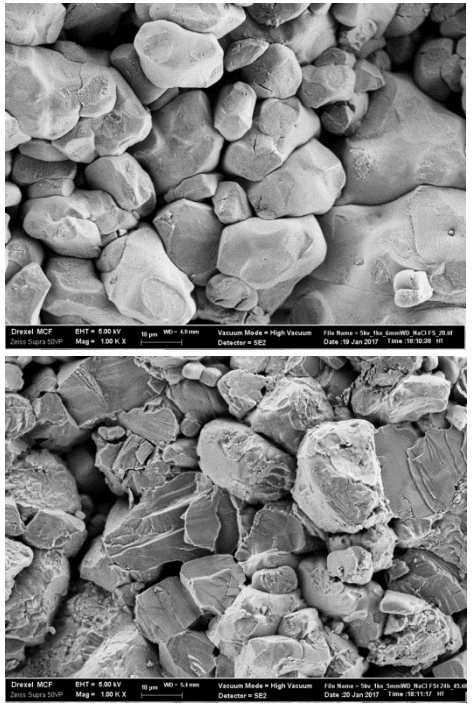

On the Post-Compaction Evolution of Tensile Strength of Sodium Chloride-Starch Mixture Tablets

Journal of Pharmaceutical Sciences 106 (2017) 2088-2096

Tensile stresses in NaCl-NaCl Contacts

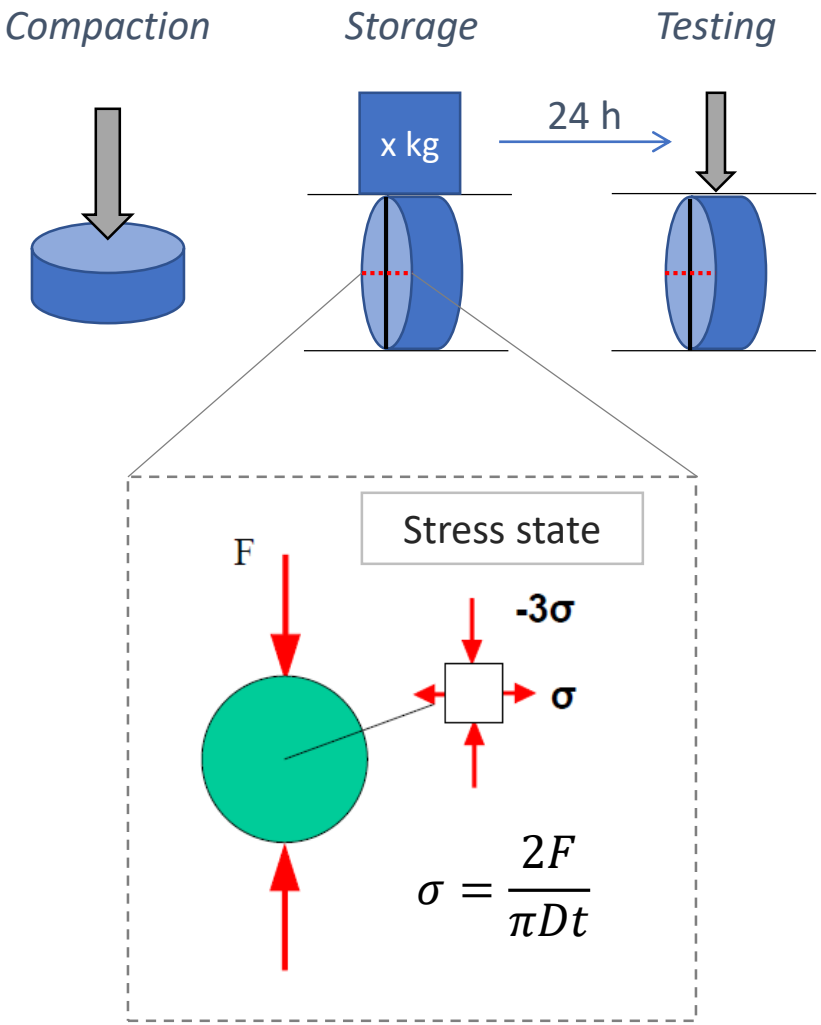

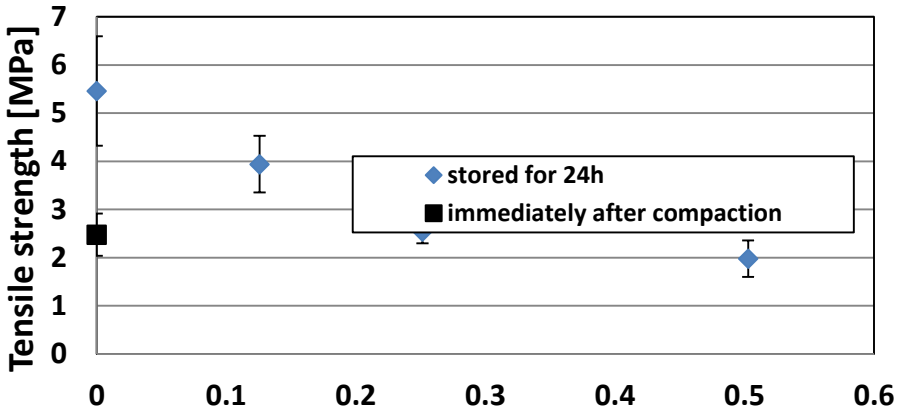

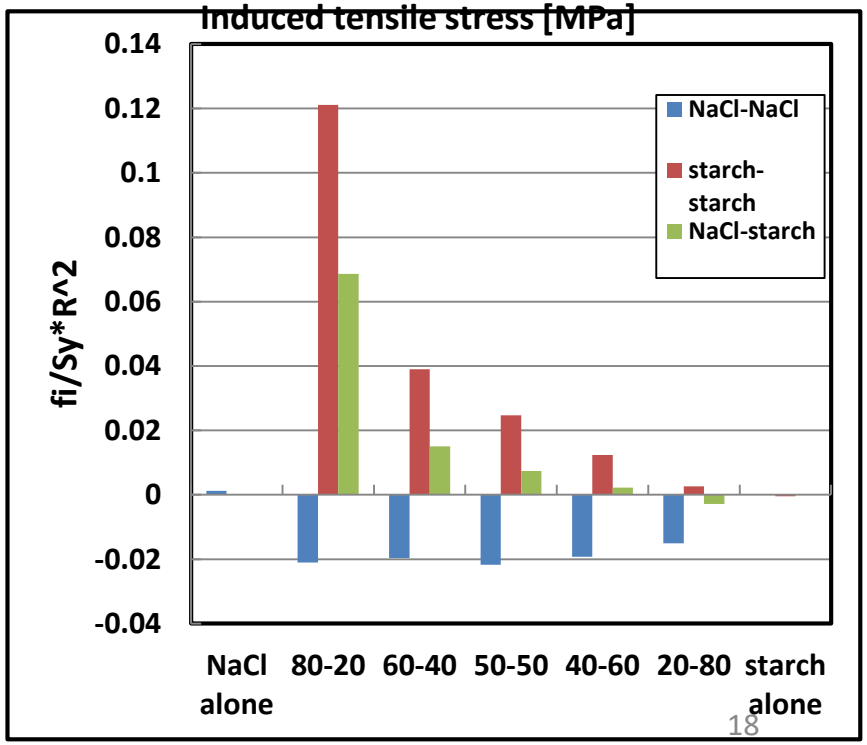

DEM predict that residual stresses is a function of the difference in moduli of the two phases

DEM simulations of compacting mixtures

Tensile stresses – negative Compression stresses - positive

Average residual stresses after ejection

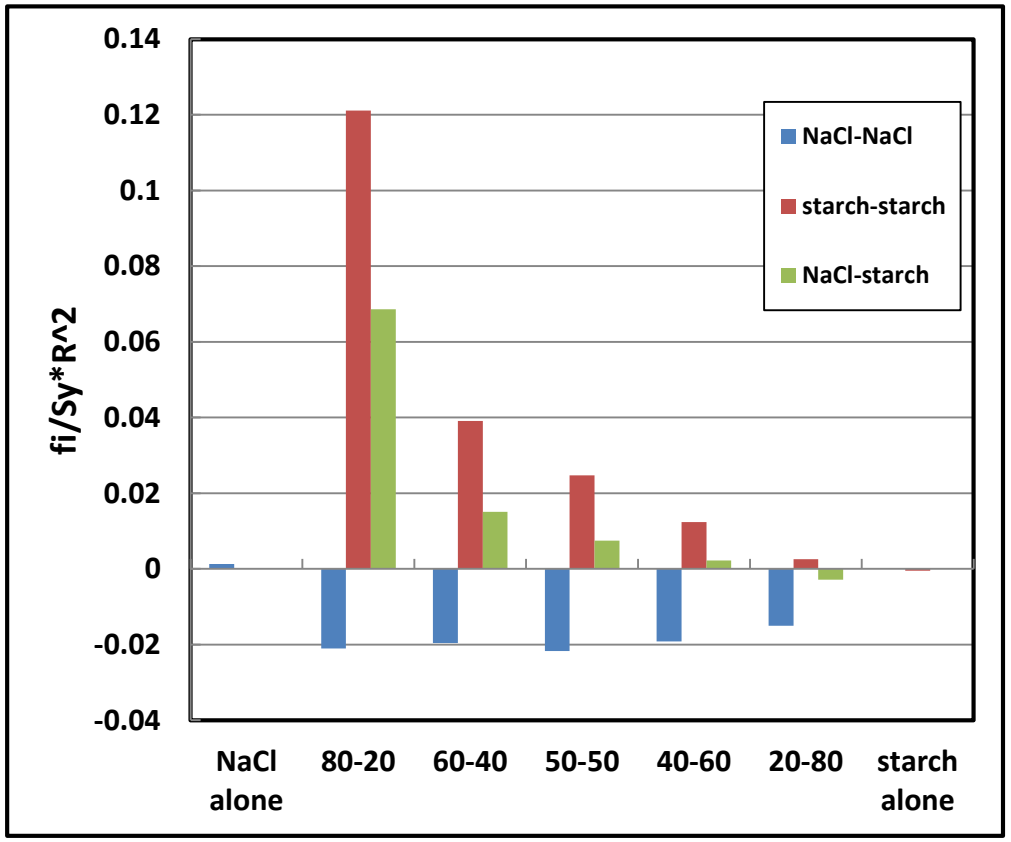

- Upon ejection NaCl-NaCl contacts are in tension and starch-starch and mixed contacts experience compressive stresses

NaCl + Starch

E (Starch) = 2 GPa

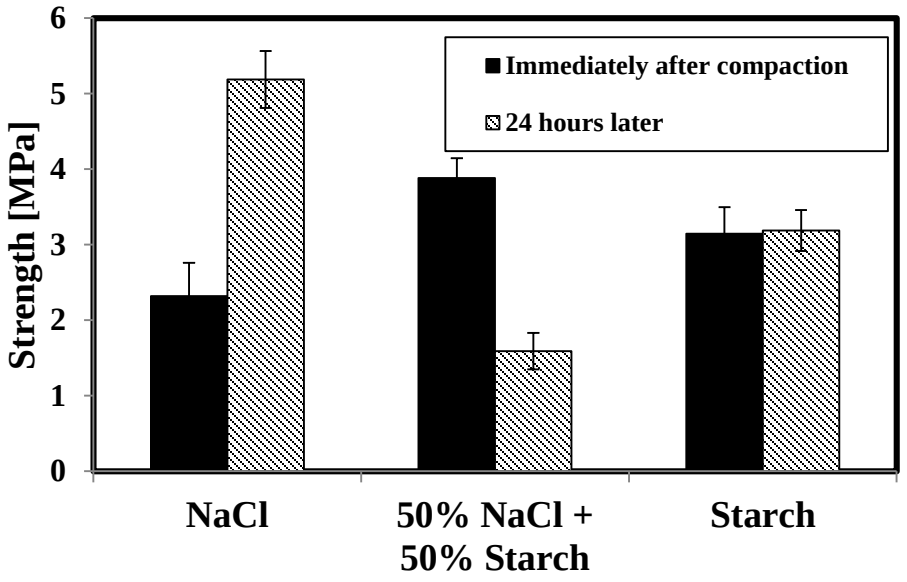

NaCl + MCC

E (MCC) = 10 GPa

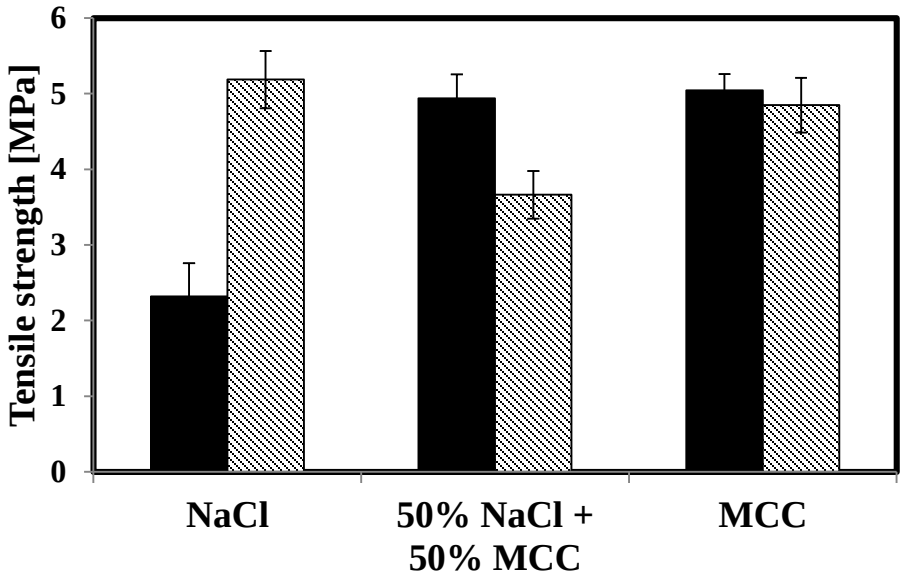

NaCl + Emcompress

E (Emcom.) = 35 GPa

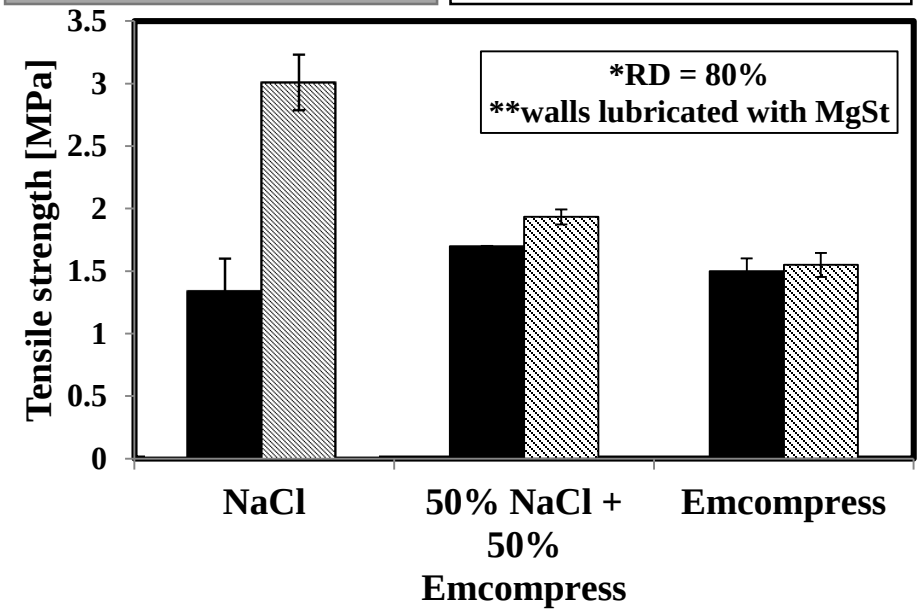

E (NaCl) = 40 GPa

- Testing the DEM supported hypothesis that smaller difference in elastic moduli between NaCl and the second phase would result in smaller residual stress leading to less or no reduction in strength of a mixture

Milled mixtures

	85% NaCl + 15% starch	50% NaCl + 50% starch	20% NaCl + 80% starch
Stored Ball Milled	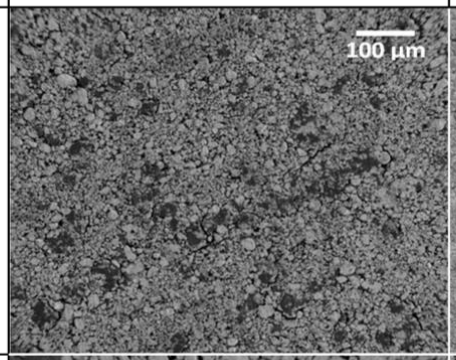	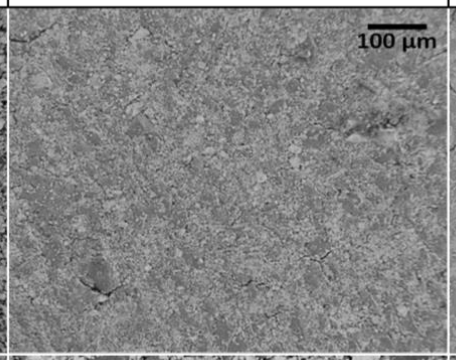	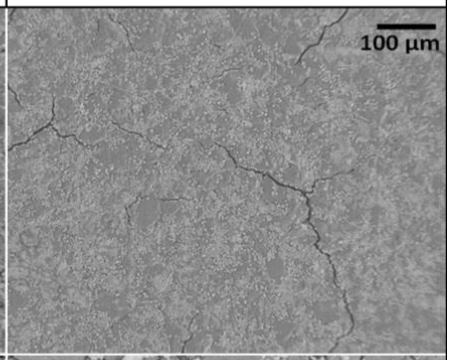
Fresh Ball Milled	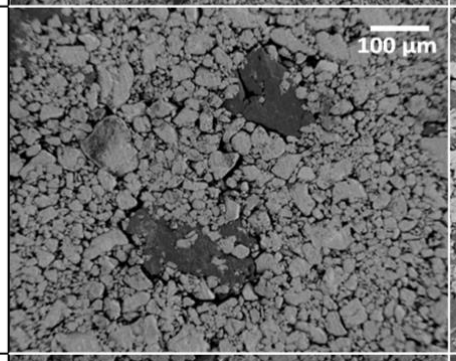	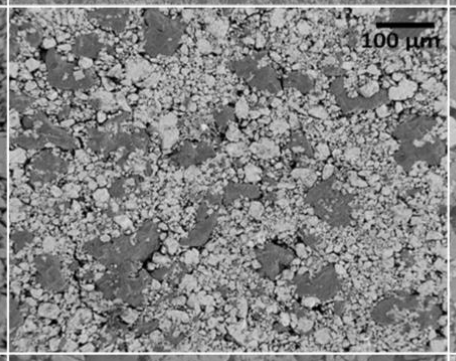	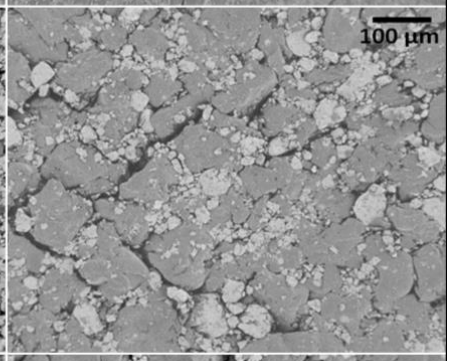
Stored Mixed	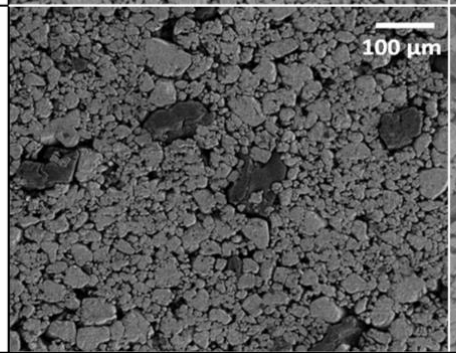	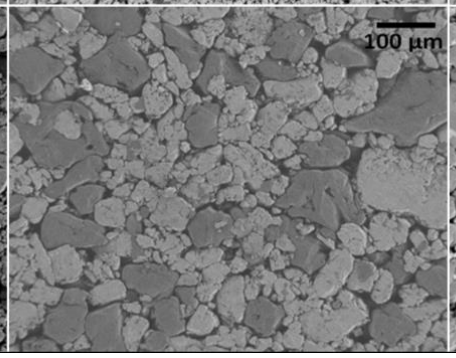	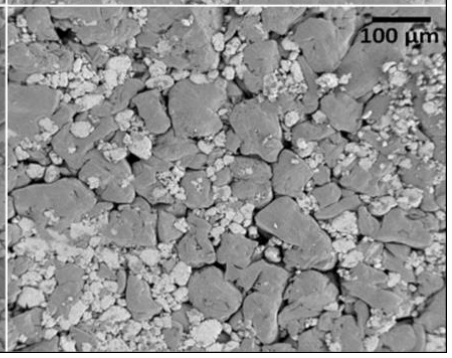

- Ball milling reduced the particle size
- Stored powders milled better than fresh powders

Evolution of strength in milled compacts

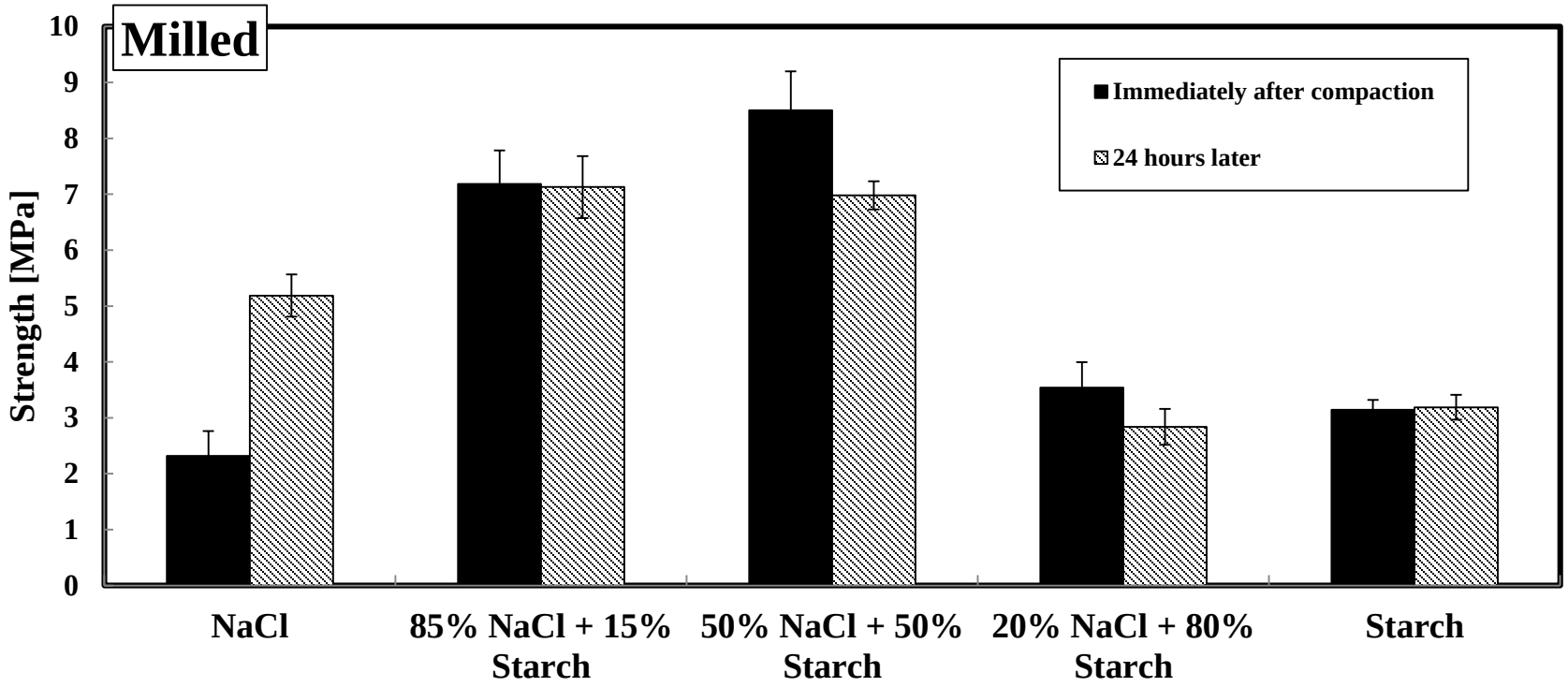

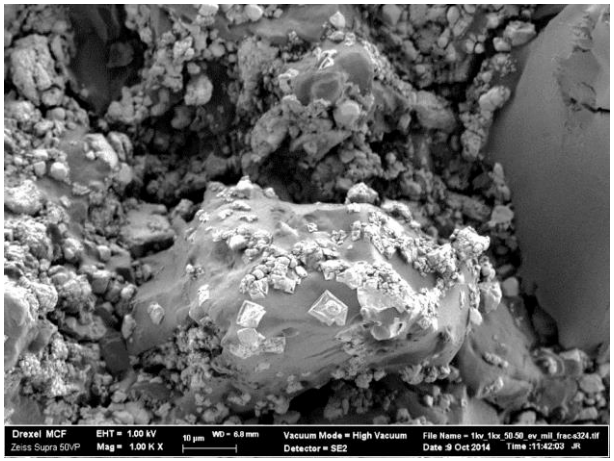

Microstructure and behavior cannot be simulated by DEM

Conclusions

- **We have pushed the DEM methodology to compactions at high densities including the associated experimental calibration**
- **Simulation of single materials are now becoming realistic and include predictions that were not possible with typical FEM continuum models.**
- **Still some aspects are not fully predicted (damage is overpredicted, expansion from die is underpredicted)**
- **For mixtures DEM can be used for understanding but not full predictions**
- **Mixtures include phenomena that lead to A+B ≠ A+B, yet the DEM models can provide extremely interesting insight that augments experimental observations and lead to explanations of relatively complex behaviors**